N-1856
December 1992

NCEL
Technical Note

By T.A. Shugar,
T.J. Holland, L.J. Malvar
and D.A. Doi

Sponsored By Office of Naval Technology

THREE-DIMENSIONAL FINITE ELEMENT ANALYSIS OF EXPLOSIVE SAFETY FACILITIES - A TECHNOLOGY ASSESSMENT

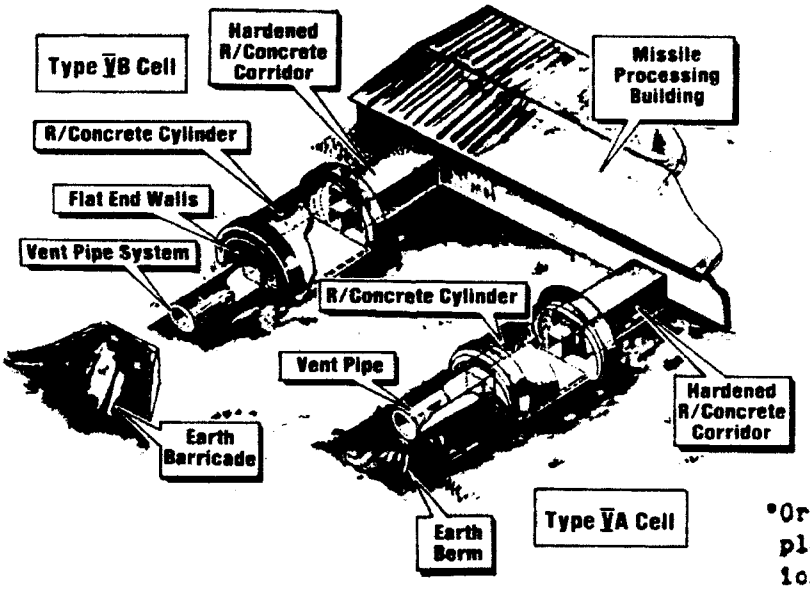

Original contains color plates: All DTIC reproductions will be in black and white

ABSTRACT To establish research requirements for development of modern, specialized software for computational structural dynamics in support of Navy explosive safety facilities, NCEL conducted baseline studies to assess commercial or currently available general purpose computer programs. Two widely available general purpose computer programs for three-dimensional nonlinear dynamic finite element analysis were applied to three types of reinforced concrete structures of interest to Navy explosive safety facility designers: (1) a novel cylindrical missile test cell concept, (2) flat slabs with variable shear steel, and (3) a soil-covered roof slab for a new high performance magazine concept. Results from codified single-degree-of-freedom (SDOF) methods for design of explosive safety structures were also considered and compared with finite element technology. This report provides an overview of these baseline studies.

NAVAL CIVIL ENGINEERING LABORATORY PORT HUENEME CALIFORNIA 93043-5003

METRIC CONVERSION FACTORS

Approximate Conversions to Metric Measures

Symbol	When You Know	Multiply by	To Find	Symbol
		LENGTH		
in	inches	*2.5	centimeters	cm
ft	feet	30	centimeters	cm
yd	yards	0.9	meters	m
mi	miles	1.6	kilometers	km
		AREA		
in^2	square inches	6.5	square centimeters	cm^2
ft^2	square feet	0.09	square meters	m^2
yd^2	square yards	0.8	square meters	m^2
mi^2	square miles	2.6	square kilometers	km^2
	acres	0.4	hectares	ha
		MASS (weight)		
oz	ounces	28	grams	g
lb	pounds	0.45	kilograms	kg
	short tons (2,000 lb)	0.9	tonnes	t
		VOLUME		
tsp	teaspoons	5	milliliters	ml
Tbsp	tablespoons	15	milliliters	ml
fl oz	fluid ounces	30	milliliters	ml
c	cups	0.24	liters	l
pt	pints	0.47	liters	l
qt	quarts	0.95	liters	l
gal	gallons	3.8	liters	l
ft^3	cubic feet	0.03	cubic meters	m^3
yd^3	cubic yards	0.76	cubic meters	m^3
		TEMPERATURE (exact)		
°F	Fahrenheit temperature	5/9 (after subtracting 32)	Celsius temperature	°C

*1 in = 2.54 (exactly). For other exact conversions and more detailed tables, see NBS Misc. Publ. 286, Units of Weights and Measures, Price $2.25, SD Catalog No. C13.10:286.

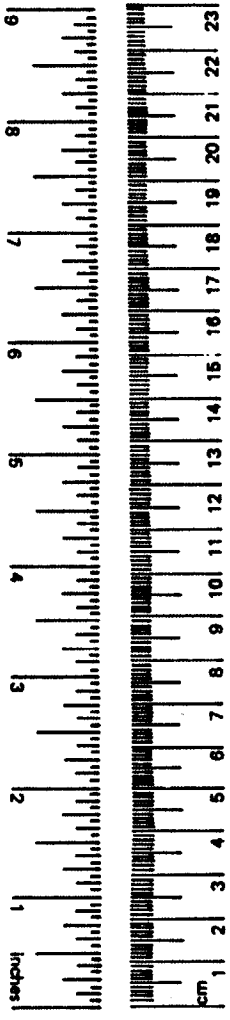

Approximate Conversions from Metric Measures

Symbol	When You Know	Multiply by	To Find	Symbol
		LENGTH		
mm	millimeters	0.04	inches	in
cm	centimeters	0.4	inches	in
m	meters	3.3	feet	ft
m	meters	1.1	yards	yd
km	kilometers	0.6	miles	mi
		AREA		
cm^2	square centimeters	0.16	square inches	in^2
m^2	square meters	1.2	square yards	yd^2
km^2	square kilometers	0.4	square miles	mi^2
ha	hectares (10,000 m^2)	2.5	acres	
		MASS (weight)		
g	grams	0.035	ounces	oz
kg	kilograms	2.2	pounds	lb
t	tonnes (1,000 kg)	1.1	short tons	
		VOLUME		
ml	milliliters	0.03	fluid ounces	fl oz
l	liters	2.1	pints	pt
l	liters	1.06	quarts	qt
l	liters	0.26	gallons	gal
m^3	cubic meters	35	cubic feet	ft^3
m^3	cubic meters	1.3	cubic yards	yd^3
		TEMPERATURE (exact)		
°C	Celsius temperature	9/5 (then add 32)	Fahrenheit temperature	°F

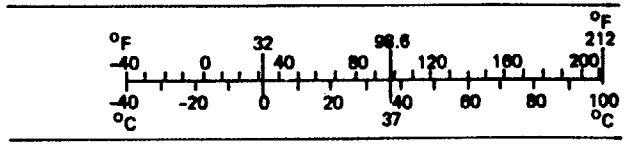

DISCLAIMER NOTICE

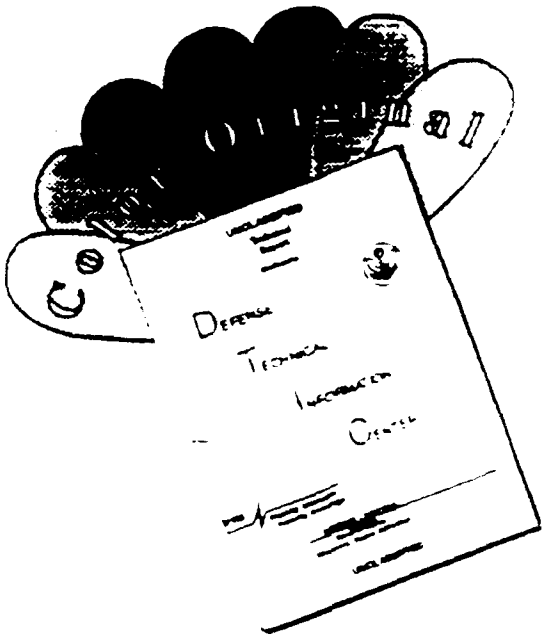

THIS DOCUMENT IS BEST QUALITY AVAILABLE. THE COPY FURNISHED TO DTIC CONTAINED A SIGNIFICANT NUMBER OF COLOR PAGES WHICH DO NOT REPRODUCE LEGIBLY ON BLACK AND WHITE MICROFICHE.

REPORT DOCUMENTATION PAGE

Form Approved
OMB No. 0704-018

1. AGENCY USE ONLY (Leave blank)	2. REPORT DATE	3. REPORT TYPE AND DATES COVERED
	December 1992	Interim: FY90 through FY92

4. TITLE AND SUBTITLE
THREE-DIMENSIONAL FINITE ELEMENT ANALYSIS OF EXPLOSIVE SAFETY FACILITIES - A TECHNOLOGY ASSESSMENT

5. FUNDING NUMBERS
PR - RM33F60-001-02-06-010
WU - DN668013

6. AUTHOR(S)
T.A. Shugar, T.J. Holland, L.J. Malvar and D.A. Doi

7. PERFORMING ORGANIZATION NAME(S) AND ADDRESS(S)
Naval Civil Engineering Laboratory
Port Hueneme, CA 93043-4328

8. PERFORMING ORGANIZATION REPORT NUMBER
TN - 1856

9. SPONSORING/MONITORING AGENCY NAME(S) AND ADDRESS(S)
Chief of Naval Research
Office of Naval Technology
Arlington, VA 22217-5000

10. SPONSORING/MONITORING AGENCY REPORT NUMBER

11. SUPPLEMENTARY NOTES

12a. DISTRIBUTION/AVAILABILITY STATEMENT
Approved for public release; distribution unlimited.

12b. DISTRIBUTION CODE

13. ABSTRACT *(Maximum 200 words)*

To establish research requirements for development of modern, specialized software for computational structural dynamics in support of Navy explosive safety facilities, NCEL conducted baseline studies to assess commercial or currently available general purpose computer programs. Two widely available general purpose computer programs for three-dimensional nonlinear dynamic finite element analysis were applied to three types of reinforced concrete structures of interest to Navy explosive safety facility designers: (1) a novel cylindrical missile test cell concept, (2) flat slabs with variable shear steel, and (3) a soil-covered roof slab for a new high performance magazine concept. Results from codified single-degree-of-freedom (SDOF) methods for design of explosive safety structures were also considered and compared with finite element technology. This report provides an overview of these baseline studies.

14. SUBJECT TERMS
Finite element modeling, structural dynamics, structural analysis, missile test cells, reinforced concrete modeling, explosive safety facilities

15. NUMBER OF PAGES
150

16. PRICE CODE

17. SECURITY CLASSIFICATION OF REPORT	18. SECURITY CLASSIFICATION OF THIS PAGE	19. SECURITY CLASSIFICATION OF ABSTRACT	20. LIMITATION OF ABSTRACT
Unclassified	Unclassified	Unclassified	UL

ABSTRACT

To establish research requirements for development of modern, specialized software for computational structural dynamics in support of Navy explosive safety facilities, NCEL conducted baseline studies to assess commercial or currently available general purpose computer programs. Two widely available general purpose computer programs for three-dimensional nonlinear dynamic finite element analysis were applied to three types of reinforced concrete structures of interest to Navy explosive safety facility designers: (1) a novel cylindrical missile test cell concept, (2) flat slabs with variable shear steel, and (3) a soil-covered roof slab for a new high performance magazine concept. Results from codified single-degree-of-freedom (SDOF) methods for design of explosive safety structures were also considered and compared with finite element technology. This report provides an overview of these baseline studies.

A commercial implicit finite element program was used to analyze the cylindrical missile test cell. Three-dimensional model construction, nonlinear concrete material modeling, and dynamic response were emphasized. Support for embedded reinforcement modeling was found to be very useful in construction of the model so as to retain the inherent anisotropic behavior of the composite structure. Concrete material modeling capability was highly sophisticated, but problematical in application when substantial cracking accumulated in the dynamic response. Results nonetheless demonstrated the value of computational structural dynamics technology in providing detailed understanding of the behavior of complex explosive safety facility designs.

Analysts used an explicit finite element program to analyze the dynamic response of two flat slabs subjected to conventional blast pressure levels. Elasto-plastic models included in the material library were used to model the material behavior of concrete and steel. The rebar pattern was modeled via the discrete reinforcement method; no embedded modeling capability existed. Measured residual deflections from field tests were compared to calculations from both three-dimensional finite element models and codified SDOF methods. In these limited data, the codified SDOF method was prone to unconservative results, while the finite element method bracketed the measured residual displacements, and further, successfully calculated observed failure modes and the onset of buckling in the reinforcement.

We also applied the explicit finite element program in the analysis of the soil-covered roof slab design. In this case, the blast load pressures were an order of magnitude higher, and the concrete material response included hydrodynamic behavior. The three-dimensional finite element model also included discrete reinforcement modeling and elasto-plastic behavior of the rebar. The dynamic response of the slab was calculated up to onset of a localized failure mode. This failure mode was consistent with initial field test observations of breach failure modes in scale models of slabs. Further, the calculated velocity field over the surface of the slab facilitated debris fallout distance prediction, an important performance aspect of the design.

This report concludes that commercial or available general purpose finite element programs for nonlinear dynamic analysis of reinforced concrete structures merit wider recognition and application in analysis and design of explosive safety facility systems. They are more encompassing and forthcoming than codified SDOF methods in this regard, though their application can sometimes be problematical. These programs have definite strengths and weaknesses, and consequently proficiency in their application must be developed to exploit them as resources.

CONTENTS

INTRODUCTION

Large structural/geotechnical systems generally represent a substantial capital investment and a substantial strategic resource for the Navy. They may also be classified as essential and/or high-risk facilities. Correspondingly, they require special attention in engineering design, hazard mitigation and maintenance, and vulnerability studies. At the same time, substantial technology in structural analysis capability exists due to advances in computational structural mechanics. Unfortunately, existing technology is relatively untapped regarding design, analysis, and vulnerability assessment of the Navy's facilities. We must gain experience in the application of this technology.

Two classes of structural analysis problems are being addressed: (1) waterfront facilities such as drydocks subjected to blast or earthquake loads, and (2) explosive containment facilities such as missile test cells subjected to internal blast loads. In each case, development of the corresponding structural analysis models for these systems must address the following issues: What structural response must be replicated accurately, and which finite element modeling tools, including elements, material models, and solution methods, are appropriate for the prescribed task. The present study describes, through demonstrations, how such modeling issues can best be resolved when using commercial/available general purpose nonlinear dynamic finite element software for analyzing explosive safety facility systems. A companion study addressed, in the same spirit, large waterfront structural/geotechnical systems such as drydocks and piers (Shugar, Holland, and Malvar, 1991).

OBJECTIVE

The objective of this study was to demonstrate and assess the effectiveness of two general purpose commercial/available computer programs for structural analysis by applying them to current technical problems involving Navy explosion containment facilities.

BACKGROUND

Explosion containment systems such as missile test cells and conventional box and high performance magazines support Fleet readiness through missile assembly and testing of missile all-up-rounds (AUR), and reduce costs through concentrated storage of munitions that reduce land encumbrances at Naval Weapons Stations.

A mishap during AUR testing could lead to inadvertent ignition of the rocket motor or detonation of the warhead. Current missile test cell designs have been made obsolete by the increased net explosives weight and changing size characteristics of new weapon systems. Testing in some current missile test cells is accomplished under safety waivers with the productivity restriction that only one missile can be tested at a time.

Current munitions storage facility designs do not exploit new materials and concepts for mitigation of sympathetic detonation of stored munitions. In some instances in foreign countries

(Republic of Korea, for example), these magazines are in noncompliance with U.S. explosive safety regulations, and they continue to operate only by exemptions or waivers.

Analysis capabilities are needed that are supportive of: (1) innovative missile test cell designs that provide for concurrent testing of missiles, and (2) high performance magazine designs that provide for high densities of stored munitions. These factors can lead to a 50 percent increase in missile testing productivity, and to dramatic reductions in ESQD (Explosive Safety Quantity Distance) arcs, as well as dramatic cost savings in optimal use of expensive real estate surrounding munitions storage facilities.

STRUCTURAL ANALYSIS MODELS STUDIED

The main body of this report is divided into three sections, each describing the analysis of a different reinforced concrete structure which is intended for explosive safety application. The structures include a novel missile test cell subjected to an internal blast load, experimental flat slabs subjected to close-in blast loads, and a soil-covered roof slab subjected to an internal blast load. The last configuration has been recently proposed for a high performance magazine concept.

The unique feature of the missile test cell analysis is the complexity of the steel reinforcement model which was constructed using the embedded reinforcement model method. In contrast to this method, discrete reinforcement models were employed for the analysis of the flat slabs and the soil-covered roof slab, both of which have comparatively very regular reinforcement schemes. The missile test cell analysis was addressed with the implicit finite element program, ABAQUS (Hibbitt, Karlsson, and Sorensen, Inc., 1989); whereas the flat slabs and soil-covered roof slab were analyzed with the explicit finite element program, DYNA3D (Hallquist and Whirley, 1989). The implicit ABAQUS code is more suitable to analyses dealing with slow, sluggish dynamic loads, while the explicit DYNA3D code is more suitable to highly transient dynamic loads. On the other hand, the reinforced concrete modeling capability is more substantial in ABAQUS than in DYNA3D.

The DYNA3D analysis of the flat slabs was noteworthy because experimental field test data were available which were used to compare the predicted and measured dynamic responses of the slabs. Two slabs were studied: one with substantial shear steel reinforcement, and the other with no shear steel reinforcement. Comparisons were also made with the dynamic response as calculated with the standard Tri-Services Guide, NAVFAC P-397 Design Manual (NAVFAC, 1991).

The unusual feature of the soil-covered roof analysis was that the blast loads were an order of magnitude higher than in the missile test cell analysis: 10,000 versus 1,000 pounds of TNT MCEs (Maximum Credible Events). This necessitated an auxiliary study of DYNA3D material models and material responses for concrete in the hydrodynamic range as well as in the shear deformation range. Techniques to simulate breaching of the slab and soil blanket, and to determine initial velocity fields for predicting fragment and debris distance, are also discussed.

STRUCTURAL ANALYSIS SOFTWARE

Though the demonstration analyses described above are the primary subject of this report, they are regarded as preliminary to future development of a specialized nonlinear structural analysis software system for selected structural/geotechnical systems in Navy facilities.

Application of commercial software products for finite element analysis to key Navy facilities often result in an adhoc project wherein the analyst must compromise project objectives to attain tractability with the software. The software architectures upon which most of these products have evolved are first generation designs which do not provide for effective translation of complex structures and dynamic loads into satisfactory models. Further, they are often found to be technologically limited because their computational algorithms are outdated.

The proposed solution is to adapt certain general methods in computational mechanics and combine them with several specific products from Navy-sponsored basic research in structural modeling to produce a special purpose, nonlinear structural analysis system. In this regard, some of these basic research products and their transition potential were reviewed in "An Evaluation of Numerical Algorithms for the Nonlinear Dynamic Analysis of Large Soil Structure Systems" (Bayo, 1987).

The flexibility to accurately and expeditiously address and determine the essential structural dynamic response of any critical facility subjected to strong motion earthquake or severe blast loads is a desirable goal, and the proposed special purpose software system will facilitate achievement of that goal. This software system concept is illustrated in Figure 1.

While commercially available technology is potent, as is demonstrated in this report, it very often does not strictly apply to complex or specialized Navy structural systems. As a result, the technical problem must inevitably be modified to accommodate the problem specification requirements of existing commercial structural analysis software products. These products have been developed for a very large market place in which the Navy is but a single customer. They provide a general purpose capability and hence, they often do not strictly apply to specialized problems. The contracting cycle is not suited to expeditious development and procurement of new or modified commercial capability. Hence, timely acquisition of the required capability most often is not an option. It is also often true that in complex nonlinear analysis problems the required capability cannot be well defined until several attempts have been made to solve the problem. All this points to the need for enhanced response via a flexible and modular software capability in nonlinear structural analysis. Toward this end, a software framework designed to provide guidance for achieving this capability was developed. Some of the issues which were considered are briefly summarized in the following. A full description is presented in "A Software Development Specification for Nonlinear Structural Analysis" (Landers, 1990). The software system proposed is primarily intended for the design and implementation of new methodologies and techniques in finite element analysis, but it can be extended to production situations as well.

Existing batch-oriented environments are conducive to creating inadvertent errors in input data which negate long costly analysis computer runs. Further, they make the development and testing of new methodologies and algorithms very difficult. Even with interactive text editors, the construction and debugging of new concepts and ideas often involves many iterations of the "edit-compile-debug" cycle.

Low-cost work stations equipped with powerful 32-bit processors, high-resolution graphic displays, and inexpensive networking facilities are appearing rapidly, while the cost of raw processing power is dropping rapidly. Further, and significantly, vendors are beginning to come

to a consensus on standards for the tools they provide for intermachine communication, graphics, and data bases.

Unfortunately, advances in structural engineering software development have not kept pace with the rapid changes in the computer marketplace. Some attempts are documented wherein existing, well-respected, monolithic finite element software systems which are traditionally run on large computers have been "downloaded" to workstation environments. However, little innovative software is available to the research and development community in structural engineering. This group requires a computational environment that is responsive to changes in the state of the art in computational mechanics and software development. Since new techniques and algorithms must be tested and debugged as they are implemented, a modular system that provides a high degree of flexibility and interaction is required.

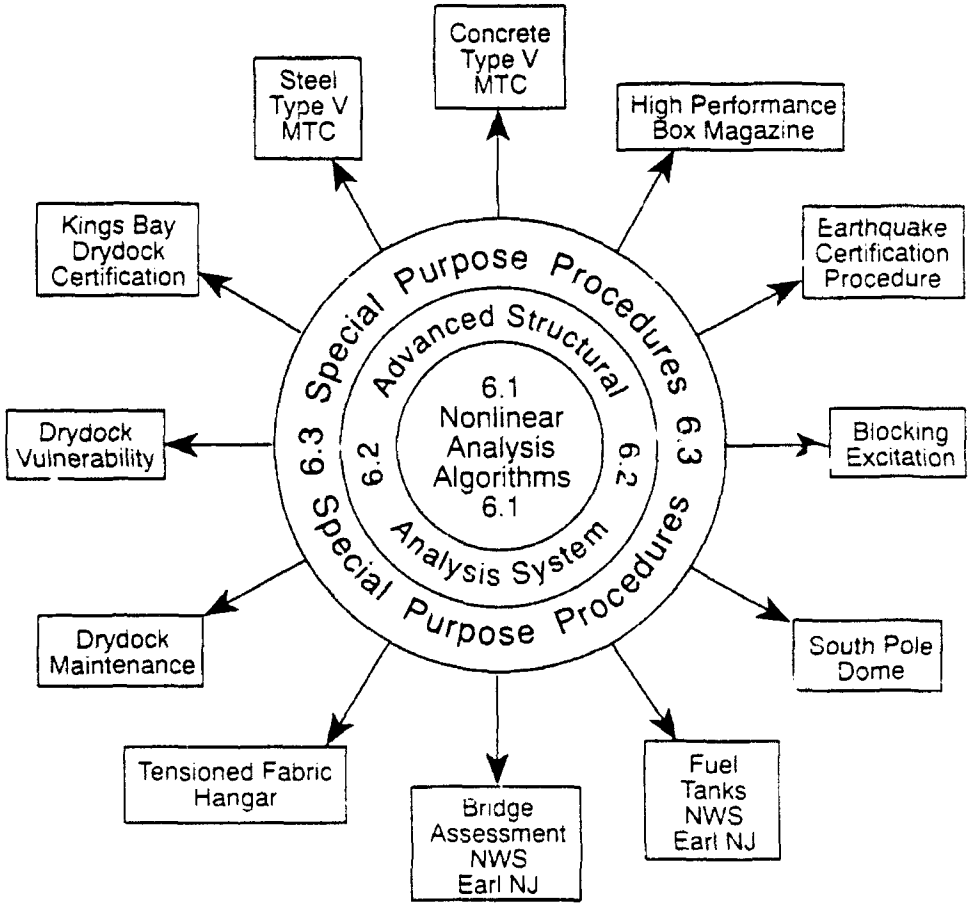

Figure 1
Structural analysis by special purpose computer programs - Concept.

SECTION 1

NONLINEAR DYNAMIC FINITE ELEMENT ANALYSIS OF REINFORCED CONCRETE MISSILE TEST CELL

INTRODUCTION

Traditional design of reinforced concrete explosive safety structures to resist blast loads has been based on structural dynamics of elastic-plastic lumped parameter single-degree-of-freedom (SDOF) models. Lumped parameter models are well explicated in the classical reference by Biggs (1964), for example. In addition to this technology, design procedures are based on field testing experience accumulated in explosive safety engineering for the past quarter century. The combination of traditional structural dynamics and field test experience has led to codification of a semi-empirical method based on SDOF models for the design of explosive safety facilities as embodied by the standard Tri-Services Guide, NAVFAC P-397 (1991).

NAVFAC P-397 does not address modern computer technology in structural dynamics using finite element models, even as an alternative method to be considered for special problems which go beyond the collective experience embodied in the codified procedure. Thus, it neither promotes nor precludes this technology in the design of explosive safety facilities.

OBJECTIVE

The objective in Section 1 of this report was the assessment of modern structural dynamics technology based on three-dimensional nonlinear finite element models for the analysis of a proposed missile test cell (MTC) concept.

SCOPE

This baseline study addressed an existing design of a reinforced concrete MTC structure subjected to internal blast loads. It employed commercial general purpose finite element software for nonlinear static and dynamic analysis. The study featured accurate replication of three-dimensional geometry and composite structural behavior for a complex reinforced concrete design. To achieve this, the embedded reinforcement model was used to represent the steel reinforcement. Modeling of reinforced concrete structures was emphasized, and the issue concerning how current technology addresses nonlinear material behavior such as cracking and crushing of concrete was studied.

Integration of the equations of motion for the MTC was accomplished by implicit methods in this study. Ordinarily, for highly transient loads such as blast loads, explicit time integration methods would be employed. However, existing commercial technology does not provide this capability in conjunction with large complex reinforced concrete structures when the latter are modeled using the embedded reinforcement modeling technique.

Construction of both two- and three-dimensional finite element models of the MTC was addressed in detail. The study included linear static analyses, linear eigenvalue analyses, and linear dynamic analyses of the MTC, and results for these analyses are briefly discussed.

Emphasis is given to presenting the numerical test results for nonlinear concrete material behavior and the nonlinear dynamic response of the MTC wall.

BACKGROUND

Loads on explosion containment facilities that result from accidental explosions of ordnance are clearly highly transient phenomena. Such loads are apt to excite deformation mode shapes corresponding to the first two thirds of the entire natural frequency spectrum of a structure. Therefore, computational methods for calculating dynamic response for blast loading must be capable of capturing high frequency response, as compared to earthquake excitation where the focus is on only a few low frequency modes. At the same time, facilities are proportioned to provide personnel safety, and a key concept in their design is ductility or the capacity of energy absorption through nonlinear material behavior and large structural deflections. This imposes a second requirement on the computational method which is the capability to handle both material and geometric nonlinear behavior. Finally, for three-dimensional analysis, computational solution methods must be numerically efficient.

The currently accepted approach appropriate to these requirements is a computational method based on explicit temporal integration of the structural dynamics equations of motion. Today, commercial finite element packages generally do not provide this capability. They are limited primarily to implicit temporal integration methods and algorithms and architectures which are numerically compatible with the implicit integration approach. There is currently a commercial rush to develop monolithic nonlinear finite element programs having true explicit temporal integration capability. However, these commercial products are only just emerging and their maturity will take some time to develop. This is especially true for reinforced concrete analysis, because it is not clear that they will support reinforced concrete modeling in their initial releases. This commercial activity is generally thought to be inspired by the availability of the DYNA2D and DYNA3D explicit finite element programs developed by Hallquist and colleagues in the Methods Development Group, Mechanical Engineering Department, Lawrence Livermore National Laboratory under the sponsorship of the Department of Energy (Hallquist, 1988; and Hallquist and Whirley, 1989).

Explicit temporal integration algorithms themselves are not complex or difficult to implement. In fact, they are implemented in most commercial implicit codes. However, explicit finite element programs can be made efficient only through special software design considerations for the surrounding finite element architecture. Implementation of special finite element formulations and material models that together promote the efficiency of explicit methods are also necessary. Thus, explicit finite element program architectures are very different from implicit program architectures.

Commercial software based on implicit temporal integration methods is more mature regarding reinforced concrete structural modeling capability, as is demonstrated in this report. Some previous examples of employing explicit codes for reinforced concrete structures subjected to blast loads do exist, however. For example, Terrier and Boisseau (1989) computed the nonlinear dynamic response of reinforced concrete slabs using DYNA3D, where they used a modified DYNA3D concrete material model. However, this material model is not well documented. Moreover, the reinforcement for the slabs was modeled by the relatively inaccurate smeared reinforcement modeling methodology. However, an accurate discrete reinforcement

model approach is available in DYNA3D and could have been used in this case because of the very regular pattern of reinforcement inherent in slab design.

In addition to having mature, shear deformable concrete constitutive models for crushing and cracking behavior, some implicit codes such as ABAQUS have superior modeling techniques for complex reinforcement designs. They include the embedded reinforcement model approach as well as the smeared and discrete approaches. There appears to be no fundamental technical reason why explicit programs cannot eventually catch up in regard to support for modeling complex reinforced concrete structures. However, they will have to employ algorithms that are simple and efficient so that they conform to the philosophy of explicit program architectures. This may be difficult because accurate reinforced concrete modeling for highly transient loads is technically complex. Additional research is required to improve concrete constitutive models for high rates of loading in three dimensions. However, steel reinforcement modeling could be enhanced by adding existing embedded reinforcement modeling capability.

Commercial computational methods that may be used for the analysis of a complex reinforced concrete missile test cell are therefore limited to ones based on implicit temporal integration algorithms. This ultimately adversely impacts the requirement for computational efficiency. For large scale problems this may mean that the analysis will be prohibitive. Codes based on implicit temporal integration are technically capable of predicting high frequency response, and technically capable of predicting both nonlinear material and nonlinear geometric behavior; they simply require enormous computational power to do so.

MISSILE TEST CELL MODEL DEVELOPMENT

A missile test cell is a key Navy facility because it supports fleet readiness through missile assembly and testing of missile all-up-rounds (AURs). One recent concept for an innovative MTC design provided for concurrent testing of missiles and close siting the MTC to the control room and other buildings of the test complex. It was estimated that these factors could afford a 20 percent reduction in testing manpower while increasing missile test production by 50 percent. One such proposed concept was the NAVFAC Type VB MTC, a design based on a thick-walled, reinforced concrete cylinder with flat circular end walls. This MTC design was the subject of the present baseline modeling study.

Blast Load and Expected Structural Response

To model the proposed MTC so that its dynamic response can be computed, the internal blast load to which it is subjected must first be determined as closely as possible. For purposes of this investigation, the MTC is presumed subjected to the design (internal) blast load graphed in Figure 2, which is based on inadvertent detonation of a missile warhead. This load was computed by Murtha and Dede (1988), and a brief description of the computation is given below.

The bilinear pressure history shown is composed of a triangular shock pressure phase followed by a triangular gas pressure phase. These triangular phases are computed separately by different methods and then combined so that superposition is suppressed where they overlap. Both calculation methods are semi-empirical, and are the current basis for determining shock and gas pressure load data in the design guide, NAVFAC P-397 Design Manual.

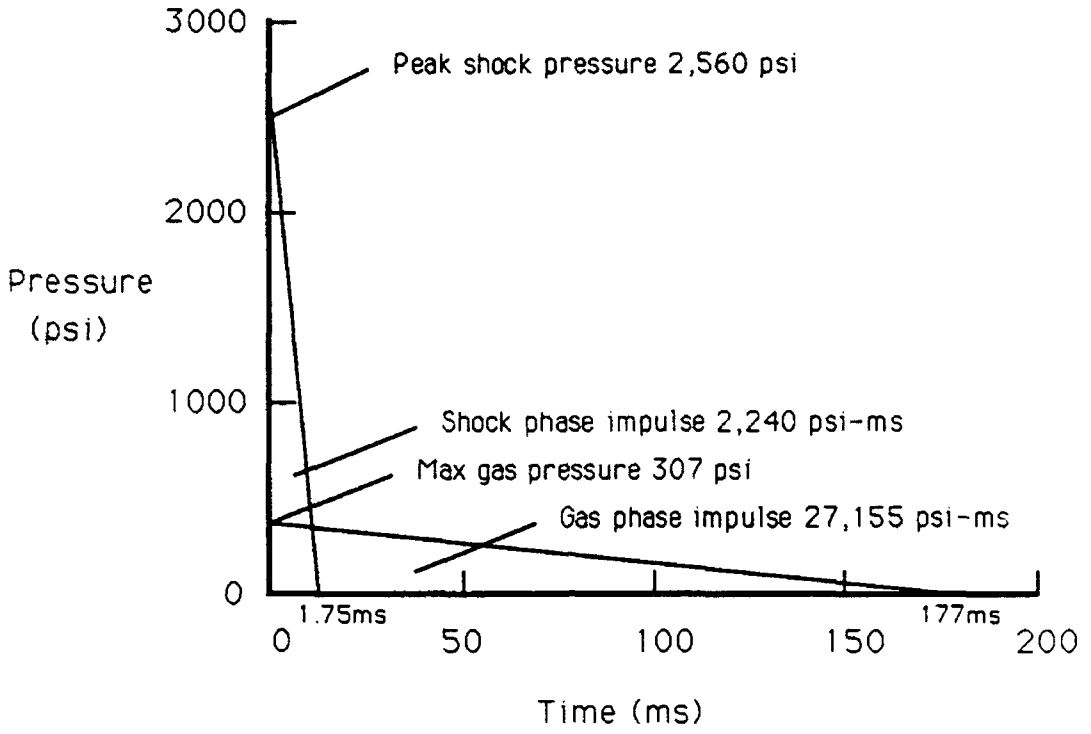

Figure 2
Assumed internal shock and gas pressure load for Type V MTC.

The calculation method for the shock phase allows for different standoff distances of a concentrically located spherical charge internal to an assumed equivalent rectangular box structure for the cylindrical MTC. Consequently, different shock pressure histories are predicted for various flat rectangular surfaces surrounding the charge. The shock pressure history selected for this study corresponds to that for the cylindrical wall of the MTC as contrasted with the flat end walls; it has a 2,560-psi peak pressure with a duration of 1.75 ms and a specific impulse of 2,240 psi-ms. For purposes of this investigation, this pressure history is assumed to be uniformly and proportionally distributed over all internal surfaces of the MTC.

The calculation of the gas phase is based on containment of the products of detonation and is a comparatively low magnitude, long duration triangular pressure history. The semi-empirical method of calculation used and the computer program developed for calculating gas pressure loads are described by Tancreto and Helseth (1984). According to this methodology, the gas pressure history depends on the shock pressure and various geometric and physical properties of any venting mechanisms present. In the case of the MTC, a frangible circular aperture in the center of the back wall constitutes a venting mechanism which is factored into the computation. The resulting triangular gas pressure history shown has a peak value of 307 psi, a duration of 177 ms, and a specific impulse of 27,155 psi-ms. Provided the MTC survives the shock phase, the larger impulse might indicate that the gas pressure phase is the dominant phase of the loading so far as structural response is concerned. However, this also depends on the relationship between the frequency spectra of the two blast load phases and the natural frequencies of the structure.

MTC Configuration and Steel Reinforcement

Structural design aspects of the proposed MTC are described in this section as they relate to the development of a three-dimensional finite element model. The basic data required are the overall three-dimensional geometry, the wall thicknesses, details of various substructural components, and steel reinforcement patterns.

The MTC is fundamentally a reinforced concrete thick-walled cylinder with thick circular plate end walls. Its overall concept is shown in Figure 3. The walls of the reinforced concrete cylinder and flat end walls of the structure are 32 inches thick, and the inside dimensions of the cylinder are approximately 20 feet in diameter and 30 feet in length. A circular apperture exists in the back wall for venting and managing the force of an accidental explosion, and a rectangular doorway exists in the front wall to provide access. These simple geometrical aspects are deceiving because the geometrical complexity of the steel reinforcement is substantial. Modeling this complexity represented the major challenge to the development of an accurate finite element model of the MTC.

Definition of the steel reinforcement in a design is a preliminary task necessary to accurate model development in complex reinforcement designs. Description of the MTC steel reinforcement design was subdivided into three sections for tractability: the cylinder, the front wall, and the back wall, as illustrated in Figure 4. These graphical data were developed using a CAD system to define and locate each major steel bar in the rebar cage design. The CAD system was essential to an accounting for, and an accurate geometric layout of, individual reinforcement bars. In this way, reinforcement data were translated directly from design drawings of the MTC into a digital form for organization, analysis, and visual display.

The layout of the hoop and longitudinal steel bars for the cylinder subsection is shown in Figure 4a. This is indicative of the density and complexity of the rebar cage. These are #11 Grade 60 bars. Groups composed of four concentric hoop bars are located at stations every 6 inches along the length of the cylinder wall as shown in Figure 4b. To each of these four rings of hoop bars, there are 156 corresponding longitudinal bars, which are spaced about the circumference at intervals of 2.3 degrees. The resulting four concentric layers of longitudinal bars in the wall are shown in Figure 4c.

The reinforcement of the back wall of the cylinder is shown in Figure 4d. It is primarily composed of two identical layers of mutually orthogonal #11 hoop and #6 radial bars. One layer each is embedded at cover depths just beneath the inside and outside concrete surfaces of the end wall. To facilitate construction of the reinforcement cage, the spacing of the hoop bars was varied with their radial location, and only every other radial bar extends completely to the inner circular opening. Also, there are four hoop bars for local reinforcement of the circular opening in the wall.

The front wall reinforcement design shown in Figure 4e is more involved since the opening is rectangular. The radial steel is similar to the radial steel in the back wall in that only every other bar extends to the opening. The radial reinforcement consists of 156 #6 bars. The hoop bars are #11 bars. There are six rectangular-shaped hoop bars around the opening to locally reinforce the rectangular doorway. As in the back wall, this pattern is repeated in two identical layers embedded at depths of cover beneath the inside and outside concrete surfaces.

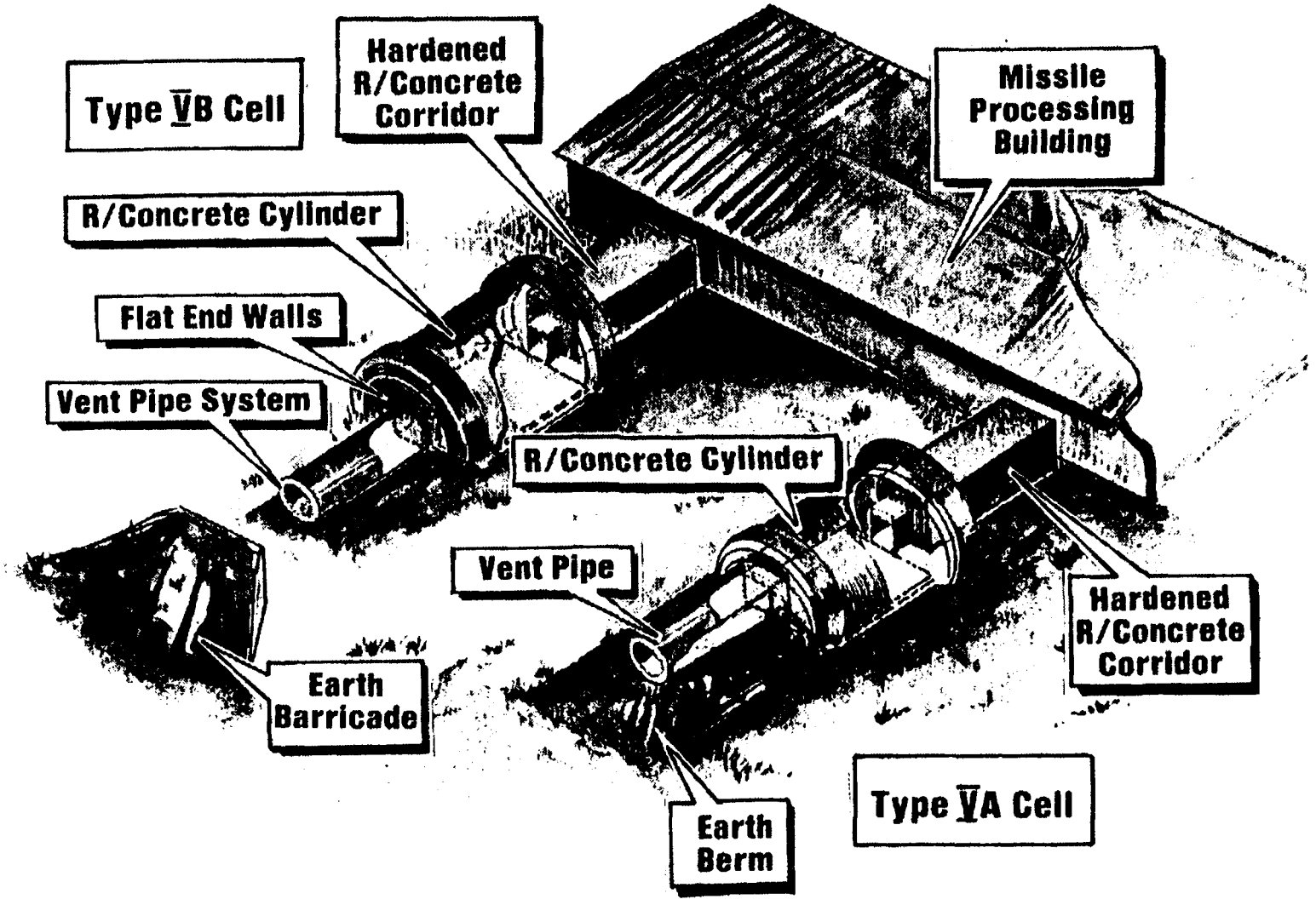

Figure 3
Proposed missile test cell concept.

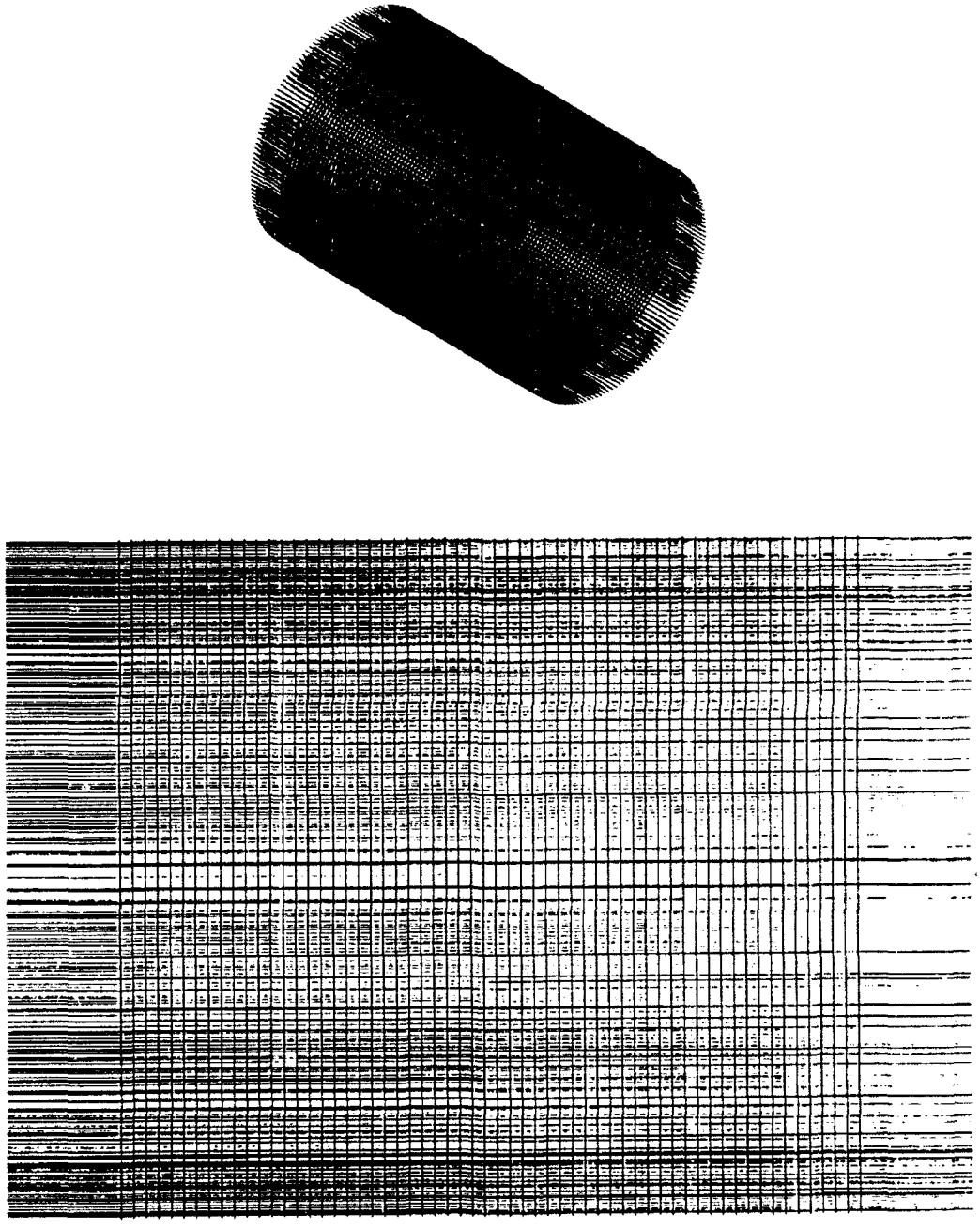

(a) Cylinder hoop and longitudinal bars.

Figure 4
MTC steel reinforcement bar layout.

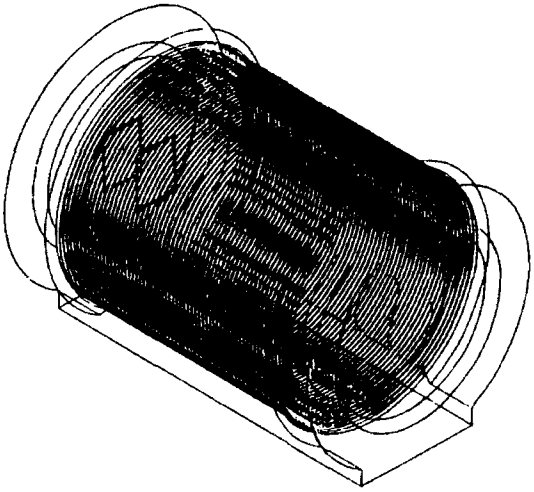

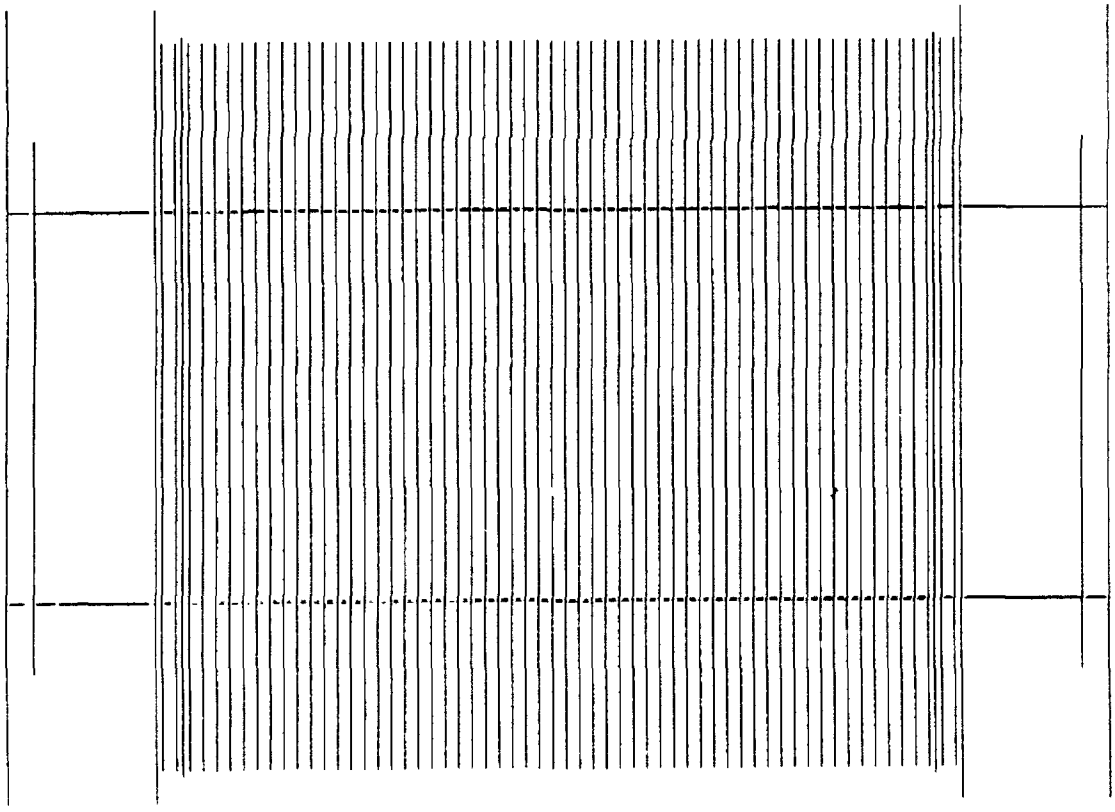

(b) Cylinder hoop steel.

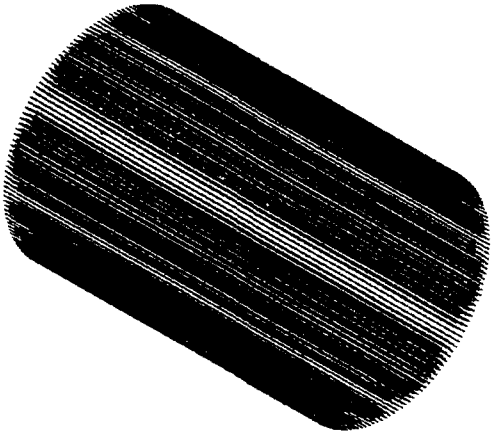

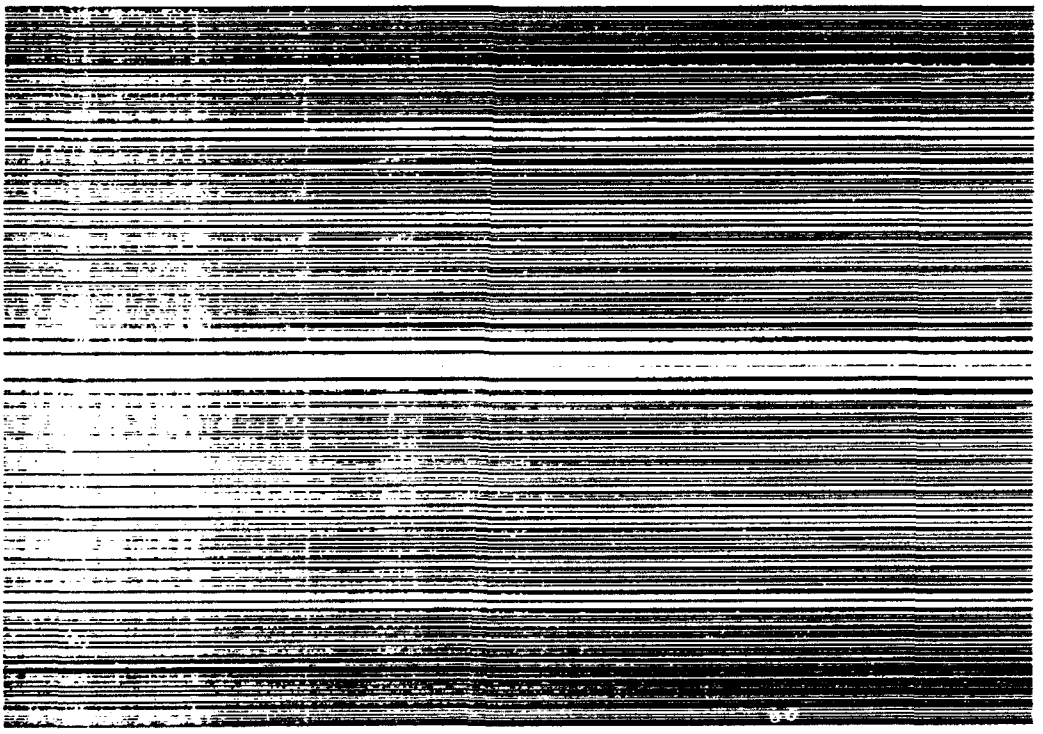

(c) Cylinder longitudinal steel.

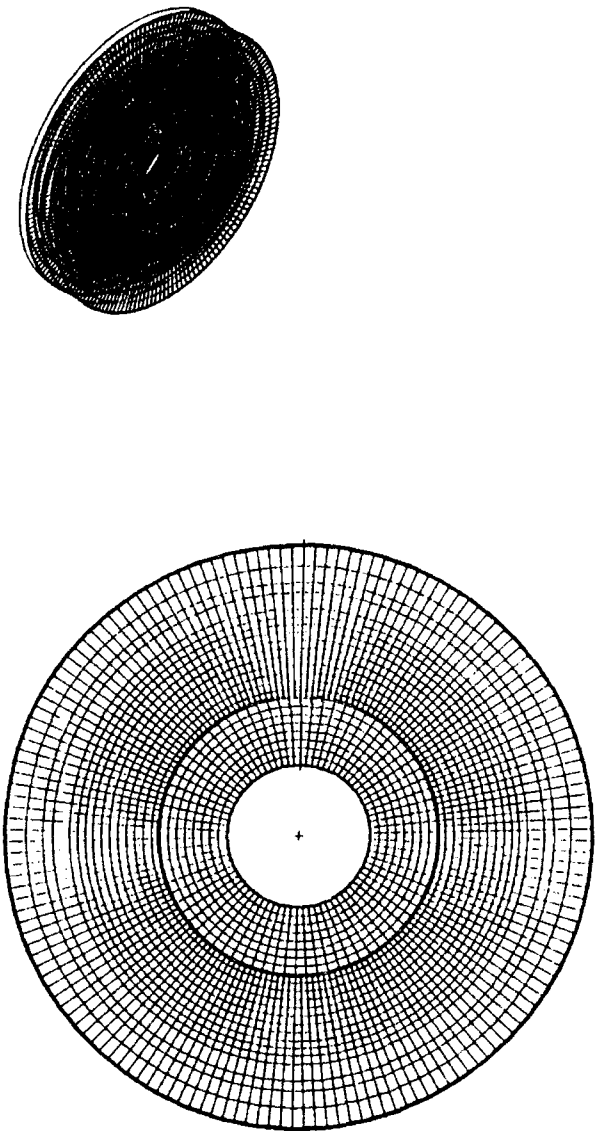

(d) Back wall hoop and radial bars.

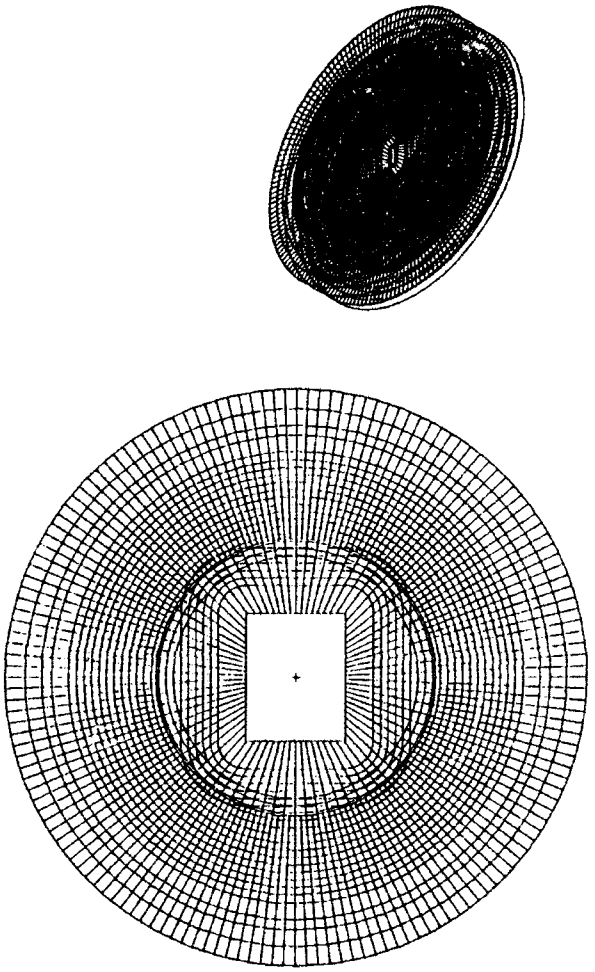

(e) Front wall hoop and radial bars.

In addition to the primary reinforcement described, the MTC walls have substantial amounts of shear steel. For example, at each 6-inch station along the cylinder wall length, stirrups are located in 156 radial planes, every 2.3 degrees around the circumference. These stirrups are intended to confine the concrete about the four concentric layers of the hoop and longitudinal steel bars in the cylindrical wall. To this end, they are tied to the inner and outer layers of the hoop and longitudinal bars.

Finally, 156 pairs of #11 crisscross diagonal bars reinforce the interface between the cylinder and the front and back walls. Each pair lies in a radial plane and is spaced at 2.3-degree intervals around the circumference. A summary of the primary reinforcing steel in the MTC design is presented in Table 1.

Other Components

In addition to the structural components of the MTC previously described, there are other components of the MTC design that relate to the issue of structural modeling. These include internal components within the enclosure of the MTC, and the external soil backfill surrounding the MTC which is designed to be embedded to one-third of its diameter below grade. Though the modeling effects of some of these components were neglected, they are discussed briefly for the sake of completeness because in other circumstances their effects might be reconsidered and they might be retained in the model.

Three secondary structural components could conceivably affect structural response: (1) a rectangular blast-resistant steel door between the MTC and the hardened access corridor, (2) a thin steel corrugated lining on the inside surface of the cylinder, and (3) a steel floor grating.

The effect of the steel door located in the front wall of the MTC was accounted for in the model by application of an equivalent line load to the door frame. The load was applied normal to the wall along the perimeter of the door frame. The magnitude of the line load is the product of the prescribed internal pressure (Figure 2) and the exposed area of the steel door, divided by the perimeter length. This approximates the effect of the steel door on the dynamic response of the MTC. The strengthening effect of the door frame on the wall is regarded as secondary. However, the dynamic response of the blast-resistant door is ordinarily of interest. Although neglected for expediency in the present analysis, it could be modeled and analyzed separately or in combination with the MTC model. Further, for the present analysis, the door is assumed not to fail, and the line load on the door frame is assumed to persist throughout the transient event as a proportional load.

The structural effects of the corrugated lining and the floor grating are completely neglected in the finite element model. The lining is intended primarily as a form to facilitate concrete placement during construction and is not meant to be a structural component. It is designed as an articulated or loosely connected series of overlapping corrugated sheets, which cannot develop the membrane stresses which otherwise could contribute to the total membrane resistance of the cylindrical shell wall. Similarly, the floor grating design was not meant to provide structural resistance or bracing of the inside wall and is therefore assumed to be structurally inert.

The circular aperture in the back wall is initially sealed by a frangible cover which is designed to fail early to vent combustion products, and thereby decrease the pressure on the cylindrical wall. This effect was accounted for in the calculation of the design pressure load history (Figure 2), and no further consideration was given to modeling the frangible cover itself.

Table 1
Summary of MTC Reinforcing Steel

Reinforcement Description		Front Wall	Cylinder Wall	Back Wall	End Wall/ Cylinder Interface
Hoop:	Layers	2	4	2	-
	Spacing	Variable	6"	Variable	-
	Size	#11	#11	#11	-
Longitudinal:	Layers	-	4	-	-
	Spacing	-	2.3 deg	-	-
	Size	-	#11	-	-
Radial:	Layers	2	-	2	-
	Spacing	2.3 deg	-	2.3 deg	-
	Size	#6	-	#6	-
Shear:	Layers	-	156	-	-
	Spacing	-	2.3 deg/6"	-	-
	Size	-	#6	-	-
Diagonal:	Layers	-	-	-	2
	Spacing	-	-	-	2.3 deg
	Size	-	-	-	#11

In the MTC design, both the rectangular and circular apertures were lined with 1-inch thick steel plating. The liners are attached to the end walls by rebar anchors extending radially into the end walls. The anchors were neglected in the reinforcement model, while the steel liner plate was included in the MTC model. A series of 32 membrane elements for the liner plate of each aperture were used for this purpose; they were assumed to be rigidly bonded to the concrete surface of the aperture.

The effect of the soil embedment was ignored as a simple matter of expediency in this study. It is otherwise believed that the soil backfill material would absorb energy through plastic deformation and the additional surrounding soil would absorb energy through radiation damping of the ground shock. This effect should enhance the performance of the MTC in resisting the design blast load. It could conceivably be modeled with nonlinear soil finite elements, albeit at much greater expense. Assessing the performance of the reinforced concrete cylinder was of the first importance, and therefore it was intended that available computational resources, as listed in Table 2, should be focused on the MTC itself. Thus, the effect of the soil was neglected and replaced with either a rigid or free boundary condition on the portion of the surface of the MTC which was in contact with the soil backfill.

Table 2
Workstation Resources for MTC Analysis

Hardware
Sun 4/260 Computer: 11 MIPS Memory: 32 Mb RAM Disks: 688Mb, 688Mb, 280Mb Seiko Color Printer, CH-5514 Apple Laserwriter II Printer Sun Tape Drive: 60MB, 1/4 inch Color Display Monitor, Keyboard and Mouse
Software
ABAQUS Version 4.8 PATRAN Release 2.4 with PAT-ABAQUS UNIX Operating System Sun Phigs 4.0 FORTRAN Compiler

Three-Dimensional Finite Element Model

The three-dimensional finite element model of the MTC is shown in Figure 5. One plane of symmetry is exploited due to symmetry of the structure, applied load, and boundary conditions. Eight-node brick elements in which the displacement fields are interpolated linearly were prescribed. Two elements were prescribed through the thickness of the wall. Larger models, such as those shown in Figure 6, were also developed with two and four elements through the thickness. Linear static runs with internal pressure loads indicated that the radial stiffness of the MTC model was the same for either two or four elements modeling the wall thickness. The MTC model possessed 1,300 nodes or 3,900 degrees of freedom, and was substantially smaller than the alternative models considered as listed in Table 3. PATRAN Plus (PDA Engineering, 1989), Release 2.4, was employed to generate the basic three-dimensional models. It has ABAQUS file format translators for basic mesh and surface load information, but it does not support the ABAQUS embedded reinforcement data files which describe the reinforcement model.

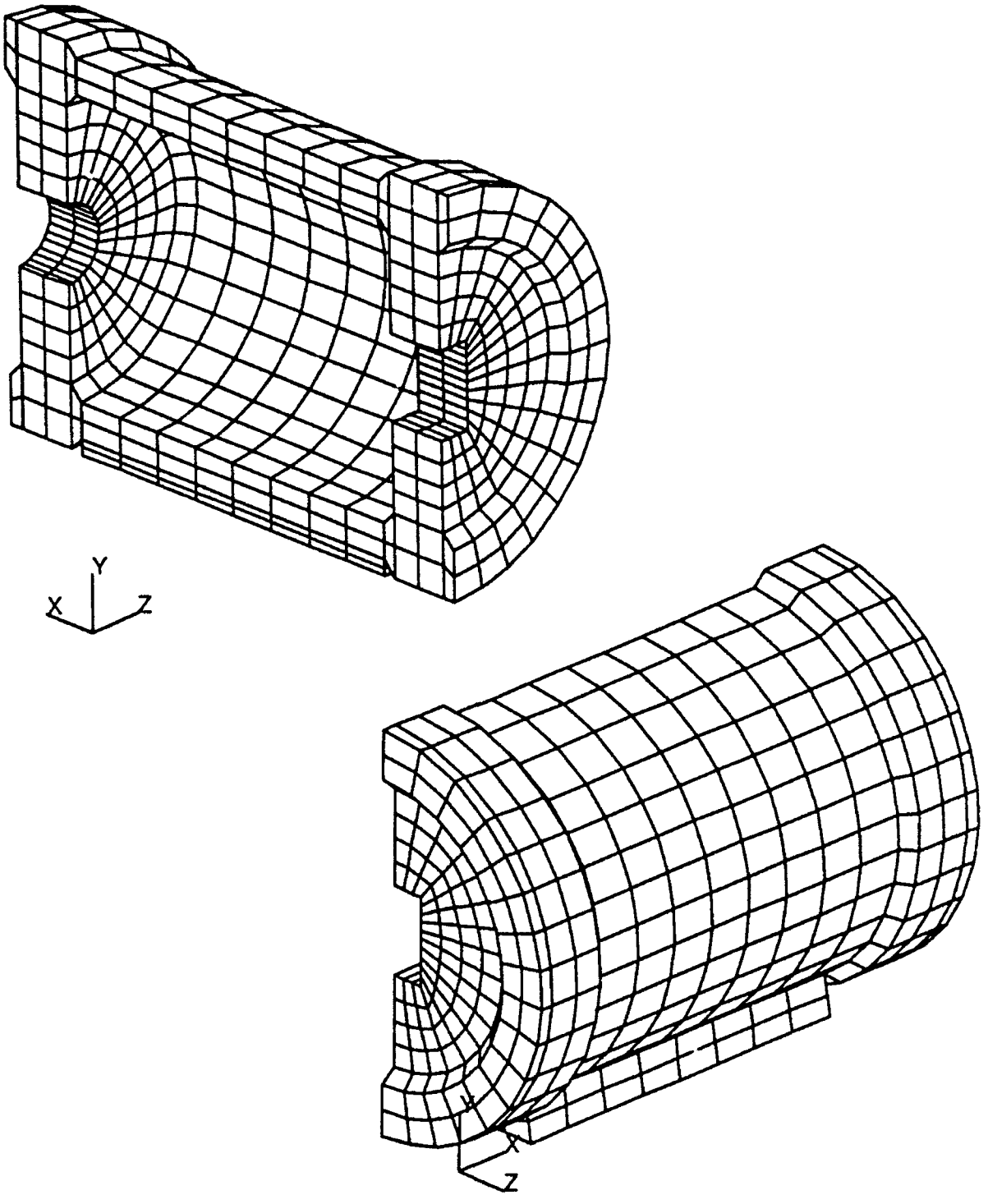

Figure 5
Three-dimensional finite element model of the MTC.

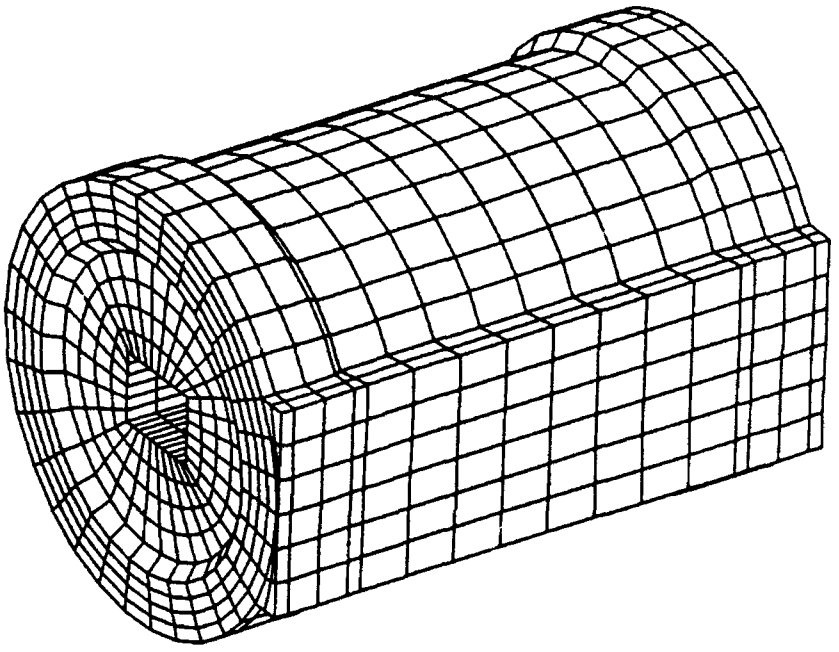

(a) Four-element wall model.

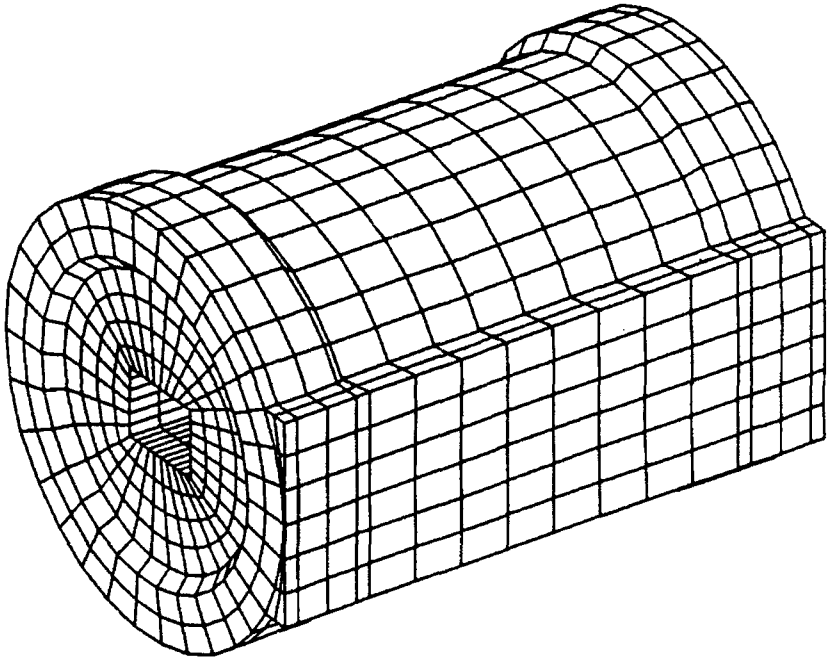

(b) Two-element wall model.

Figure 6
Preliminary MTC models.

Table 3
Three-Dimensional Model Data

Description	Nodes	DOF	Element Aspect Ratios
Four-Element Wall Model	8400	25,200	1 x 1 x 1 to 3 x 3 x 1
Two-Element Wall Model:			
Full	2600	7,800	1 x 1 x 1 to 1 x 1 x 2
Half (MTC Model)	1300	3,900	1 x 1 x 1 to 1 x 1 x 2

Embedded Reinforcement Model

Description of Embedded Element. The steel reinforcement is represented by the embedded reinforcement model (Zienkiewicz, et al., 1972). The advantage of this model is that it provides a reasonably accurate replication of the effect of reinforcement while being convenient and expedient to implement into an existing finite element mesh. No changes to the finite element model (in this case, see Figure 5) are required to introduce the reinforcement, no matter how complex the reinforcement pattern. A more recent discussion is provided by Cervera, Hinton, and Hassan (1987). However, the ABAQUS implementation of this model removes the restriction that prevented the consideration of reinforcement in an arbitrary position inside the element.

A sketch of an embedded element is shown in Figure 7. This element is typical of the cylindrical wall portion of the MTC model, so that the principal directions are labeled hoop, longitudinal, and radial in the figure. The thickness of the cylindrical wall is 32 inches and two such elements, each 16 inches thick, model the wall through its thickness. This is the inner element with the bottom node lying in the internal cylindrical surface of the wall and the top node lying in the middle surface of the cylindrical wall. There are four layers of steel reinforcement in the wall, so that two layers exist within this element.

The location of the two layers shown correspond exactly to the actual location of the two reinforcement layers as measured from the middle surface of the cylindrical wall. The embedded reinforcement model assumes that a group of parallel reinforcing bars running through an element may be modeled as an equivalent continuous thin layer of steel. The thickness of the layer is automatically computed according to the prescribed cross-section area and spacing of the bars in the group. When, as in this case, the amount of steel in one direction (hoop) differs from the amount in the other direction (longitudinal), two thicknesses are assigned to one layer. In this case, there is a hoop thickness and a longitudinal thickness assigned to each of the two layers shown.

To retain the directional behavior of bars, the steel layers of the embedded reinforcement model are mechanically shearless in the plane of the layer. With this restriction, layers may be described as orthotropic since the layer stiffness in the orthogonal hoop and longitudinal directions may differ. However, the mechanical behavior in the two directions of the layer is uncoupled.

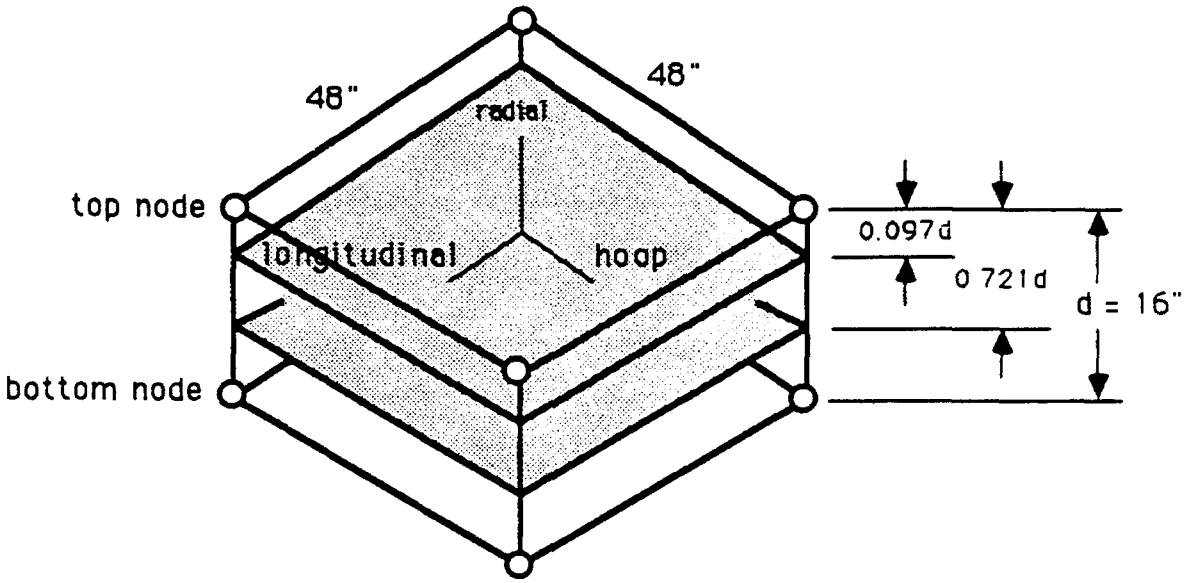

Figure 7
Typical embedded element for MTC model.

The mechanical properties in the radial direction would otherwise not be affected by the steel layers for the element shown. However, radial layers were included in these elements to represent the shear steel reinforcement (stirrups) in the design of the MTC cylindrical wall. They were omitted in this discussion for clarity.

Mathematically, the embedded element formulation is based on superposition of the stiffness matrix for the parent concrete element and the stiffness for thin layers of steel. As implemented in ABAQUS, the edges of the steel layers are constrained to remain compatible with the parent concrete element as the element deforms under load (Rebelo, 1989). The internal forces generated in the steel layers are distributed to the nodes in a manner consistent with the kinematics (of bilinear shape functions) for the parent element as well as with the location and orientation of the layers. The embedded reinforcement formulation avoids the necessity of additional nodes and elements that would otherwise model the reinforcement layers directly, as is done in the alternative discrete reinforcement modeling approach. The advantages over the smeared approach are: (1) proper location of the rebar, and (2) anisotropic behavior, i.e., accurate representation of the anisotropy due to the directional behavior of steel reinforcement.

Perfect Bond Hypothesis. In commercially available general purpose computer programs for reinforced concrete finite element analysis, the assumption is made that the concrete-to-steel bond remains perfect throughout the entire load-deflection behavior, even for gross failure or highly nonlinear behavior. No bond-slip behavior is allowed at the concrete-steel interface despite the fact that relative displacement at the interface is regarded as a common occurrence in nonlinear behavior. This assumption is implied in the present analysis of the MTC. This is generally true regardless of the type of reinforcement model used. Using the discrete reinforcement method, slide line or gap elements may be included to model frictional sliding of

bars. However, bond-slip relations are not characterized by friction phenomena alone. Coulomb frictional behavior cannot model crushing and splitting due to the lugs on bars which dominate bond-slip behavior.

Potentially important energy absorbing mechanisms involving friction and crushing are neglected as a result of the perfect bond hypothesis. The importance of these mechanisms will vary according to application. They may be more important for earthquake analysis than for blast analysis, for example. The energy lost due to historetic bond-slip effects under cyclic loads may be regarded as important. However, for highly transient loads the concrete is often separated from the steel early (i.e., in the first or second cycle) in the dynamic response, and from then on the concrete strength does not participate in resisting the applied transient load.

Bond-slip models are the subject of ongoing basic research under the auspices of the Naval Civil Engineering Laboratory's (NCEL's) Structural Modeling Project (Cox and Herrmann, 1992) as well as elsewhere. Such models have been used with embedded reinforcement models for steel by some investigators (Elwi and Hrudey, 1989). However, the technique remains tentative and embryonic as the discussion by Pandey (1991) suggests. Others such as Schnobrich (1989) suggest that application of bond-slip models is prohibitively costly in connection with large, nonlinear finite element analysis of reinforced concrete structures.

Single Embedded Reinforcement Element Analysis. Forces were applied to the nodes of the embedded element (Figure 7) to numerically assess its elastic load-deflection behavior. The node forces were applied in the longitudinal, hoop, and radial directions in separate tests, and they were predetermined such that without the steel layers, the element would experience 1-psi normal stress in each case. The numerical results of the three tests are compiled in Table 4.

Table 4
Embedded Element Behavior

Nodal Load Direction	Node Displacement (in. x 10^5)		Concrete Stress* (psi)	
	Without Steel Top/Bottom	With Steel Top/Bottom	Without Steel Top/Bottom	With Steel Top/Bottom
Longitudinal	1.600/1.600	1.261/1.317	1.000/1.000	0.800/0.810
Hoop	1.600/1.600	1.240/1.310	1.000/1.000	0.790/0.800
Radial	0.533/0.533	0.533/0.533	1.000/1.000	1.000/1.000

*Concrete stresses are reported at the top and bottom Gauss points.

The computed top and bottom node point displacements and element concrete stresses agreed with the expected solutions in the absence of the steel. Comparison between these values and the computed values with the steel layers included demonstrates the effect of the steel layers, particularly the anisotropic behavior of the embedded reinforcement. For example, the numerical results show that the steel reinforcement adds more stiffness to the upper portion of the element in both the longitudinal and hoop directions, as would be expected from the placement of the two steel layers in the upper part of the element. Correspondingly, the element concrete stresses diminish because a portion of the load is redistributed to the steel reinforcement.

Embedded Reinforcement Model Description. The embedded reinforcement model is described by constructing a *REBAR input data file which is part of the overall ABAQUS input data file for the MTC analysis. Constructing this file was a substantial effort, and a description of the procedure used along with an example embedded element is presented in Appendix A.

To verify and display the results of the embedded reinforcement model, ABAQUS also provides procedures within a post-processor, ABAPOST. This program reads the *REBAR data file and creates a graphics output file, ABAPLOT, which in turn drives a plotter to produce black and white images of reinforcement models in impressive detail. The parent finite element structure is also shown superimposed on the reinforcement images. During construction of the *REBAR file for the MTC model, several data input errors were uncovered and corrected using this capability; this capability was invaluable to modeling the MTC reinforcement design. Figure 8 illustrates typical plots of the embedded steel reinforcement for the three-dimensional MTC model.

A vertical slice through the steel rebar cage is shown in Figure 8a. This view shows a longitudinal section that, for clarity, is only one element deep in the direction perpendicular to the section. The four layers of longitudinal steel running through the cylinder wall and terminating in the end wall sections are clearly visible at both the top and bottom. The unusually thick layers are actually the edges of thin layers seen at a slight incline. These four layers model the four concentric layers of hoop and longitudinal steel in the cylindrical wall design.

These graphics also show the crisscross diagonal bars in the haunch design of the MTC model including their development lengths. This modeling capability facilitates unprecedented accuracy in modeling crucial interaction between the cylinder and end walls. Design of haunches, whether in the MTC or in a conventional box magazine, aims to provide fixity against rotation to develop the strength in adjoining walls and slabs. Yet, conventional analytical procedures supporting design typically ignore this interaction which nonetheless is important to overall structural behavior.

The hoop and radial steel reinforcement model of the front end wall is shown in Figure 8b. The rectangular aperture included in the circular front wall was more difficult to accommodate, but the elliptical hoop bars (see Figure 4e) surrounding the aperture were eventually modeled successfully. Elsewhere in this wall, the hoop steel is circular and easier to model. The back end wall reinforcement model is shown in Figure 8c. In the MTC design, the radial steel is not always continuous through the wall (see Figures 4d and 4e), and this discontinuity in radial reinforcement is modeled in both end walls. Except for the radial lines of the parent finite element discretization shown in the graphical images, only every other radial line (reinforcement layer) may be seen to extend to the aperture. In Figure 8d, top and bottom layers of hoop and radial steel are shown.

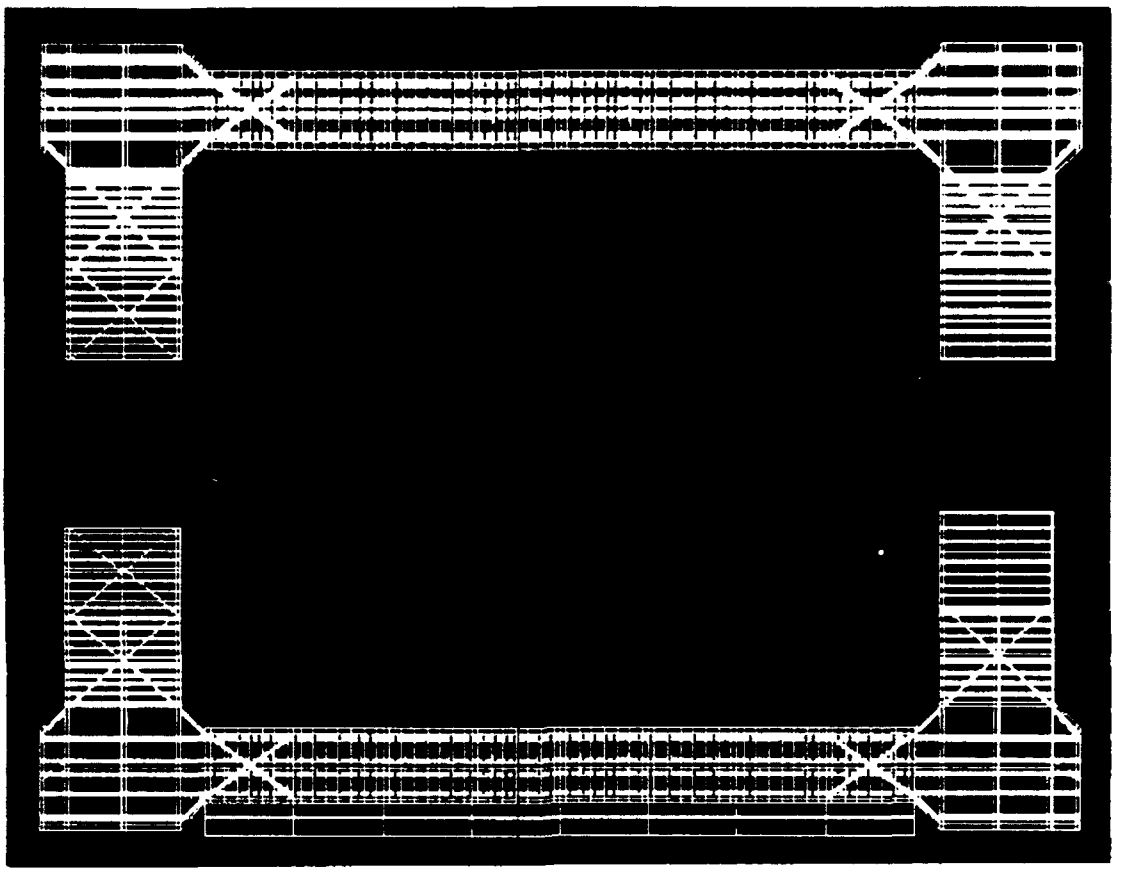

(a) Elements in vertical plane.

Figure 8
Embedded reinforcement model for MTC.

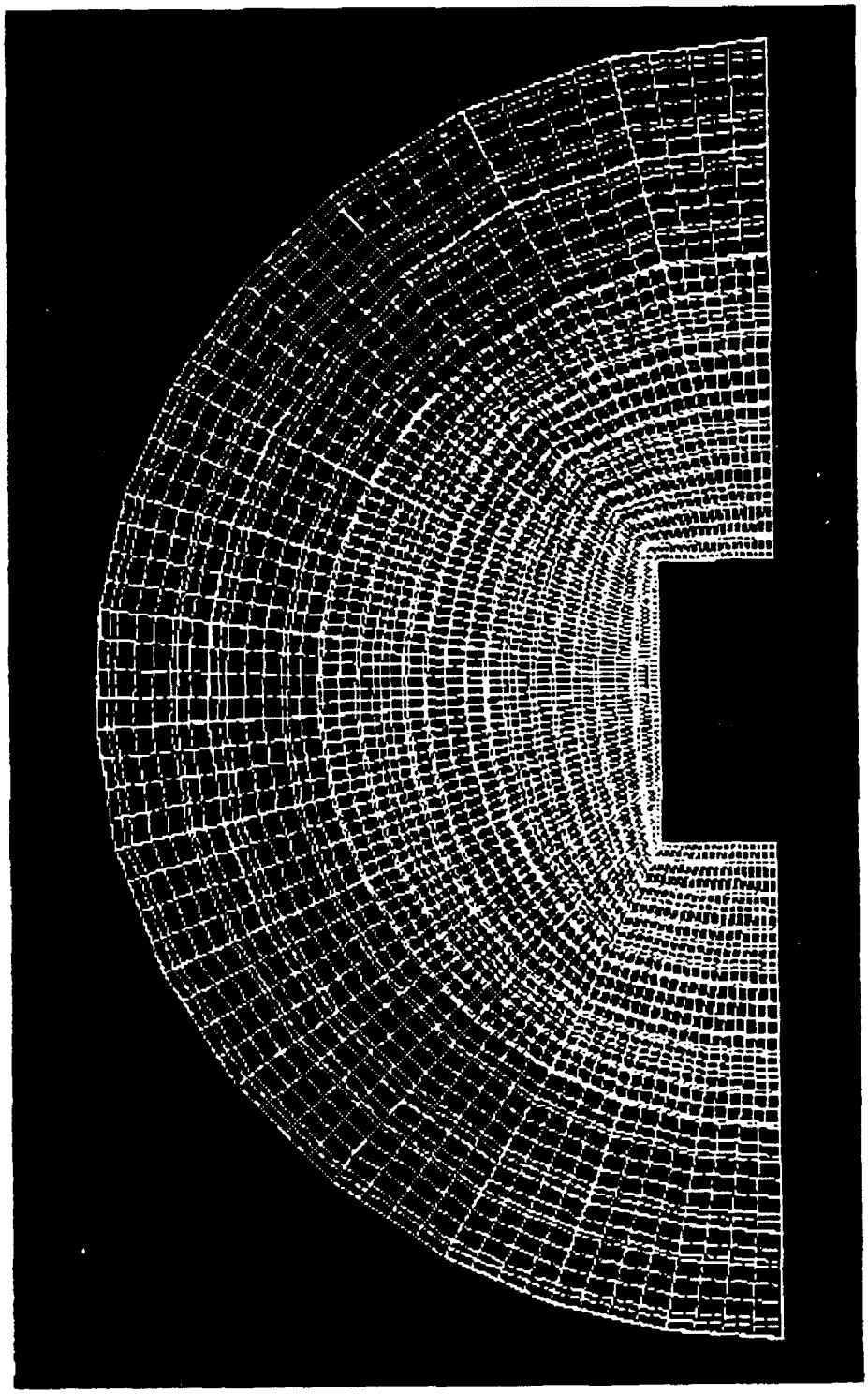

(b) Front wall elements.

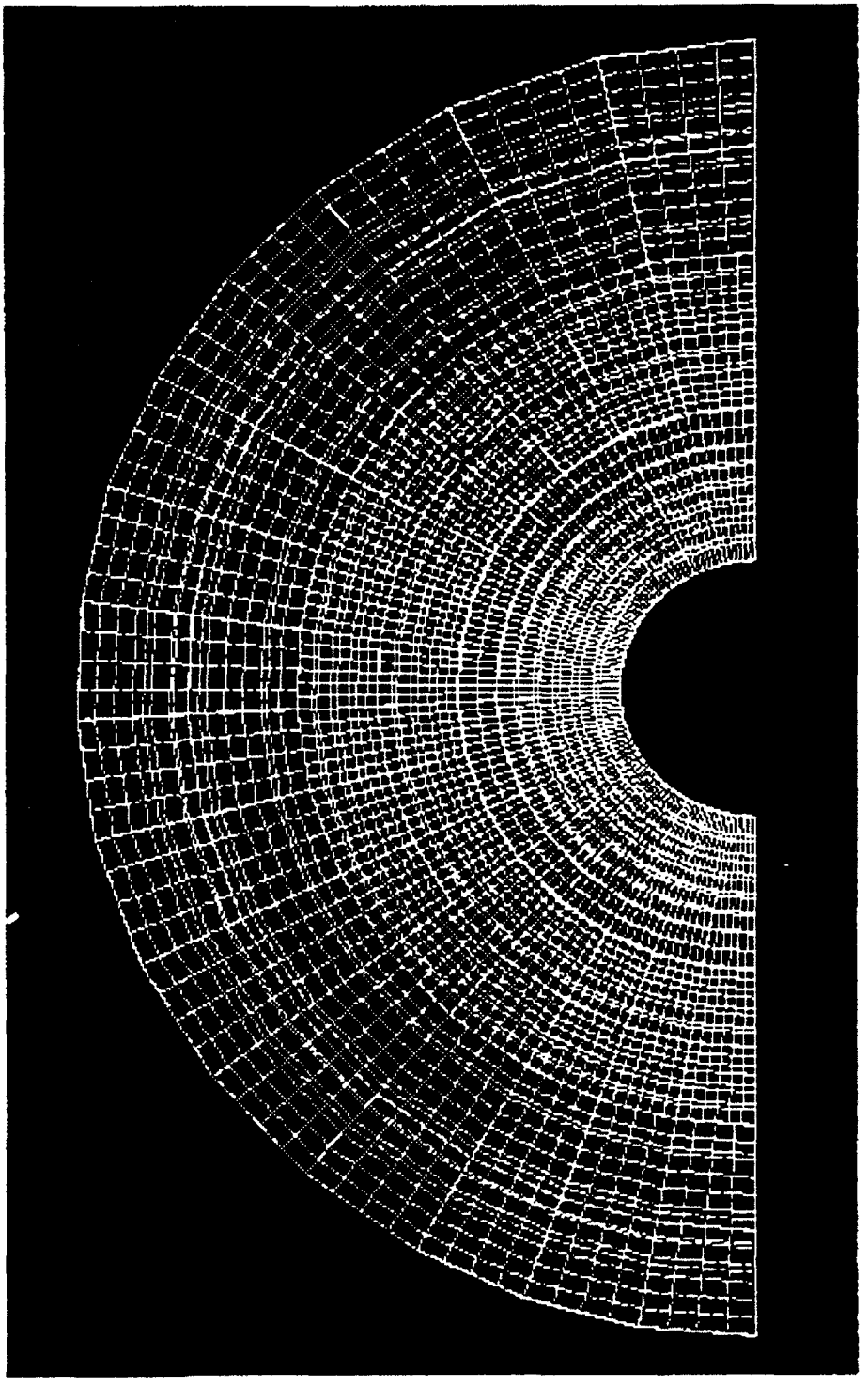

(c) Back wall elements.

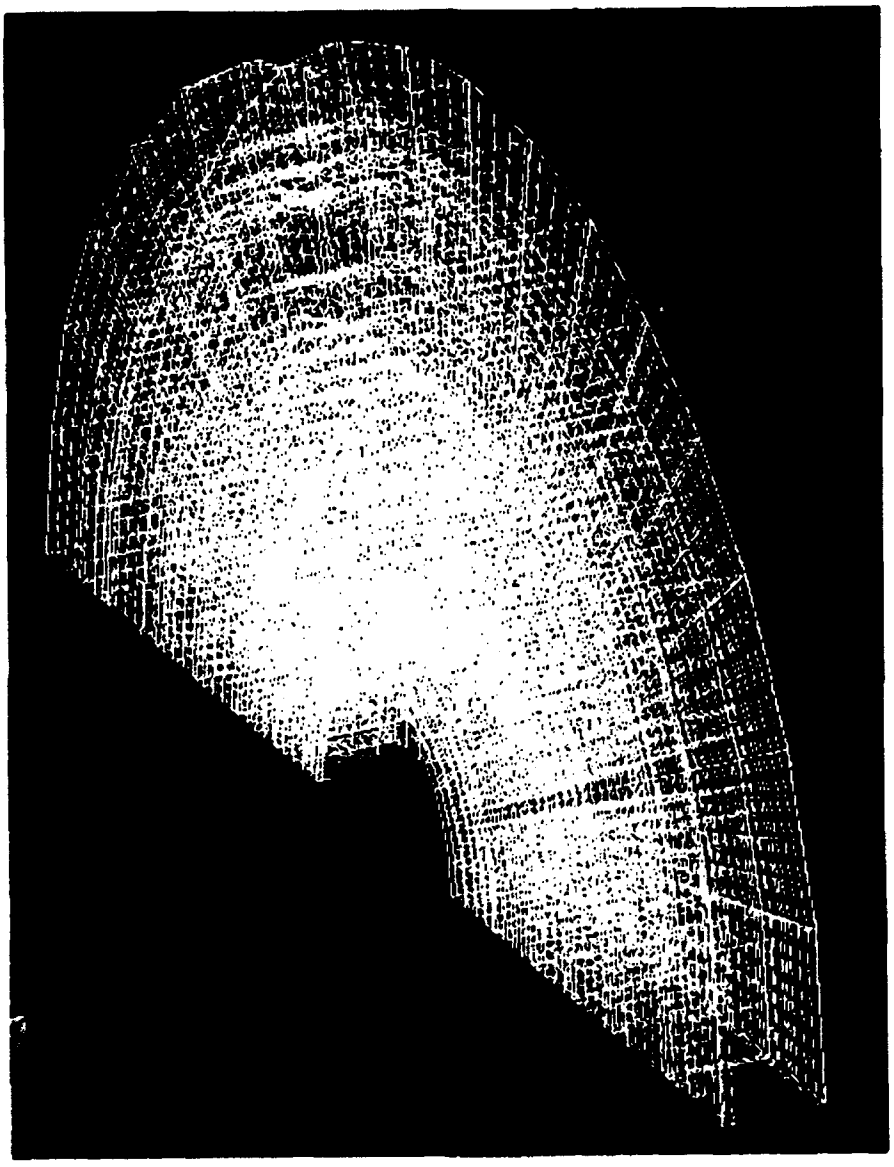

(d) Isometric view of back end wall model.

LINEAR ANALYSIS

The following describes preliminary three-dimensional analyses of the MTC which were conducted to develop and demonstrate analytical technique while working toward a full nonlinear study. The analyses include the computation of stresses in the MTC due to a static internal pressure, and the computation of natural frequencies and mode shapes for the low end of the MTC spectrum. A linear dynamic analysis was also conducted to determine computer run time for the three-dimensional model which could then be used to estimate nonlinear run time. Due to the inherent nonlinear behavior of the structure, particularly in concrete material behavior, the structural analysis information provided by these linear analyses is limited.

Three-Dimensional Static Finite Element Analyses

Two separate static analyses of the MTC model were conducted to assess at least the initial affect that the steel reinforcement would have in reducing the level of concrete stresses. A uniform internal pressure was applied to the model with and without steel reinforcement, the highest stresses at various regions of the MTC were identified, and the percent reduction in stress was calculated. These results are presented in Table 5.

Table 5
Reduction in Concrete Stress Due to Reinforcement in
Various Locations of the MTC

Rectangular Aperture	Wall/Cylinder Interface	Circular Aperture	Cylinder Wall
13%	20%	22%	29%

The locations of stress concentrations in the concrete material are depicted in Figure 9 where the distribution of stresses (von Mises stress) throughout the three-dimensional domain of the unreinforced MTC model is shown. The most severe stress concentration occurred at the corners of the rectangular aperture. The next most severe stress concentration was located at the wall/cylinder interface followed by the region near the circular aperture. The least severe stress concentration was in the cylinder wall at top dead center, where the maximum static displacement of the MTC wall was 0.057 inches. It was concluded from these observations that the steel reinforcement in the MTC tended to be less effective in reducing concrete stress where the stress concentrations tended to be more severe.

Natural Frequencies and Mode Shapes

It is generally agreed that the natural vibration properties of a structure are important to an understanding of its dynamic response. The linear, and to some extent the nonlinear, dynamic

response of a structure can be thought of as a combination of the structure's natural modes of vibration. The natural modes with frequencies that closely match the frequency spectrum of the applied load history can be expected to dominate the response. To the extent that this theory is relevant to the response of the MTC, the following natural vibration study is presented.

The design of the MTC by Ammann and Whitney Consulting Engineers (Ayvazyan, et al., 1988) was based upon an assumption that the MTC would vibrate in one particular natural mode. That mode was assumed to be a radial dilation or membrane mode for a thick-walled cylinder (which excluded bending in the walls). This was consistent with a design procedure founded in SDOF vibration theory. It isolates the cylinder and does not directly consider the constraining effect of the end walls on the dynamic response of the cylinder. However, the dynamic response of the MTC would likely include many vibration modes because of the transient nature of blast loads, and because it is a three-dimensional contiguous assembly of two thick circular plates and a thick cylindrical shell which are subject to bending as well as membrane action. To examine this further, it is necessary to calculate a portion of the natural frequency spectrum of the MTC.

ABAQUS employs the subspace iteration algorithm (see Bathe and Wilson, 1972) for computing a specified number of natural frequencies and corresponding natural mode shapes for very large finite element models. In this case, the first 10 modes of the MTC model were requested and computed. The results are presented in Table 6 in which an attempt has also been made to identify the mode types (see Blevins, 1979). To again assess the effect of steel reinforcement, these modes were computed for the unreinforced MTC model as well.

The effect of the steel reinforcement was to increase the natural frequencies from 1.5 to 8.2 percent for the first through the tenth modes. This was a consequence of the added stiffness provided by the reinforcement.

Calculation of the natural modes for the MTC model was extended to include the first 20 modes. (ABAQUS required two hours to compute these modes on the Sun 4 workstation.) The MTC model was then modified by halving the percentage of steel reinforcement. The modification was accomplished with only minor difficulty, and was based on simply doubling the prescribed design spacing of the rebar in the *REBAR input data file for the reinforcement model. Then the first twenty natural modes were recomputed. The corresponding reduction in the magnitude of the calculated natural frequencies was least for the first mode and greatest for the twentieth mode. The natural frequency for the tenth mode was reduced by 5 percent and represented an average reduction among the first twenty modes. Thus, an average change of only 5 percent in the fundamental dynamic properties of the MTC model results from a 50 percent change in the steel reinforcement. The linear dynamic properties of the MTC model were relatively insensitive to the percentage of reinforcement.

The ten natural modes computed are dominated by bending deformations in the cylinder of the MTC as shown in Figure 10. It may be useful to compare these shapes to the undeformed model (Figure 5). The first few modes are pure modes of deformation, but the higher modes become increasingly involved because they include combinations of higher order cylinder and end wall bending deformations. A cylindrical membrane mode such as was assumed in the MTC design was evidently not among the first ten modes. Such membrane modes for plate and shell structural elements are known to be higher frequency modes. It is likely to exist, but its natural frequency is clearly greater than 114 hertz.

Figure 9
Distribution of von Mises stress in the MTC without reinforcement - linear analysis.

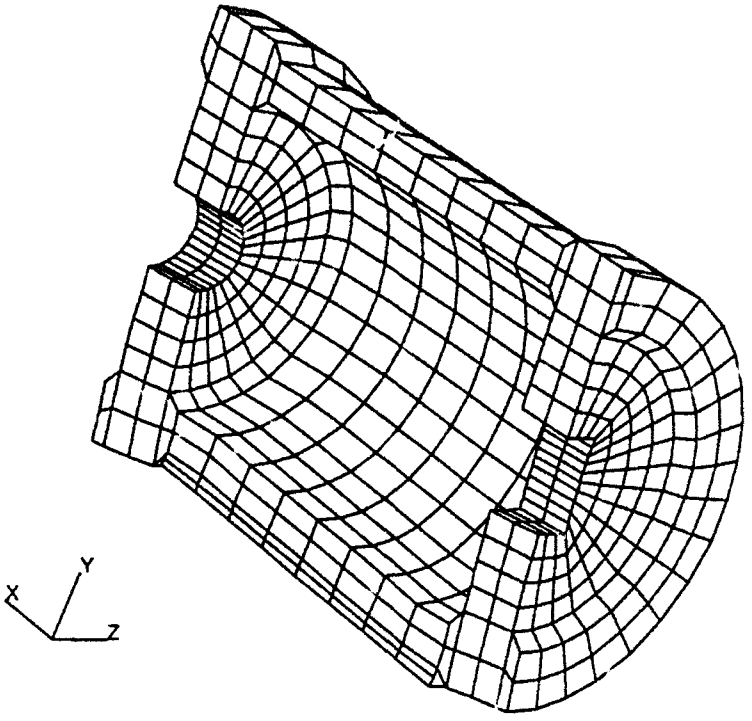

(a) Mode 1, f_1 = 19.8 Hz.

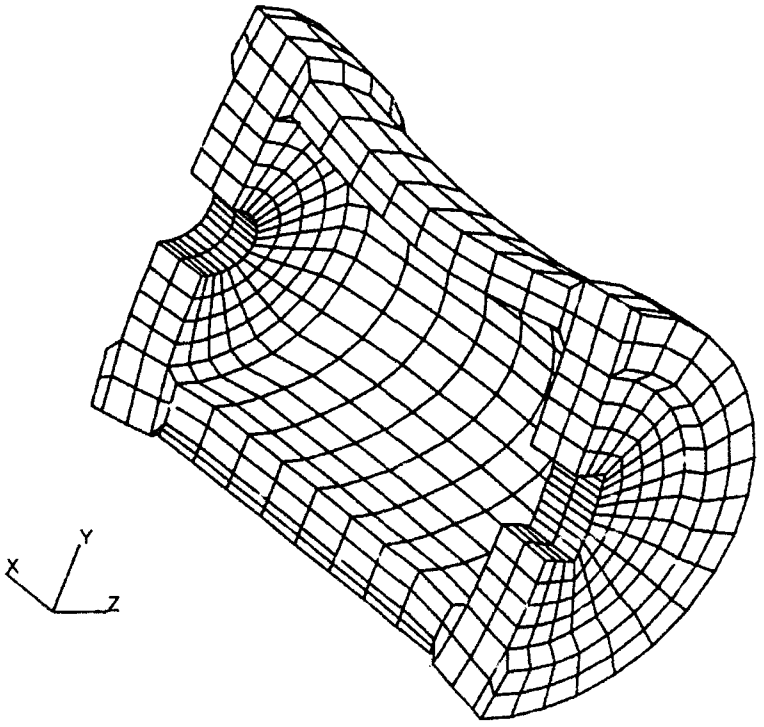

(b) Mode 2, f_2 = 36.4 Hz.

Figure 10
Natural mode shapes for MTC model.

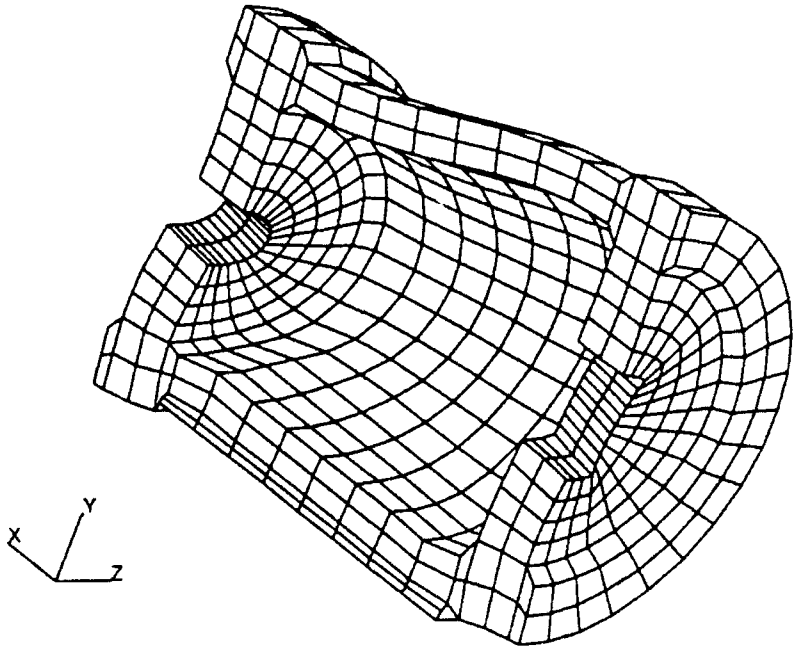

(c) Mode 3, f_3 = 58.7 Hz.

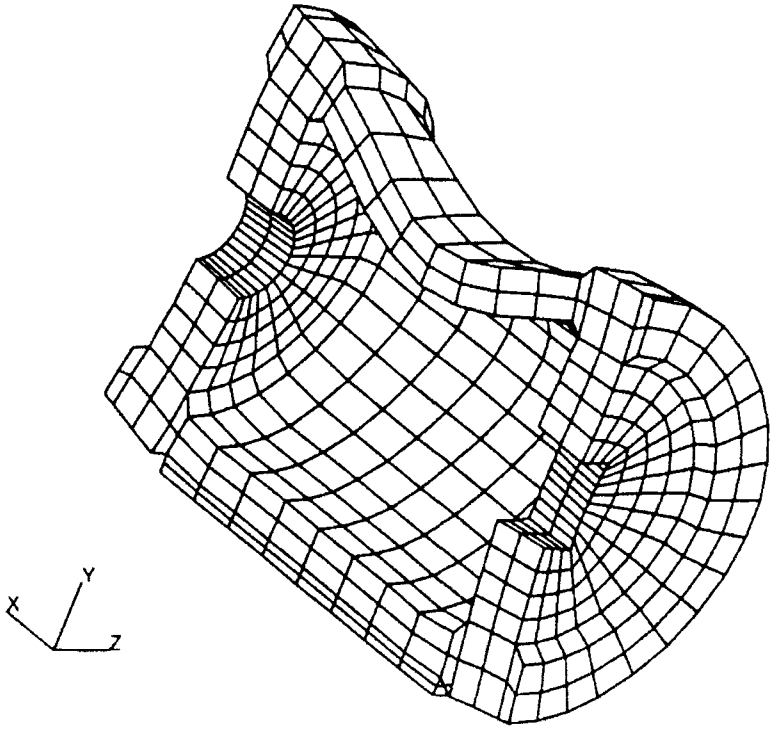

(d) Mode 4, f_4 = 67.4 Hz.

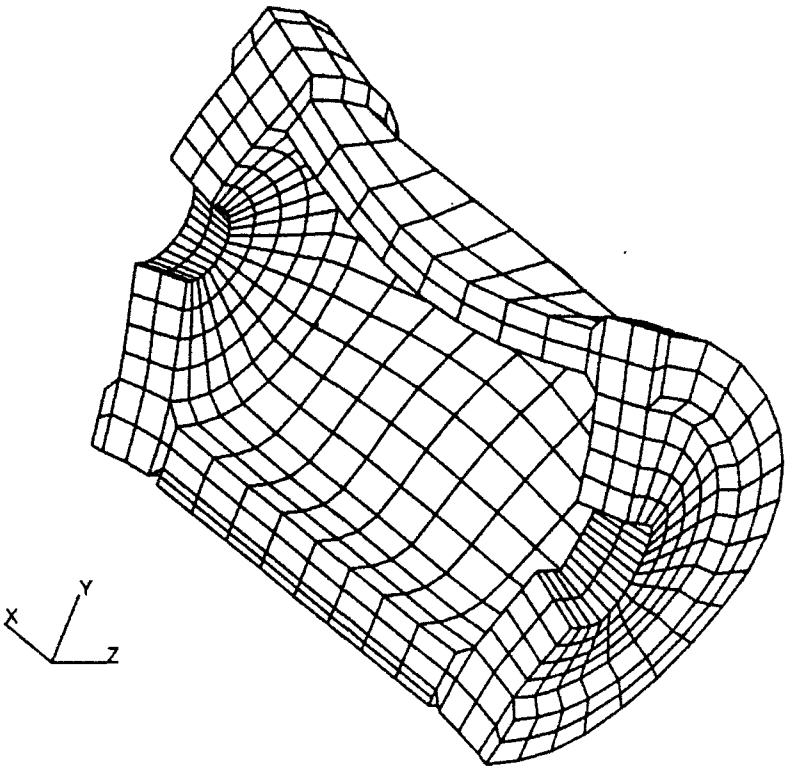

(e) Mode 5, f_5 = 83.7 Hz.

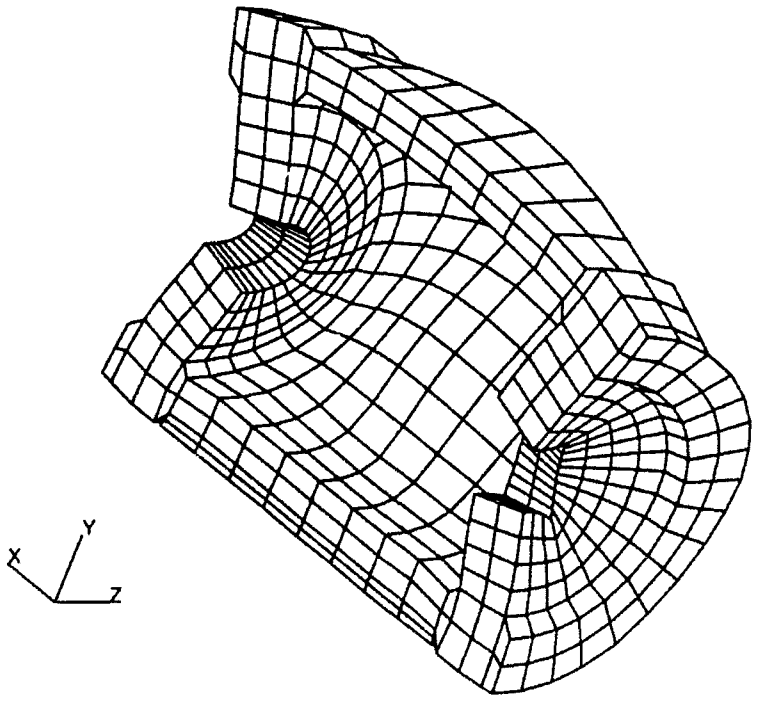

(f) Mode 6, f_6 = 87.4 Hz.

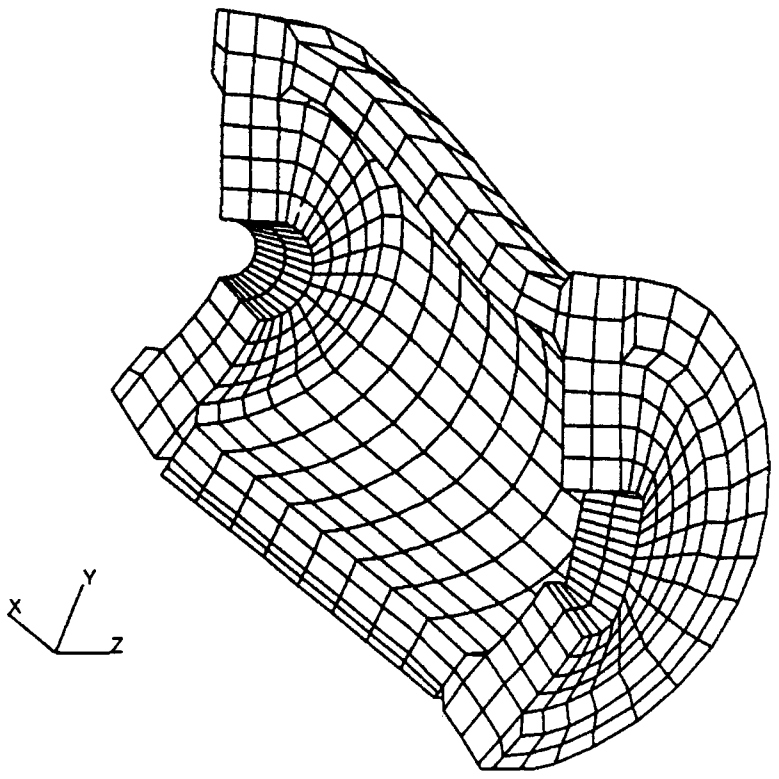

(g) Mode 7, f_7 = 91.2 Hz.

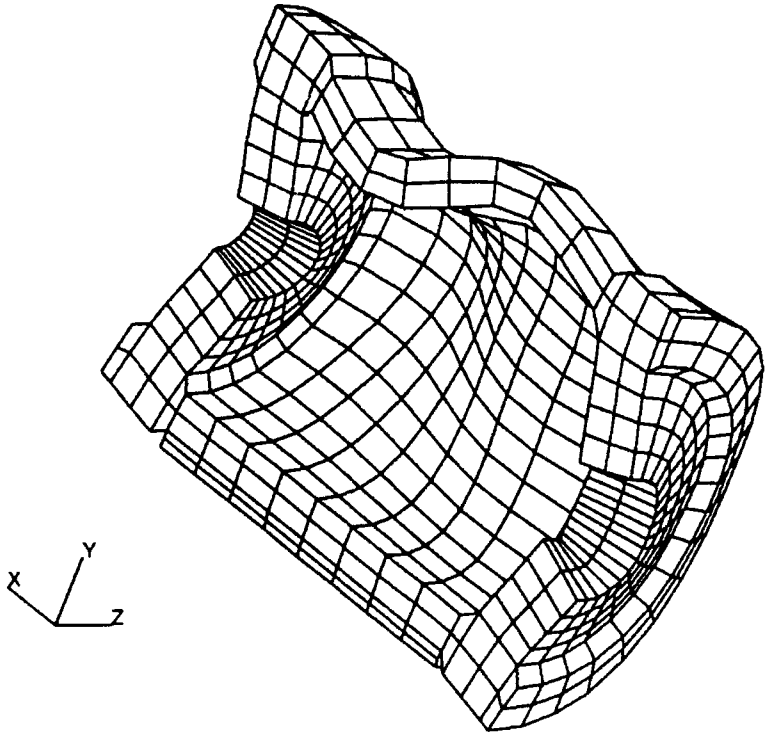

(h) Mode 8, f_8 = 102.5 Hz.

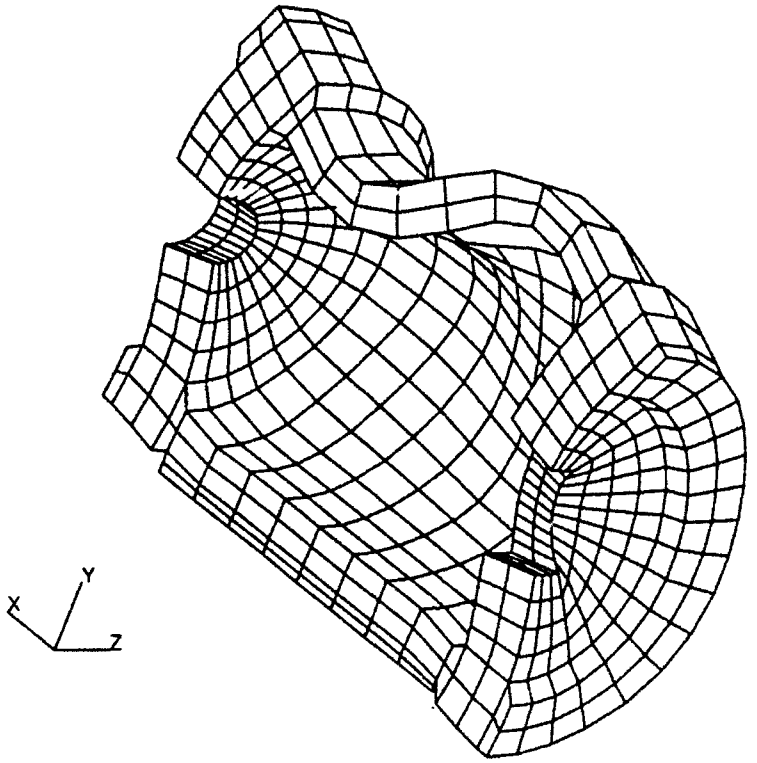

(i) Mode 9, f_9 = 110.8 Hz.

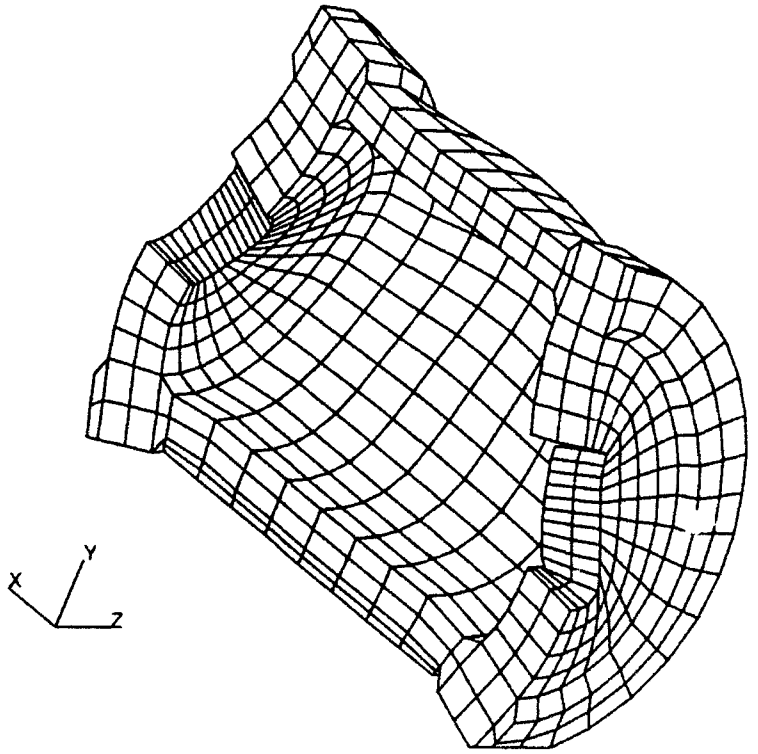

(j) Mode 10, f_{10} = 113.9 Hz.

Table 6
Lowest Ten Natural Frequencies and Symmetrical Natural Modes of MTC*

Mode No.	W/O Rebar (Hz)	W/Rebar (Hz)	Mode Type Description
1	19.5	19.8	Longitudinal shear mode or racking of MTC
2	34.6	36.4	Transverse bending in cylinder or cylinder pinching
3	57.8	58.7	Vertical shear or racking of MTC
4	63.3	67.4	Longitudinal bending in cylinder
5	77.2	83.7	2nd transverse bending mode in cylinder
6	82.9	87.4	Mode 5 plus end wall bending mode
7	86.0	91.2	2nd longitudinal bending mode in cylinder plus end wall bending mode
8	97.8	102.5	3rd longitudinal bending mode in cylinder plus end wall bending mode
9	104.3	110.8	3rd longitudinal bending mode in cylinder plus 2nd end wall bending mode
10	105.3	113.9	Longitudinal stretching plus 2nd end wall bending mode

*These results do not account for the increase in mass due to steel rebar displacing lighter concrete in the embedded reinforcement model.

The computed modes are symmetrical with respect to the longitudinal plane of symmetry of the MTC; the MTC model excludes antisymmetrical modes such as torsional modes of vibrations. Analysis of fully three-dimensional models (see Figure 6) showed that three torsional type modes are included in the first ten modes. If the blast loading is symmetric with respect to the longitudinal plane of symmetry (as has been assumed in determining the design load), torsional modes would not be excited and therefore would not participate in the dynamic response of the MTC. Otherwise, they would be expected to participate in the response.

The frequency spectra for the two phases of the idealized design blast load time history (see Figure 2) were calculated in an auxiliary analysis to ascertain which of the natural modes of vibration would likely be more important to the dynamic response of the MTC. This is accomplished by evaluating the Fourier transform of the two idealized triangular load pulses for the shock pressure load phase and for the gas pressure load phase. Details of the calculations are given in Appendix B. The graphs of these spectra are shown in Figure 11. Figure 11a shows that the gas pressure phase dominates a low frequency range below 143 rad/s (22 hertz),

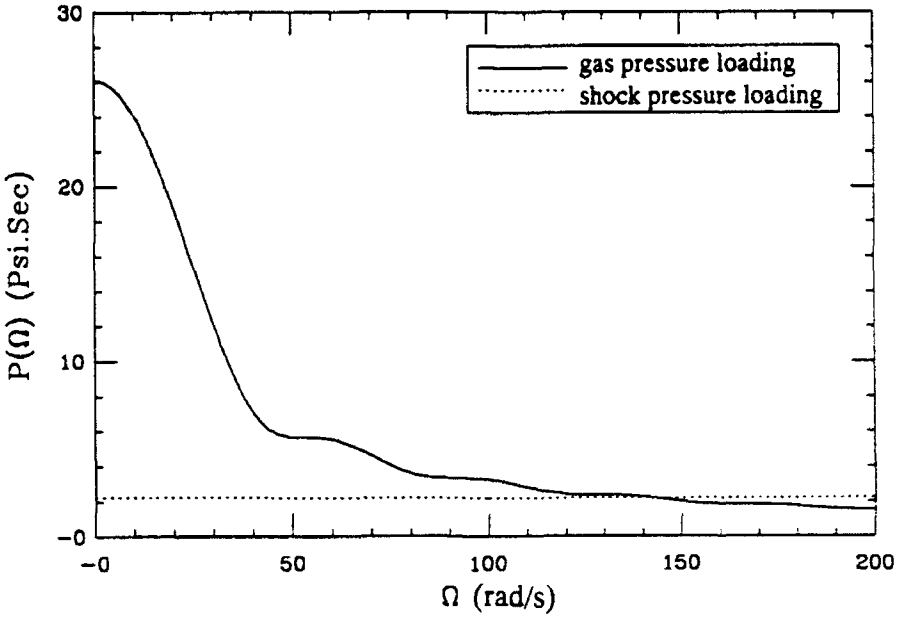

(a) Low range.

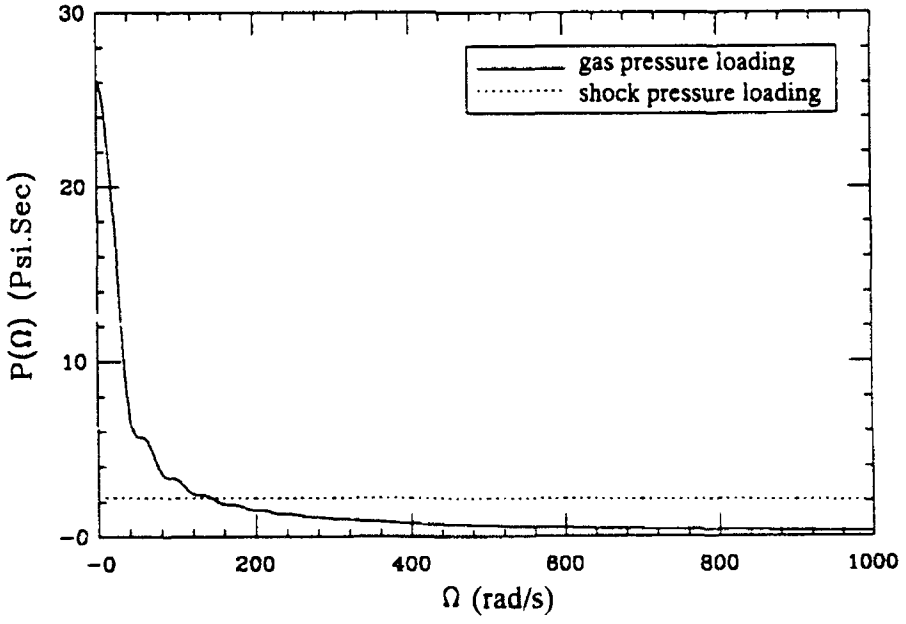

(b) High range.

Figure 11
Frequency spectra for design load.

and the shock pressure phase dominates a high frequency range above 143 rad/s. The gas pressure phase is associated with much higher energy.

Since the lowest natural mode calculated for the MTC model is about 20 hertz, which is near the upper end of the low frequency range dominated by the gas pressure phase, the MTC design would have apparently successfully avoided the most severe part of the design load spectra. Thus, the importance of the (higher impulse) gas pressure phase of the load to the MTC response would likely be substantially diminished. Further, the frequency spectra showed that the (lower impulse) shock phase would excite uniformly all the MTC natural modes up to 160 hertz (1,000 rad/s) and beyond. In such cases as when no particular frequency is dominant, the load is referred to as white noise loading.

To the extent that these results apply to the nonlinear response of the MTC, it may be concluded that essentially all natural modes of vibration for the MTC design would be equally excited, and would equally participate in the dynamic response. Further, the gas pressure phase of the loading would have been successfully managed by the venting mechanism in the MTC design.

The design objectives for the MTC clearly excluded total containment of the blast pressure. In such cases, it has often been natural to disregard the shock phase of the resulting design load, and design the MTC to manage the gas pressure phase of the load since it is associated with much greater impulse (see Figure 2, for example). However, the natural vibration analysis as presented here demonstrates that the issue is not necessarily straightforward, and the shock phase cannot always be conveniently disregarded, in favor of the gas phase.

Three-Dimensional Linear Dynamic Response

The linear dynamic response of the MTC model was addressed prior to attempting lengthy nonlinear dynamic response computer runs. In particular, the expected computer run time for the three-dimensional nonlinear finite element model can be estimated using data from the linear model. This also entailed studying the effects of input data parameters associated with *DYNAMIC, *AMPLITUDE, and *STEP data sets in ABAQUS. Additionally, the performance of the implicit temporal integration scheme employed by ABAQUS, and time step sizes which were reasonable for use in analysis of the MTC model, were sought in this preliminary study.

The *DYNAMIC data set controls the overall implicit integration procedure including the step size, and whether or not the step size should be automatically adjusted while under program control. The *AMPLITUDE data set specifies in a pointwise manner the magnitude and shape of the applied pressure load history, in this case a triangular load pulse. The *STEP data set controls the length of the computer run time and specifies a maximum number of time steps.

ABAQUS employs the Hilber, Hughes, and Taylor (1978) implicit temporal integration algorithm to integrate the equations of motion for either a linear or nonlinear finite element model. This algorithm features a numerical damping control parameter, α, for stability of the direct integration process. Stability is not guaranteed for nonlinear problems. When α is set to zero, the algorithm reduces to the Newmark ß (ß=1/4) algorithm which is unconditionally stable for linear problems. A small amount of damping is otherwise prescribed by the default value in ABAQUS, $\alpha = -0.05$. This dampens artificial transients that tend to occur when the time step Δt is suddenly adjusted, to promote either accuracy or economy, under automatic program control. The damping also has a minimal effect on low frequency response accuracy while eliminating high frequency response, which is generally unwanted in implicit finite element analyses.

Automatic control of the time step subsequently proved to be a valuable aid in facilitating nonlinear analysis of the MTC. It employs the "half-step residual" procedure proposed by Hibbit and Karlsson (1979). The residual or out-of-balance force calculated at time $t + \Delta t/2$ is compared to a user-supplied force value HTOL (a *DYNAMIC parameter) which is typically based on the applied load. The time step size is adjusted during integration of the equations of motion, according to behavior of the norm of the half step residual force. Generally, if the norm increases, the step size is reduced to promote accuracy, and if the norm decreases, the step size is increased to promote economy.

The user prescribed HTOL parameter nevertheless became a burden and a constant source of concern as its specification had to be adjusted often during subsequent nonlinear dynamic analysis in attempts to control the frequency of time step changes. Furthermore, since the applied load was changing, it was not clear how a good value of HTOL was to be calculated. When solution progress was difficult, this parameter was often recalculated in an ad hoc manner in attempts to control the solution. At the time of this writing, we learned that the HTOL parameter was eliminated in Version 5 of ABAQUS.

The linear dynamic response of the MTC is shown in Figure 12 where the vertical displacement history of the inside wall of the cylinder at top dead center (TDC) is graphed. The applied load was the gas pressure phase of the loading (Figure 2), and also included an equivalent line load applied to the rectangular door jam of the MTC which varied proportionally with the gas pressure phase. The maximum response computed was 0.075 inches and occurs just off the graph in Figure 12(a) at 0.015 seconds. The shape of this graph, as is expected for a transient analysis, generally follows that of the applied triangular load pulse. Similarly, after 0.177 seconds, the response was free vibration. The time step size specified was $\Delta t = 0.018$ seconds, which was based on requiring ten steps for the duration of the load pulse.

A second analysis was conducted to refine the initial portion of the dynamic response. Eighty time steps were prescribed for the first 30 ms of the response, yielding a time step size $\Delta t = 0.35$ ms. The dynamic response for 12 ms is shown in Figure 12(b). The maximum response was 0.144 inches, occurring at 11 ms. That this response was almost twice the previous value (Figure 12a) demonstrates the importance of choosing the time step size carefully. The linear response yielded a dynamic load factor (DLF) of 2.53, based on the previously calculated static deflection (0.057 inches). The actual response is nonlinear, but this DLF would otherwise not be unreasonable.

Eighty linear time steps required 19 hours of compute time on the Sun 4 workstation, or 14.2 minutes per time step for the three-dimensional MTC model. The run was actually accomplished in two successive working days by using the restart file capability in ABAQUS.

A final linear analysis was conducted with the full loading, including the initial shock phase as well as the gas pressure phase of the design load. The maximum response increased to 0.57 inches, and the time of the maximum response reduced to 9.4 ms. The prescribed time step size was reduced to $\Delta t = 0.1$ ms for 100 time steps. The run time required only 14 hours or only 8.4 minutes per time step. This constituted a 59 percent decrease in the compute time per step. This reduction was accomplished by flagging the LINEAR parameter option in the *STEP input data set. This option prescribes that the analysis is linear, and causes the system to calculate and factor the structure stiffness matrix only once at the beginning of the computation. However, if one is interested in estimating the compute time for subsequent nonlinear investigation, it is more relevant to omit this parameter causing the system to assume the analysis to be nonlinear and to recalculate the structure stiffness matrix and resolve the linear system for each time step.

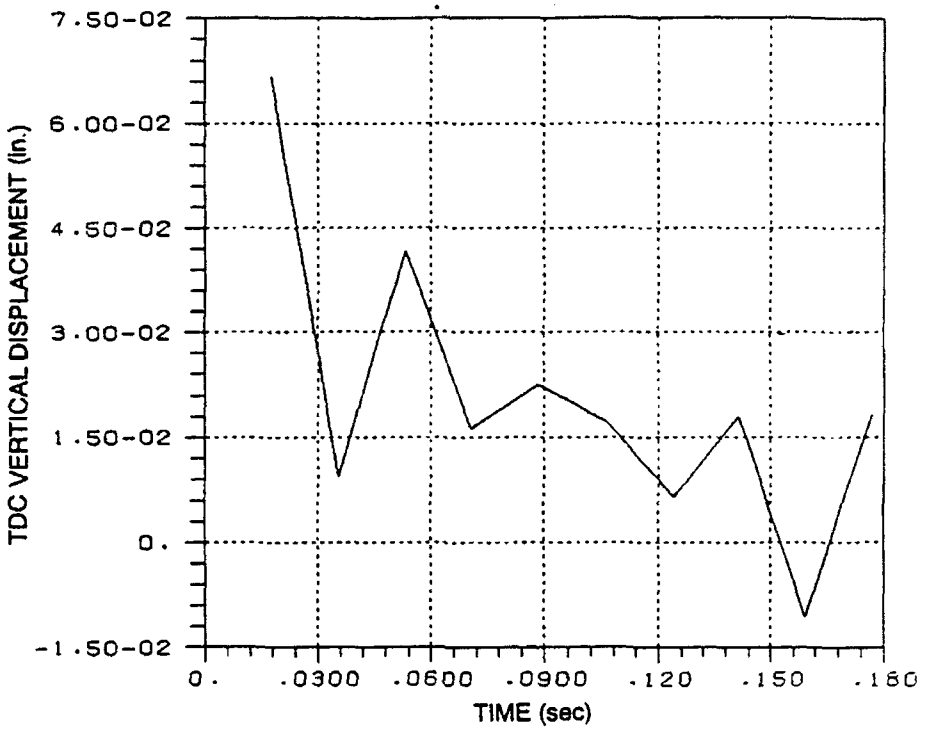

(a) Coarse analysis.

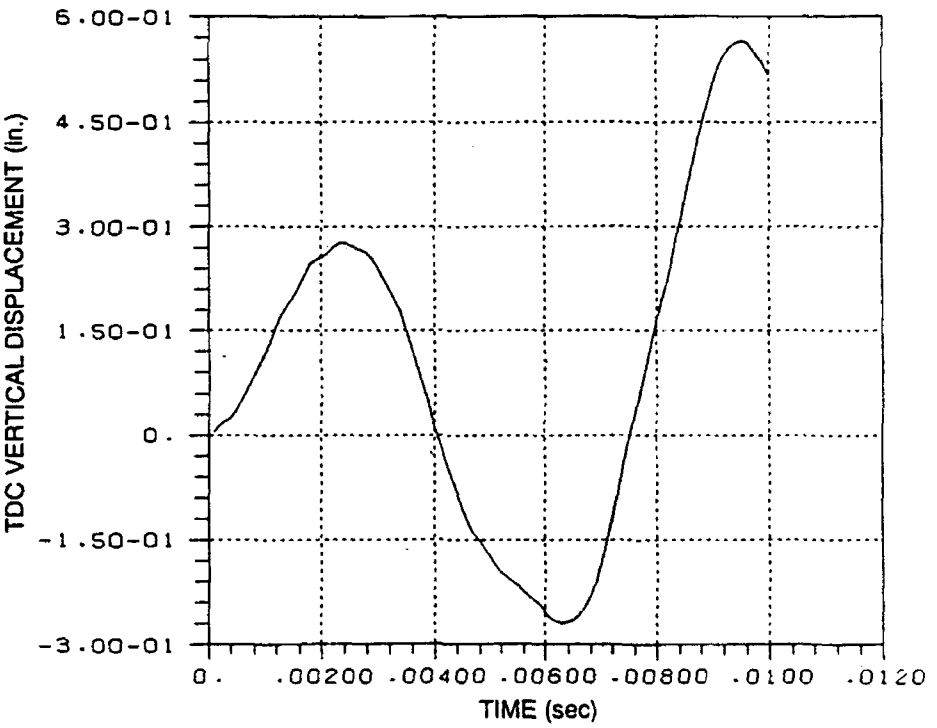

(b) Refined analysis.

Figure 12
Linear dynamic response of the MTC subjected to the gas pressure load phase.

Summary of Linear Analyses

The linear analysis study of the MTC was primarily conducted to gain experience with the three-dimensional MTC model prior to beginning more complex and time consuming nonlinear analyses of the MTC. Except for the mode shapes, linear analysis results were neither reported in absolute terms or discussed in detail since they were not relevant to the MTC structural behavior, which is clearly nonlinear. However, some of the results discussed bear summarization.

A three-dimensional linear static finite element analysis of the MTC revealed the relative magnitudes of various stress concentrations that existed throughout the structure. A significant stress concentration existed at the interface between the cylinder wall and the end walls. The analysis shows that the steel reinforcement in this region tended to be less effective in reducing concrete stress than at other regions.

An eigenvalue analysis for the three-dimensional MTC model determined that the natural frequency range for the lowest twenty natural modes was between 20 hertz and 160 hertz. The corresponding natural mode shapes were characterized by combinations of shear and bending deformations in the cylinder wall and end walls. A simple, uniform dilation mode for the MTC, similar to the mode implied in the MTC design procedure, was not found to exist among the computed lower natural modes.

A frequency spectrum analysis of the design blast load revealed that the frequency content of the shock pressure phase more closely matched the natural frequency range of the MTC than the frequency content of the gas pressure phase of the design load. Further, the MTC excitation due to the shock pressure phase was shown to be essentially white noise excitation. These results show that a tendency to de-emphasize the role of the shock phase in such designs may not always be appropriate.

The results of a linear dynamic analysis study using the three-dimensional MTC model are summarized in Table 7. To expect reasonable simulation times for the entire 177-ms forced response and any free vibration response afterward, specification of very coarse time step sizes must be anticipated. However, it was shown that the maximum response in the cylinder wall occurred within 10 ms and that refined time step sizes are needed for accuracy.

Table 7
Linear Dynamic Response Results

Blast Load	Time Step Sizes (ms)	Max Wall Response (in.)	Time of Max Wall Response (ms)	Compute Time per Step (min)
Gas Pressure Phase	18.0	0.075	< 18	14
Gas Pressure Phase	0.35	0.144	11	14
Shock + Gas Pesssure	0.10	0.57	9.4	8

NONLINEAR CONCRETE MATERIAL MODEL

There seems to be an understanding among those who design explosive safety systems to manage internal explosions that, compared to the steel reinforcement, the concrete contributes little to the restoring forces within the structure, while contributing more substantially to the inertial forces resisting the load. Indeed, concrete tends to crack and to release internal restoring forces to the reinforcement very early in the dynamic response. It is therefore believed to contribute primarily inertial resistance forces throughout the majority of the dynamic response. In view of this, it is sometimes concluded that modeling of concrete material behavior is not an important requirement for purposes of design in such cases.

On the other hand, the necessity of modeling the linear and nonlinear material behavior of concrete in explosive safety applications of finite element technology seems reasonable when it is considered that these structures are often designed to sustain severe damage while containing or managing internal explosions. The anticipated extent of nonlinear material behavior might well vary with the particular facility, and therefore modeling this behavior may be more important for some explosive safety designs than for others. Compression behavior in the concrete material is important. Compressive stresses equilibrate tension forces in steel rebar in cracked sections which are subject to flexure. Even when the compressive strength is not exceeded, the stress-strain behavior of concrete may still exhibit nonlinear behavior. Moreover, in most cases, failure of concrete in tension precipitates cracks which propagate and control subsequent dynamic response causing nonlinear structural behavior. Therefore, nonlinear concrete material modeling is necessary for accurate determination of the initial fracture modes that tend to govern the subsequent dynamic response of the structure.

At the same time, nonlinear concrete material models are generally very complex from both a theoretical and a computational viewpoint. To achieve accurate simulation of the nonlinear structural response in the aforementioned sense, it will be necessary to sustain the price of this complexity.

The overall complexity of modeling reinforced concrete is reduced somewhat by the common strategy of separately modeling the reinforcement (e.g., using either the discrete or the embedded reinforcement model) and the concrete. However, the interaction between the two, known as bond-slip behavior, is generally not included. Instead the perfect bond hypothesis is generally implied in reinforced concrete analysis.

Theoretical Aspects

Theoretical complexity derives from the concepts of the theories of plasticity and continuum damage mechanics as applied to the failure of brittle materials which exhibit very different behavior for compression and tension loadings. Both theories require a nonlinear path-dependent formulation. The ABAQUS concrete material model uses the former for crushing behavior in compression and the latter for cracking behavior in tension. These theories are used to derive a nonlinear constitutive, or stress-strain, law for the material behavior. The constitutive law is ultimately expressed as a system of several nonlinear differential equations.

There are two basic approaches to modeling concrete fracture behavior. The discrete fracture approach seeks to model the initiation and propagation of cracks by providing for actual discontinuities in the finite element model for representing cracks. The smeared crack approach seeks to model the initiation and propagation of cracks by an equivalent continuous model exhibiting a softening behavior in the stress-strain relationship in regions of tensile failure. This

approach may be further subdivided into either a smeared crack approach based on plasticity theory, or a smeared crack approach based on continuum damage mechanics. The ABAQUS concrete material model employs the latter approach to model the tension behavior of concrete.

Continuum damage mechanics postulates that a single variable (either a scalar, vector, or tensor quantity) called a damage parameter can represent progressive degradation of the elastic properties of concrete. ABAQUS uses a scalar damage parameter. An evolution law controls the rate at which damage progresses (i.e., the rate at which the elastic properties degrade and soften). A crack detection technique and post-failure model for tensile cracking, which is due to Resende (1989), governs tension behavior.

In addition to elastic behavior, the ABAQUS plasticity concrete model includes a yield surface, a flow rule, and a hardening rule to describe compressive behavior. This plasticity model is a modified version of the model developed by Chen and Chen (1975) and it is discussed by Chang, et al. (1987).

Computational Aspects

The constitutive law must be integrated in a manner analogous to an initial value problem. In this case, the initial value problem is constrained. The constraints arise from the yield surfaces and hardening laws that restrict the admissible stress states. The initial values are the stress increments from the previous integration step. Computational complexity derives from material behavior which can change drastically (yield, crush, crack, load, unload, etc.), and from the path- or history-dependent nature of plasticity models. In these models, the determination of the direction of the change in material behavior (material loading or unloading) is not straightforward. An incremental analysis formulation of stress and strain in which the variables are analyzed as stress and strain rates is required.

Various numerical algorithms are used to integrate the constitutive system of nonlinear differential equations along the highly nonlinear stress-strain path. The integration is specified at special points within each finite element known as stress points or Gauss points. The nonlinear concrete material model implemented in ABAQUS, as described by Resende (1987, 1989), contains over 4,000 lines of code. In an implicit nonlinear dynamic finite element analysis, this code sequence must be traversed for each Gauss point, within each element, for each iteration, within each load step, over the history of the dynamic response. For a single three-dimensional analysis using the MTC model, this could amount to over one million traverses of the material model loop. Clearly these analyses are not suited to personal computers, and require at least very powerful workstations. Supercomputers are even more suited to this type of analysis when multiple analyses are required for evaluating alternative design concepts.

In the ABAQUS strategy for integrating conventional plasticity models, Hibbitt (1985) describes an implicit solution procedure to advance the material response solution along the stress-strain path. In the context of dynamic problems, ABAQUS is historically also an implicit code, and therefore this strategy seems natural. Further, the unconditional convergence performance usually associated with implicit methods for linear problems, provides an expectation of enhanced robustness for the nonlinear material model solution. Further, the conditional convergence and stability limit of the alternative explicit solution methods for integrating the constitutive equations restricts increments of strain to small values (compared to the yield strain magnitude).

A backwards Euler implicit algorithm is used to numerically discretize the nonlinear analytical form of the constitutive equations in the description by Hibbitt. The primary algorithm

used to solve the resulting nonlinear algebraic form is Newton's method. This is also the method used to solve the global system of equilibrium equations for the structural model in ABAQUS. Thus, the process of integrating along the path-dependent stress-strain curve using a local Jacobian matrix (material matrix at a point) is analogous to the process of integrating along the nonlinear load-displacement path using the global Jacobian matrix (tangent stiffness matrix of the structure). Since the local problem solution is nested within the global solution, it is important that the local problem be solved with a tight convergence criterion so that the global solution does not accumulate error and converges satisfactorily. However, for plasticity models such as the concrete model, the potential for breakdown in the overall solution exists, and therefore robust behavior can in fact be problematic. The high cost of nonlinear analysis of reinforced concrete structures is largely due to the difficulties encountered in the stability and accuracy of these solutions. These difficulties are a direct consequence of the specific numerical implementation of the concrete material nonlinearities (Bathe, et al., 1989).

Practical Aspects

Despite their apparent sophistication, nonlinear concrete material models have limitations on their application. The ABAQUS concrete material model seeks a balance between capturing essential behavior and numerical reliability. It sacrifices some modeling detail for numerical tractability as discussed below.

The ABAQUS nonlinear concrete model is limited to confining pressures below three to four times the concrete compressive strength, f_c'. The model incorporates an associative flow rule which is valid for concrete for a low range of confinement pressures. At higher pressures the direction of flow in the material (i.e., the plastic strain) would no longer be expected to be normal to the failure surface as assumed by an associated flow rule model. Thus, calculations would not be reliable in this domain. To overcome this pressure limitation, hydrodynamic material model capability is required. This capability is available in the computer program DYNA3D, which is discussed in later sections of this report.

Furthermore, while the ABAQUS concrete model handles reasonably severe loading, well beyond the elastic response, it is limited to relatively monotonic loads. This is a result of using a simplified hardening rule that cannot replicate accumulation of damage to the material due to successive cycles of loading.

The ABAQUS concrete material model should therefore be applicable to problems involving overpressurization of containment structures such as nuclear reactor containments or missile test cells. Conversely, it is not suited to high performance magazine concepts wherein design pressures are of an order magnitude higher than f_c', or to severe seismic loads because such problems involve cyclic inelastic response.

Usage of the ABAQUS concrete material model requires three input data sets for definition of material properties as follows:

1. The *ELASTIC data set defines the elastic properties.

2. The *CONCRETE data set defines the compressive stress-strain relationship outside the elastic range.

3. The *TENSION STIFFENING data set defines the post-failure stress-strain behavior across a smeared crack.

Additionally, an optional *SHEAR RETENTION data set is prescribed to define the reduction in shear modulus associated with crack surfaces, as a function of the tensile strain across the smeared crack.

The *ELASTIC data set consists of the modulus of elasticity and the Poisson ratio for concrete. These data are presented in Table 8 for the MTC analysis, along with the compressive and tensile strengths for the material model.

Table 8
Mechanical Properties for the Concrete Material
Model Specified for the MTC Analysis

Property	Prescribed Value
Modulus of Elasticity, E	4.415×10^6 psi
Poisson Ratio, ν	0.20
Shear Modulus, G	1.840×10^6 psi
Compressive Strength, f_c'	6,000 psi
Tensile Strength, f_t'	540 psi

The *CONCRETE data set is a prescribed list of coordinate points along a uniaxial stress-strain curve, beyond the elastic limit, in compression. The data set used in the MTC model is graphed in Figure 13. The compressive strength f_c' is specified in this manner and in this case allowance for high rates of loading has resulted in a value of 6,000 psi. The elastic limit was set at 4,000 psi. The nonlinear behavior prior to failure of the material is clearly represented in these data which were processed from test data reported in Park and Pauly (1975). Unloading in compression occurs along a straight line having a slope equal to the modulus of elasticity, E.

The *TENSION STIFFENING data set is likewise a prescribed list of coordinate points describing stress-strain behavior. In this case the behavior of interest is tensile and it applies only after fracture has occurred. It represents the relationship between tensile stress and strain acting normal to the face of a smeared crack. In this sense, stress and strain are fictitious since a crack is in fact a free surface. However, the artificial stiffening concept, called tension stiffening, allows for the effects of the interaction of reinforcement with the concrete (perfect bond effects) to be simulated in a simple manner. Further, cracking is assumed to occur over a portion of the finite element associated with an integration point. The data used to describe this behavior for the MTC analysis are graphed in Figure 14 where the stress is normalized on the uniaxial tensile strength, f_t', and the strain is the total strain minus the strain at cracking. These data are based on deformation-controlled tests on concrete conducted by Cornellissen, Hordijk, and Reinhardt (1986) where the emphasis was on measurement of the descending branch of stress-strain behavior, also termed strain softening behavior.

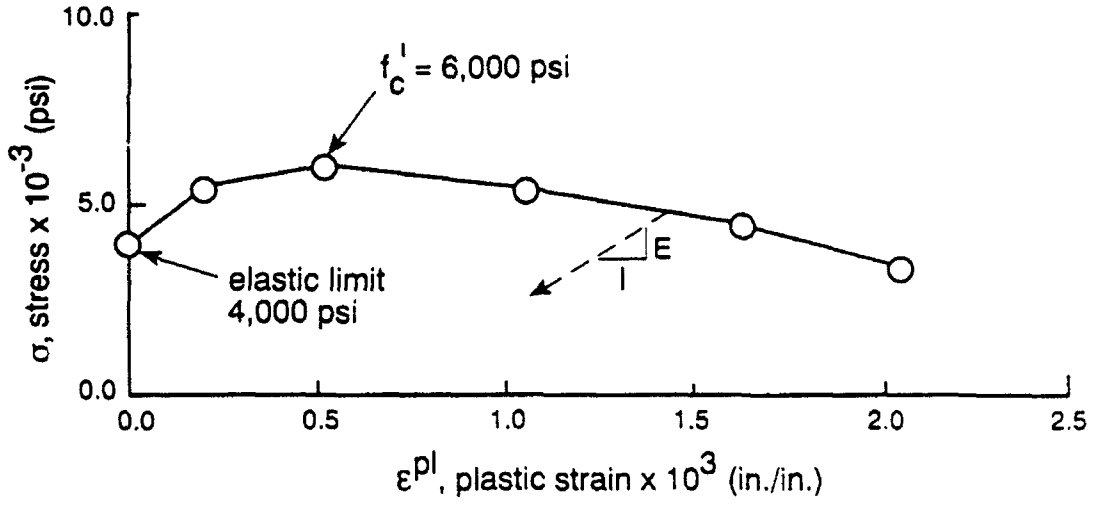

Figure 13
Nonlinear uniaxial compression behavior.

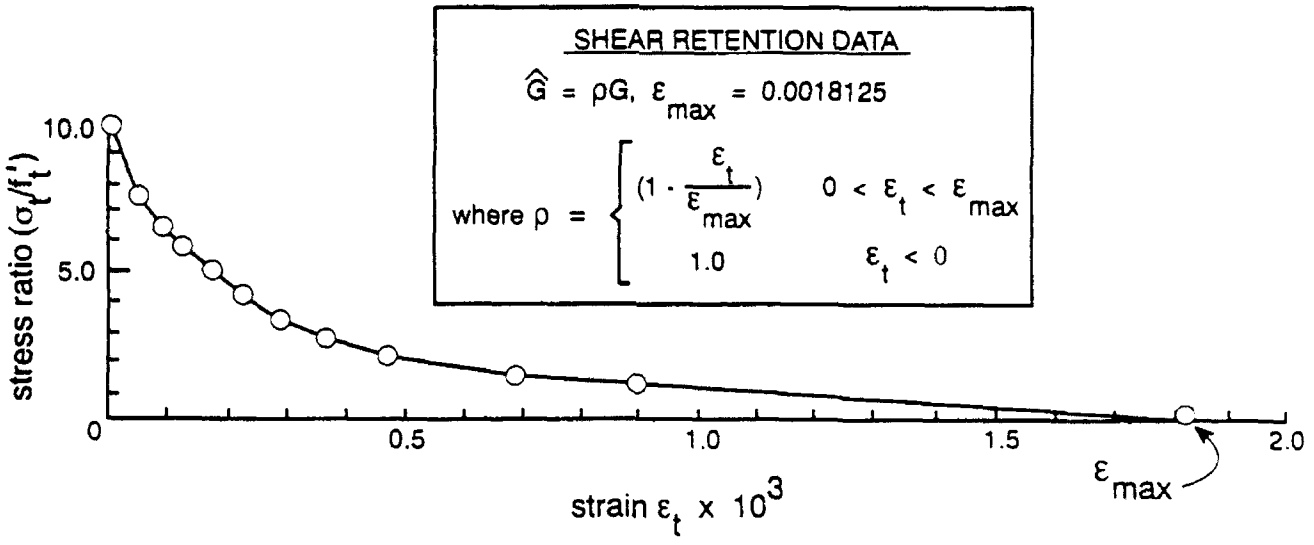

Figure 14
Prescribed tension stiffening data.

The *SHEAR RETENTION data used for the MTC analysis are presented in the inset of Figure 14. These data provide a multiplying factor, ρ, which defines the shear modulus of cracks, ρG, where G is the elastic shear modulus of intact concrete. (The value for G is determined automatically from the prescribed values for E and ν.) The shear retention model assumes that the shear stiffness of smeared cracks reduces linearly to zero as the crack opening increases. In the expressions, ϵ_t denotes the normal strain at the smeared crack, and ϵ_{max} denotes the opening at which both the normal and shear stress become zero. Provision is also made for crack closing by restoring the shear modulus to the initial elastic value.

Once a crack forms in the ABAQUS model, the direction of the crack is recorded. Subsequent element stress and strain calculations are made in the corresponding local coordinate system defined by the crack direction. Subsequent or secondary cracks are constrained to directions orthogonal to the primary crack direction.

Single Element Tests

Single element tests were conducted to verify the nonlinear concrete material model. Static, displacement-controlled numerical tests were conducted using a single three-dimensional finite element having a size typical of the elements used to model the MTC cylinder wall (48 by 48 by 16 inches). Large displacements and large strains were permitted to allow for nonlinear behavior. The resulting nonlinear concrete model behavior for a uniaxial tension test is shown in Figure 15. A smeared crack forms at the prescribed value of 540 psi and subsequent loading indicates a gradual nonlinear strain softening behavior of the smeared crack. Upon unloading and reloading, the behavior is constrained to a straight line directed toward the origin. That the slope of this line is less than the intact concrete stiffness, E, is significant and an indication of accumulated damage to the material. It is a consequence of the elastic damage model assumed for tension behavior. There is a progressive loss of material stiffness for unload/reload cycles at increased levels of strain softening. Conversely, no progressive damage occurs for successive loading cycles along the same unloading line.

NONLINEAR DYNAMIC RESPONSE OF THE MTC WALL

The nonlinear dynamic response of the MTC using the aforementioned three-dimensional model could not be computed satisfactorily. This was apparently due to extreme sensitivity of the concrete material model when simulating cracking. In the material model, cracks form when the direct stress exceeds the tensile strength of concrete. Secondary cracks form in planes orthogonal to the plane containing the initial or primary crack. At most, only the first 1.6 ms of the dynamic response was simulated before secondary cracking took place, which apparently could not be handled by the material model. This deficiency has since been documented in ABAQUS version 4.9.

Simplified Model of the MTC Wall

To determine the cause of the difficulty, a simpler model of the MTC wall was constructed as shown in Figure 16. This model consisted of a transverse section through the cylinder, and was formed directly from a ring of solid elements from the center of the three-dimensional model. Plane strain conditions were imposed on this layer of elements, so that the

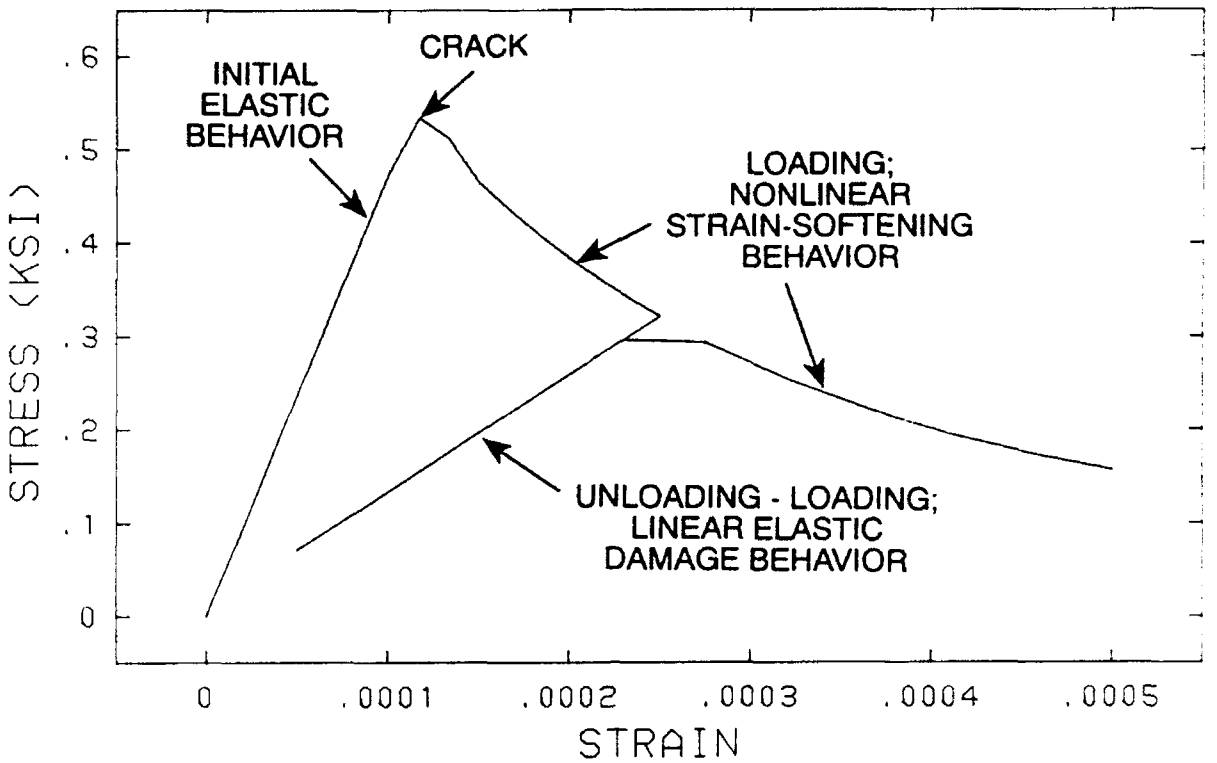

Figure 15
Behavior of a single concrete element in tension.

subsequent dynamic response computed with this model would be strictly applicable to the wall of an infinitely long tube possessing the cross-sectional shape of the MTC.

Attempts to run the simplified model were eventually successful, but not before many failed attempts occurred which were similar to those experienced with the three-dimensional model.

Post-mortem data of failed runs indicated that primary radial cracks had formed in the wall in a rational manner, but that the directions of secondary cracks which also formed were arbitrary and meaningless. Furthermore, the occurrences of secondary cracks were correlated with occurrences of hashing in the reported hoop stress data in the MTC wall. The hashing, or occurrence of large spikes in the response, was spurious since subsequent to formation of radial cracks, the concrete hoop stress response should have diminished smoothly to zero with continued loading according to the elastic damage model assumed for tension behavior.

Boundary conditions at the base of the MTC induced high bending moment in the wall which caused severe cracking to occur, and this overburdened the concrete material model's capacity to handle cracking correctly. The difficulty in running the simplified model was finally resolved when boundary conditions representing support at the base of the model were removed. Subsequent to that adjustment, the simplified model ran reasonably successfully.

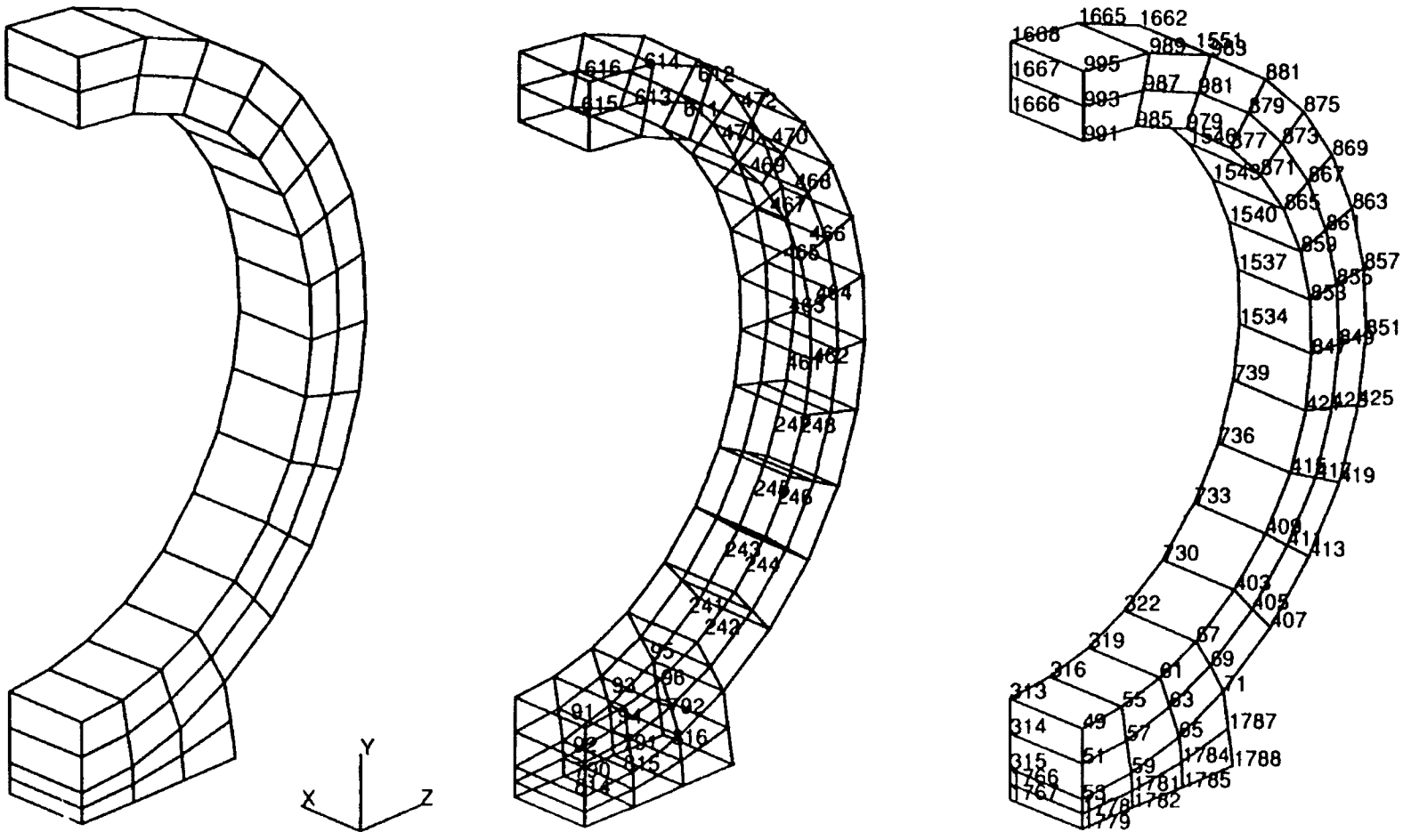

(a) Mesh. (b) Elements. (c) Nodes.

Figure 16
Nonlinear dynamic ring model.

Unfortunately, similar adjustment to the boundary conditions at the base of the three-dimensional MTC model did not noticeably improve subsequent simulation attempts. This model is more challenging to the concrete material model since the additional geometrical complexity induces severe stress concentrations, particularly at the interface between the cylinder and end walls, which lead to widespread cracking. These stress concentrations were clearly visible in the results of preliminary linear static runs with the three-dimensional model (Figure 9).

Dynamic Response of the MTC Wall

Using the unrestrained simplified model of the MTC wall, the nonlinear dynamic response was computed relative to the prescribed blast load (Figure 2). The simulation terminated after 33 ms. The displacement fields at four intermediate stages of the response are depicted in Figure 17 where the basic behavior of the radial expansion of the wall and base are indicated (shown exaggerated for clarity).

Wall Section Behavior at TDC

The nonlinear dynamic response at top dead center (TDC) of the wall is shown in Figure 18. The first peak occurred at 12 ms and the second peak occurred at about 28 ms, as shown in Figure 18a. The second peak is slightly larger at 2.3 inches displacement on the cylinder inner radius.

The hoop stress response at TDC is shown in Figure 18b. These data are remarkable because they show the relationship between radial cracking of concrete and the progressive transfer of hoop force to steel reinforcement at this section. This information is important to a detailed understanding of how the MTC wall behaves in resisting load. It would otherwise be difficult to obtain this information experimentally in full-scale or model field tests of any reinforced concrete structure or structural element subjected to severe blast loading. It typifies the potential contribution of modern computational structural dynamics methods in supplementing information gained from full-scale or model tests in explosive safety research.

The radial stress response in the concrete at TDC is shown in Figure 18c. The initial and peak response is 2,560 psi. This is as expected since the peak pressure applied on the inside wall surface of the MTC is 2,560 psi (Figure 2), and it is a result of satisfying the stress boundary condition on that surface. A beating phenomena is also present in which two frequencies predominate. The lower frequecy corresponds to the oscillation in dynamic response of the wall (Figure 18a). The higher frequency could be that of the radial stress wave traveling between the inner and outer surface of the 32-inch wall. However, it has a period of about 1 millisecond which is twice that for an elastic plane wave in a 32-inch concrete slab. The combined oscillation has a mean amplitude of approximately 500-psi compression, and a dynamic amplitude of 500 psi, so that the radial stress oscillates between 0- and 1,000-psi compression during the post-shock phase of the response. A measure of material damping, which was provided indirectly by specifying the maximum possible numerical damping in the temporal integration algorithm, was included in the simulation. The effect of this damping was barely evident in dissipating the radial stress oscillation and it was not very effective.

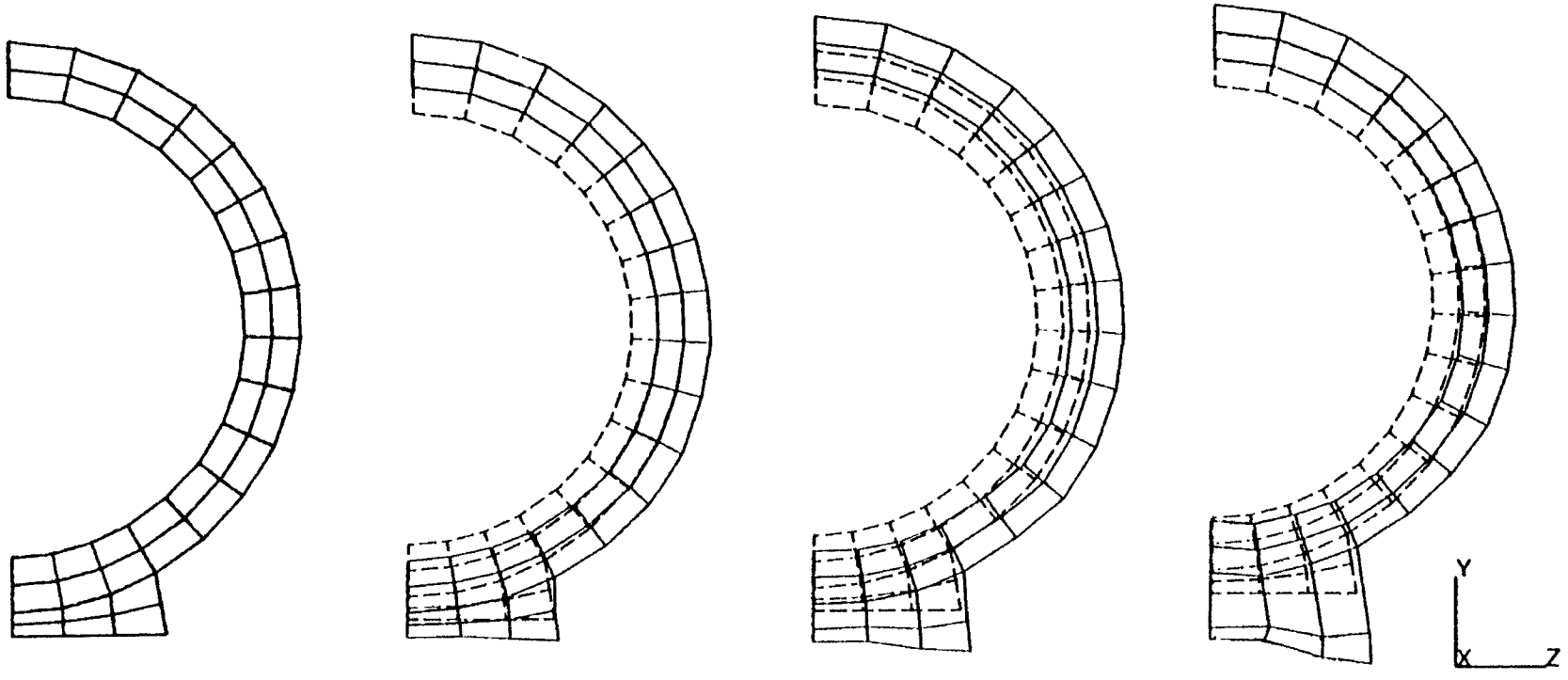

(a) t = 0.44 ms. (b) t = 6.03 ms. (c) t = 12.00 ms. (d) t = 20.04 ms.

Figure 17
Dynamic response of nonlinear ring model.

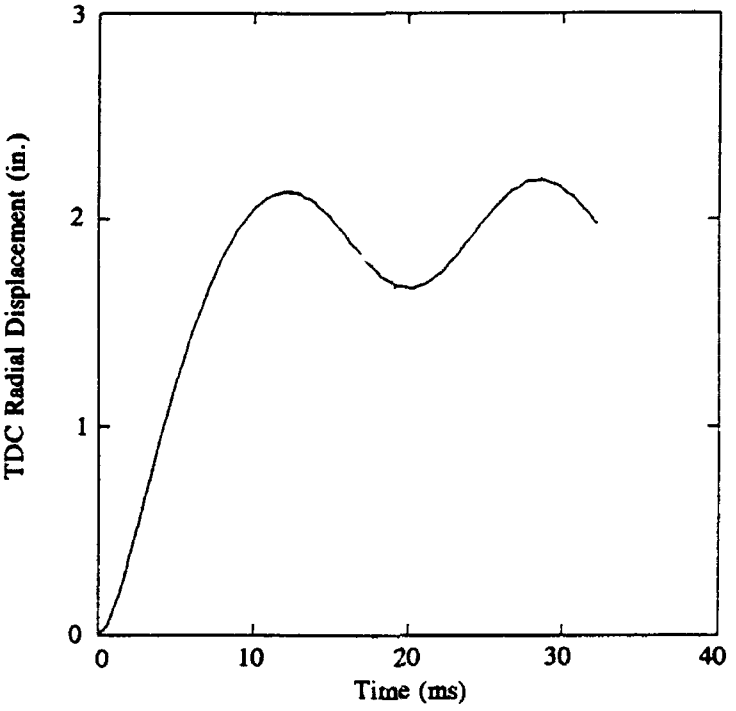

(a) Radial displacement at nodes 991 and 1666.

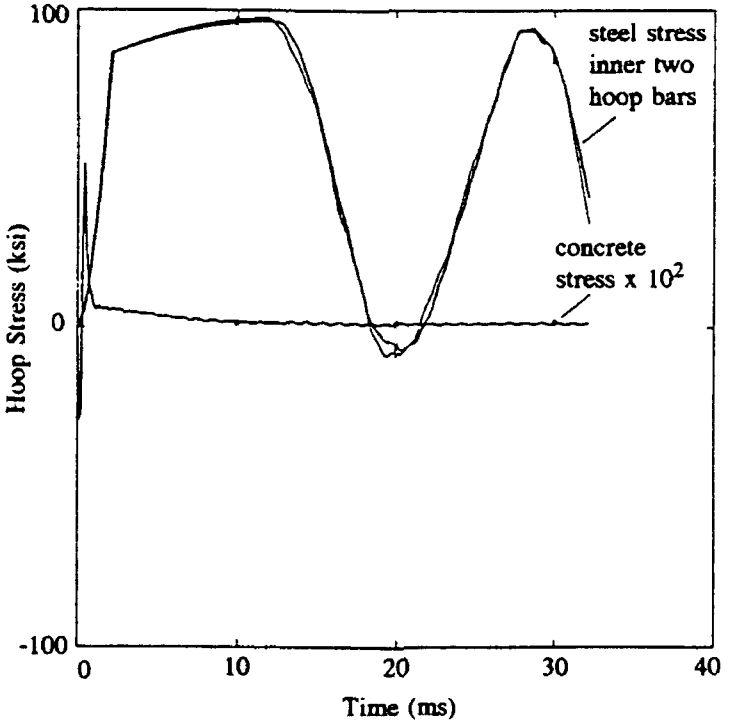

(b) Hoop stress, element 615.

Figure 18
Dynamic response at TDC.

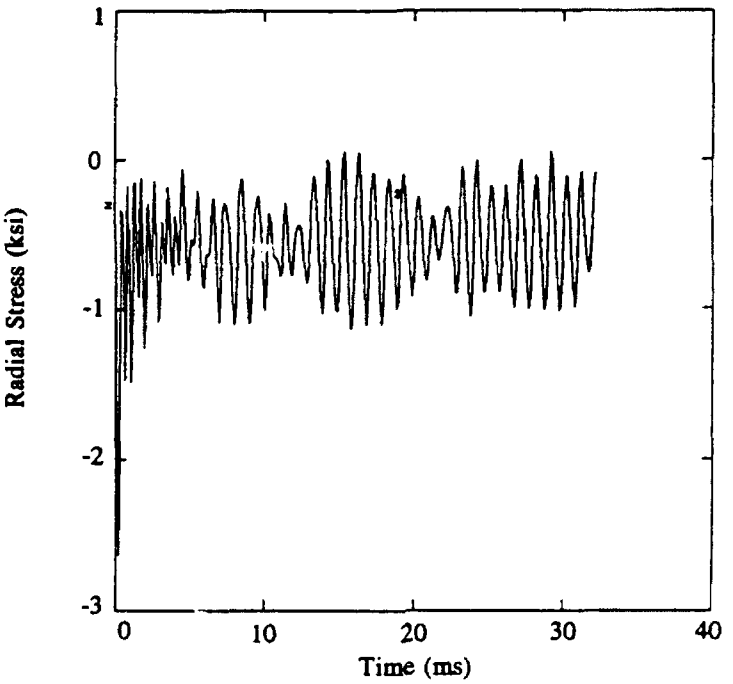

(c) Radial stress, element 615.

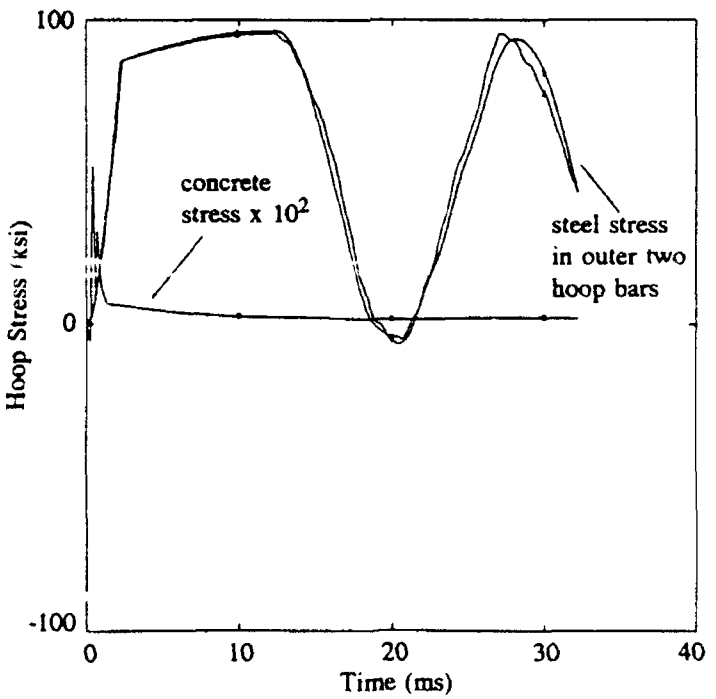

(d) Hoop stress, element 616.

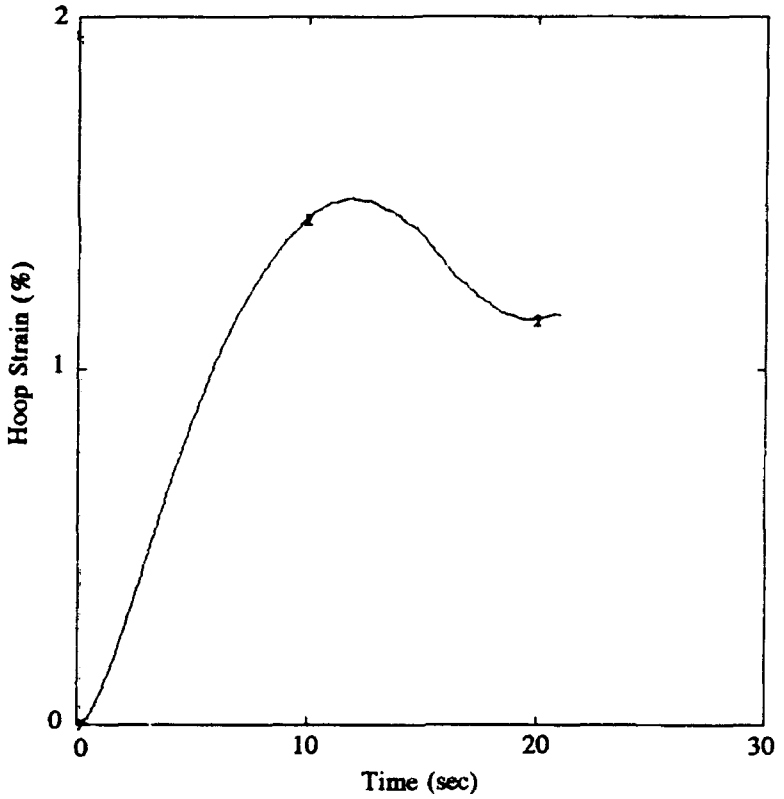

(e) Hoop strain - inner two rebars at TDC.

The aforementioned response results are from the inner finite element at TDC. Similar results also occurred for the outer element as shown in Figure 18d, thus indicating that the 32-inch wall was completely fractured at TDC. The peak tensile stress shown for the concrete is 540 psi, which was precisely the value prescribed in the material model for the tensile strength of concrete. The section completely cracks within the first millisecond. That is, the concrete strength of the section was not a factor after the first millisecond in resisting the residual gas pressure impinging on the wall.

The hoop steel reinforcement was seen to carry the load for the great majority of the dynamic response. These results tend to corroborate the assumption made in the MTC design that the concrete strength plays a negligible role in resisting the internal blast load and may be ignored (Ayvazyan, et al., 1988).

The two inner layers of hoop reinforcing bars are shown to yield at the prescribed value of 86.7 ksi (Ayvazyan, et al., 1988) within the first 3 ms. Again, these data were typical of the entire section. Prescribed strain hardening of the bars was also evident in the response data (subsequent to yield) until such time as the wall rebounded, after 12 ms had elapsed, causing the bars to unload. Complete unloading of the hoop reinforcement was indicated, and in fact the bars momentarily experienced compression before the onset of the second cycle of the response. These data warn that buckling of the reinforcing bars designed primarily to resist tension forces is often a possibility due to rebound. A similar observation is made in a subsequent description of the computed dynamic response of reinforced concrete slabs (see Section 2).

Hoop strain response in the steel bars is graphed in Figure 18e. The maximum value of strain for the two inner hoop bars is 1.5 percent. If the yield strain value is taken as 0.3 percent, this represents a ductility ratio of 5, which is close to the design goal of 6 for the MTC. Yet there is far more ductility to exploit in the stress-strain behavior of Grade 60 steel bars, as shown in Figure 19. The potential of high strength bars in this regard for MTC designs is also indicated (see ASTM A722-88a, 1989).

Wall Section Behavior at 90 Degrees from TDC

To investigate the response of the MTC wall further, the displacement, hoop stress, and radial stress histories were graphed for the section 90 degrees from TDC. These data are shown in Figures 20a through 20d. In Figure 20a, the maximum dynamic response is 2.5 inches on the inside radius of the MTC, slightly greater than at TDC. Otherwise, when compared to the corresponding data from the TDC section (Figure 18), the responses at both sections were seen to be very similar. Thus, the aforementioned discussion of the dynamic response of the section at TDC generally applied to the entire MTC wall.

Overall Stress Response for the Wall

Maximum principal stress contour data for concrete in the MTC wall are shown in Figure 21. These data were very similar to hoop stress data (not shown) where the primary action was due to tensile hoop forces in the wall. The stresses are shown to increase to the specified cracking level in Figure 21b and then to diminish simultaneously throughout most of the wall. The stresses diminished with loading according to the prescribed tension stiffening data (Figure 14). Radial cracks through the 32-inch wall were implied by the data to have occurred throughout this region during the first millisecond of response.

SUMMARY

Two- and three-dimensional finite element analyses of a proposed novel missile test cell (MTC) design constructed of reinforced concrete were conducted. A two-dimensional nonlinear dynamic analysis of this structure was carried out using the general purpose implicit finite element program, ABAQUS. The finite element models account for a very complex steel rebar cage design by using the embedded reinforcement model capability provided in ABAQUS. Unfortunately, the fully three-dimensional model could not be successfully processed due to an error discovered in the ABAQUS concrete material model which caused spurious oscillations in concrete stress to occur once secondary cracks formed in the MTC wall. These oscillations became unstable and contaminated the global solution which caused the computer simulation to crash very early in the simulation. The error is now documented in version 4.9 of ABAQUS. It is noted that the version of ABAQUS used (version 4.8) is fundamentally an implicit finite element code, and the nonlinear dynamic analysis of the MTC model was a particularly challenging problem for any such code, and probably better suited to solution by an explicit finite element code.

Nonetheless, substantial information was obtained on the nonlinear dynamic response of the cylindrical wall of the MTC by using a simplified model consisting of a two-dimensional slice from the center of the cylinder in the three-dimensional model. By virtue of its simpler

geometry, this model was better behaved. Analysis of the calculated dynamic response showed that the 32-inch-thick cylindrical wall would completely fracture radially all around the circumference within the first 1.5 ms, which is during the shock phase of the simulated blast load. Also, section hoop forces were redistributed to the hoop steel, all of which is loaded into the plastic range within 2 to 3 ms. This redistribution of load within the wall and the dynamic response of the wall were clearly explicated by the analysis and computer graphics. For example, the gas pressure phase of the loading continued to cause forced vibration of the cylindrical wall after the shock phase. The hoop steel was shown to unload and reload two times, elastically, during the first 33 ms of this load phase. Maximum radial deflection was about 2.5 inches on the 10-foot inside radius of the cylinder during this interval, and it occurred on the second oscillation at about 28 ms. The two-dimensional simulation eventually terminated abnormally at 33 ms for the same reason as discussed above for the full three-dimensional model.

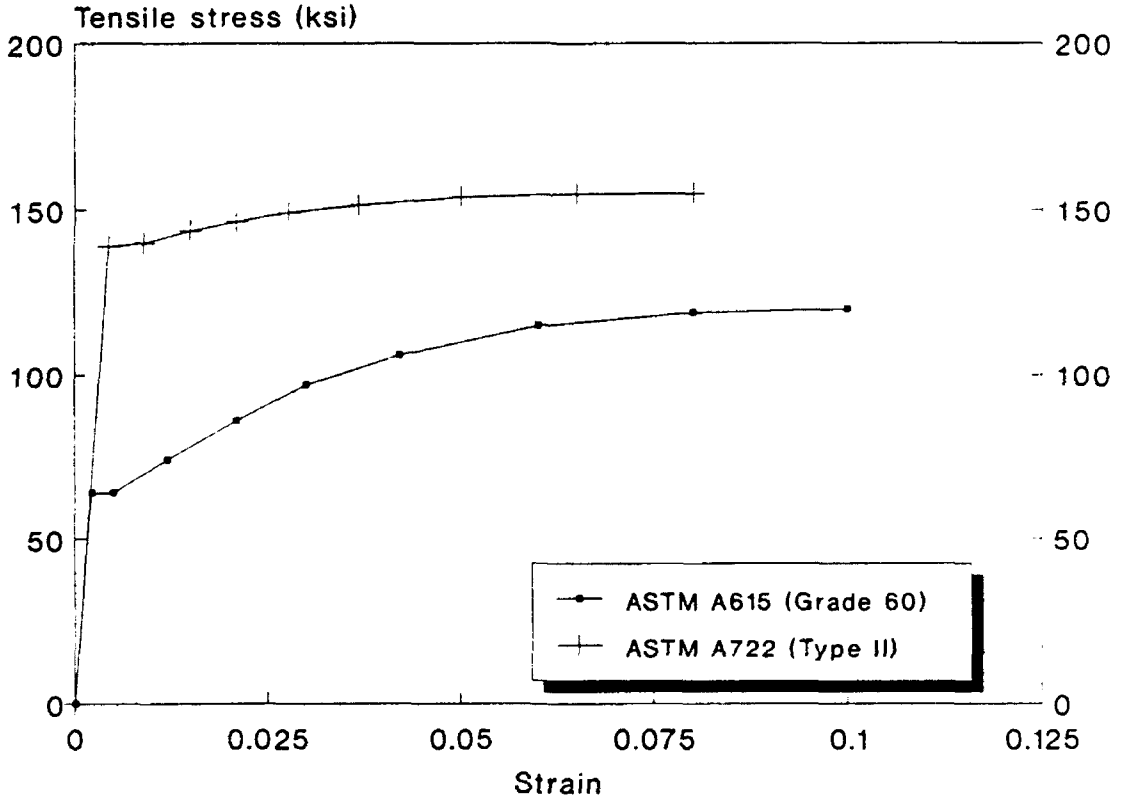

Figure 19
Ductility of high strength steel.

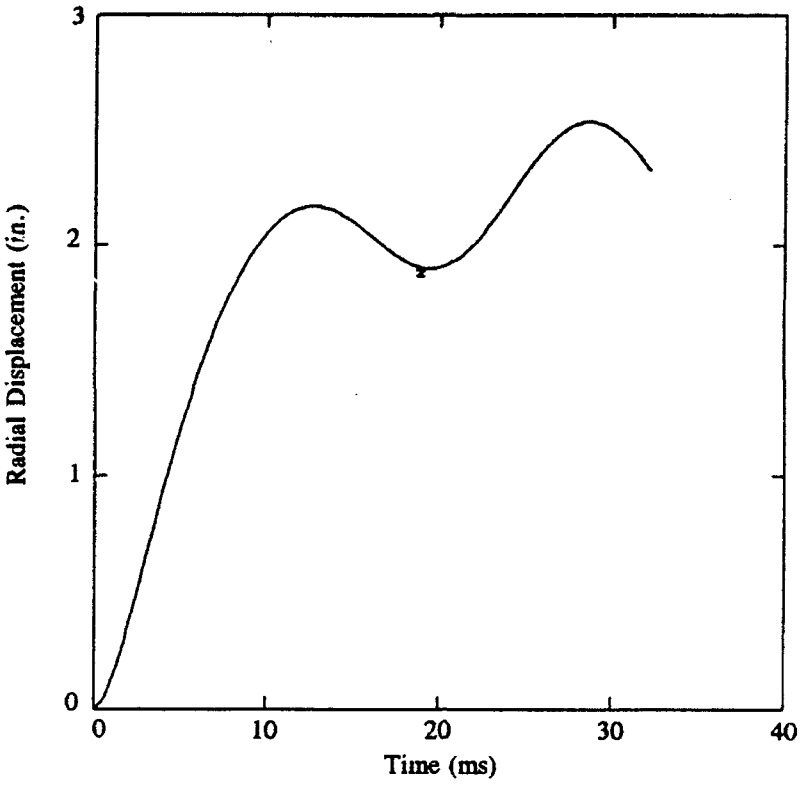

(a) Radial displacement at both nodes 421 and 739.

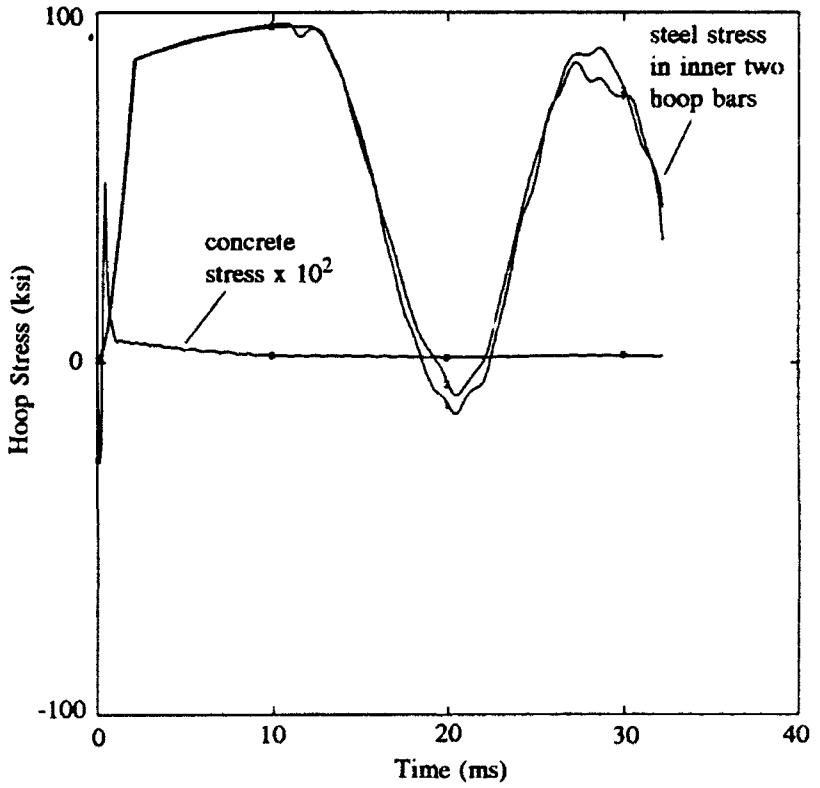

(b) Hoop stress, element 463.

Figure 20
Dynamic response at 90 degrees from TDC.

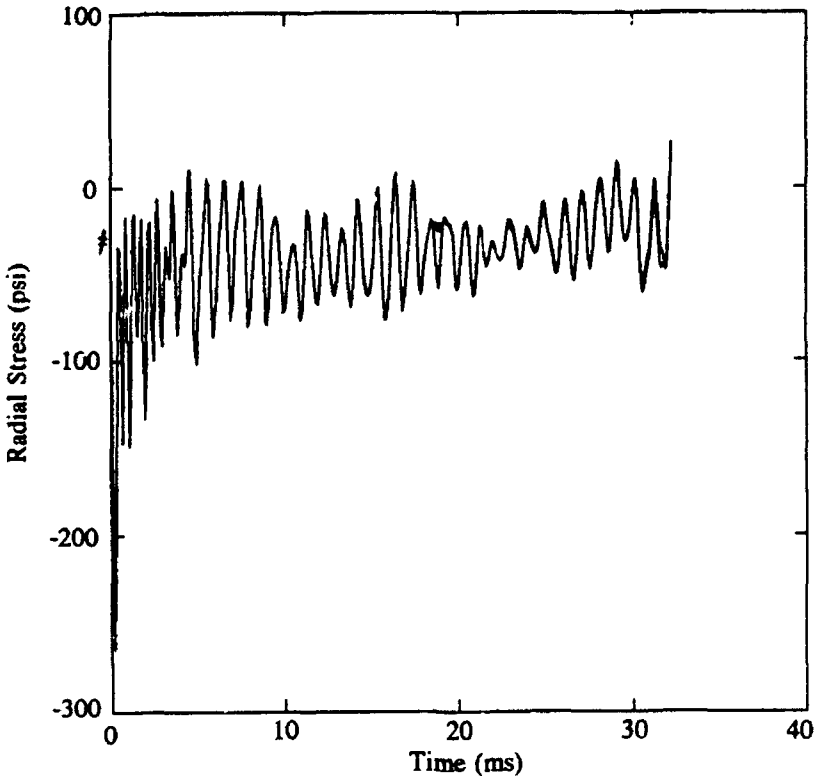

(c) Radial stress, element 463.

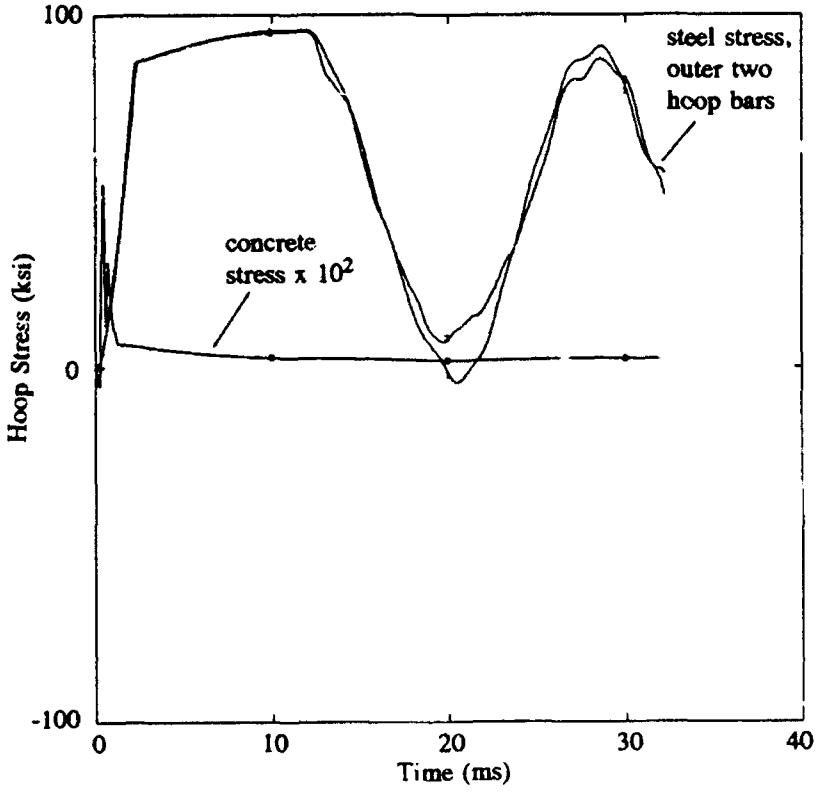

(d) Hoop stress, element 464.

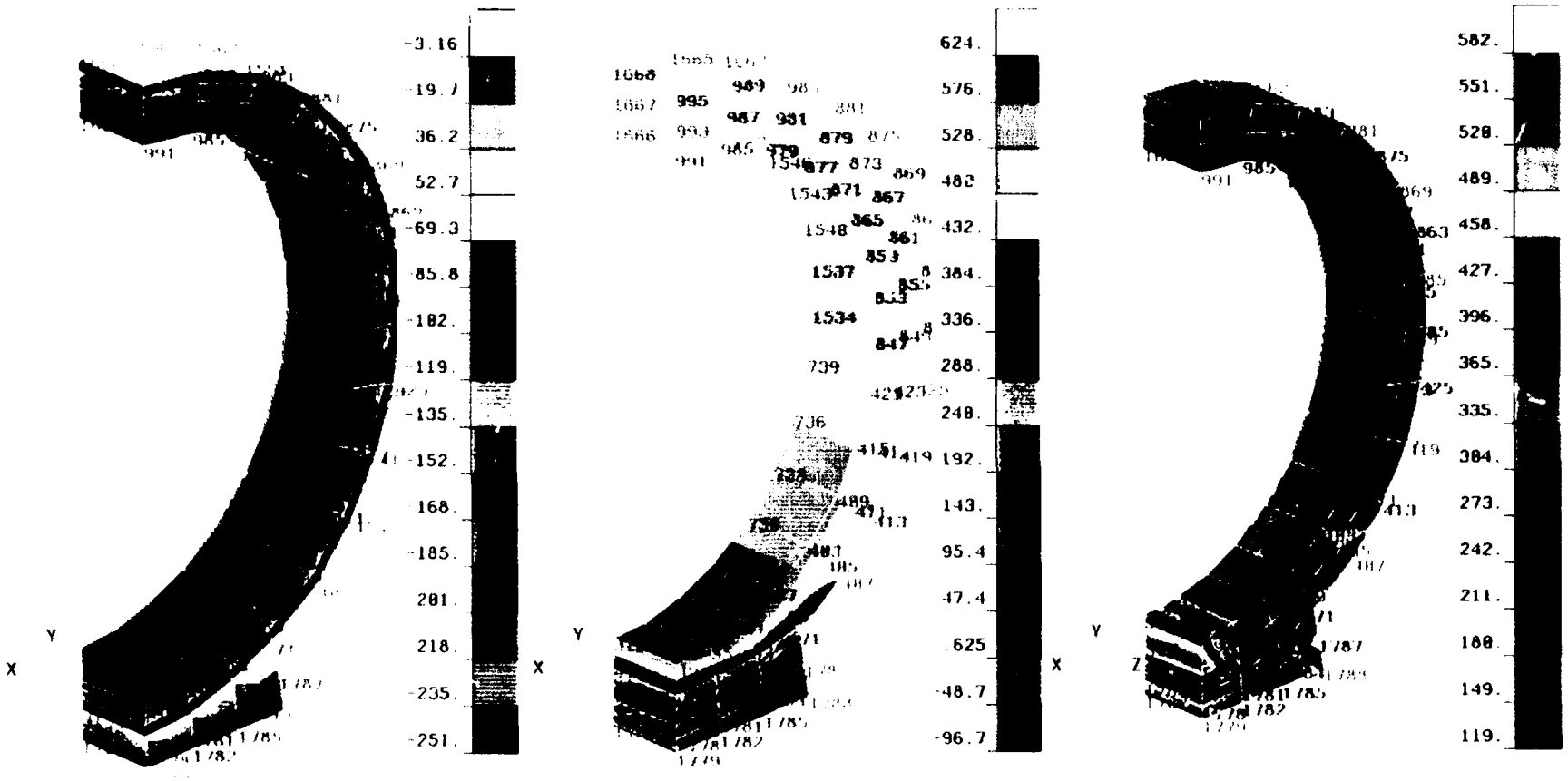

(a) t = 0.131 ms. (b) t = 0.422 ms. (c) t = 0.787 ms.

Figure 21
Maximum principal concrete stresses in MTC wall.

SECTION 2

NONLINEAR DYNAMIC FINITE ELEMENT ANALYSIS OF REINFORCED CONCRETE SLABS SUBJECTED TO BLAST LOADS

INTRODUCTION

Critical Navy reinforced concrete structures such as missile test cells and graving drydocks are designed to withstand large deformations under severe blast and strong-motion earthquake loads. The development of design criteria for these structures requires the evaluation of their response in the nonlinear range. Due to their complex configuration, consideration for their three-dimensional geometry is also required. Current finite element technology offers the capability of handling large three-dimensional nonlinear models, although these are computationally intense and expensive. In this regard, the Naval Civil Engineering Laboratory (NCEL) has evaluated existing technology and its applicability to specific Navy problems.

The discussion in this section represents an assessment of the explicit finite element code DYNA3D (Whirley and Hallquist, 1991). In this study, DYNA3D is used to predict the response of two, two-way reinforced concrete slabs subjected to blast loads. A three-dimensional nonlinear reinforced concrete model was employed to accurately represent the progressive crack formation and to reflect the consequent stiffness degradation associated with the dynamic response of the slabs. The results of DYNA3D calculations are compared to test results and to results from standard NAVFAC P-397 single-degree-of-freedom (SDOF) methods.

BACKGROUND

Dynamic blast load tests were conducted on 12 two-way reinforced concrete slabs to verify shear steel reinforcement criteria for NAVFAC P-397 (Tancreto, 1988). The scaled standoff distance of the bare explosives was small (0.65 to 1.10 ft/lb$^{1/3}$) to verify the criteria in relation to breach failure of slabs. Tests were also designed to obtain large deflections for verification of the criteria in the presence of tension membrane effects. Test specimen variables included main steel percentage (0.15 to 2.54 percent); shear reinforcement type (lacing, stirrups, or none); spacing of stirrups (d/2 to d); slab thickness (4.5 to 10 inches); and L/d ratios (10 to 30).

Results of the first six tests were reported by Tancreto (1988) and Woodson (1990). Results of all 12 tests and preliminary comparisons of the measured response to that predicted by SDOF models and DYNA3D were reported by Tancreto and Malvar (1991).

OBJECTIVES

The numerical simulation was directed at:

- Predicting the load-displacement time history of the center of the slabs.
- Comparing the predicted deflections with measured residual values.

- Comparing predicted and measured residual deflections with design values based on NAVFAC P-397.

- Evaluating the steel rebar stress/strain histories, including the buckling potential and the need for confining steel.

- Evaluating deflected shapes to predict failure modes.

TEST PROGRAM

Test Setup

The test setup is shown in Figures 22 and 23. A 7.5- by 7.5- by 8-foot deep cubicle was used to support the test slabs. The 10.5- by 10.5-foot slabs (with a two-way clear span of 7.5 by 7.5 feet) were bolted to the top of the cubicle with a steel fixture that clamped the outer 1.5-foot width. The steel fixture was held via a total of 32 1-3/4-inch diameter A325 bolts installed through 2-1/2-inch diameter holes provided in each slab. The clamping procedure developed the moment capacity of the slab and provided lateral friction resistance. The slabs' oversize holes could have allowed some lateral slippage, but none was observed during the tests.

Test Specimens

Only two test slab configurations (slabs I and V) were analyzed. Slab I was the baseline configuration with stirrups at each longitudinal steel intersection. Slab V had no shear steel but was thicker (6 inches instead of 4.5 inches). The main (longitudinal) steel for these two slabs was the metric equivalent of #2 deformed bar with a measured yield stress, f_y, of 74.5 ksi. The wire shear reinforcement (ASTM designation W1) used in slab I had a yield strength of about 60 ksi.

Slab I had 1.06 percent (each way, each face) longitudinal steel (#2 bar) at d/2 spacing; W1 stirrups at each intersection of the longitudinal steel; a thickness of 4.5 inches; an effective depth, d, of 3.1 inches; and a clear span to effective depth ratio, L/d, of 29. Slab V had a low steel percentage of 0.31 percent with #2 bars at d, no shear steel, a slab thickness of 6.0 inches, an effective depth of 4.0 inches, and an L/d ratio of 23. The steel cage for slab V is shown in Figure 24.

Explosive Charge

Spherical composition C4 explosives were used to obtain the blast loads. Explosive weights of 60 pounds were used for these two slabs (with a TNT equivalency by weight of 1.13). The scaled standoff distances were 0.69 and 1.1 $ft/lb^{1/3}$ for slabs I and V, respectively.

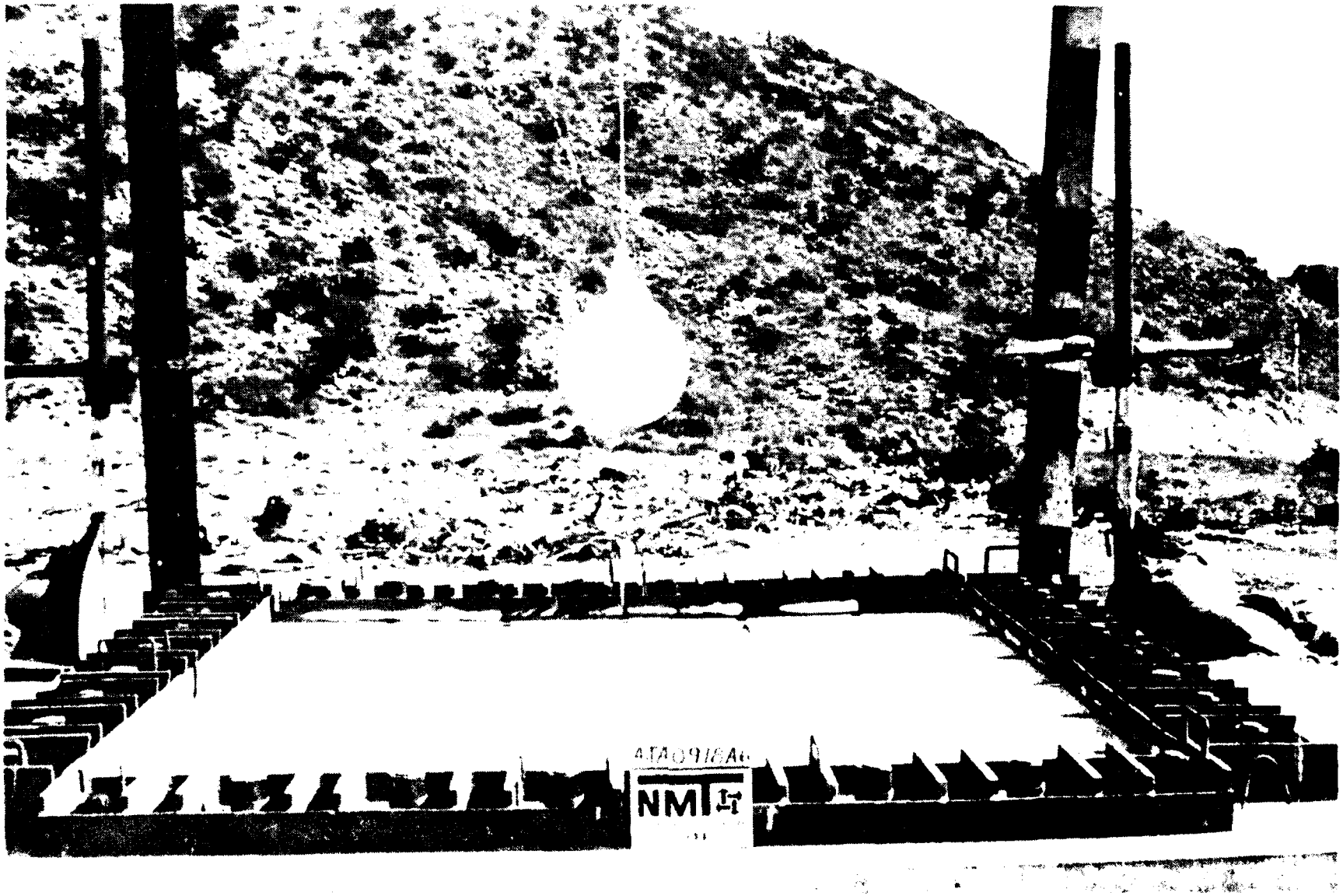

Figure 22
View of test setup.

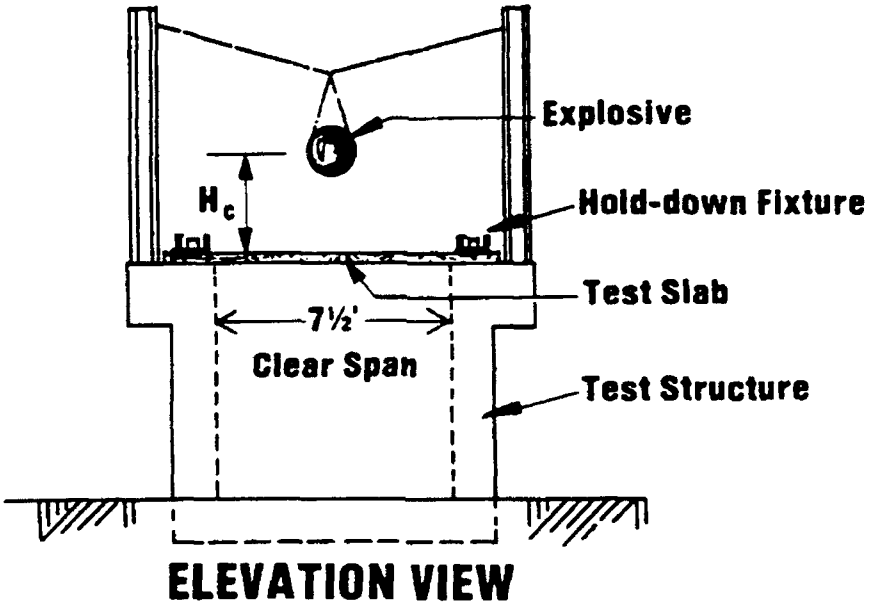

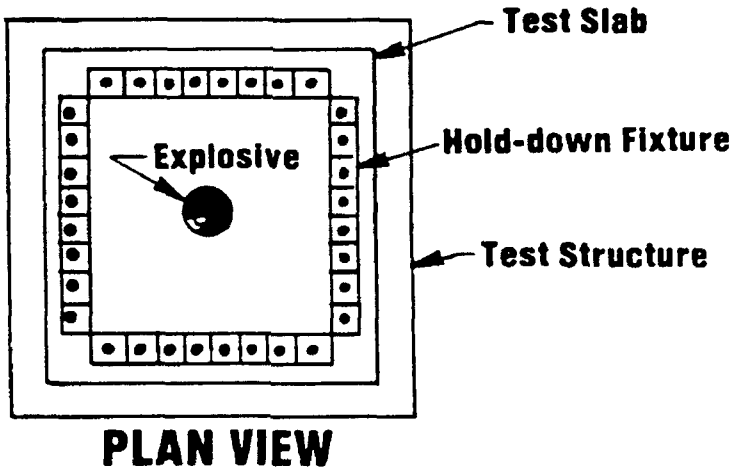

Figure 23
Test setup schematic.

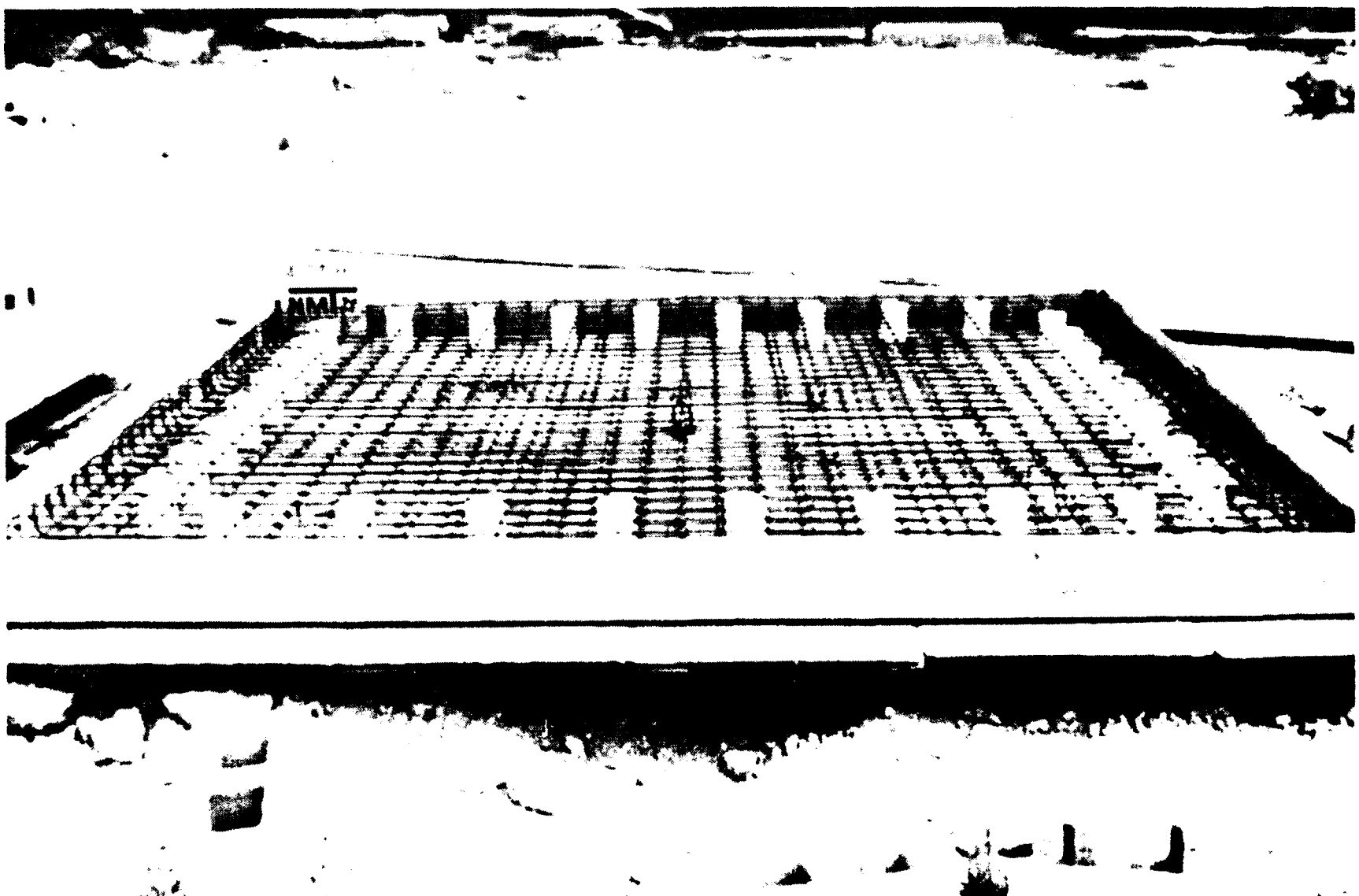

Figure 24
Rebar cage for slab V.

FINITE ELEMENT MODEL

A brief description of the three-dimensional nonlinear finite element models used in conjunction with DYNA3D for analysis of reinforced concrete slabs is presented. The development of the models featured a substantial examination of available material models, the details of which are included in Appendix C.

Model Discretization and Simulated Load

The explicit finite element program DYNA3D was used to model slabs I and V. Eight-node solid elements were used to represent the concrete and 2-node truss elements were used to represent the steel bars. The latter modeling technique is referred to as a discrete reinforcement model.

Due to double symmetry, only one-fourth of the slabs needed to be discretized. Figure 25 shows a typical 45-inch by 45-inch mesh. The 8-node solid elements are 3 inches by 3 inches with variable thickness through the depth. A discrete reinforcement model was employed. The steel truss elements are located below the thin first layer on each face. Wherever the reinforcement spacing did not coincide with the mesh size, the corresponding steel area was lumped at 3 inches on center in the discrete reinforcement model. Transverse steel was also lumped accordingly.

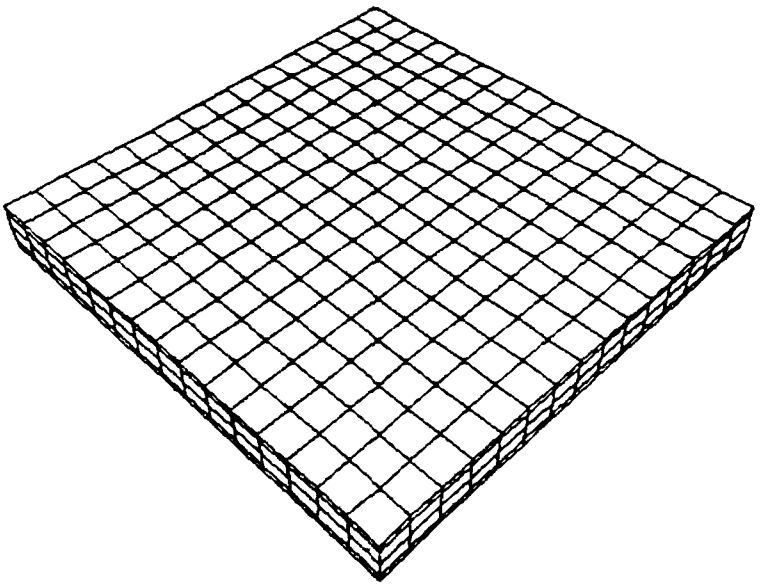

Figure 25
Finite element (quarter) mesh for slab models.

To provide for a direct comparison to SDOF models, which are based upon codified procedures that ordinarily assume uniform load conditions, the load was first assumed to be uniformly distributed over the slabs in the finite element analysis. The equivalent uniform load was obtained using the program SHOCK* which determined impulses and pressures from which the time histories were derived. For slab I, the simulated load decreased linearly from an initial 5,724 psi to 0 psi in 0.2 ms. For slab V, it decreased linearly from 3,564 psi to 0 psi in 0.264 ms. A subsequent analysis considered a more realistic nonuniform load distribution which was also obtained via SHOCK. In this case, the load intensity varied across the surface of the slab, and with respect to time, the load distribution varied in a proportional manner. In addition to a description of the slab geometry, input data for the program SHOCK included the explosive weight and standoff distance.

Material Properties

The material properties used in the predictions were:

Concrete	Steel
$E = 4{,}000$ ksi $\mu = 0.20$ $f_{dc}' = 6{,}000$ psi (DIF = 1.25)	$E = 29{,}000$ ksi $\mu = 0.30$ $f_{dy} = 97$ ksi (DIF = 1.3) $f_{du} = 102$ ksi (DIF = 10.5)

where E = modulus of elasticity
μ = Poisson's ratio
f_{dc}' = dynamic concrete compressive strength
f_{dy} = dynamic steel yield stress
f_{du} = dynamic steel ultimate stress
DIF = dynamic increase factor

Each dynamic quantity is the product of the static quantity and the corresponding DIF, (e.g., $f_{dy} = 1.3\, f_y$). DIF values were obtained from NAVFAC P-397 for close-in design range. For the steel yield stress, the DIF was refined based on calculated strain rates. A measured value for f_c' was not available and 4,800 psi was assumed. Concrete pressure versus volumetric strain curves for the equation of state used were obtained from Whirley and Hallquist (1991) and Matuska, et al. (1982).

*Naval Civil Engineering Laboratory. SHOCK User's Manual, Version 1.0. Port Hueneme, CA, Jan 1988. The user's manual has not been published as of this writing.

Steel Material Model

To examine the behavior of the different DYNA3D material models available to represent steel, a single truss element was subjected to tension then compression and the load displacement response analyzed. These simple numerical models showed reasonably good agreement with the expected elastic-plastic behavior of steel bars in tension or compression when Material 3 was prescribed (see Appendix C). This is an elastic-plastic material model with isotropic or kinematic (or both) hardening. Isotropic hardening was specified with a tangent modulus of 48 ksi (0.17 percent of E). This material model was used in the analyses of the slabs.

Concrete Material Models

To examine the DYNA3D concrete material models, a unit concrete cube was modeled with a single 8-node solid element and was tested both under tension and compression. The applied load (or stress) was quasi-statically incremented linearly with time so that the time axis can effectively be replaced directly by a stress axis for the purpose of graphing stress-strain behavior.

Material 17 was first considered because of its simplicity. Although a hardening modulus was specified and lateral confinement on all eight nodes provided, it was not possible to obtain a yield plateau in compression: typically, the compression stress would reduce to zero as soon as the yield stress was reached (see Appendix C). It was not possible to include an equation of state to handle very high pressures with this model. In tension, the model cracked at the specified fracture strength and released the stress satisfactorily, but exhibited an erroneous modulus of elasticity. This use of this material model was limited to an initial run.

Material 16 was then considered, with an internally generated equation of state (equation of state 0). It was found to behave properly and was used in the simulations. Material 16 has been used previously in similar DYNA3D analyses of reinforced concrete slabs (Terrier and Boisseau, 1989).

NONLINEAR DYNAMIC RESPONSE OF SLABS

The nonlinear dynamic response of the two reinforced concrete slabs is discussed. The data from the field-tested slabs were limited to knowledge of the explosive charge weight and close-in standoff distances, measurements of post-test or residual deflections at the center of the slabs, and post-test photographs of the slabs. The measured residual deflections were compared with residual deflections from two different computational procedures for the dynamic response of slabs. The discussion focuses on the accuracy of the DYNA3D computational procedures. The discussion is also extended to the observed and computed failure modes of the slabs, the computed stress response of the main steel reinforcement, and the effects of confinement steel.

Measured Residual Deflections and Observed Failure Modes

Large deflections and rotations were observed in the field-tested slabs. The post-test or residual deflections were measured and were generally less than the maximum deflections that occurred during the tests due to rebound. The residual deflections at the center were 8 and 8.3 inches for slabs I and V, respectively. The corresponding support rotations were 10.1 and 10.4

degrees.* These rotations exceeded the maximum allowable design rotation which is 8 degrees for slabs assuming tensile membrane resistance and no lacing shear steel.

Slab I developed a classic crisscross yield line as can be seen in Figure 26. In contrast with this, slab V, which had no shear steel, developed a circular yield line with a radius of approximately 37 inches as shown in Figure 27. Slab V also developed a 2.5-foot-long concrete shear crack along that yield line, with no failure of the main steel. The shear crack is visible in the figure and runs parallel to the foreground support and about 18 inches from it. The slab did not lose tensile membrane resistance. It should be noted that the standoff distance of the explosive (1.1 $ft/lb^{1/3}$) was much less than the minimum allowable, which is 3 $ft/lb^{1/3}$ for slabs without stirrups. Figures 28 and 29 show the cracking at the bottom of slabs I and V, respectively.

Computed Response with Codified SDOF Models

Design deflections which account for membrane action in slabs, were calculated based upon the SDOF model procedures from NAVFAC P-397. These procedures have been coded in two SDOF computer programs developed at NCEL, BARCS (Ferritto, 1977) and SOLVER (Holland, 1989). Due to the small variation in results from both programs (less than 4 percent), only the results from SOLVER are reported.

Using SOLVER, center deflections of 5.5 and 6.1 inches for slabs I and V, respectively were computed. These design values were unconservative since they were less than the measured values of residual deflection.

The design procedure in NAVFAC P-397 allows the use of a constant plastic resistance function to simplify the response calculation. The idealized design resistance function, shown in Figure 30, averages the actual resistance function for slab edge rotations up to 8 degrees. It is higher than the actual function just after spalling of the concrete cover, and lower elsewhere. This procedure also ignores membrane action.

Using this simplified procedure, the maximum deflections predicted were 6.1 and 6.4 inches, respectively, for slabs I and V. These values are higher than the ones found with membrane action but still lower than measured residual values.

The maximum deflections were again recalculated using the simplified procedure, with a slight variation in material properties. For concrete, a design compression strength of 4,000 psi with a DIF of 1.25 was used as before. However, for steel, a yield stress of 70 ksi and a standard DIF value of 1.23, instead of 1.30, was used. The maximum center deflection was found to be 6.8 inches for slab I, and 6.9 inches for slab V. These values are closer to the measured residual values and represent upper bounds for slab calculations based upon codified SDOF models in this study.

The foregoing SDOF deflection values are maximum values, as distinct from residual values, for the time history responses. Analysis of the lightly damped oscillations in these responses indicates that the residual deflections would probably be between 6.4 and 6.8 inches for slab I, and between 6.8 and 6.9 inches for slab V.

*Support or edge rotation is defined as the rotation of a rigid semiaxis line for the slab. This is different from the usual definition of slab rotation which is the slope of the deformed surface of the slab.

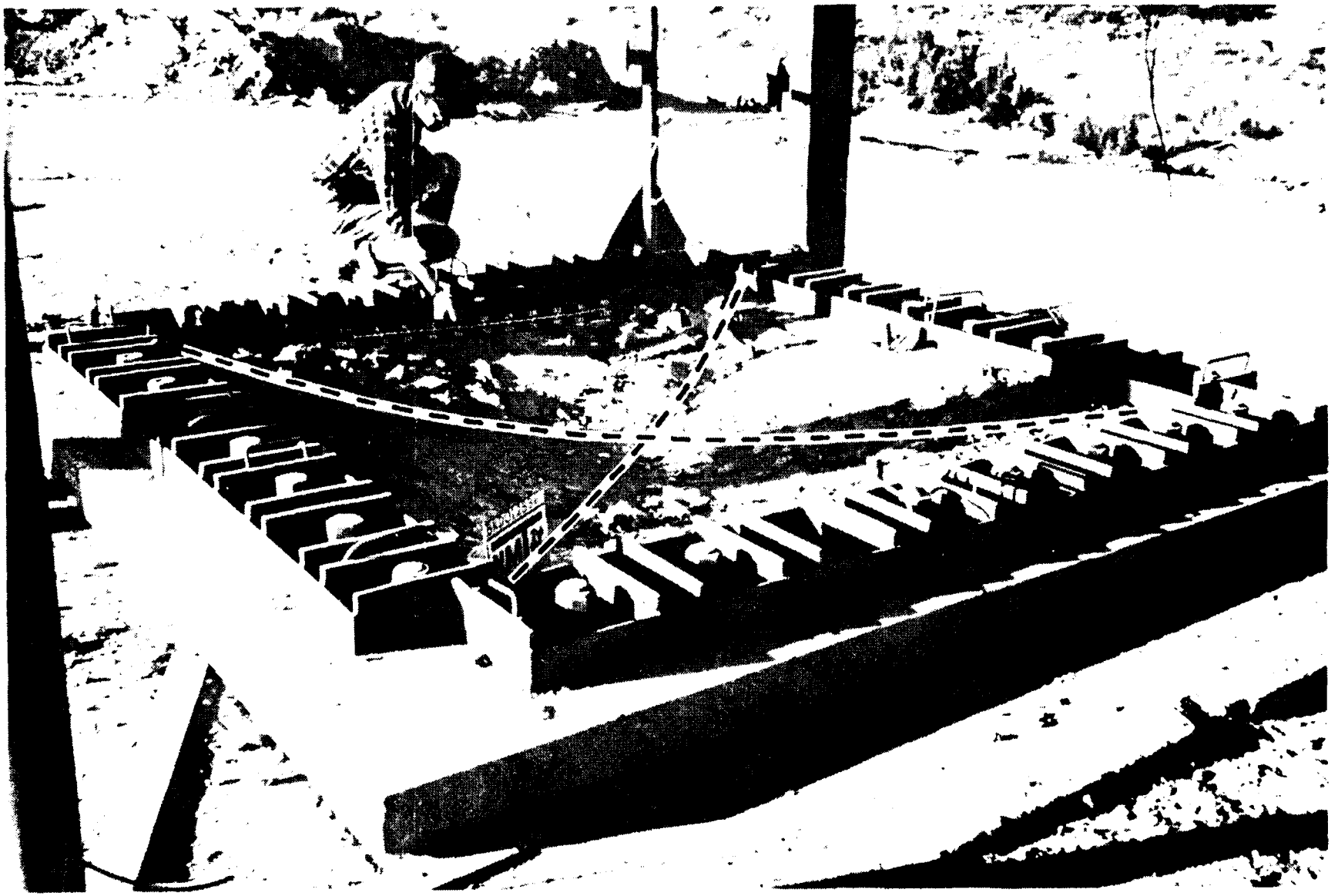

Figure 26
Top view of slab I after failure.

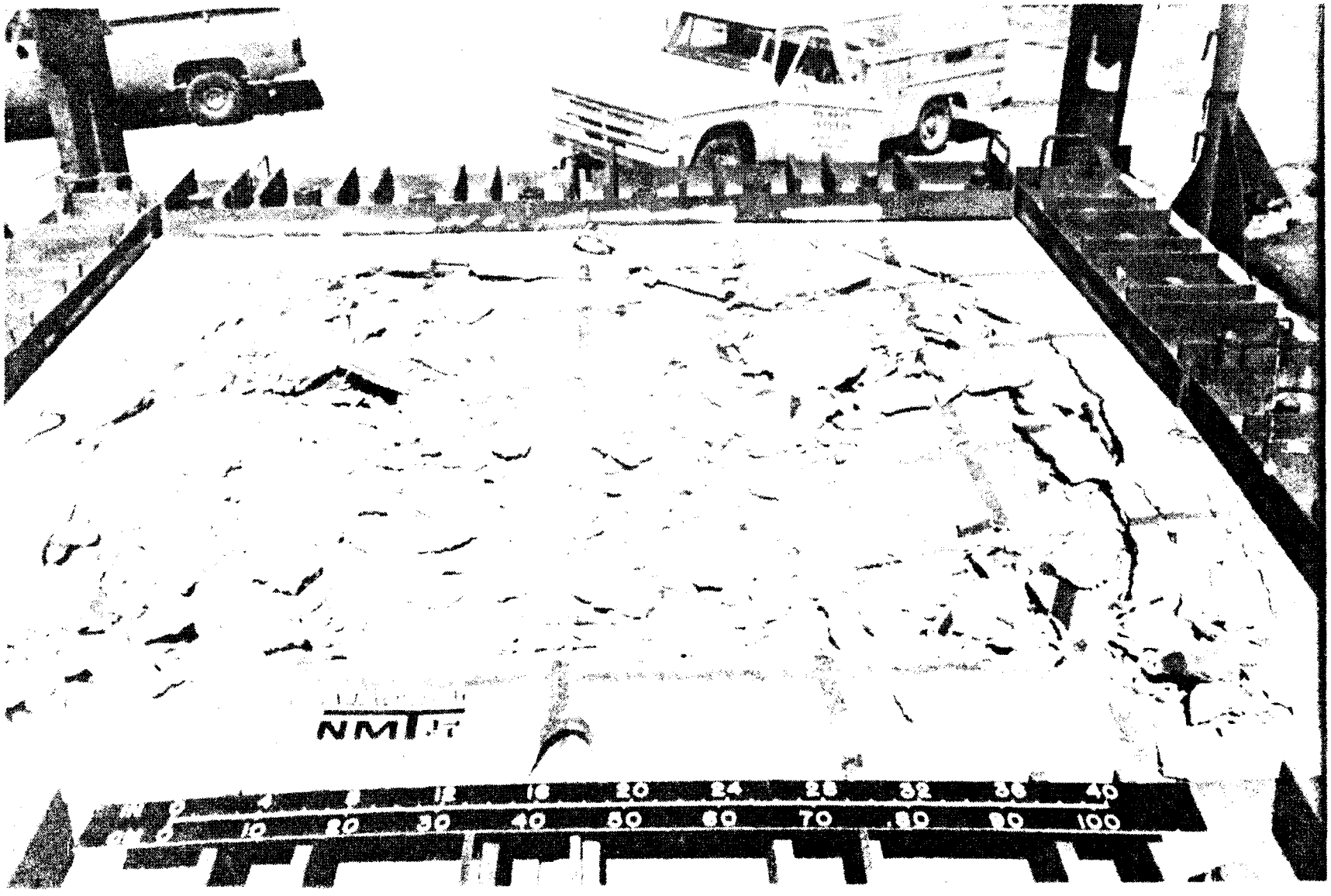

Figure 27
Top view of slab V after failure.

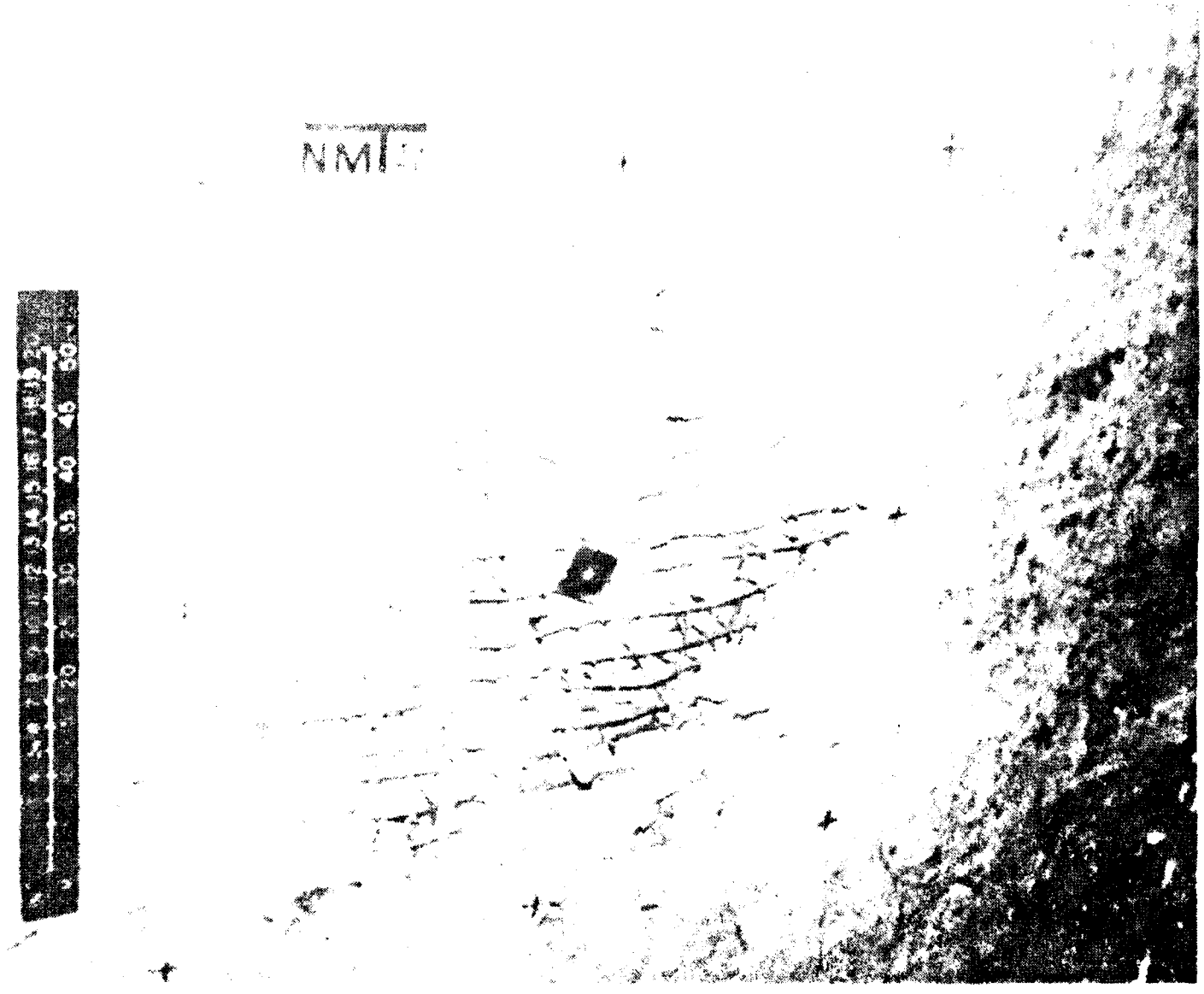

Figure 28
Bottom view of slab I after failure.

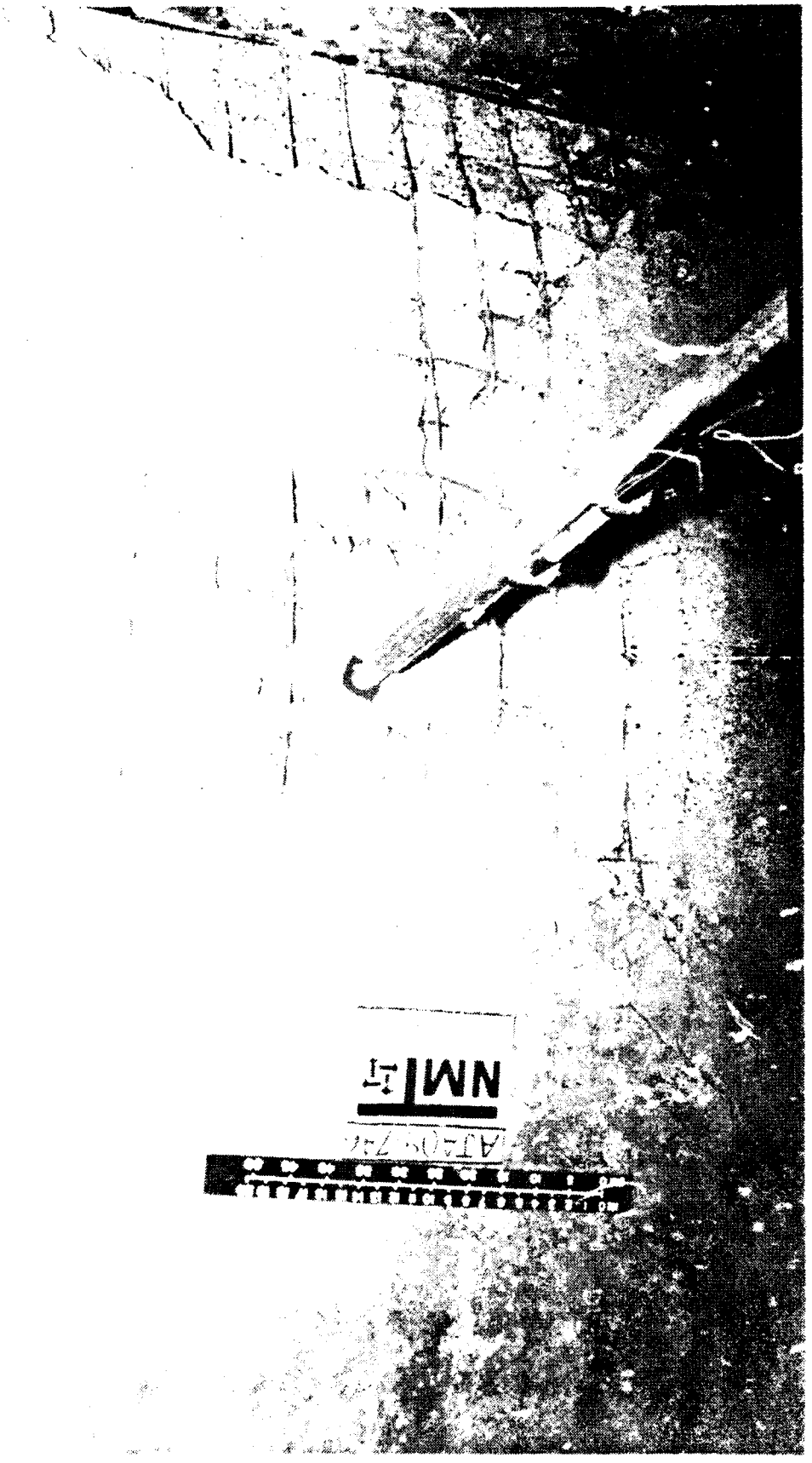

Figure 29
Bottom view of slab V after failure.

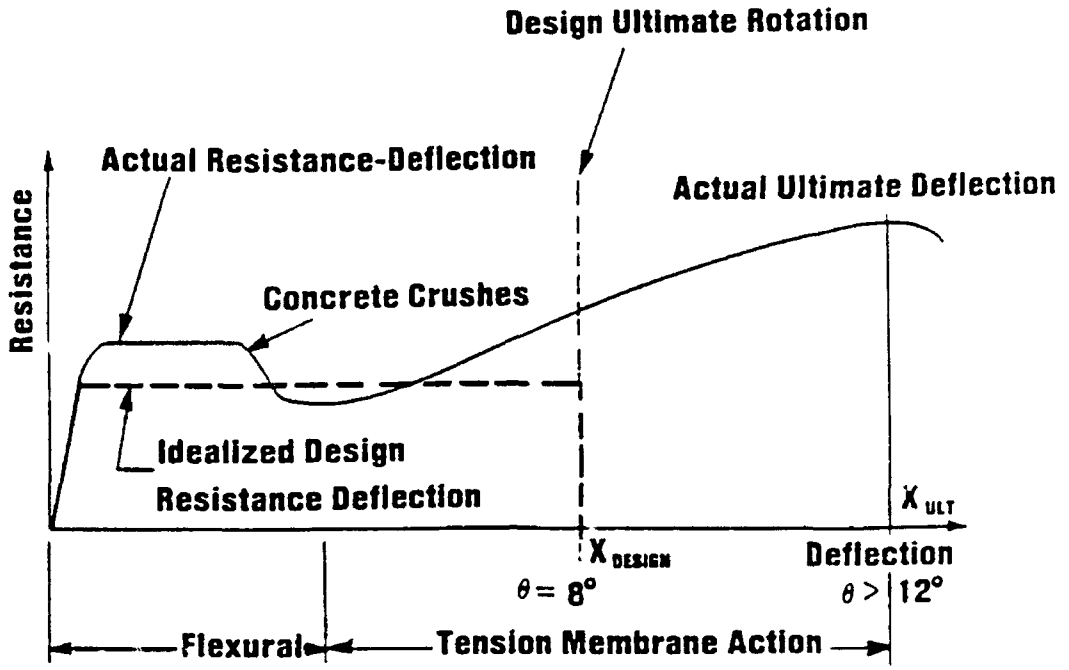

Figure 30
Resistance function for SDOF models of slabs.

In all cases, predictions from SDOF models were less than the measured deflections at the slab centers. Even the upper bound values (maximum design response) of 6.8 and 6.9 inches were less than the measured residual deflections of 8 and 8.3 inches for slabs I and V. Although these predictions are only about 15 percent off, they are unconservative. This could be due to the fact that the codified SDOF methods used here assume a uniform (average) load distribution, whereas the present test data refer to very close-in explosions (small-scaled distances) which will focus the load at the center of the slab.

Computed Response with DYNA3D

Figures 31 through 33 show the dynamic response of both slabs I and V using DYNA3D, and compares them with the response from codified SDOF methods as well as with measured residual displacements. Initially a uniform load condition was employed to provide a more direct comparison with the SDOF methods (Figures 31 and 32), then a more realistic, nonuniform load condition was used (Figure 33). Material models 16 and 17 were both used for concrete where indicated in the figures.

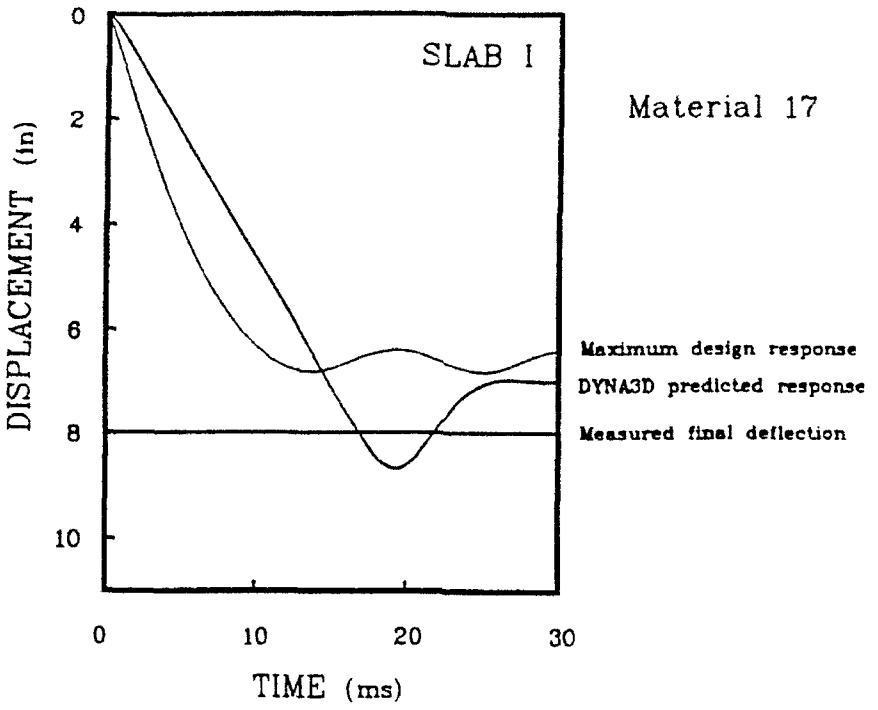

(a) Vertical Deflection, Center of Slab I

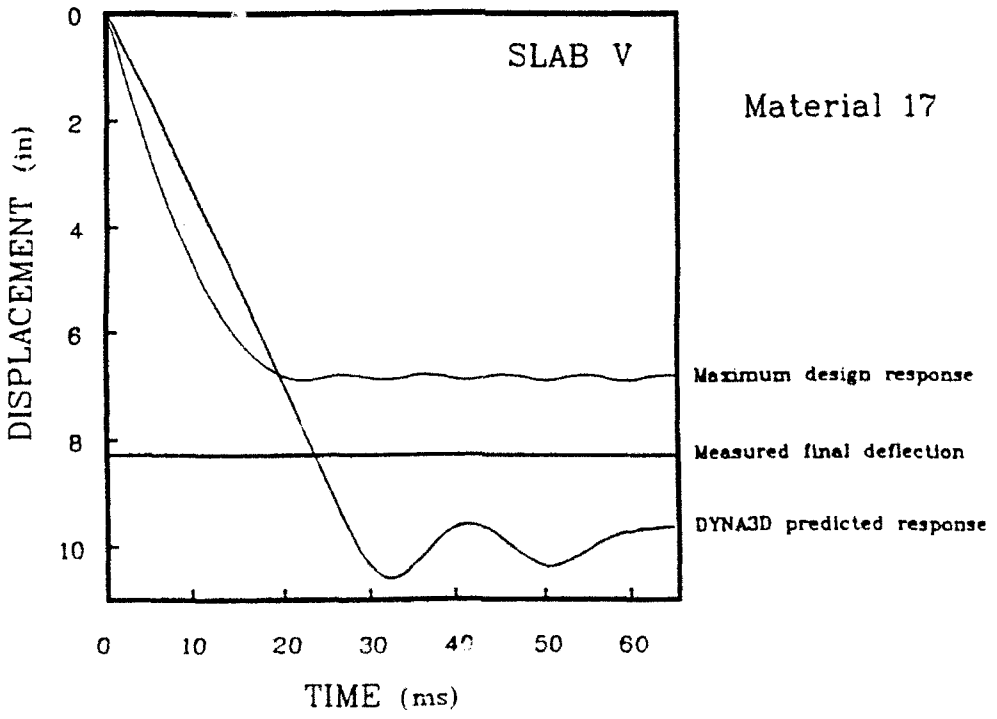

(b) Vertical Deflection, Center of Slab V

Figure 31
Predicted responses using Material 17 and uniform load.

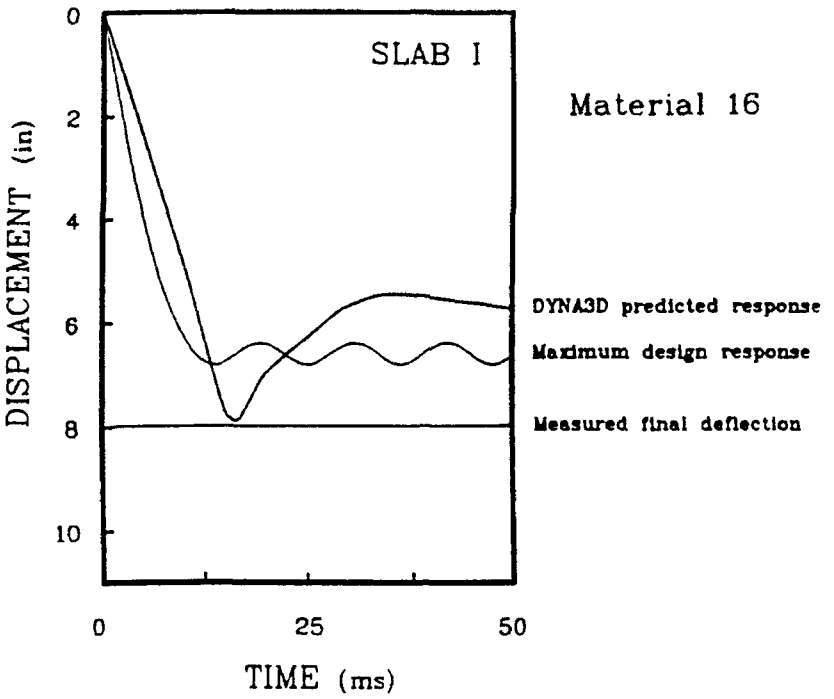

(a) Vertical Deflection, Center of Slab I

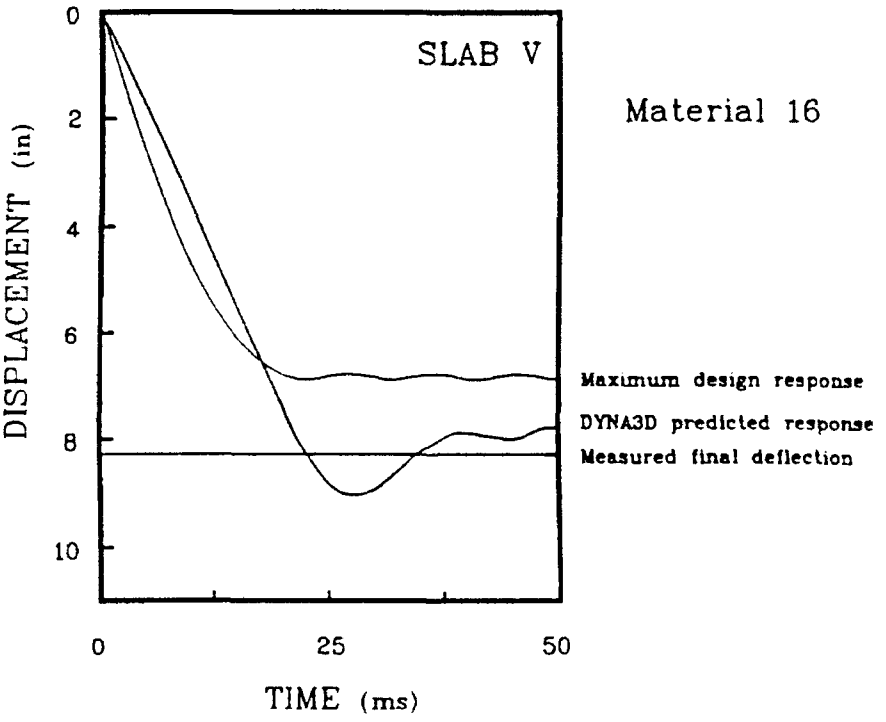

(b) Vertical Deflection, Center of Slab V

Figure 32
Predicted responses using Material 16 and uniform load.

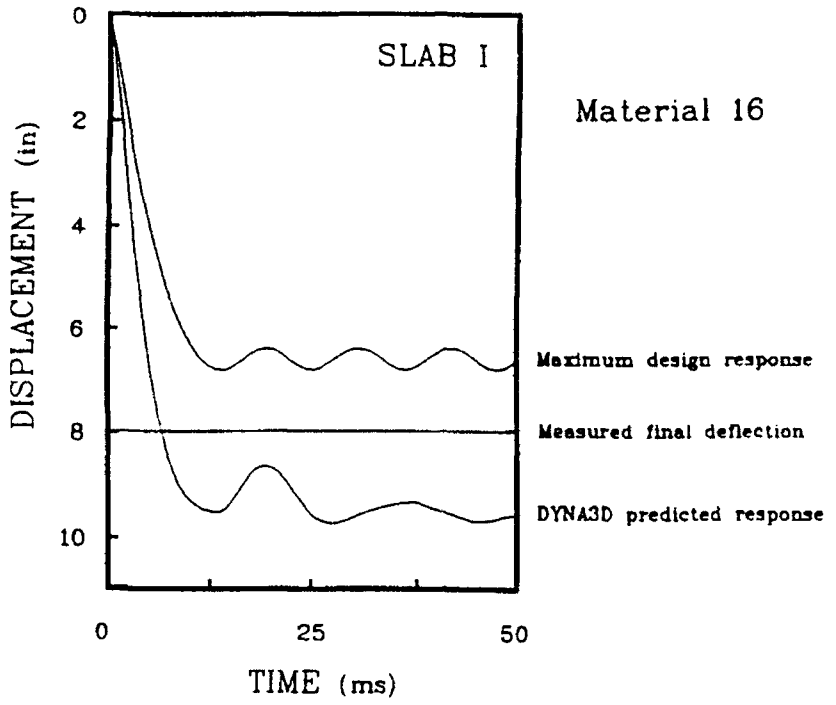

(a) Vertical Deflection, Center of Slab I

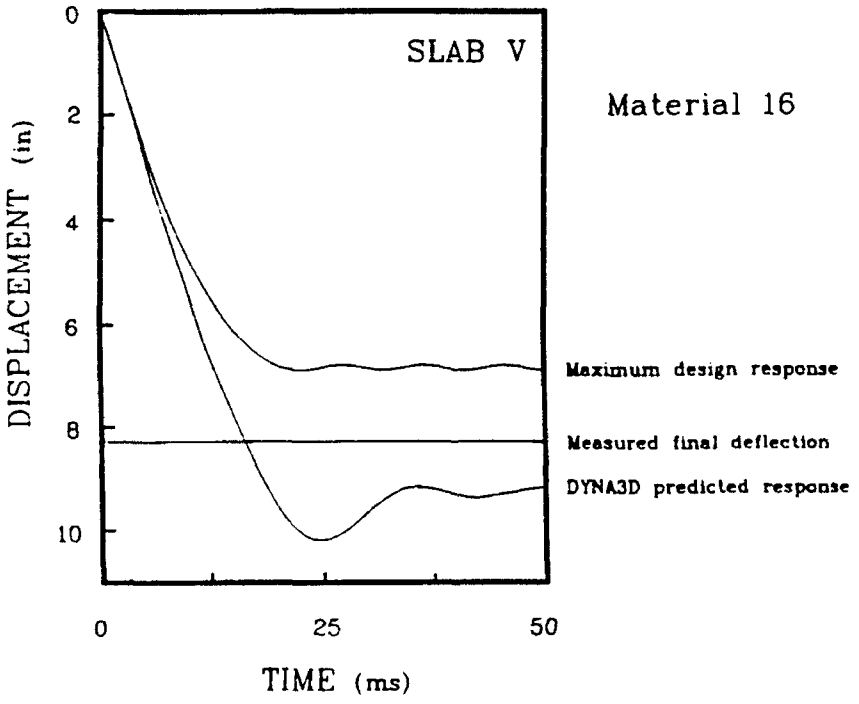

(b) Vertical Deflection, Center of Slab V

Figure 33
Predicted responses using Material 16 and variable load.

Initial DYNA3D analyses of both slabs using Material 17 and a uniform load distribution yielded residual deflections which were in closer agreement with experimental results than the SDOF method (Figure 31). Since Material 17 did not satisfactorily represent concrete behavior beyond crushing (Appendix C), Material 16 was then used. Computations based on Material 16, due to its post-crushing resistance, yielded smaller deflections than those based on Material 17 (Figure 32). For slab I, the computed residual deflection was unconservative, although the computed maximum response was close to the measured residual deflection. For slab V, the DYNA3D calculations were much improved and within 5 percent.

It was expected that a nonuniform load distribution would produce more accurate results, and yield larger deflections. This is verified in Figure 33 where, for the same Material Model, the maximum response for both slabs have increased by 20 percent for the nonuniform load case. Further, the DYNA3D calculations yielded conservative values for residual deflection in both slabs.

The measured residual deflections fall between the residual deflections computed by DYNA3D for the uniform and nonuniform load cases (Figures 32 and 33). The initial velocities (slopes) for the SDOF predictions fall between the initial velocities for the DYNA3D predictions for the uniform and nonuniform load cases.

Figure 34 shows the deformed shape of slab I at peak displacement, under uniform and nonuniform loads. Figure 35 shows the deformed shape of slab V at 50 ms, and in Figure 35b the vertical displacements have been enhanced by a factor of 4 to illustrate the discontinuity in the displacement gradient.

Figures 36 and 37 indicate the stress-time history of the main steel reinforcement bars at the slab center for both slabs as calculated by DYNA3D. Both the top and bottom steel go into compression (less than 16 ksi for both slabs) for a very short time during the initial shock phase of the load. Thereafter, both top and bottom steel go into tension, indicating that membrane action is taking place in the slabs. Yielding of the bottom steel occurred at about 4.7 ms and 5.5 ms, respectively, for slabs I and V. The prescribed yield stress (97 ksi) and strain hardening behavior are clearly indicated in these results.

During the subsequent rebound phase, the DYNA3D calculations indicate that both top and bottom bars go into a relatively high apparent compression state, reaching almost yield stress for the case of slab I. Since the reinforcement was not prevented from buckling, these elevated compressive states most likely did not occur. However, these calculations did indicate that buckling of the top and bottom reinforcement should have occurred. Indeed, it is apparent that buckling did actually take place during the rebound phase from the post-test photographs of the slabs (Figures 28 and 29).

As a consequence, the calculated rebound in the dynamic response of the slabs (Figure 33) may have been underpredicted because the finite element model of the slabs overestimates lateral resistance by having ignored the effect of buckling in the reinforcement. The numerical model would then also predict an excessive residual displacement. This would explain the difference between measured and computed residual displacements.

A typical DYNA3D analysis with a nonlinear load distribution and a simulation time of 50 ms would involve about 9,000 time steps and would require about 8,800 seconds (CPU time) on a SUN Sparc 2 workstation.

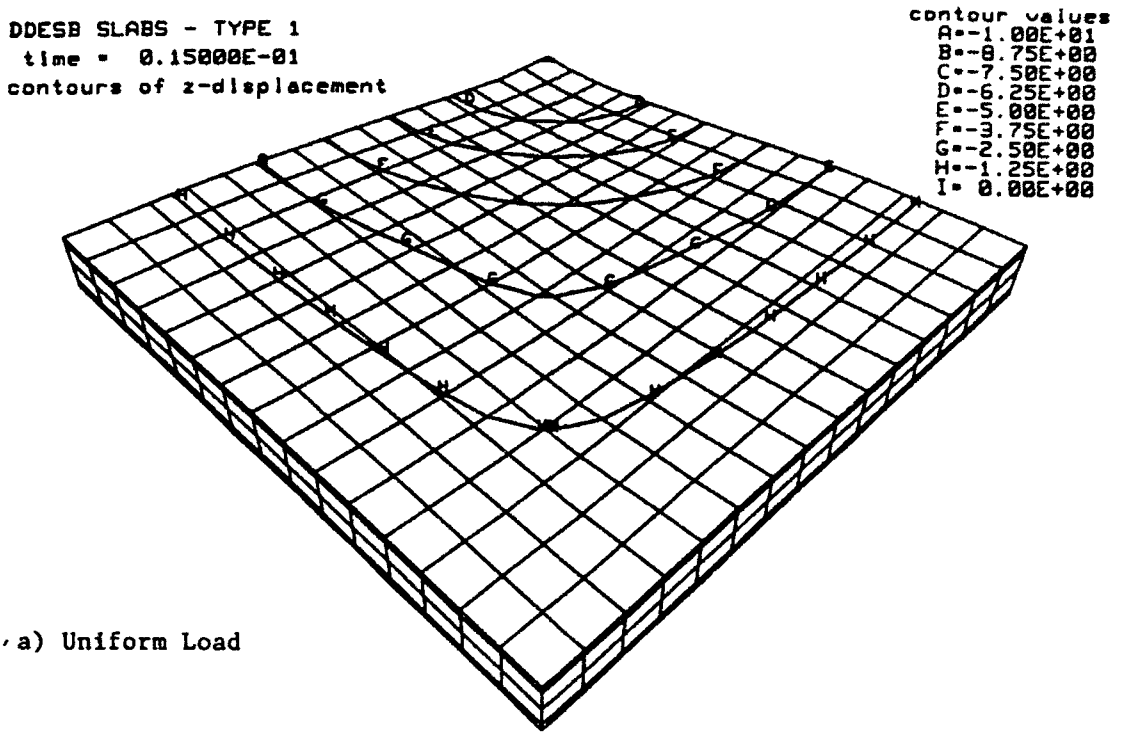

a) Uniform Load

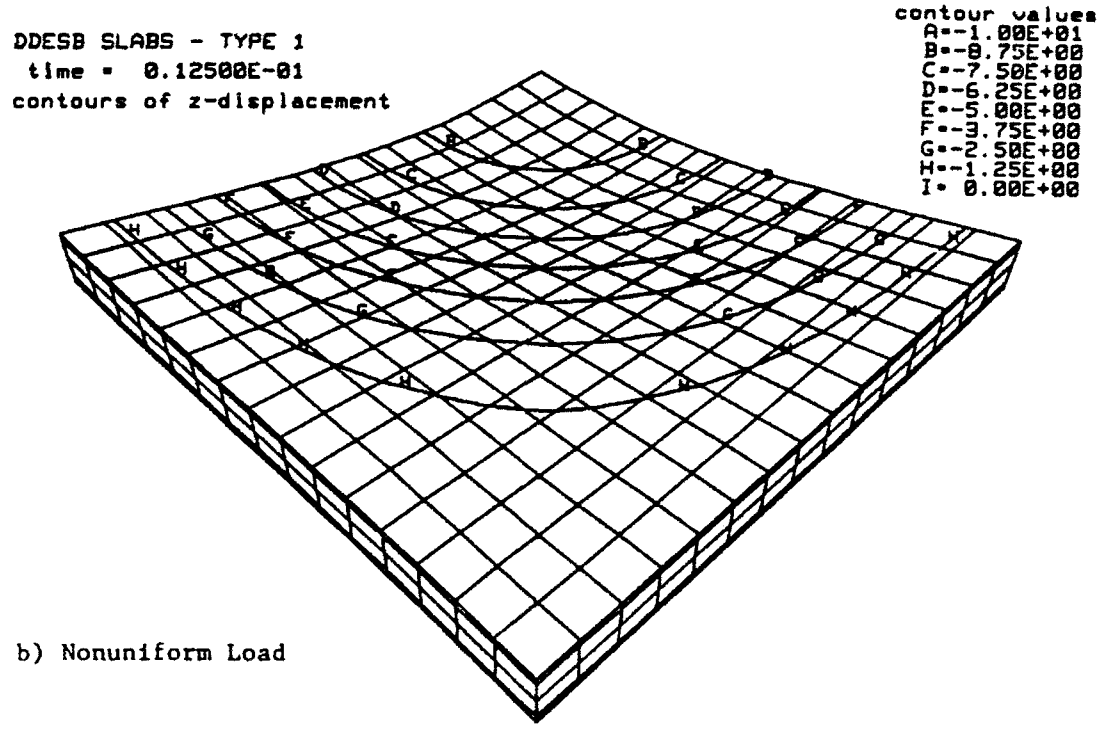

b) Nonuniform Load

Figure 34
Deformed shape of slab I at peak displacement.

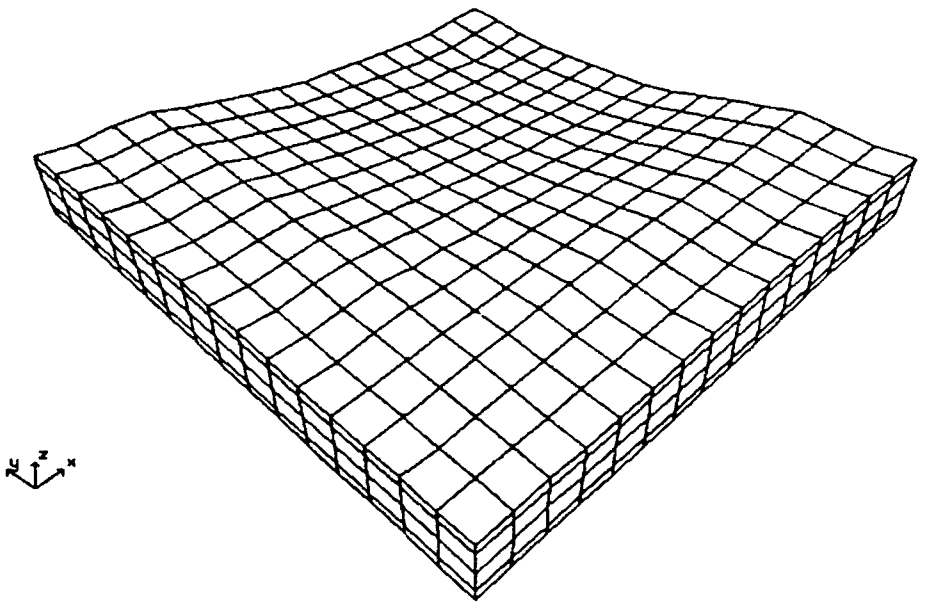

(a) Displacement scale factor = 1

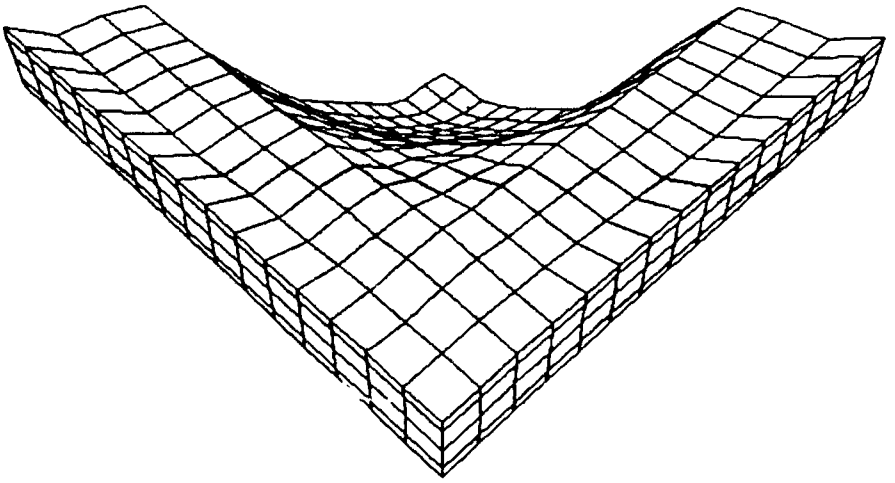

(b) Displacement scale factor = 4

Figure 35
Deformed shape of slab V at 50 ms.

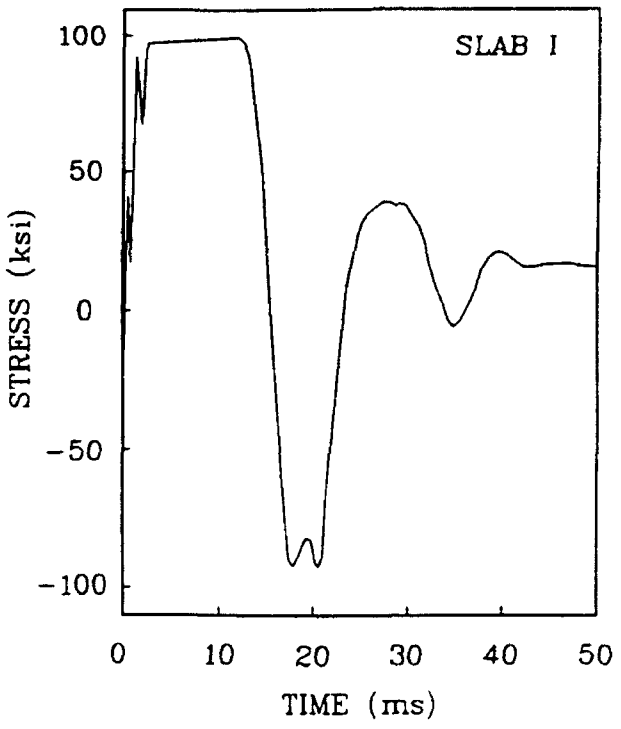

(a)
Material 16
Nonuniform Load
Center, Top Bar

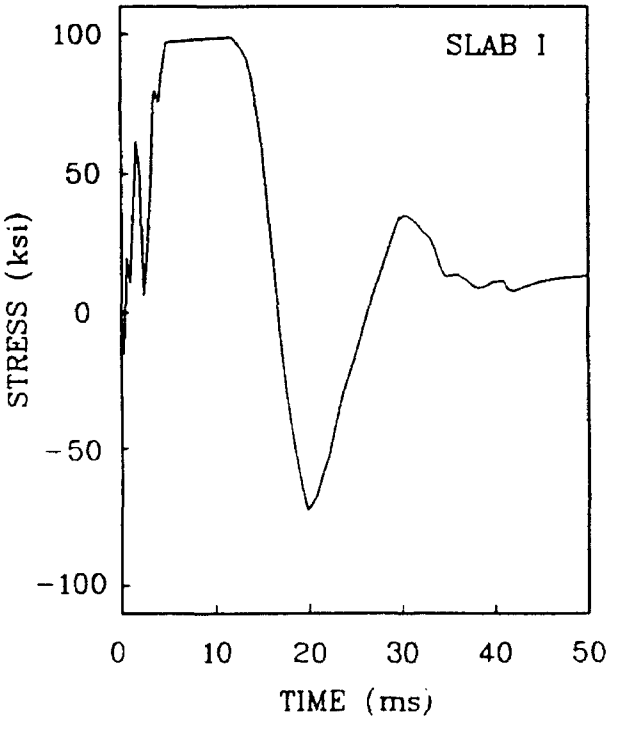

(b)
Material 16
Nonuniform Load
Center, Bottom bar

Figure 36
Top and bottom center bars stress-time history, slab I.

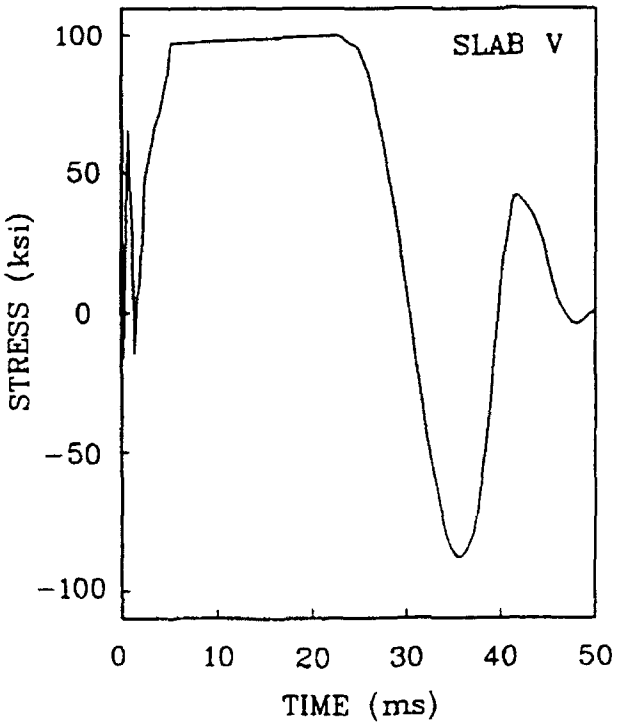

(a)
Material 16
Nonuniform Load
Center, Top Bar

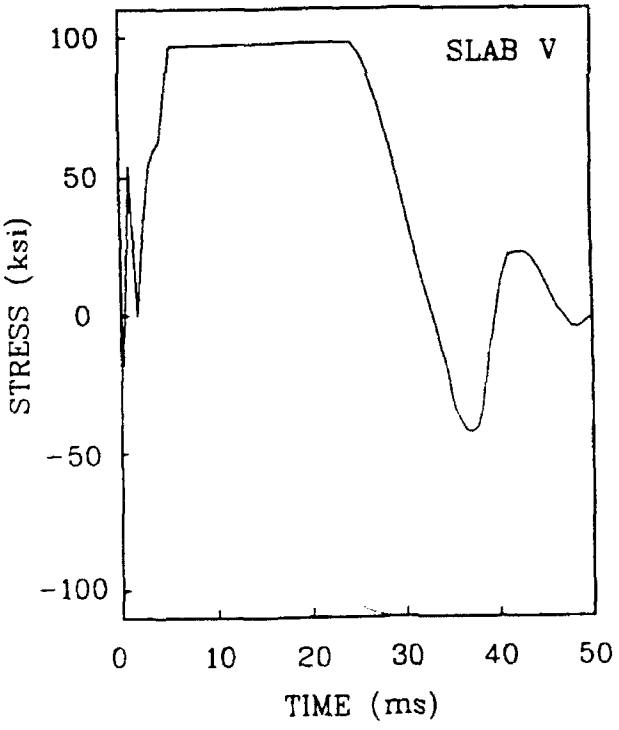

(b)
Material 16
Nonuniform Load
Center, Bottom bar

Figure 37
Top and bottom center bars stress-time history, slab V.

In Figure 34, the contours of vertical displacement are mostly circular toward the center of slab I. Toward the edges, however, they appear to show increased deflections along the slab diagonals. This points to the formation of classical yield lines as were found experimentally (Figure 26). For slab V, however, the observed yield lines were circular and more pronounced (Figure 27). The numerical model predicted a circular localized deformation with a radius of 36 inches (Figure 35a), which was very similar to the observed yield line.

There is little guidance for the design of confinement steel reinforcement for blast-loaded reinforced concrete slabs. It has been suggested that seismic design criteria be considered. For seismic design of reinforced concrete flexural members, the ACI code (ACI, 1989) requires transverse reinforcement spacing to be the least of: (1) d/4, where d is the effective depth of the section, (2) eight times the diameter of the smallest longitudinal bar, (3) 24 times the diameter of the hoop bars, and (4) 12 inches. The purpose of this transverse reinforcement is to provide for lateral confinement of the compression steel and prevent it from buckling during the formation of plastic hinges. Since the codified SDOF method employs yield line theory in the evaluation of slab resistance, stability of compression bars is also implied in this method.

It was discovered that buckling of the reinforcement did occur in both slabs during the rebound phase. However, preventing this buckling may or may not be critical to the designer who is often concerned with only maximum dynamic response. During the very initial loading phase, the compression stresses which were noted in the reinforcement, are much lower, and the duration of this compression is very short, indicating that no premature bar buckling would take place, and that the slab resistance would likely not be adversely affected. Therefore, from these limited results, it appears that consideration of additional transverse steel for confinement purposes may not be necessary to ensure the integrity of useful (pre-rebound) slab resistance.

SUMMARY

The dynamic responses of reinforced concrete slabs were calculated by using codified SDOF models and DYNA3D finite element models of the slabs. The results were compared with each other and with limited measurements from two field-tested slabs.

Measured residual deflections exceeded residual deflections computed by using codified SDOF models, which provide for tensile membrane action, by about 30 percent. These predictions were unconservative. The discrepancy is believed to be due to the assumption of uniform load distribution over the surface of a slab. This condition does not apply to close-in explosions, and codified procedures should consider nonuniform load conditions for these cases. Measured residual deflections exceeded codified SDOF maximum design predictions which were based upon a simplified resistance function by about 15 percent. These predictions were also unconservative, but were close to DYNA3D predictions with uniform loading.

Measured residual deflections fell between the residual values predicted by DYNA3D assuming uniform and nonuniform load cases and using Material Model 16 for concrete. Calculations with nonuniform loading exceeded measured residual deflections by about 15 percent. DYNA3D calculated failure modes which were similar to those observed in both slabs. These failure modes appeared to be consistent with yield line theory even though test standoff distances were small. The DYNA3D results also predicted potential buckling in the reinforcement, which was in fact observed in post-test photographs. This observation also provided an explanation for the noted discrepancy in residual deflection, because the DYNA3D finite element model did not account for the reduction in slab bending resistance that would

accompany rebar buckling. This is also true of the SDOF models, except that the corresponding discrepancy is exacerbated because the deflections were unconservative. It was found that additional transverse reinforcement for confinement purposes may not be warranted for the case of clamped slabs when design performance is largely based upon the maximum dynamic response.

The use of DYNA3D provided an inexpensive and accurate way to obtain detailed information on the dynamic response of reinforced concrete slabs which is not available using codified SDOF models.

SECTION 3

NONLINEAR DYNAMIC FINITE ELEMENT ANALYSIS OF A SOIL-COVERED ROOF SLAB SUBJECTED TO AN INTERNAL BLAST LOAD

INTRODUCTION

The explicit finite element code DYNA3D was applied to a problem involving much higher blast pressure loads on reinforced concrete. A high performance magazine concept which includes a soil-covered roof slab is currently under development at NCEL. The roof slab was the subject of this demonstration of nonlinear dynamic finite element technology. The demonstration features hydrodynamic behavior in the material model which was employed for concrete.

OBJECTIVE

The objective of the numerical analysis was to determine the dynamic response of the roof slab due to a very high pressure explosion in one of the cells of the high performance magazine. This includes an evaluation of DYNA3D's material models for their suitability to high pressure behavior. In addition, the determination of the velocity field for the concrete fragment debris which emanated from the failed slab was also an important objective.

BACKGROUND

The function of the high performance magazine concept is storage of large amounts of munitions in a small area so as to reduce the encumbered land around storage facilities required for safety. Preliminary design for the magazine involves a large buried structure with munitions stored in "cells," as shown schematically in Figure 38. The cells are designed so an explosion in one cell will not propagate to the remainder of the magazine. Thus, the safe distance is a function of the explosive charge in a single cell, not the entire magazine.

The roof is a 2-foot-thick reinforced concrete slab constructed using 4,000-psi concrete weighing 150 lb/ft^3 with top and bottom reinforcement consisting of Grade 60, #9 bars running in both directions at 10 inches on center. Shear reinforcement consisting of Grade 60, #4 bars connects each intersection of the longitudinal bars across the top and bottom of the slab.

In the design, the roof primarily functions as a one-way, simply supported slab carrying 4 feet of soil cover weighing 110 lb/ft^3. It is supported only by the outer walls and the middle wall in the long direction, and it is only lightly connected to these walls. It offers no structural resistance to uplift due to the explosion, only inertial resistance. The soil cover is designed to provide mass for kinetic dissipation of the blast energy. It is presumed to be unreinforced and therefore elastic resistance forces are negligible. Only inertial resistance forces are contributed by the soil cover.

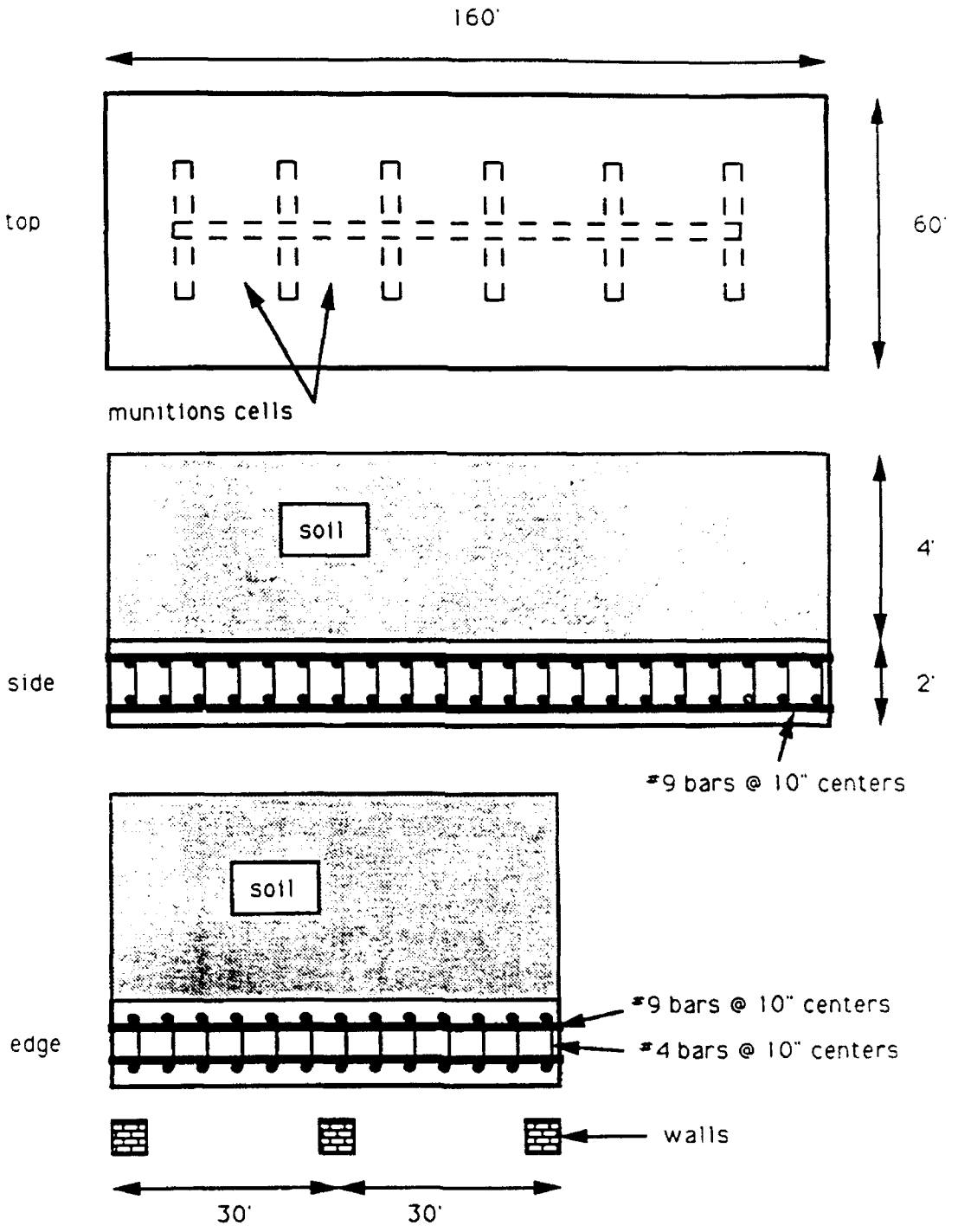

Figure 38
Preliminary design concept for high performance magazine roof.

LOADING

The walls of the cells are designed to prevent an explosion in one cell from detonating the munitions stored in adjacent cells (sympathetic detonation). The roof, however, will be subjected to the full force of the explosion and is designed to suffer considerable damage and absorb most of the energy released from the explosion. Due to the cell arrangement, the blast load on the slabs will be off center and nonuniform, as shown in Figure 39a.

Blast load pressure descriptions were obtained using the program SHOCK.* A charge of 10,000 pounds detonated in a central cell was simulated. Figure 39a shows the shock wave scaled impulse loading (units are psi-ms/$lb^{1/3}$). Pressure values are obtained from:

$$P = \frac{2I}{t}$$

where I = scaled impulse x 24.27 (scaling factor, $lb^{1/3}$)
t = load duration (assumed constant over the roof)
= 4.06 ms

The maximum load time history at a point above the charge is shown in Figure 39b. It includes both the shock load and the gas pressure. The gas pressure is relatively low but lasts for close to 20 seconds.

FINITE ELEMENT MODEL

The description of the roof slab finite element model is divided into two sections, the finite element discretization and the material models.

Reinforcement and Roof Slab Discretization

A discrete reinforcement model of the steel in the roof was implemented. This method is more accurate than a smeared or an embedded reinforcement model when reinforcement patterns are regular. Although an embedded model would have been more efficient and sufficiently accurate, it is not available in DYNA3D. Top and bottom steel meshes were modeled using 10,706 discrete 2-node truss elements. The concrete slab was represented by 3,456 8-node three-dimensional solid elements. Two were used through the 2-foot depth of the slab. The model had a total of 5,436 nodes and about 16,000 degrees of freedom.

Top and bottom steel truss elements were located at 20 inches on center, twice the actual rebar spacing. Each truss modeled the cross-sectional area of two bars lumped together. Similarly, the shear reinforcement was lumped at 20 inches on center, with each truss modeling the cross-sectional area of four bars lumped together.

*Naval Civil Engineering Laboratory. SHOCK User's Manual, Version 1.0. Port Hueneme, CA, Jan 1988. The user's manual has not been published as of this writing.

To simplify the model further, the soil cover was not modeled directly. Its mass was added to the core of the concrete slab. Element generation was carried out using INGRID (Stillman and Hallquist, 1985) with the help of a custom-made preprocessor written specifically for this project.

A top view of the finite element mesh is shown in Figure 40. The single plane of symmetry for this problem is exploited through assignment of appropriate boundary conditions. Otherwise, assigned boundary conditions at the supports replicated a free/free slab boundary condition. Figure 41 details the mesh cross section at several locations though this figure is not to scale (e.g., the middle wall is actually centered). Finite element results were subsequently retrieved at the identified element and node locations.

Reinforcement and Concrete Material Models

Material Model 3, an elastic-plastic model, was selected (see Appendix C) to model the behavior of steel rebar. This was the material model used for rebar in the foregoing section on reinforced concrete slabs. Based on the limited experience discussed, the following properties were prescribed:

Young's modulus	E	=	29,000,000 ksi
Poisson's ratio	μ	=	0.3
Yield stress	σ_o	=	82.5 ksi (DIF 1.25)
Tangent modulus	E_t	=	447 ksi
Hardening parameter	β	=	1 (isotropic hardening)

For concrete, linear and nonlinear responses with Material Models 5, 16, 17, and 25 were evaluated. In the case of concrete, tension testing would reveal the nonlinear capacity of the model to represent cracking, whereas confined compression testing indicated the model's response to high hydrostatic stresses at points on the slab near the source point of the blast load.

Test input load data to evaluate the response of the solid element to controlled uniaxial strain with various material models is indicated in Table 9.

Table 9
Material Test Loads

Direction of Loading	Compression Tests	Tension Tests
x	$\epsilon_x = 0$ to -0.024	$\sigma_x = 0$
y	$\epsilon_y = 0$	$\epsilon_y = 0$
z	$\epsilon_z = 0$	$\epsilon_z = 0$ to 0.002

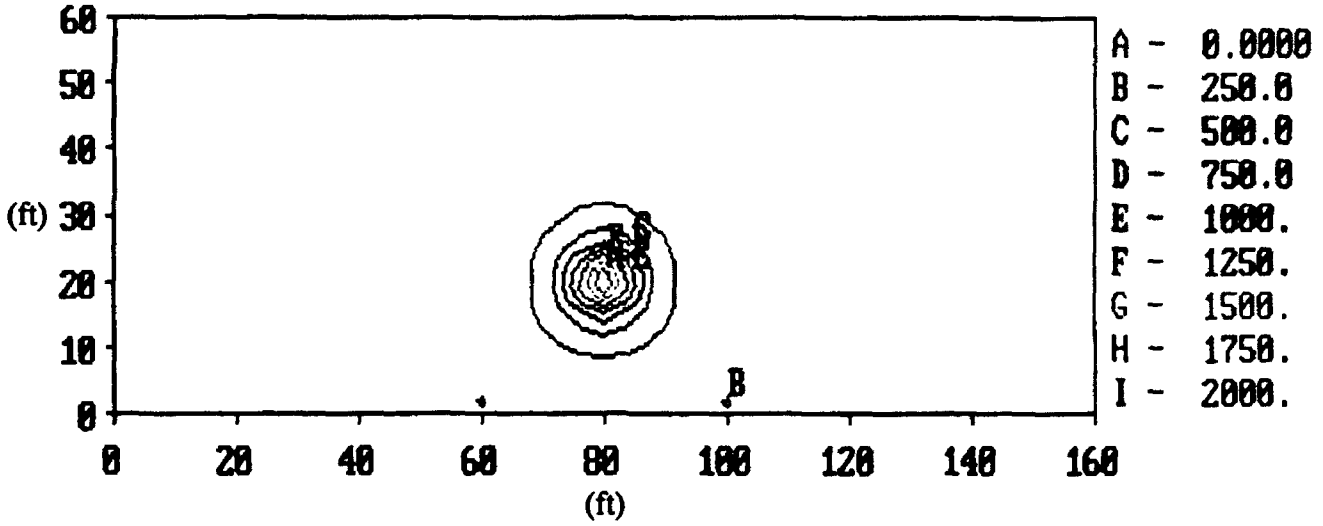

(a) Scaled shock impulse distribution (psi).

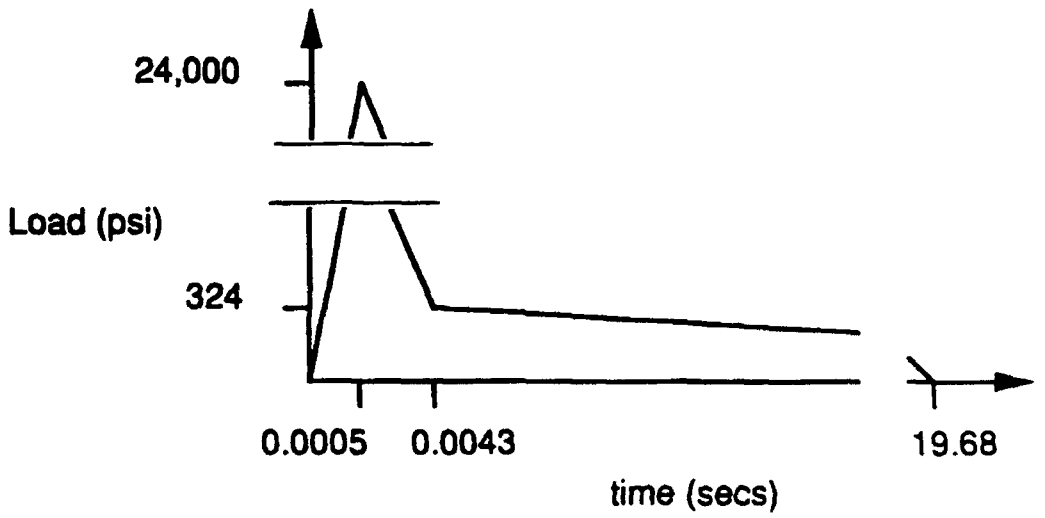

(b) Load history at maximum location point.

Figure 39
Design roof slab load.

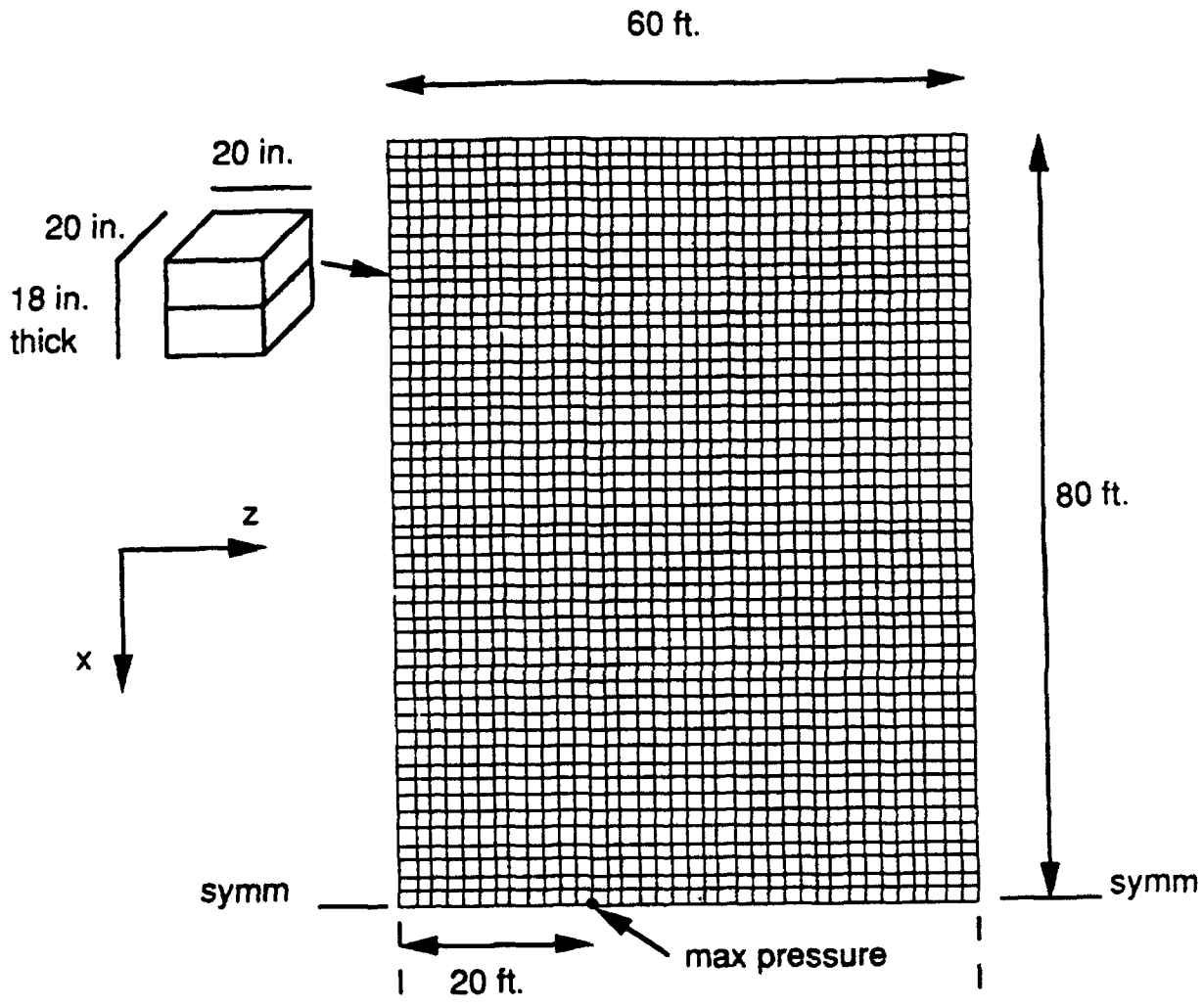

Figure 40
Finite element mesh.

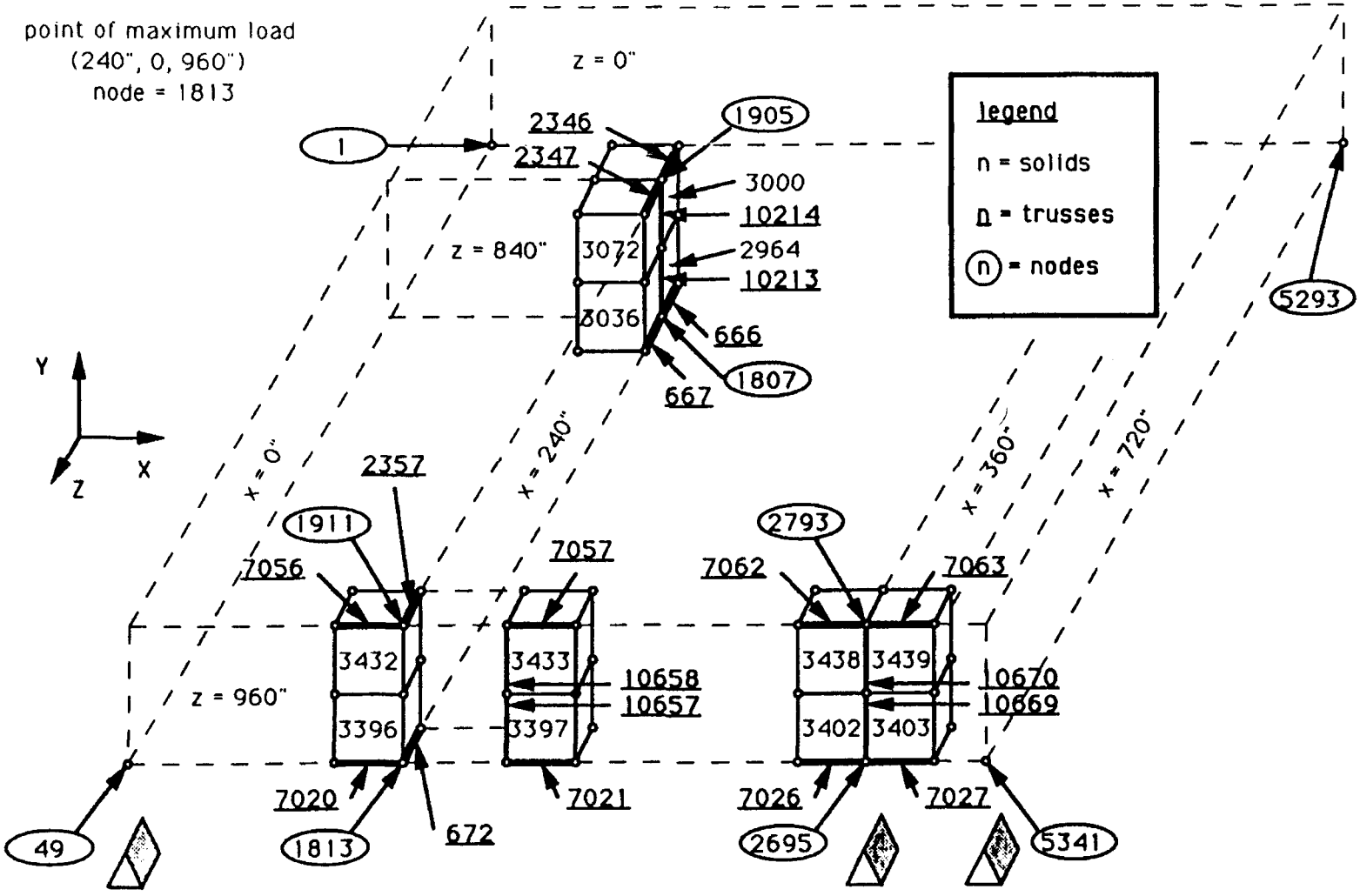

Figure 41
Significant nodes, solid and truss elements.

Material 17 showed normal behavior up to crushing but then abruptly dropped to zero. This model was to show a transition to fluid behavior to carry the hydrostatic pressures, but several attempts to incorporate the corresponding fluid equations of state proved futile (Appendix C).

Material 16 allows representation of steel reinforcement using a smeared model. With no smeared steel, it behaved as expected. However, with 2 percent smeared steel, the post-cracking behavior in tension was again excessively stiff, i.e., the yield strain was about one-sixth the expected value (Appendix C). A default equation of state was prescribed to handle hydrodynamic material behavior beyond yield stress. This equation is internally generated by DYNA3D.

Materials 5 and 25 are discussed in Appendix C (see also Ju, et al., 1985). Both Materials 5 and 25 exhibited acceptable response in compression but did not release the tensile stresses in tension upon cracking, therefore they did not properly represent true concrete behavior.

For modeling concrete, Material 16 (with no smeared steel) was used exclusively with the following properties:

Poisson's ratio	μ	=	0.2
Compressive strength	f_c'	=	6,000 psi
Cohesion	a_0	=	-1

DYNA3D internally generates the remaining concrete properties. Yield stress and compressive strength were adjusted upward to account for strengthening due to high strain rates.

A summary of this material model study is given in Table 10.

NONLINEAR DYNAMIC RESPONSE OF SOIL-COVERED ROOF

Two aspects of the soil-covered roof slab are important to its design, the dynamic response and the distance over which the debris from the reinforced concrete slab will travel.

Response and Yield Behavior

The deformed shape of the roof slab (enhanced five times for clarity) is shown in Figure 42 at two different time steps. The load is clearly of such an intensity that the roof fails by breaching rather than by flexure. Figure 43 shows the dynamic response at five selected node points, the four corners of the mesh and the point of maximum load (refer also to Figure 41). It is observed in the difference between these responses that these data show that the displacement field is very localized, consistent with a breach failure mode. However, there is clearly also a rigid body displacement component in the roof response. The entire soil-covered roof is predicted to lift off the walls about 8 inches at 30 ms.

Table 10
Summary of DYNA3D Reinforced Concrete Material Model Study*

Material Model	Concrete Behavior		Steel Reinforcement Model		
	Compression	Tension	Smeared	Embedded	Discrete
#5 Soil/Foam	Okay	Erratic after cracking	No	No	Yes
#16 Concrete/ Geological	Okay	Okay	Yes	No	Yes
#17 Isotropic Concrete	Unreliable after crushing	Okay	No	No	Yes
#25 Concrete Cap	Okay	Nonzero after cracking	No	No	Yes

*Model #5 is often used for gross concrete.
Model #16 is recommended for this study.
Model #17 is not well supported at LLNL.
Model #25 is the latest model.

Figure 44 shows the response for concrete stress in the plane of the roof slab in four elements near the point of maximum load (Figure 41). Upon arrival of the shock wave, the concrete goes temporarily into compression, then unloads, cracks in tension, and loses all load-carrying capability within the first 4 ms. The two elements closest to the load are subjected to a longer lasting and more severe compression, as should be expected due to local bending action. Cracking of the top elements occurs at 2.5 ms. After element cracking, the concrete mass is still acting on the system. It is expected that the concrete cover would then begin to separate from the roof slab and generate debris. Figure 45 shows the vertical stress response in the same four elements. They are very similar since these stresses are indicative of the shock wave traveling through the slab thickness.

Contours of effective plastic strain (strain in excess of yield) are shown in Figure 46, indicating the localized nature of the plastic deformation. At 17 ms this is the extent of the roof surface involving yield in the concrete. Its diameter is about 23 feet.

Figure 47 shows the stresses in ten lower reinforcing bars along the plane of symmetry, five on each side of the point of maximum load (see Figure 41). Some of these bars are seen to reach yield between 16 and 18 ms. At that point, it is expected that additional debris will begin to be generated and separate from the roof slab.

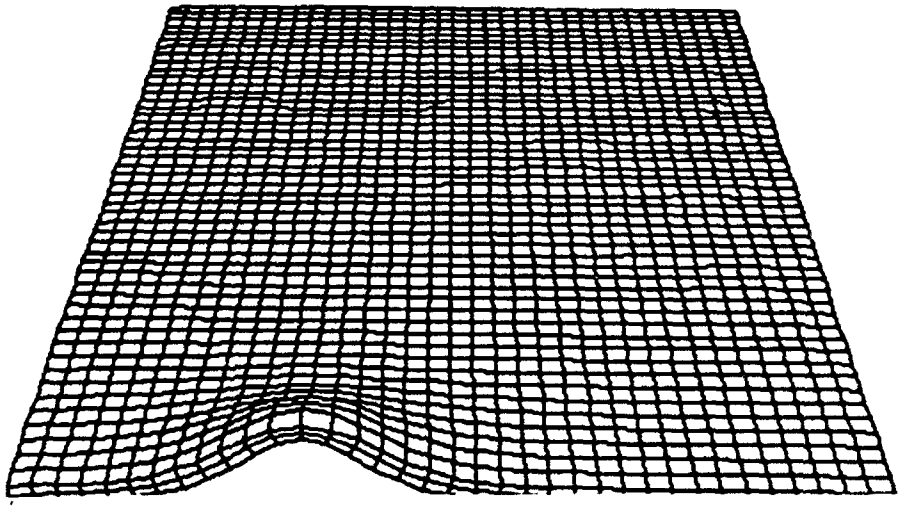

(a) Time = 7 ms.

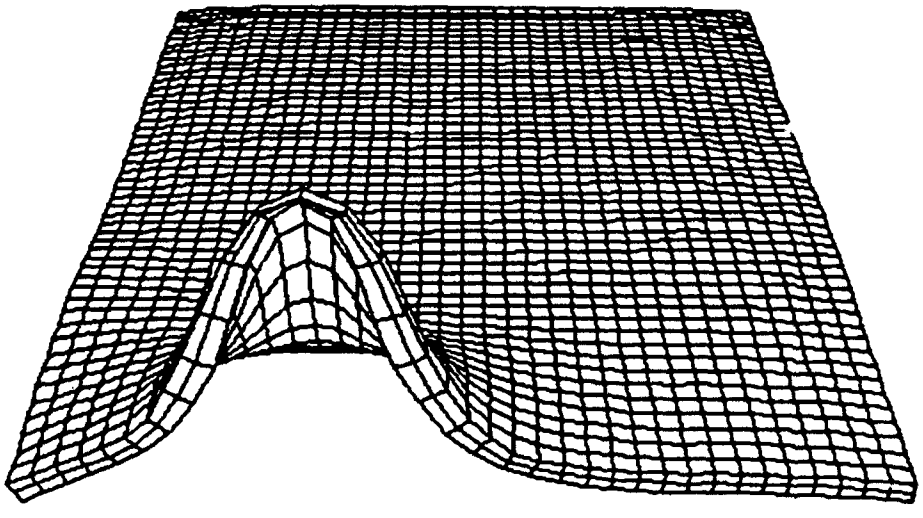

(b) Time = 27 ms.

Figure 42
Deformed shape (enhanced 5 times).

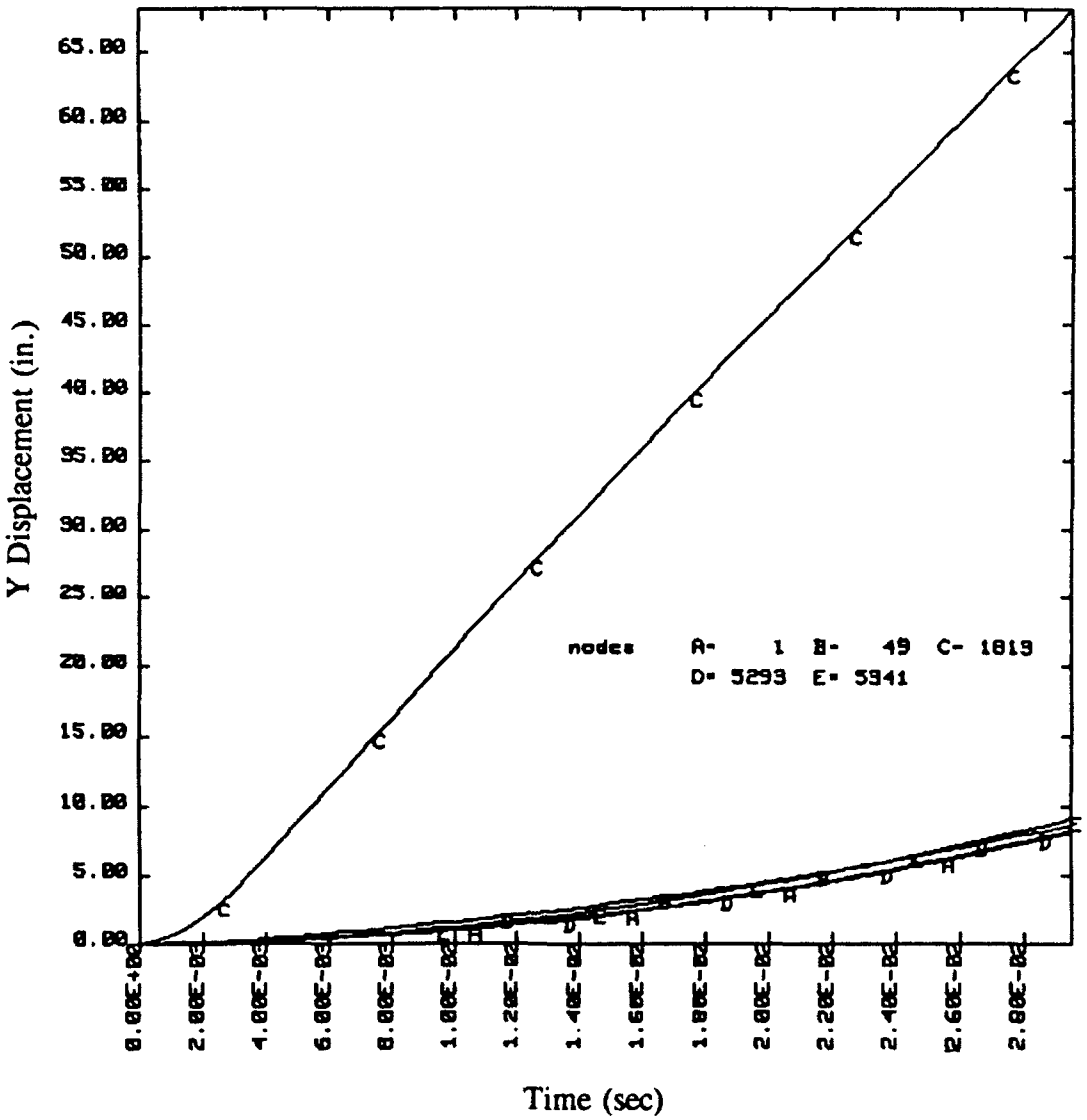

Figure 43
Dynamic response of soil-covered roof slab.

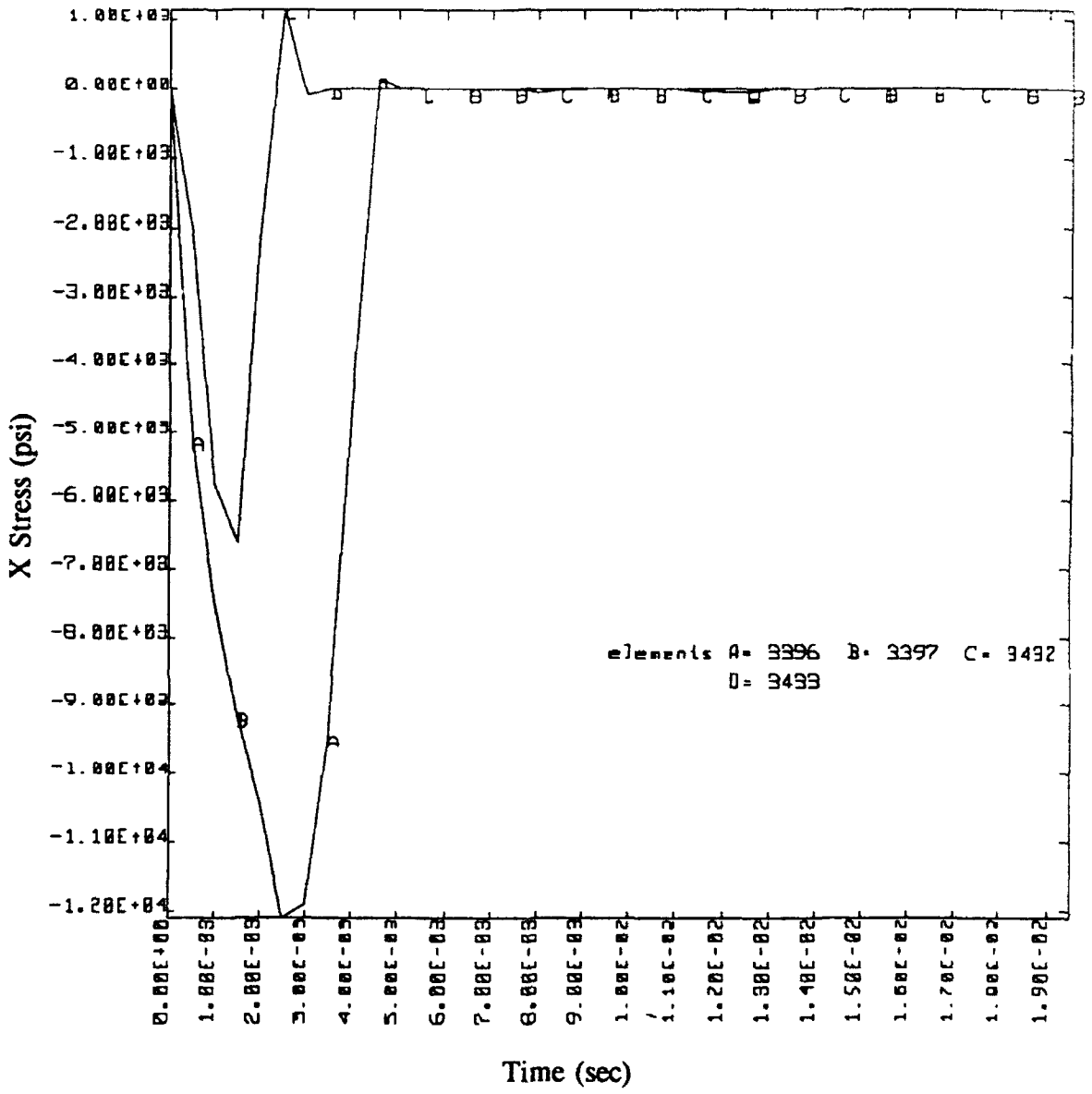

Figure 44
Horizontal concrete stresses.

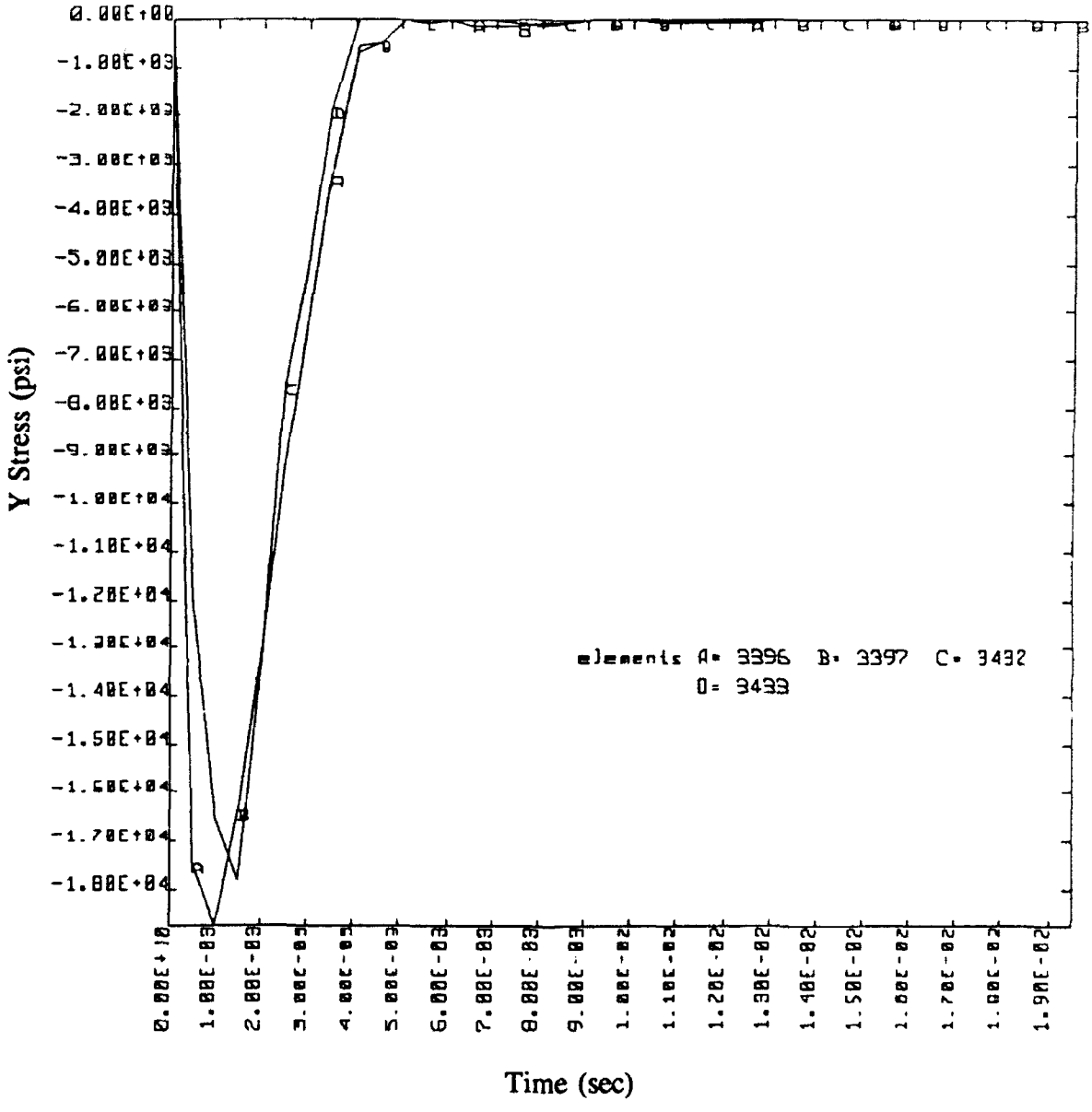

Figure 45
Vertical concrete stresses.

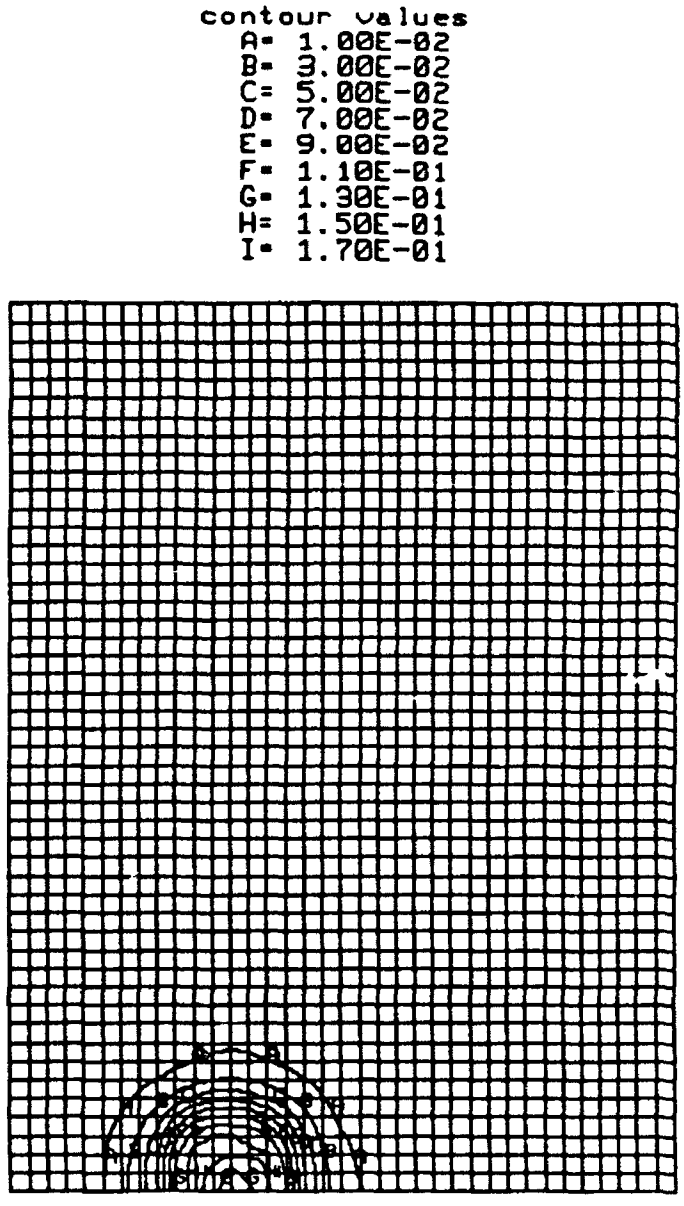

Time = 17 ms

Figure 46
Effective plastic strain in the roof slab.

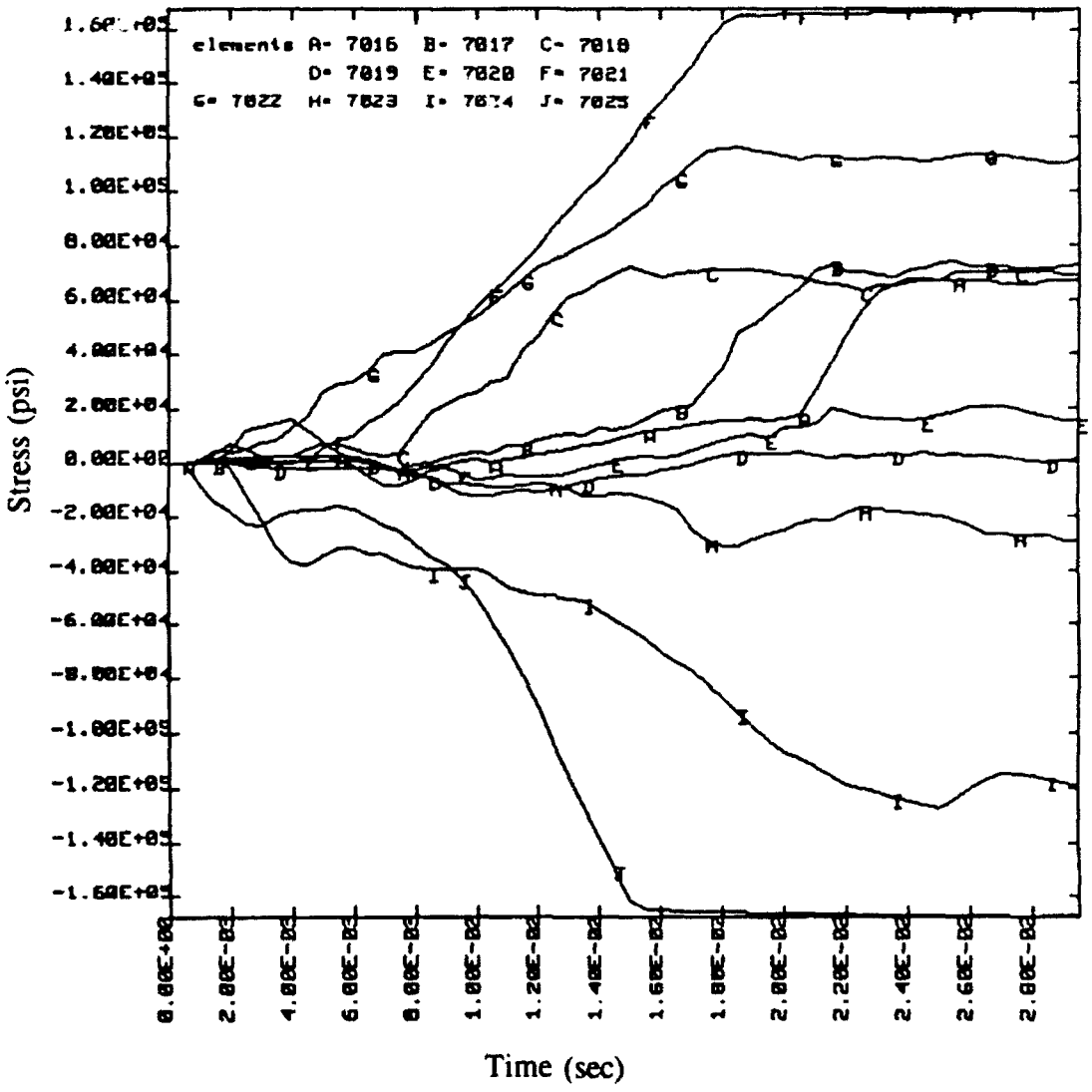

Figure 47
Reinforcing bar stress response.

Knowledge of velocity fields for the roof slab at various times is the basis for computing debris distance, which in turn will characterize the effectiveness of the proposed roof slab design. Figure 48 indicates the velocity time history at the five previously selected node points. The maximum velocity is 2,500 in./sec and it is reached at about 8.5 ms. Figures 49a and 49b show contours of the velocity field at times 7 and 27 ms, respectively. As evident in the latter figure, these velocity contour data are graphed along with the displacement field. These data therefore may be more easily related to initial debris velocities.

Relationship to Debris Distance

These calculations of the dynamic response of the high performance magazine roof slab indicate that blast effects on the roof will be very localized. NCEL tests on a one-tenth scale model of a high performance magazine (Murtha, 1992) confirmed the localization of the deformations and breaching of the roof above the cell which has been predicted by these results. The concrete directly above the blast should crush early, then carry the pressure hydrostatically during the shock load phase, i.e., the first 4 ms. Calculations also indicate that the rebar directly above the blast load will yield and should snap around 17 ms, reducing the concrete confinement and releasing parts of the roof slab as debris. The model does not allow for direct prediction of actual debris sizes and failure of bars, and the predicted response ceases to be strictly valid as soon as the reinforcing bars reach their ultimate capacity. However, debris distance predictions can be obtained indirectly as follows:

- Knowledge of the concrete stress field allows for the determination of time of debris separation.
- Knowledge of the velocity field as a function of time allows the determination of initial debris velocities.
- Once debris initial velocities are known, debris distances can be calculated.

In this regard, similar calculations of debris velocity using DYNA3D have been reported before (Terrier and Boisseau, 1989).

Recent independent calculations using the NCEL program FRANG (Wager and Connett, 1989) determined the average velocity of debris from a 16- by 28-foot breached area directly above the cell. The program FRANG calculates pressure histories resulting from an explosion in a room with vents and frangible panels (i.e., panels designed to break loose and provide additional vent areas). Displacement, velocity, and acceleration histories of the frangible panels are also determined.

It was found that for a 4-foot soil cover, the average maximum velocity of the debris would be 2,400 in./sec as shown in Figure 50. Those calculations assumed the fragments had been separated from the rest of the roof and the velocities were expected to be somewhat higher than the ones found with DYNA3D. From Figures 48 and 49 it is observed that the velocity field above the cell at 8.5 ms (maximum values) varies between 700 and 2,500 in./sec for an area of about 20 feet in diameter. Assuming the maximum velocity, zero drag and a 45-degree trajectory, the maximum throw distance would be 1,346 feet.

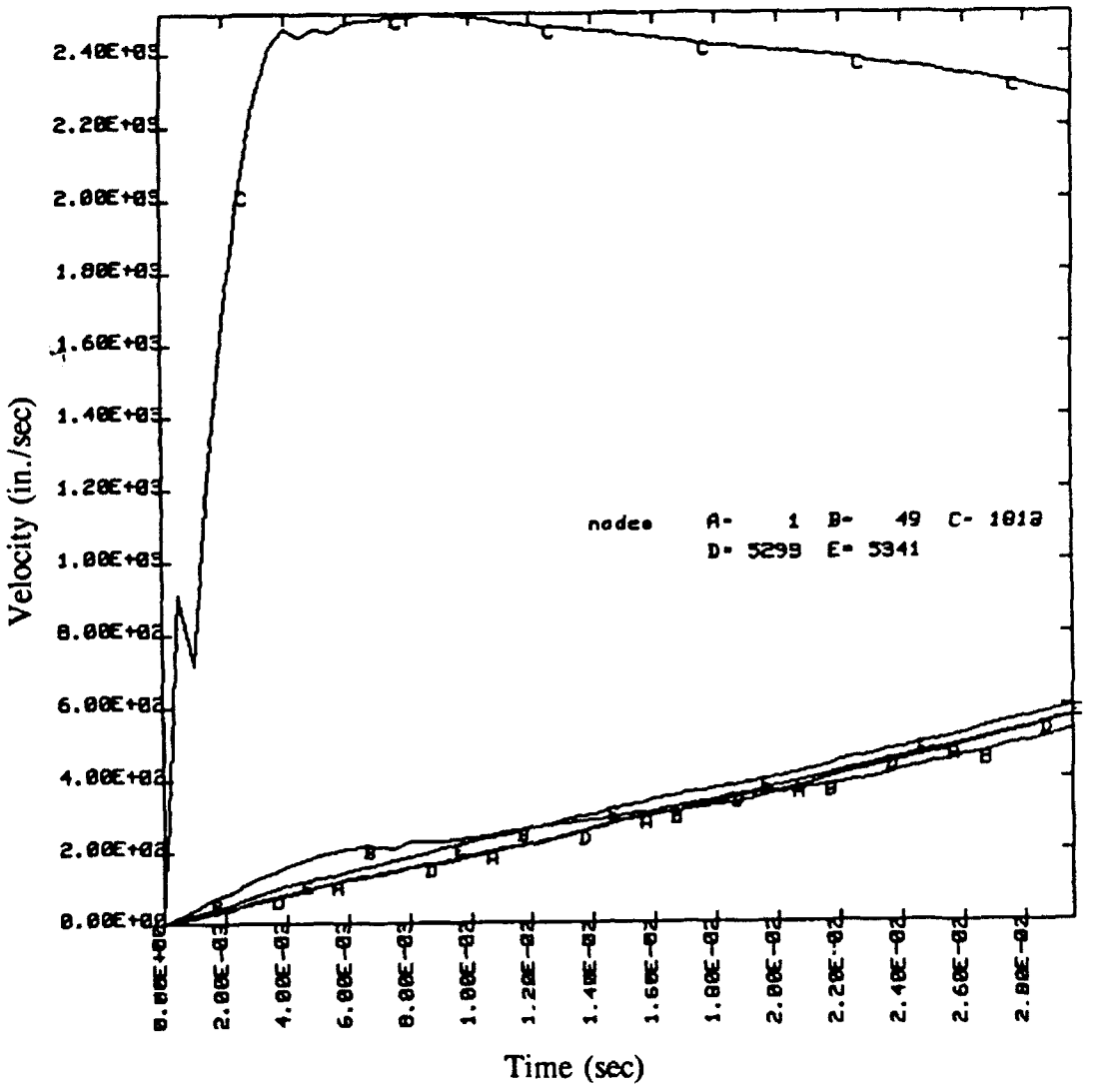

Figure 48
Vertical velocity histories in the roof slab.

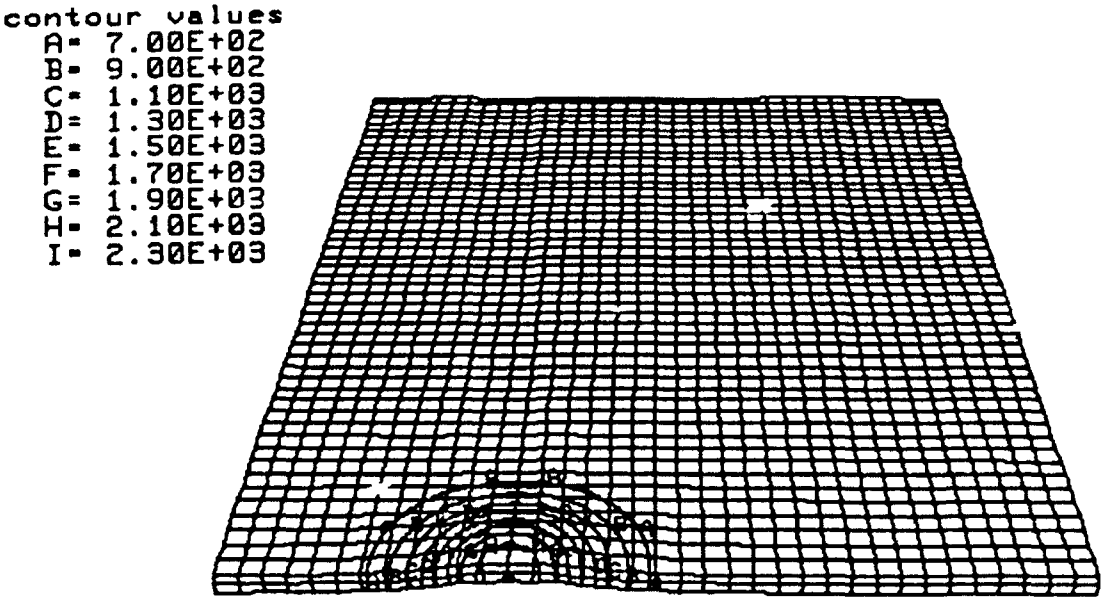

(a) Time = 0.007 sec.

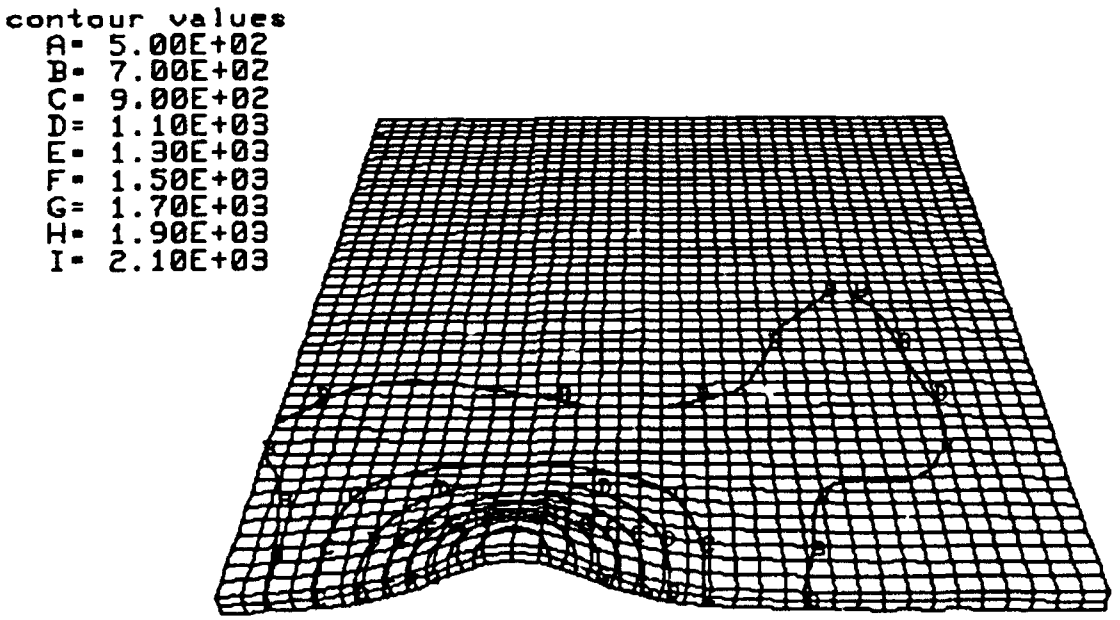

(b) Time = 0.027 sec.

Figure 49
Vertical velocity fields of the roof slabs.

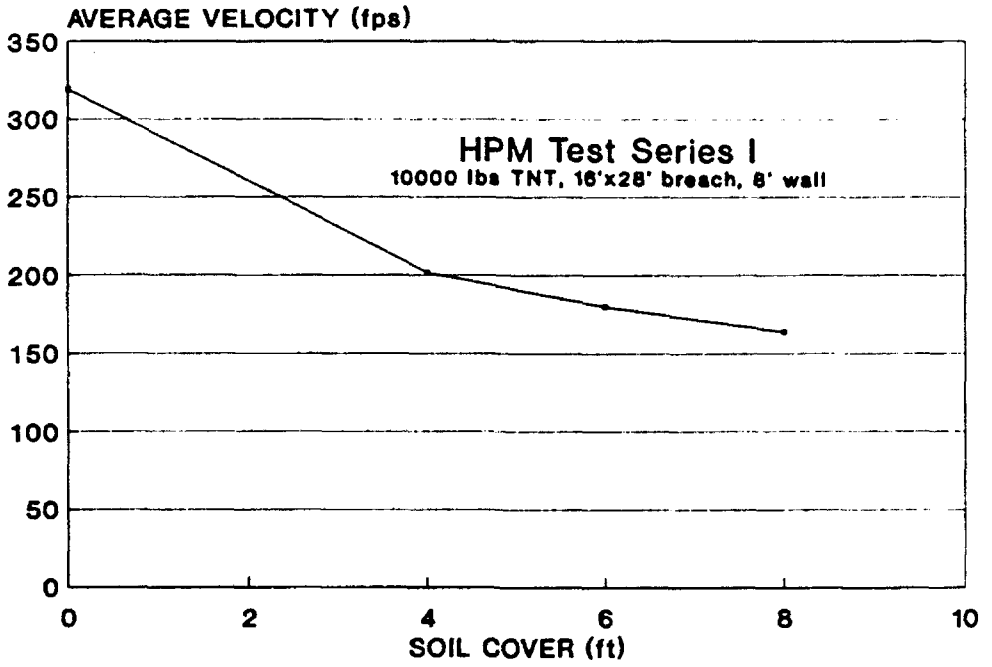

Figure 50
Average debris velocity using FRANG.

SUMMARY

The explicit finite element program DYNA3D was successfully used to determine the nonlinear dynamic response of a soil-covered roof slab for a proposed high performance magazine concept. Concrete and reinforcing bar stress histories have been obtained, yielding detailed information on cracking, concrete cover separation, bar yielding, and rupture. Initial debris velocities were estimated, which in turn allowed for the estimation of debris distances for the proposed soil-covered roof design.

It is expected that this program will be a useful tool for designers of reinforced concrete structures to contain or manage explosions. The following are specific recommendations on the use of the program.

In the absense of an embedded reinforcement model capability, a discrete reinforcement model was used to model regular patterns of reinforcement in the roof slabs. Some compromises were necessary in the roof slab discretization using this method. Truss elements with an elastic-plastic material model (Material 16) were employed satisfactorily in this regard. The concrete/geological Material Model 16 should be used to model concrete. This material model also offers a smeared reinforcement model capability which allows for modeling larger elements, but it is not necessarily to be preferred and it has not been evaluated.

CONCLUSIONS

Three-dimensional nonlinear dynamic finite element studies have been carried out for three classic problems in Navy explosive safety facilities engineering, these include: (1) a specialized missile test cell design concept, (2) reinforced concrete slabs with variable shear steel design, and (3) a soil-covered roof design for a proposed high performance magazine. Two widely available general purpose computer programs were applied in these analyses, one based on implicit and the other based on explicit temporal integration of the equations of motion. They are state-of-the-art programs, and they are highly regarded programs that are indicative of the industry.

Application of these computer programs can provide a viable alternative to codified single-degree-of-freedom (SDOF) methods currently used in the design and analysis of explosive safety structures. This modern technology can be at least as accurate as historical SDOF methods for computing dynamic response, and can provide substantially more detail on structural behavior, particularly when special structural concepts are encountered.

Concrete material models that have been implemented in commercial implicit computer programs are sophisticated, but they can be unreliable and cause simulations to terminate prematurely. This difficulty may be partially offset in programs that allow users to supply their own specialized material model subroutines which may be more suited to specialized problems. Implicit programs were found to provide for excellent reinforcement modeling capability when they supported embedded reinforcement modeling. This capability is important for explosive safety because many designs include heavily reinforced sections and complicated reinforcement patterns in both two- and three-dimensional configurations.

The large-scale equation solver capability that is implemented in commercially available implicit codes is outdated and limited. With present capability, only abbreviated three-dimensional models may be considered using modern computer workstation power. Improved solution algorithms do exist that have been developed to further exploit available computer resources. However, these algorithms are not always implemented in commercial technology. When they are implemented, the average lag time between research and implementation is 5 years or more.

Explicit programs are more robust regarding large-scale numerical solutions of highly nonlinear equations of motion describing the dynamic response of explosive safety structures. However, concrete material models in explicit programs are less mature than corresponding material models in implicit programs. Moreover, reinforcement modeling is not as well supported in explicit programs. Although they can reasonably model regular patterns of reinforcement, often found in slab designs for example, they cannot model more complex patterns efficiently because they do not as yet have embedded reinforcement modeling capability.

In summary, general purpose computer programs for three-dimensional nonlinear dynamic finite element analysis represent a powerful tool for specialized problems in explosive safety, as well as an attractive alternative for codified SDOF methods. Accurate models of specialized reinforced concrete missile test cells and magazines can be constructed more efficiently using available implicit programs, whereas, available explicit programs yield successful simulations with less difficulty.

RECOMMENDATIONS

Several technical problems in computational mechanics related to explosive safety remain. Problems also exist that involve user-friendliness of computer programs associated with the application of computational mechanics methods to the field of explosive safety engineering. Nevertheless, applications of this technology are becoming more prevalent in the open literature, and it is soon apt to make a larger impact on design and analysis in this field. An additional section on the application of this technology intended for guidance when confronted with a novel design problem should be considered for the next revision of NAVFAC P-397. It could include a discussion of the potential solutions using modern computerized methods in structural dynamics when the design problem goes beyond the collective experience upon which current codified methods are based, and usage of high-tech methods appear to be a definite option. For example, inherent assumptions attending the analytical methods can be reviewed, examples can be included or referenced for additional information, and recommendations for both the required engineering experience and the required levels of skill in usage of computer programs could be included in the new section. This would help to minimize the risk of misusing the technology, and would promote objectivity in dynamic response solutions and results obtained from its application.

ACKNOWLEDGMENTS

The Computer Aided Design Division, Code 1082, NWTC, Point Mugu, California, supplied the Sun Workstation used in the MTC study; Jim Thompson was instrumental in the MTC modeling work. At HKS (West), Inc., Nuno Rebelo and Todd Dalrymple provided valuable user support in the application of ABAQUS. Robert Whirley at Lawrence Livermore National Laboratory kindly supplied DYNA3D tapes and documentation to NCEL. At NCEL, Bob Murtha and Jim Tancreto provided useful discussions on aspects of explosive safety design practice and recent field test results.

REFERENCES

American Concrete Institute (1989). Building code requirements for reinforced concrete, ACI 318-89. Detroit, MI, 1989.

American Society of Testing and Materials (1989). Standard specification for uncoated high strength steel bar for prestressing concrete, ASTM A722-88a. Philadelphia, PA, Apr 1989.

Ayvazyan, H.E., M. Dede and N. Dobbs (1988). Design of NAVFAC Type VB missile test cell, Ammann and Whitney Consulting Engineers. New York, NY, Aug 1988.

Bathe, K.-J., J. Walczak, A. Welch and N. Mistry (1989). "Nonlinear analysis of concrete structures," Computers and Structures, vol 32, no. 3/4, 1989, pp 563-590.

Bathe, K.-J. and E.L. Wilson (1972). "Large eigenvalue problems in dynamic analysis," in Proceedings of the ASCE, EM6, 98, 1972, pp 1471-1485.

Bayo, E. (1987). An evaluation of numerical algorithms for the nonlinear dynamic analysis of large soil structure systems, Naval Civil Engineering Laboratory, CR 88.002. Port Hueneme, CA, Dec 1987.

Biggs, J.M. (1964). Introduction to structural dynamics. New York, NY, McGraw-Hill Book Co., 1964.

Blevins, R.D. (1979). Formulas for natural frequency and mode shape, Chapter 12. New York, NY, Van Nostrand Reinhold Co., 1979.

Cervera, M., E. Hinton and O. Hassan (1987). "Nonlinear analysis of reinforced concrete plate and shell structures using 20-noded isoparametric brick elements," Computers and Structures, vol 25, no. 6, 1987, pp 845-869.

Chang, T.Y., H. Taniguchi and W.F. Chen (1987). "Nonlinear finite element analysis of reinforced concrete panels," Journal of Structural Engineering, ASCE, vol 113, no. 1, Jan 1987.

Chen, A.C.T. and W.F. Chen (1975). "Constitutive relations for concrete," Journal of the Engineering Mechanics Division, ASCE, vol 101, no. EM4, Aug 1975.

Cornelissen, H.A.W., D.A. Hordijk and H.W. Reinhardt (1986). "Experiments and theory for the application of fracture mechanics to normal and lightweight concrete," Fracture Toughness and Fracture Energy of Concrete, Ed. F.H. Whitman. Elsevier Science Publishers B.V., Amsterdam, 1986.

Cox, J.V. and L.R. Herrmann (1992). "A plasticity model for the bond between matrix and reinforcement," 6th Japan-U.S. Conference on Composite Materails, Orlando, FL, 22-24 Jun 1992.

Craig, R.R. (1981). Structural dynamics, an introduction to computer methods. New York, NY, John Wiley and Sons, 1981.

Dameron, R.A., R.S. Dunham and Y.R. Rashid (1990). Concrete containment integrity software: Procedure manual and guidelines, Electric Power Research Institute, NP-6263-M. Palo Alto, CA, Jun 1990.

Elwi, A.E. and T.M. Hrudey (1989). "Finite element model for curved embedded reinforcement," ASCE Journal of Engineering Mechanics, vol 115, no. 4, 1986. (Discussion by P.C. Pandey, vol 117, no. 3, Mar 1991, pp 714-715.)

Ferritto, J.M. (1977). BARC user manual, Naval Civil Engineering Laboratory, Technical Note N-1494, Optimum dynamic design of nonlinear reinforced concrete slabs under blast loading. Port Hueneme, CA, Jul 1977.

Hallquist, J.O. (1988). User's manual for DYNA2D, Lawrence Livermore National Laboratory, UCID-18756, Rev 3. University of California, Livermore, CA, Mar 1988.

Hallquist, J.O. and R.G. Whirley (1989). DYNA3D user's manual, Lawrence Livermore National Laboratory, UCID-19592, Rev. 5. University of California, Livermore, CA, May 1989.

Hibbitt, H.D. (1985). "Some practical issues in nonlinear structural analysis with finite element methods," paper presented at Office of Naval Research Workshop, Stanford University, Stanford, CA, Mar 26-27, 1985.

Hibbitt, H.D. and B.I. Karlsson (1979). Analysis of pipe whip, Electric Power Research Institute, Report NP-1208. Palo Alto, CA, 1979.

Hibbitt, Karlsson, and Sorensen, Inc. (1989). ABAQUS user's manual, Version 4.8. Providence, RI, 1989.

Hilber, H.M., T.J.R. Hughes and R.L. Taylor (1978). "Collocation, dissipation and 'overshoot' for time integration schemes in structural dynamics," Earthquake Engineering and Structural Dynamics, vol 6, 1978, pp 99-117.

Holland, T.J. (1989). SOLVER user's guide, Version 2.2: Dynamic response analysis of single degree of freedom systems, Naval Civil Engineering Laboratory, CAE Structures Library, UG-0020. Port Hueneme, CA, Aug 1989.

Hughes, T.J.R. and J. Winget (1980). "Finite rotation effects in numerical integration of rate constitutive equations arising in large deformation analysis," International Journal of Numerical Methods in Engineering, vol 15, 1980, pp 1862-1867.

Ju, J-W, J.C. Simo, K.A. Pister and R.L. Taylor (1985). A parameter estimation algorithm and extensive numerical simulations for the CAP model, Defense Nuclear Agency, Contract 001-84-C-0304. Alexandria, VA, 30 Nov 1985.

Landers, J.A. (1990). A software development specification for nonlinear structural analysis, Naval Civil Engineering Laboratory, CR 90.016. Port Hueneme, CA, Jul 1990.

Matuska, D.A., R.E. Durrett and J.J. Osborn (1982). Hull user guide for three-dimensional linking with EPIC-33, Orlando Technology Inc., ARBRL-CR-0084. Shalimar, FL, Jul 1982.

Murtha, R.N. (1992). Personal communication on small-scale high performance magazine roof and soil cover tests, Naval Civil Engineering Laboratory, Port Hueneme, CA, 1992.

Murtha, R.N. and M. Dede (1988). Test plan for explosives safety certification of NAVFAC standard type V missile test cell, Naval Civil Engineering Laboratory, Memorandum to files. Port Hueneme, CA, Dec 1988.

Naval Facilities Engineering Command (1991). Structures to resist the effects of accidental explosions, NAVFAC P-397 Design Manual. Alexandria, VA, 1991 (also Army TM5-1300 and Air Force AFM 88-22).

Newmark, N.M. (1962). "A method of computation for structural dynamics," in Transactions of the ASCE, vol 127, 1962, pp 1406-1435.

Park, R. and T. Paulay (1975). Reinforced concrete structures. New York, NY, John Wiley and Sons, 1975, pg 12.

PDA Engineering (1989). PATRAN Plus user manual, Release 2.4. Costa Mesa, CA, Sep 1989.

Rashid, Y.R. (1968). "Analysis of prestressed concrete pressure vessels," Nuclear Engineering and Design, vol 7, no. 4, Apr 1968, pp 334-344.

Rebelo, Nuno (1989). Personal communication, HKS (West), Inc., Newark, CA, 21 Nov 1989.

Resende, L. (1987). "A damage mechanics constitutive theory for the inelastic behavior of concrete," Computer Methods in Applied Mechanics and Engineering, vol 60, 1987, pp 57-93.

Resende, L. (1989). Personal communication, ABAQUS Training Course, Providence, RI, Oct 1989.

Schnobrich, W.C. (1989). "Reinforced concrete shells: Some problems," Analytical and Computational Models of Shells. Noor, Belytschko and Simo, Eds. Computers in Engineering Division, vol 3, ASME, 1989.

Selna, L.G., L.J. Malvar and R.J. Zelinski (1989). "Box girder bar and bracket seismic retrofit devices," American Concrete Institute Structural Journal, vol 86, no. 5, Sep - Oct 1989.

Shugar, T.A., T.J. Holland and J. Malvar (1991). Advanced finite element analysis of drydocks and waterfront facilities - A technology assessment, Naval Civil Engineering Laboratory, Technical Note N-1835. Port Hueneme, CA, Oct 1991.

Stevens, D.J. and T. Krauthammer (1991). "Analysis of blast-loaded, buried RC arch response. I: Numerical approach," ASCE Journal of Structural Engineering, vol 117, no. 1, Jan 1991.

Stillman, D.W. and J.O. Hallquist (1985). INGRID: A three-dimensional mesh generator for modeling nonlinear systems, Lawrence Livermore National Laboratory. University of California, Livermore, CA, Jul 1985.

Tancreto, J.E. (1988). "Dynamic tests of reinforced concrete," in Proceedings of the 23rd Department of Defense Explosives Safety Board Seminar, Atlanta, GA, Aug 1988.

Tancreto, J.E. and E.S. Helseth (1984). "Effect of frangible panels on internal gas pressures," Minutes of the Twenty-First Explosives Safety Seminar, Department of Defense Explosives Safety Board, Aug 1984.

Tancreto, J.E. and L.J. Malvar (1991). "Response of reinforced concrete slabs to close-in explosive loads," in Proceedings of the Fifth International Symposium of Interaction of Conventional Munitions with Protective Structures, Bundesakademie fuer Wehverwaltung und Wehrtechnik, Mannheim, Federal Republic of German, Apr 1991.

Terrier, J.M. and J.F.X. Boisseau (1989). "Numerical simulation of reinforced concrete structure response subjected to high explosive detonation," in Proceedings of the Fourth International Symposium on the Interaction of Non-nuclear Munitions with Structures (vol 1), Panama City Beach, FL, Apr 17-21, 1989.

Wager, P. and J. Connett (1989). FRANG user's manual, Naval Civil Engineering Laboratory. Port Hueneme, CA, 1989.

Whirley, R.G. and J.O. Hallquist (1991). DYNA3D user's manual, Lawrence Livermore National Laboratory. University of California, Livermore, CA, May 1991.

Woodson, S.C. (1990). Response limits of blast-resistant slabs, Waterways Experiment Station, Corps of Engineers, Technical Report SL-90-11. Vicksburg, MS, Oct 1990.

Zienkiewicz, O.C., D.R.J. Owen, D.V. Phillips and D.C. Nayak (1972). "Finite element methods in the analysis of reactor vessels," Nuclear Engineering and Design 20, 1972, pp 507-541.

Appendix A

PROCEDURE FOR SPECIFYING REINFORCEMENT DATA IN THE ABAQUS MTC MODEL

The most labor intensive task involved with constructing the MTC finite element model was preparation of the embedded reinforcement input data, specifically the generation of the ABAQUS *REBAR input data file. Because of this, it is worthwhile documenting the procedure which was developed to achieve a representation of the reinforcement for the MTC model. This procedure is meant only as a supplement to the ABAQUS User Manual regarding *REBAR data preparation.

The procedure consists of four steps. It requires two kinds of finite element model data: the element connectivity data for mapping of actual node numbers to a generic set of node numbers 1 through 8 for the solid element, and the node topology data relative to the reinforcement within each element. These data provide a complete picture of the embedded element with its steel layers placed relative to the element nodes.

Step 1: Locate Isoparametric Directions 1, 2, and 3 for the Element

As an example, consider a typical element of the MTC model for which the mapping between the element connectivity data and generic node numbers is shown in Figure A-1. The generic element is selected from the ABAQUS User's Manual. In this mapping, the isoparametric directions 1, 2, and 3 are respectively defined to correspond to the generic node directions 1-2, 1-4, and 1-5. Correspondingly, in the example embedded element, these directions are respectively defined by the actual node directions 1616-1619, 1616-1617, and 1616-1628.

Step 2: Determine Reference Edge Number

The location and orientation of the reinforcement layers within the embedded element are referred to the reference edge number. The edge number must refer, in turn, to one of the three isoparametric directions. To obtain the edge number, first select any isoparametric direction, and enter this into the appropriate *REBAR data field. If, in the example element, direction 3 is selected, the element's reference orthogonal face is defined by nodes 1616, 1619, 1620, and 1617; this face is orthogonal to axis 3, where axis 3 must be an inward normal by ABAQUS convention. Next, select an edge of the orthogonal face from which the distances to the reinforcement layers in the embedded element are measured. A convenient choice is edge 3. It is defined as the 1617-1620 edge (the direction implied in the edge definition is significant for specifying angular orientation data in the fourth step of the procedure) when the selected isoparametric direction is 3.

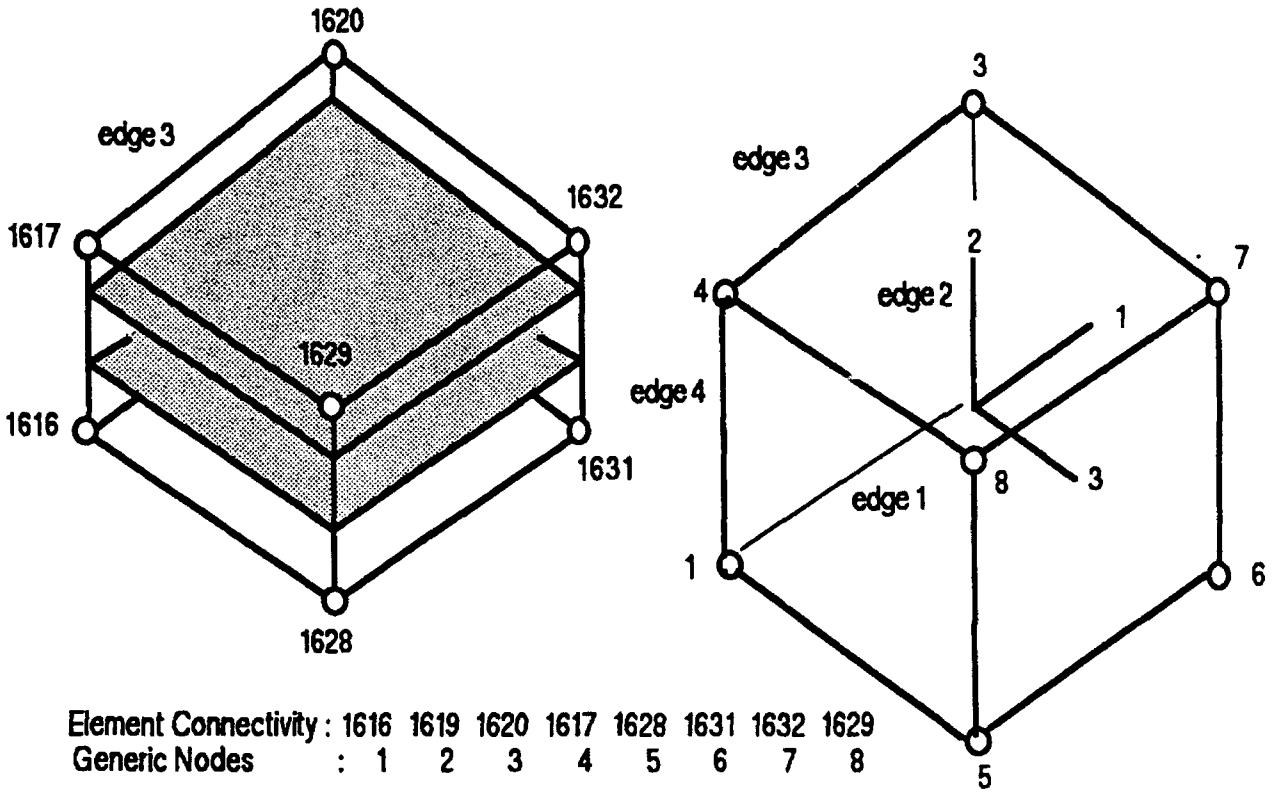

Figure A-1
Construction of typical embedded element for MTC model.

Step 3: Calculation of Fractional Distances

A fractional distance is the distance from the reference edge to a reinforcement layer, divided by the element size in that direction. Using edge 3 as the reference edge, the fractional distances in the example are (refer to both Figure 7 in the main text and Figure A-1):

(a) 0.097 for the upper steel layer in the hoop direction
(b) 0.097 for the upper steel layer in the longitudinal direction
(c) 0.721 for the lower steel layer in the hoop direction
(d) 0.721 for the lower steel layer in the longitudinal direction

Step 4: Calculation of Orientation Angles

The direction of the reinforcement is measured relative to the direction of the reference edge defined in Step 2. In this example, the reference edge is 3. If the rebar direction is parallel to this edge, the orientation angle is 0 degrees, and if it is perpendicular to this edge, the orientation angle is 90 degrees. In this example, the orientation angle data are:

(a) 0 degrees for the two layers of hoop steel
(b) 90 degrees for the two layers of longitudinal steel

More generally, the orientation angle is defined as the angle subtended by the direction of the rebar and the line formed by the intersection of the reinforcement layer with the selected orthogonal face. The line of intersection also has a positive sense which is defined by the generic node direction, 3-4 in the example element. The orientation angle is subtended by this positive direction and the direction of the rebar within the element.

Specification of the *REBAR data for the cylindrical portion of the MTC model was easier than for the end walls, since the reinforcement pattern is more regular in the cylinder than in the end walls. However, once the four-step procedure is used for several elements, the task becomes routine for the remainder of the model.

Additional strategy was required to manage the substantial variation in reinforcement patterns throughout the MTC. This was accomplished by assigning code names to various regions of the MTC model as shown in Figure A-2. The code names define groups of elements in which the reinforcement pattern is common. These code names are entered in the *REBAR data file, as seen in the sample included as Table A-1.

Other similar research projects have recognized and employed the embedded reinforcement modeling capability of ABAQUS. The Electric Power Research Institute (EPRI) in Palo Alto, California, has supported substantial development of this capability for application to reinforced concrete nuclear containment structures. In one such project Dameron, et al., (1990) attempted to overcome the labor intensive task of developing complex reinforcement models in conjunction with ABAQUS. The result was an auxiliary automated software procedure for generating *REBAR data files.

In this connection, it should be mentioned that despite the formidable finite element pre- and post-processing capability of PATRAN Plus, no provision is made in its ABAQUS interface program, ABAPAT, for interpreting and graphically displaying *REBAR data. PATRAN Plus does not support reinforced concrete analysis when the embedded reinforcement model technique is employed. However, the ABAQUS post-processor, ABAPOST, is available and was very useful for displaying and checking the reinforcement model (see Figure A-2).

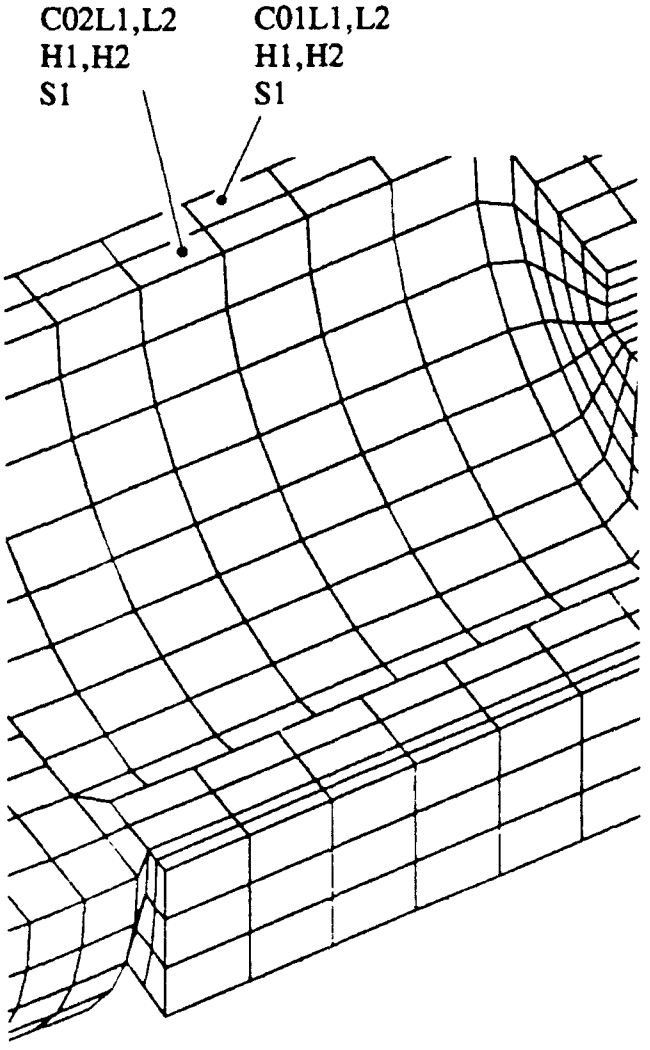

Figure A-2
Sample of *REBAR group codes for MTC model.

Table A-1
Sample of *REBAR Input Data File for ABAQUS MTC Model

```
**Rebar Definition For Cylinder
**
**  Rebar Mesh of Cylinder Group 1
**
**     Hoop
**
*REBAR, ELEMENT=CONTINUUM, MATERIAL=STEEL, GEOMETRY=ISOPARAMETRIC, NAME=C01H1
   C01,1.23,6.00,90,0.097,3,2
*REBAR, ELEMENT=CONTINUUM, MATERIAL=STEEL, GEOMETRY=ISOPARAMETRIC, NAME=C01H2
   C01,1.23,6.00,90,0.721,3,2
**
**     Stirup
**
*REBAR, ELEMENT=CONTINUUM,' MATERIAL=STEEL, GEOMETRY=ISOPARAMETRIC, NAME=C01S1
   C01,1.23,6.00,0,0.1429,2,2
   C01,1.23,6.00,0,0.2857,2,2
   C01,1.23,6.00,0,0.4286,2,2
   C01,1.23,6.00,0,0.5714,2,2
   C01,1.23,6.00,0,0.7143,2,2
   C01,1.23,6.00,0,0.8571,2,2
   C01,1.23,6.00,0,0.9999,2,2
**
**     Longitudinal
**
*REBAR, ELEMENT=CONTINUUM, MATERIAL=STEEL, GEOMETRY=ISOPARAMETRIC, NAME=C01L1
   C01,1.23,6.55,0,0.097,3,2
*REBAR, ELEMENT=CONTINUUM, MATERIAL=STEEL, GEOMETRY=ISOPARAMETRIC, NAME=C01L2
   C01,1.23,6.15,0,0.721,3,2
```

Appendix B

FREQUENCY SPECTRA CALCULATION FOR IDEALIZED TRIANGULAR PRESSURE-TIME HISTORY

A triangular pressure-time history is often used to idealize blast loads in explosive safety analyses of Navy facilities. For the missile test cell design, the load was idealized as shown in Figure 2 in the main text of this report. This information can also be considered in terms of its frequency content or frequency spectrum. In this case, the idealized pressure pulse is divided into two triangular pulses, one for the shock phase and one for the gas pressure phase. A triangular pulse is mathematically defined as:

$$p(t) = \begin{cases} p_o(1 - t/t_o) & 0 \le t \le t_o \\ 0 & t \ge t_o \end{cases} \qquad \text{(B-1)}$$

where t denotes time and p_o and t_o are, respectively, magnitude and duration constants.

The frequency spectrum of a triangular pulse is obtained by calculating its Fourier transform,

$$\bar{P}(\Omega) = 1/2\ \pi \int_{-\infty}^{\infty} p_o(1 - t/t_o)\, e^{i\Omega t}\, dt \qquad \text{(B-2)}$$

where Ω denotes circular frequency in rad/s. The result is

$$\bar{P}(\Omega) = \frac{p_o}{\Omega^2 t_o}\left[(1 - \cos(\Omega t_o) + i(\sin(\Omega t_o) - \Omega t_o)\right] \qquad \text{(B-3)}$$

The modulus or magnitude of $\bar{P}(\Omega)$ is the frequency spectrum, $P(\Omega)$. It is obtained by multiplying $\bar{P}(\Omega)$ by its complex conjugate $\bar{P}^*(\Omega)$,

$$P(\Omega) = \bar{P}(\Omega) \times \bar{P}^*(\Omega) \qquad \text{(B-4)}$$

The result is,

$$P(\Omega) = \frac{p_o}{\Omega^2 t_0}\sqrt{2 - 2\cos(\Omega t_o) - 2\,\Omega t_o \sin(\Omega t_o) + (\Omega t_o)^2} \qquad \text{(B-5)}$$

This frequency spectrum is graphed in Figure 11 for both the shock and gas pressure time-histories shown in Figure 2.

Appendix C

DYNA3D MATERIAL MODELS FOR REINFORCED CONCRETE

An evaluation of the material models available in DYNA3D was performed to find suitable models for both the reinforcing steel and the concrete for use in finite element models of reinforced concrete slabs. The evaluation consisted of primarily uniaxial compressive and tensile analyses on single truss and solid elements in the expected stress and strain ranges. Materials 3, 17, 16, 5, and 25 were selected as candidate models and analyzed.

The analyses utilized the material driver option in DYNA3D and a single element calculation. The material driver option allows inputs and calculates the material's response. DYNA3D has no static analysis capability per se. Displacements were imposed quasi-statically via prescribed velocities at the nodes on one side of the element. The velocity is integrated over the prescribed time (which is much larger than the element's fundamental period) to verify that the prescribed displacement history has been imposed correctly. A constant velocity results in a displacement which increases linearly with time, and the time axis can be replaced by a displacement axis.

MATERIAL 3

Material 3 is an elastic-plastic material model with either kinematic, isotropic, or a combination of kinematic and isotropic hardening. Material 3 is well suited for modeling steel trusses. Material 12 is an elastic-plastic model with isotropic hardening which is reported to be more efficient than Material 3 (with a hardening parameter $\beta' = 1$), but it is not available for use with beam or truss elements.

The properties for steel used in Material 3 were as follows:

Young's modulus	$E = 29{,}000$ ksi
Poisson's ratio	$\mu = 0.30$
Yield stress	$\sigma_o = f_y = 97$ ksi (DIF = 1.3)
Tangent modulus	$E_t = 48$ ksi
Hardening parameter	$\beta' = 1$ (isotropic hardening)

A single truss element was subjected to tension, then compression, and the load displacement response analyzed. The stress was increased linearly with time to simplify the graphs of stress-strain behavior.

From Figure C-1 it is apparent that the steel yielded both in tension and compression at the specified value of 97 ksi. Yielding occurred at a strain of about 0.0033, which is in agreement with the expected value of 97/29,000. This material model was used to represent steel for all the numerical analyses of the slabs.

MATERIAL 17

Material 17 is an isotropic elastic-plastic oriented crack model not currently supported by the Lawrence Livermore National Laboratory.

A 1- by 1- by 1-inch concrete cube (a single 8-node solid element) was analyzed under tension and compression. The applied load (or stress since the area is 1 $in.^2$) was incremented linearly with time so that the time axis could be replaced directly by a stress axis.

The input for this model was:

Young's modulus	E	= 4,000 ksi
Poisson's ratio	μ	= 0.20
Yield stress	σ_o	= f_{dc} = -6,000 psi (DIF = 1.25)
Tangent modulus	E_t	= 1,000 ksi
Fracture strength	σ_f	= f_t = 500 psi
Pressure cutoff	p_c	= 7,500 psi

In tension, and with all nodes free to displace laterally, the concrete cracked at the specified tensile strength, but exhibited a very low modulus of elasticity. This case was run again with all nodes laterally fixed. The results are shown in Figure C-2. Cracking again occurred at 500 psi but exhibited a modulus of elasticity of only 2,300 ksi.

In compression (with all nodes laterally restrained), the modulus of elasticity was in agreement with the specified value. However, the concrete did not yield until the stress reached 7 ksi, in excess of the specified dynamic strength. Subsequent to yield, the material model lost all strength and no plastic behavior could be obtained. Equation of state 1, supplemented with data from Matuska, et al. (1982), was specified to observe the material model response in elevated states of confined compression. Attempts at obtaining an acceptable response did not succeed.

This material model had been used in some of the initial numerical simulations of the slabs with the understanding that the concrete slab should have no post-crushing load carrying capacity. This enabled an evaluation of the effects of post-crushing resistance on load deflection by comparison with simulations carried out with Material 16. It is, however, recommended that Material 17 not be used in any future simulation for modeling concrete.

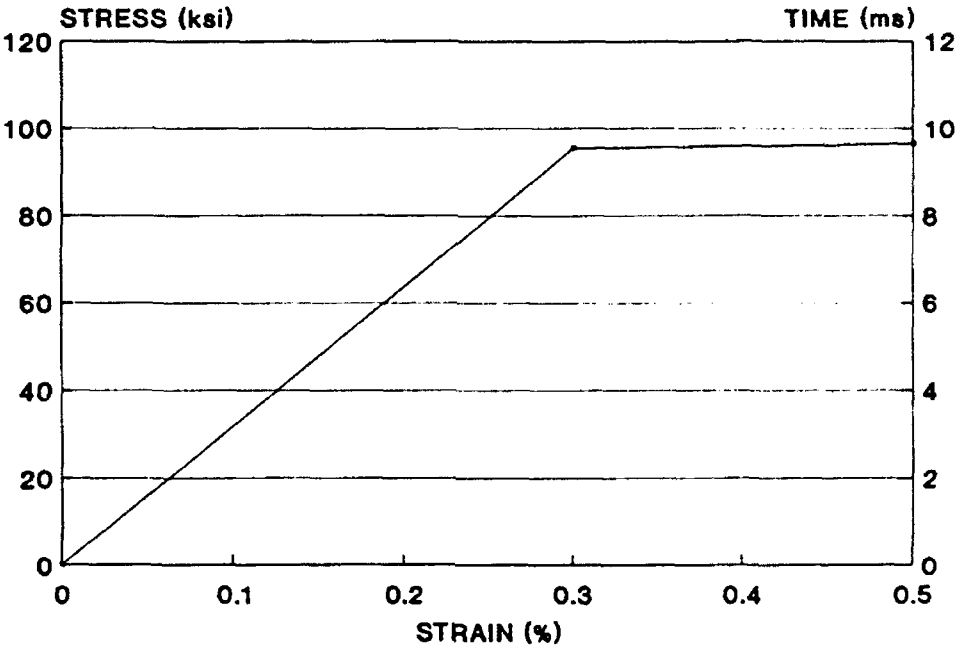

(a) Tension.

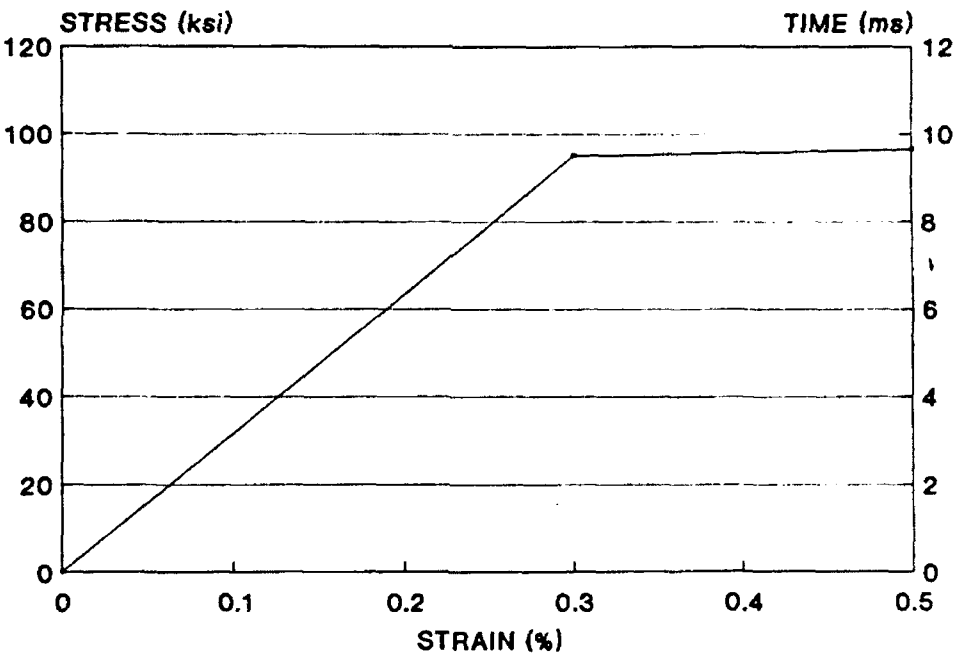

(b) Compression.

Figure C-1
Truss elements - Material 3.

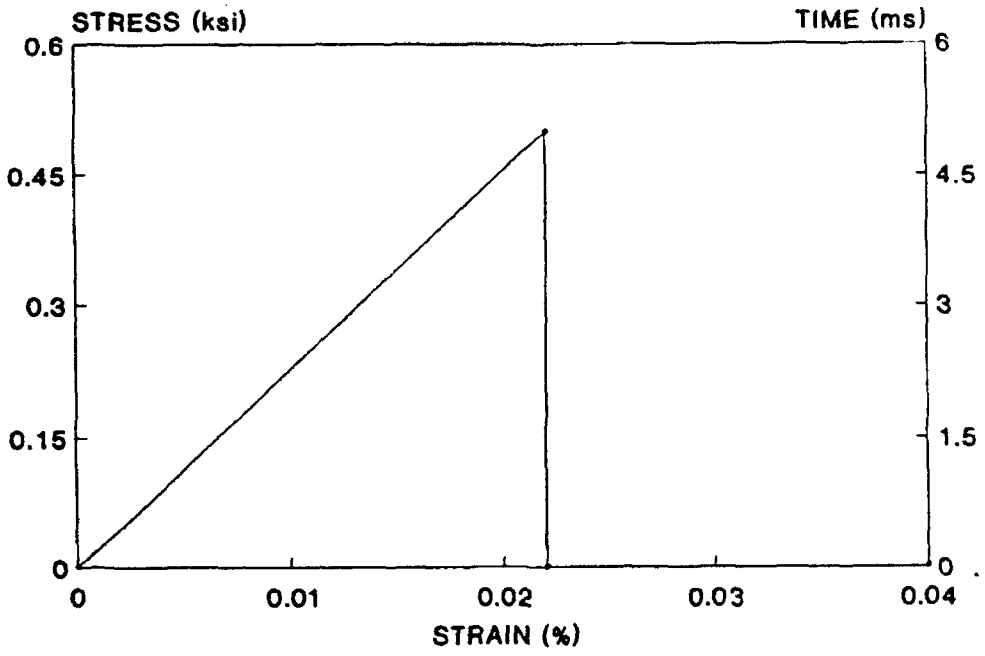

(a) Tension.

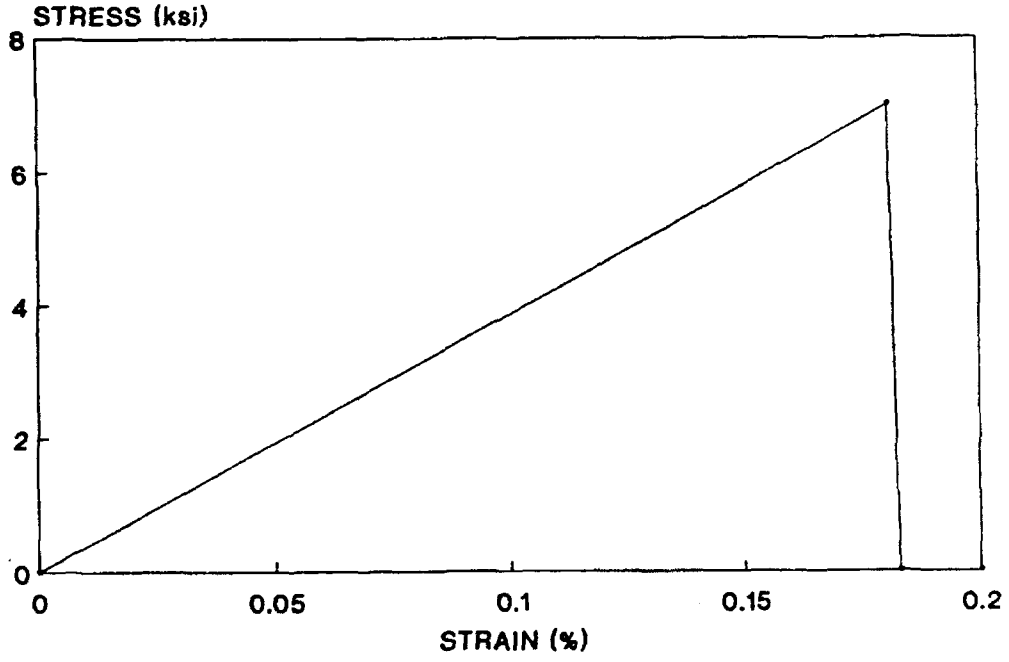

(b) Compression.

Figure C-2
Solid elements - Material 17.

MATERIAL 16

Material 16 is called the concrete/geological material model. A unit concrete cube represented by a single 8-node solid element was analyzed under tension and compression. Under tension, all nodes were free to contract laterally. Under compression, lateral movement of the nodes was prevented. The applied load (or stress) was incremented linearly with time so that the time axis was replaced directly by a stress axis.

Input

All concrete properties were defined by entering:

Card 3:
- μ = 0.20 (Poisson ratio)
- f_c' = 6,000 psi (compressive strength)
- a_o = -1 (generates f_t)

The program internally generated a corresponding value of tensile strength, f_t = 561 psi. By specifying the equation-of-state (EOS) as 0, a trilinear EOS type 8 is automatically generated internally.

This model allows for the inclusion of steel bars which are smeared into the element via a rule of mixtures. This is referred to as a smeared reinforcement model. Two sets of smeared steel properties were used:

Set 1 (no steel)

Card 4: 0

Set 2 (2 percent steel)

Card 4:
- percent = 2.0
- modulus = 29,000,000 psi
- μ = 0.30
- σ yield = 97,000 psi
- E_t = 48,000 psi

Cards 5 through 8 were blank.

Results for Set 1 - No Steel

In tension, the stress resistance was cut off exactly at f_t and quickly reduced to 0 as shown in Figure C-3. The strain at failure was 0.00013 and the initial modulus of elasticity, E_o, was about 4.4 x 10^6 psi, which are both acceptable results.

In compression, the concrete yielded at about 0.0016 (close to the 0.002 typically accepted strain at maximum stress), and the corresponding yield stress was 6,000 psi as prescribed. The initial modulus of elasticity, E_o, was about 6 x 10^6 psi, and the tangent modulus at yield, E_t, was about 4 x 10^6 psi. The initially generated equation of state provided for increased resistance due to the confinement condition of the concrete cube. This is also demonstrated in Figure C-3.

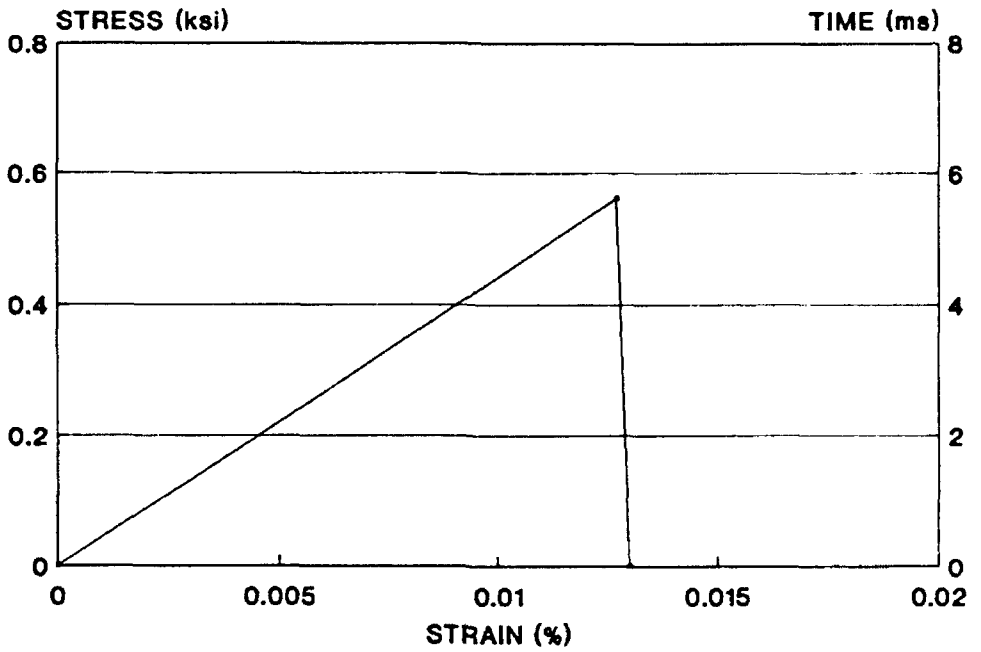

(a) Tension - no steel.

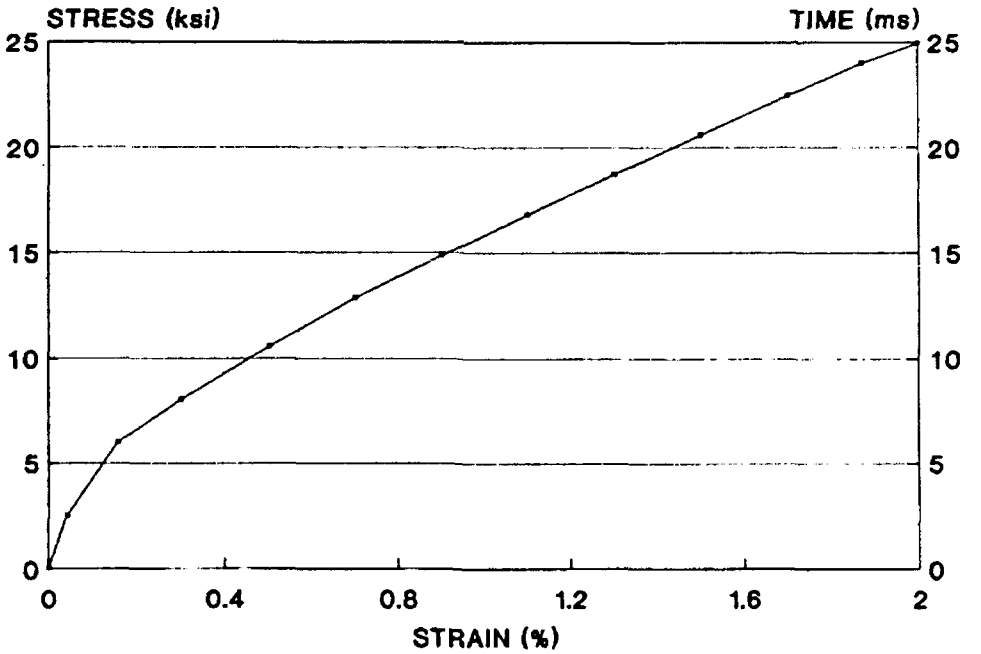

(b) Compression - no steel.

Figure C-3
Solid elements - Material 16.

Results for Set 2 - 2 Percent Steel

In compression, with all nodes laterally restrained, the stress-strain curve, which is shown in Figure C-4, is similar to the one without steel (Figure C-3). At 0.0016 strain - the previous concrete yield strain - the stress in the concrete is 6,000 psi, and the load in the steel is 940 pounds. Superposing the concrete and steel stresses, the total section stress is then 6,940 psi. Since the compression stress-strain curve does go through the point (6,940 psi, 0.016 strain), the smeared material model appears to work correctly in compression.

In tension, with all nodes laterally free, concrete cracking occurred close to the expected value of 637 psi (561 psi due to the concrete and 76 psi due to the steel). The model also accurately predicted yielding in the cube at 1,940 psi, which corresponds to 97 ksi for 2 percent steel. However, the steel yield strain was too small (0.00077 instead of 0.00334). The apparent steel stiffness was 4 times too large. The cause for this discrepancy could not be determined.

Recommendations

For representing pure concrete, Material Model 16 should be used. For concrete with smeared steel, the noted discrepancy in stiffness will introduce error.

MATERIAL 5

This material model came highly recommended for modeling the gross behavior of concrete, and is called the Soil and Crushable Foam Model, Type 5. This model was reported to have been heavily used in the community, and to be well supported and well debugged.

The material parameters for this model were specified as follows:

Shear modulus	G	=	1,456 ksi
Bulk unloading modulus	K_u	=	2,427 ksi
Yield stress	σ_y	=	4 ksi
Tangent modulus	E_t	=	37.7 ksi

The compressive test results are shown in Figure C-5a. The material yielded at approximately 6.5 ksi and at a strain of 0.0015. The calculated stiffness was 6,000 ksi and the calculated linear tangent stiffness was 600 ksi. Overall, the behavior under confined compression was judged as adequate.

Tensile results are given in Figure C-5b. The tensile stress response shows what appears to be an elastic rebound. The rebound is centered around 0.5 ksi which is the input fracture stress. Attempts to solve this problem by slowing the prescribed displacements below 1 in./sec resulted in the same behavior. However, increasing the loading rate to 100 in./sec resulted in a clean fracture curve, as shown on Figure C-5b. In this model, the fracture shows a peak stress of 0.9 ksi at a strain of 0.0002, then maintains a constant residual stress of 0.5 ksi instead of zero residual stress. Although this is a low stress level when compared to the compressive stresses, it can adversely affect dynamic behavior by introducing an artificial resistance force at

cracked sections. This is because a large solid element can have a large crack surface area so that, even for a small artificial residual stress, the artificial residual forces on the cracked section introduced are not necessarily small.

MATERIAL 25

This model is referred to as an inviscid two invariant geologic cap model. The cap model was historically developed for soils, and later it was applied to concrete. It was the latest model implemented into the DYNA3D program. The implementation was consistent with the Berkeley version of the cap model (Ju, et al., 1985) and includes their parameter calibration fit to the "Colorado" data set for concrete. The "Colorado" data set is made up of 67 different tests. The procedure was to calibrate the cap model on six tests and then evaluate the model on how well it predicted the results of the other 61 tests. The cap model was reported to be successful in this regard. The model was refined to run in DYNA3D and performs exceptionally fast within the explicit finite element framework. Although it was reported to be a supported model, it has so far seen little use by the community.

The material parameters for the cap model (Ju, et al., 1985) are as follows:

Initial bulk modulus	$K = 2{,}100$ ksi
Initial shear modulus	$G = 1{,}700$ ksi
Failure envelope parameter	$\alpha = 3.87$
Failure envelope linear coefficient	$\theta = 0.1$
Failure envelope exponential coefficient	$\tau = 1.16$
Failure envelope exponent	$\beta = 0.444$
Cap axis surface ratio	$R = 4.43$
Hardening law exponent	$D = 0.00322$
Hardening law coefficient	$W = 0.429$
Hardening law parameter	$X_o = 16.0$
Tension cutoff	$T = -0.3$ ksi

The results for our compressive test are given in Figure C-6a. The material yielded at a stress of 6.3 ksi and a strain of 0.0016. This appears to be within an acceptable range for confined concrete in that it is generally accepted that the compression strength is reached at a strain of 0.002. The initial stiffness was about 3,940 ksi compared to 4,016 ksi, expected, and the hardening stiffness was about 277 ksi. The cap model therefore properly captured compressive behavior throughout the given range.

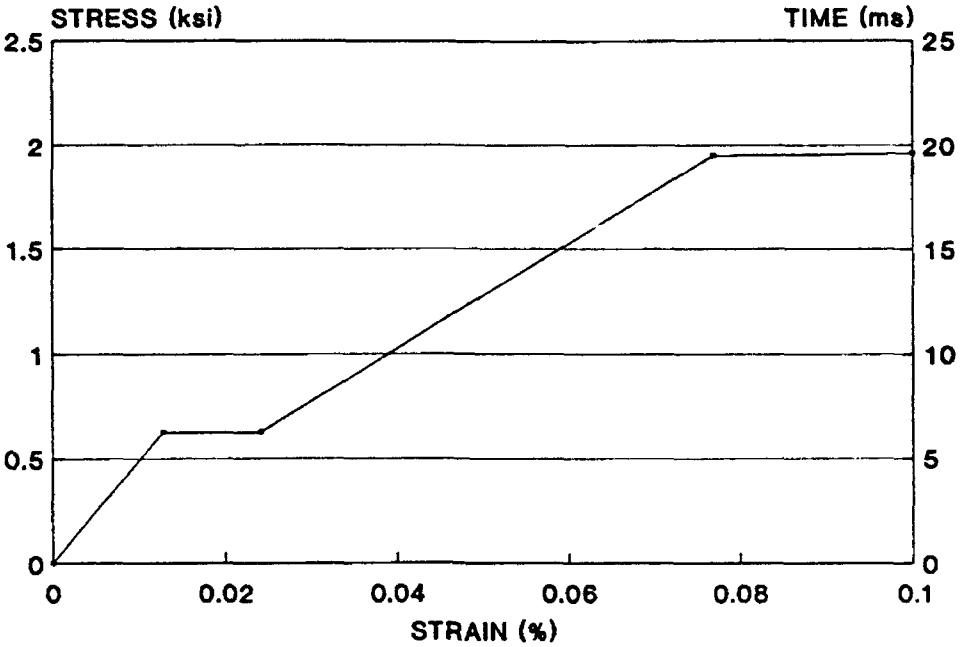

(a) Tension - 2% steel.

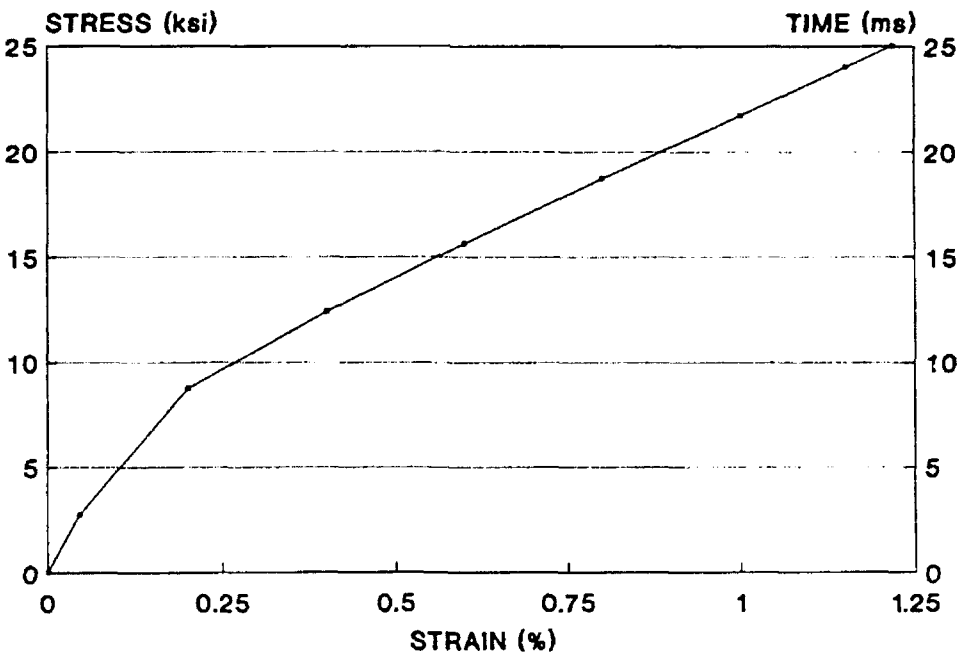

(b) Compression - 2% steel.

Figure C-4
Solid elements - Material 16.

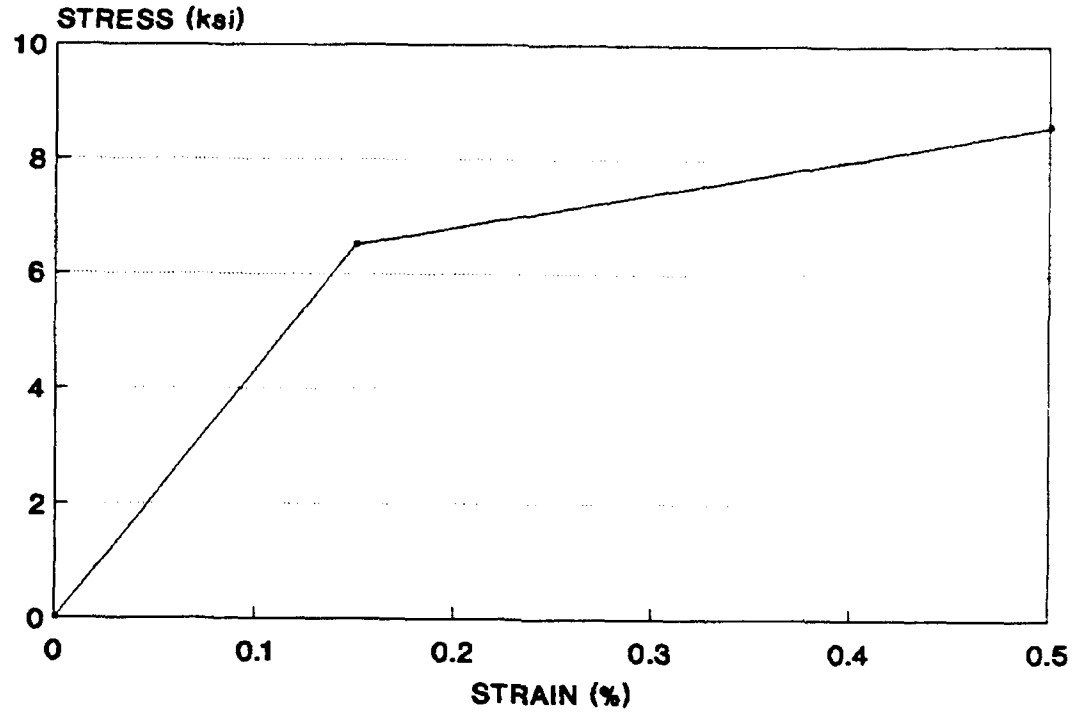

(a) Compression.

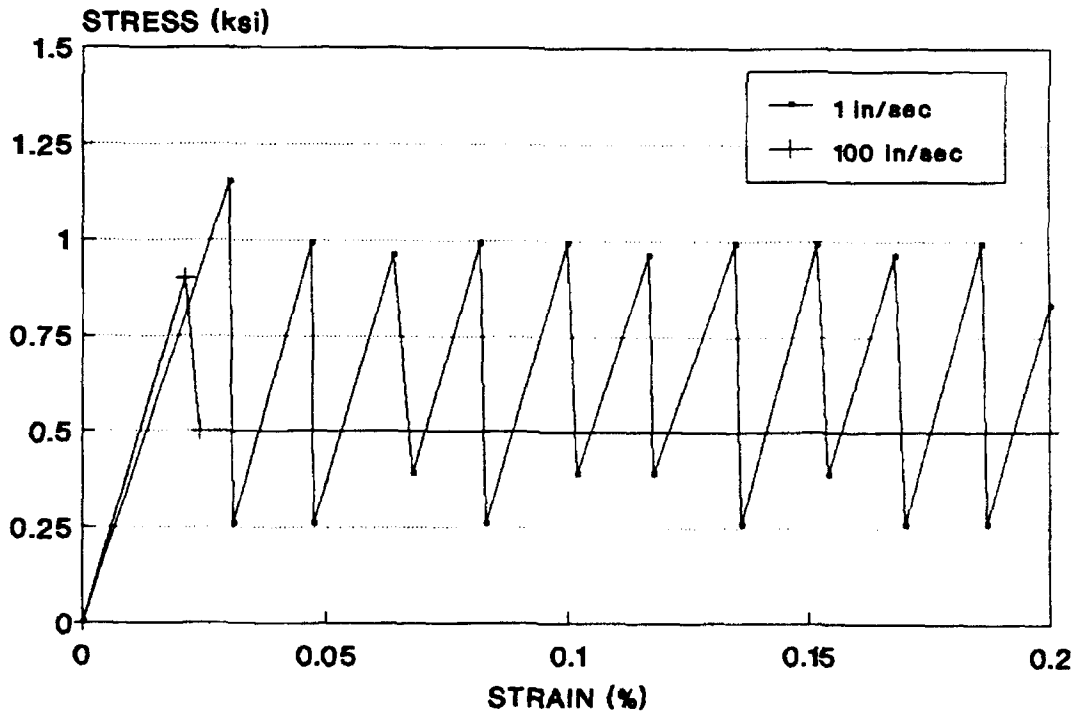

(b) Tension.

Figure C-5
Solid elements - Material 5.

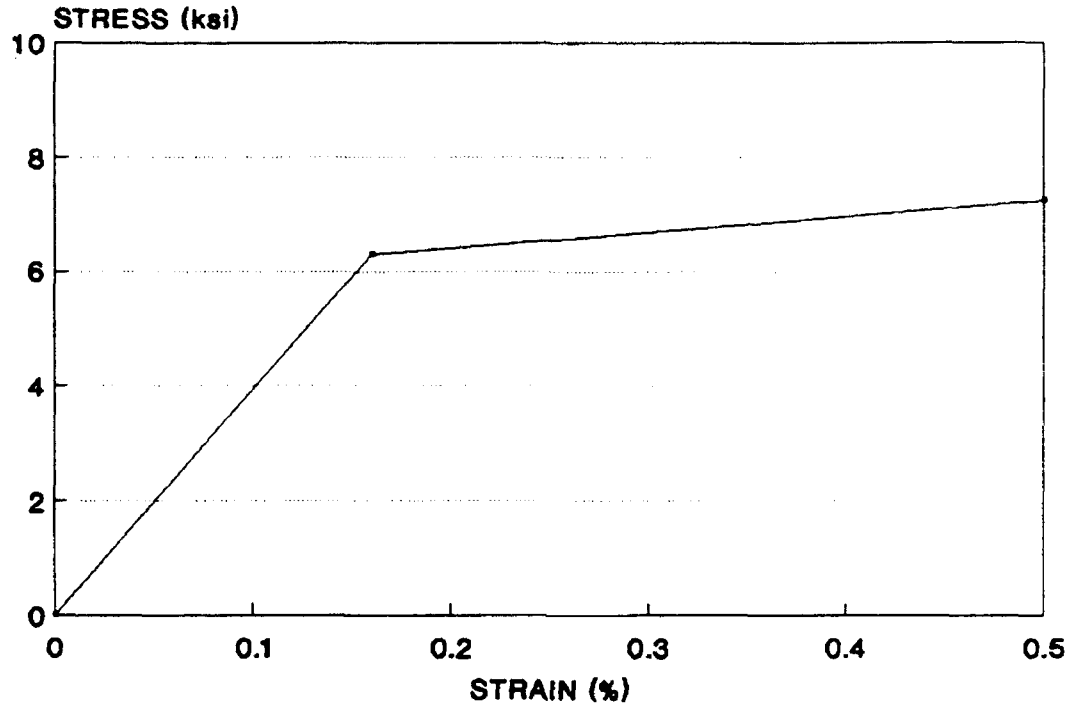

(a) Compression.

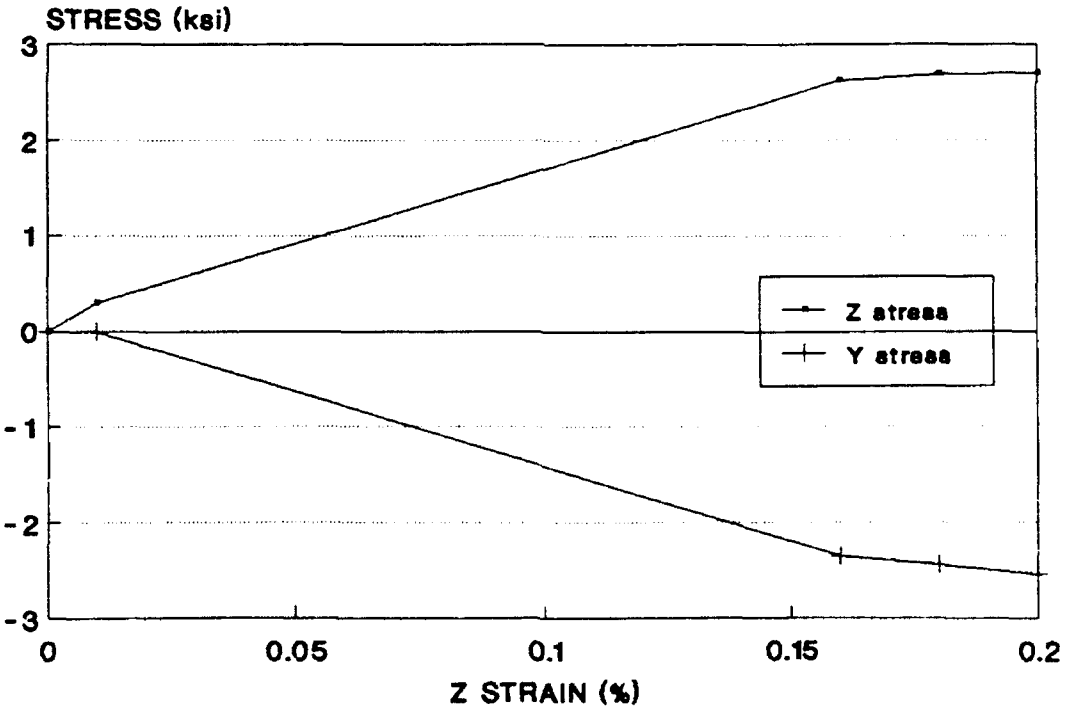

(b) Tension.

Figure C-6
Solid elements - Material 25.

The tensile test results for a transversely unconstrained unit solid element are shown in Figure C-6b and indicate inconsistent behavior. At the prescribed tensile cutoff (pressure = -0.3 ksi), the stress-strain curve in the z-direction shows a change in slope at a strain of 0.0001, but the stress keeps increasing to 2.7 ksi before the curve flattens. The stress-strain response in the y-direction (with $\epsilon_y = 0$) is also graphed. After fracture (or cutoff) the stress became compressive when it should have dropped to zero. This is inconsistent with expected concrete behavior.

In the cap model, it was assumed that the tensile cutoff mechanism was implemented as an additional failure surface besides the J_2 failure surface and the cap itself. To further investigate this assumption, a triaxial tension test was conducted by prescribing a strain in the x-direction and constraining the lateral displacements to zero. Using the aforementioned elastic properties, the triaxial stresses were evaluated at $\epsilon_x = 5 \times 10^{-5}$, which is near the point where the model indicates a change of slope in Figure C-7. The resulting stresses were:

$$\sigma_x = 0.2183 \text{ ksi}$$

$$\sigma_y = 0.0483 \text{ ksi}$$

$$\sigma_z = \sigma_y$$

$$\text{pressure} = \sigma_x + \sigma_y + \sigma_z = 0.3149 \text{ ksi} \approx T$$

The value for pressure indicates that tensile cutoff should have occurred and the volumetric stress-strain graph in Figure C-8 indicates that it did occur.

Assuming that the tension cutoff acts as a failure surface, any increase in stress due to further strain should be available via the incremental nonlinear stress-strain equation:

$$\Delta\sigma_{ij} = D_{ijkl}\,\Delta\epsilon_{kl}$$

$$D_{ijkl} = L_{ijkl} - \frac{((3KU_{,J1})\delta_{ij} + (GU_{,\sqrt{J2}}/\sqrt{J2})\sigma_{ij})\,((3KF_{,J1})\,\delta_{kl} + (GF_{,\sqrt{J2}}/\sqrt{J2})\,\sigma_{kl})}{K_p + 9KF_{,J1}U_{,J1} + GF_{,\sqrt{J2}}U_{,\sqrt{J2}}}$$

where $L_{ijkl} = K\delta_{ij}\delta_{kl} + G(\delta_{ik}\delta_{jl} + \delta_{il}\delta_{jk} - (2/3)\delta_{ij}\delta_{kl})$

- G = shear modulus = 1,700 psi
- K = bulk modulus
- F = failure surface
- U = flow direction
- J1 = σ_{kk}
- J2 = $1/2\ s_{ij}s_{ij}$
- K_p = plastic modulus
- ϵ_{ij} = strain tensor component
- S_{ij} = deviator stress tensor component
- σ_{ij},etc. = stress tensor component
- δ_{ij},etc. = Kronecker delta function

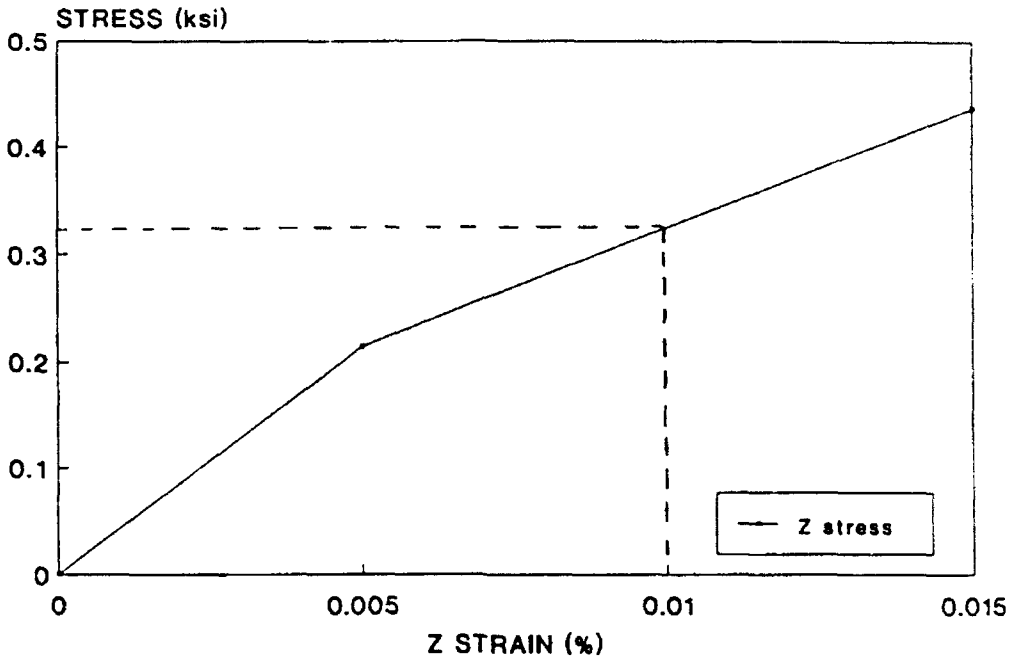

Figure C-7
Solid elements - Material 25,
laterally constrained tension.

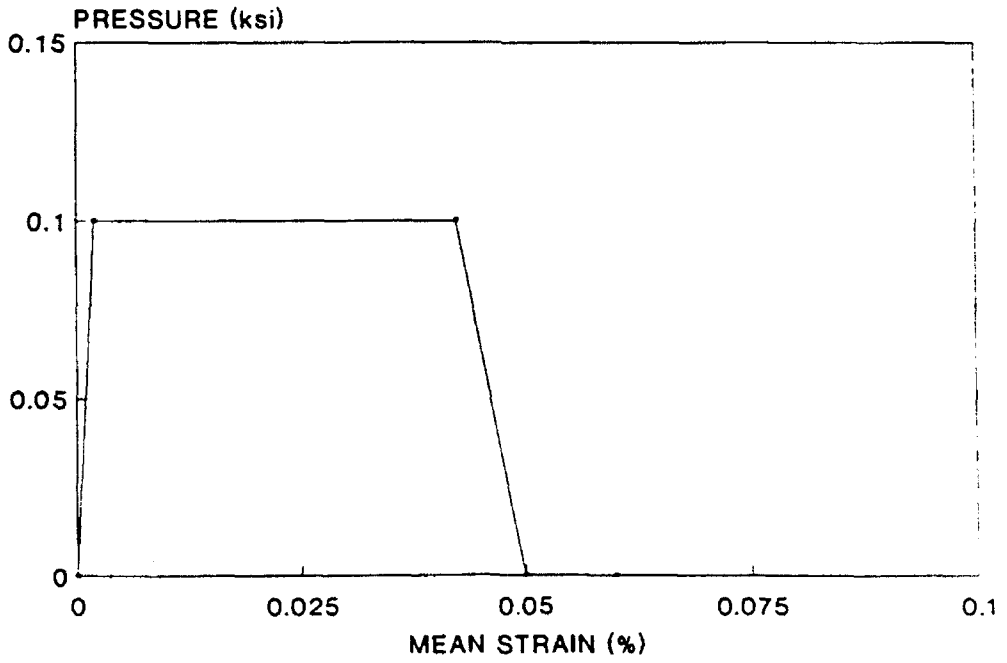

Figure C-8
Solid elements - Material 25, tension.

In the expression for the elasto-plastic modulus, D_{ijkl}, a comma indicates differentation with respect to either the J1 or $\sqrt{J2}$ stress invariant, and repeated subscripts indicate summation over the range i,j,k,l = 1,2,3.

The failure surface for the tensile cutoff can be defined as:

$$F = J1 - 0.3 = 0$$

With this definition, it is noted that the derivatives with respect to $\sqrt{J2}$ vanish and since there is no hardening when replicating brittle tension failure, $K_p = 0$. Also, assuming the cap model uses an associative flow rule for the tensile failure surface, F=U. The elasto-plastic modulus therefore reduces to:

$$D_{ijkl} = L_{ijkl} - \frac{(3KF_{,J1}\delta_{ij})(3KF_{,J1}\delta_{kl})}{9KF_{,J1}F_{,J1}}$$

For i,j,k,l = 1, the first term becomes (K + 4/3 G) and the second term becomes K. Therefore,

$$D_{1111} = \left(\frac{4}{3}\right)G = 2{,}267 \text{ ksi}$$

The incremental stress was calculated for a strain increment of $\Delta\epsilon_{11} = 0.00005$ as follows:

$$\Delta\sigma_{11} = D_{1111}\,\Delta\epsilon_{11} = 2{,}267 \times 0.00005 = 0.1133$$

The resulting stress at a total strain of 0.0001 is:

$$\sigma_{11} = \sigma_x = 0.2183 + 0.1133 = 0.3316 \text{ ksi}$$

which is confirmed in Figure C-7. This simple test establishes that the tensile cutoff in the cap model is being treated as a failure surface with an associative flow rule.

One of the problems of treating the tensile cutoff as a failure surface in invarient stress space is as follows: The pressure (J1) versus the mean strain, $\epsilon_{mean} = (\epsilon_x + \epsilon_y + \epsilon_z)$ 13, is shown in Figure C-8. Upon reaching the tensile cutoff, the pressure will remain constant at the cutoff value. The problem arises when the x-direction strain ϵ_x continues to increase and the stress σ_x continues to grow. The σ_y and σ_z must go into compression to maintain the constant pressure constraint (i.e., to remain on the tensile failure surface). This can also be confirmed by looking at the elasto-plastic modulus for the increment in transverse stress $\Delta\sigma_{22}$ due to an increment in axial strain $\Delta\epsilon_{11}$:

$$D_{2211} = L_{2211} - \frac{(3KF_{,J1})(3KF_{,J1})}{9KF_{,J1}F_{,J1}}$$

$$D_{2211} = -\left(\frac{2}{3}\right)G$$

The negative sign indicates that the increment of stress subracts from the elastic tensile contribution and at some point exceeds it, causing compressive stress in the transverse direction.

Based upon the direct formulation approach, it can be seen that the tension cutoff in the cap model is being treated as an associative flow rule failure surface. Figure C-6b indicates that as tensile strain increases, the strain follows an associative flow rule for the tension cutoff failure surface (i.e., the flow is perpendicular to the tension cutoff surface). As the stresses increase, the J2 component increases until the cone failure surface is touched. At this point, the flow rule for the new failure surface is observed. This is the flat region of the stress response seen in Figure C-6b. Although the model follows conventions for direct plasticity correctly, its numerical behavior for the tensile region of concrete is not appropriate.

DISTRIBUTION LIST

ADINA ENGRG, INC / WALCZAK, WATERTOWN, MA
AEWES / LIB, VICKSBURG, MS; PETERS, VICKSBURG, MS
AFESC / TECH LIB, TYNDALL AFB, FL
AFOSR / NA HOKANSON, WASHINGTON, DC
AMERICAN CONCRETE / LIB, DETROIT, MI
AMMANN & WHITNEY / NEW YORK, NY
ANTARCTIC / STAFFO, ALEXANDRIA, VA
APPLIED RSCH ASSOCIATION / HIGGINS, ALBUQUERQUE, NM
APTEC / SCHWER, SAN JOSE, CA
ARMSTRONG AERO MED RSCH LAB / OVENSHIRE, WRIGHT PATTERSON AFB, OH
ARMSTRONG, W. / MYSTIC, CT
ARMY / DEF AMMO CEN & SCOL, SARAC-DEV (R HILL), SAVANNA, IL; ENGR CEN, ATSE-DAC-LC, ALLAN, FORT LEONARD WOOD, MO; ENGR CEN, ATSE-DAC-LC, BERSTRAND, FORT LEONARD WOOD, MO; HQDA (DAEN-ZCM), WASHINGTON, DC
ARMY CECOM R&D TECH LIBRARY / ASNC-ELC-I-T, FORT MONMOUTH, NJ
ARMY CERL / CECER-FME (HAYES), CHAMPAIGN, IL; ENERGY SYS DIV, CHAMPAIGN, IL; LIB, CHAMPAIGN, IL
ARMY EWES / LIB, VICKSBURG, MS; WES (NORMAN), VICKSBURG, MS
ARVID GRANT & ASSOC / OLYMPIA, WA
ASSOCIATED SCIENTISTS/ MCCOY, WOODS HOLE, MA
ATLANTIC RICHFIELD CO / RE SMITH, DALLAS, TX
BATTELLE / D. FRINK, COLUMBUS, OH
BECHTEL CIVIL, INC / K. MARK, SAN FRANCISCO, CA
BETHLEHEM STEEL CO / ENGRG DEPT, BETHLEHEM, PA
BING C YEN / IRVINE, CA
BLAYLOCK ENGINEERING GROUP / T SPENCER, SAN DIEGO, CA
BRITISH EMBASSY / SCI & TECH DEPT (WILKINS), WASHINGTON, DC
BROWN, ROBERT / TUSCALOOSA, AL
BULLOCK, TE / LA CANADA, CA
BUREAU OF RECLAMATION / D-1512 (GS DEPUY), DENVER, CO
CAL STATE UNIV / C.V. CHELAPATI, LONG BEACH, CA
CALIF INST OF TECH / PASADENA, CA
CASE WESTERN RESERVE UNIV / CE DEPT (PERDIKARIS), CLEVELAND, OH
CATHOLIC UNIV / CE DEPT (KIM) WASHINGTON, DC
CENTRIC ENGINEERING SYSTEMS INC / TAYLOR, PALO ALTO, CA
CHAO, JC / HOUSTON, TX
CHEE, WINSTON / GRETNA, LA
CHESNAVFACENGCOM / CODE 402 (FRANCIS), WASHINGTON, DC; CODE 407, WASHINGTON, DC; YACHNIS, WASHINGTON, DC
CHEVRON OIL FLD RSCH CO / ALLENDER, LA HABRA, CA
CHILDS ENGRG CORP / K.M. CHILDS, JR., MEDFIELD, MA
CLARK, T. / SAN MATEO, CA
CLARKSON UNIV / CEE DEPT, POTSDAM, NY
CLIFTON, B. / SPRINGFIELD, VA
COGUARD / SUPERINTENDENT, NEW LONDON, CT
COLLEGE OF ENGINEERING / CE DEPT (GRACE), SOUTHFIELD, MI
COLLINS ENGRG, INC / M GARLICH, CHICAGO, IL
COLORADO SCHOOL OF MINES / GOLDEN, CO

COLORADO STATE UNIV / FORT COLLINS, CO; CE DEPT (CRISWELL), FORT COLLINS, CO; CE DEPT (W CHARLIE), FORT COLLINS, CO
COLUMBIA GULF TRANSMISSION / HOUSTON, TX
COM GEN FMF / PAC, SCIAD (G5), CAMP HM SMITH, HI
CONRAD ASSOC / LUISONI, VAN NUYS, CA
CONSOER TOWNSEND & ASSOC / DEBIAK, CHICAGO, IL
CONSTRUCTION TECH LABS, INC / G. CORLEY, SKOKIE, IL
CORNELL UNIV / ITHACA, NY; KULHAWY, ITHACA, NY
CRREL / CECRL-IC, HANOVER, NH; KOVACS, HANOVER, NH
DAMES & MOORE / LIB, LOS ANGELES, CA
DAVY DRAVO / WRIGHT, PITTSBURG, PA
DAY ZIMMERMAN/BASIL CORP / FITZGERALD, HAWTHORNE, NV
DEPT OF STATE / FOREIGN BLDGS OPS, BDE-ESB, ARLINGTON, VA
DIA / DB-6E1, WASHINGTON, DC; OGA-4B2, WASHINGTON, DC; VP-TPO, WASHINGTON, DC
DOBROWOLSKI, JA / ALTADENA, CA
DOD / EXPLOS SAFETY BRD, ALEXANDRIA, VA
DOT / TRANSP SYS CEN (TONG), CAMBRIDGE, MA
DTRCEN / (CODE 1720), BETHESDA, MD; CODE 172, BETHESDA, MD; CODE 1760, BETHESDA, MD
EDWARD K NODA & ASSOC / HONOLULU, HI
ENGINEERING DATA MANAGEMENT / RONALD W. ANTHONY, FORT COLLINS, CO
FAA / ARD 200, WASHINGTON, DC
GEI CONSULTANTS, INC. / T.C. DUNN, WINCHESTER, MA
GEIGER ENGINEERS / FUNSTON, BELLINGHAM, WA
GEOCON INC / CORLEY, SAN DIEGO, CA
GEORGE WASHINGTON UNIV / ENGRG & APP SCI SCHL (FOX), WASHINGTON, DC
GEORGIA INST OF TECH / CE SCHL (KAHN), ATLANTA, GA; CE SCHL (SWANGER), ATLANTA, GA; CE SCHL (ZURUCK), ATLANTA, GA
GEOTECHNICAL ENGRS, INC / MURDOCK, WINCHESTER, MA
GERWICK INC / SAN FRANCISCO, CA
GIORDANO, A.J. / SEWELL, NJ
GSA / HALL, WASHINGTON, DC
HALEY & ALDRICH, INC. / CETIN SEYDEMIR, CAMBRIDGE, MA
HAN-PADRON ASSOCIATES / DENNIS PADRON, NEW YORK, NY
HARDY, S.P. / SAN RAMON, CA
HARTFORD STEAM BOILER INSP & INS CO / SPINELLI, HARTFORD, CT
HAYNES & ASSOC / H. HAYNES, PE, OAKLAND, CA
HAYNES, B / LYNDEN, WA
HEUZE, F / ALAMO, CA
HJ DEGENKOLB ASSOC / W. MURDOUGH, SAN FRANCISCO, CA
HKS INC / PAWTUCKET, RI
HOIDRA / NEW YORK, NY
HQ AFESC / RDC (DR. M. KATONA), TYNDALL AFB, FL
HQ AFLC / CAPT SCHMIDT, WRIGHT PATTERSON AFB, OH
HUGHES AIRCRAFT CO / TECH DOC CEN, EL SEGUNDO, CA
HYPERBARIC CENTER / DURHAM, NH
INFOTEAM INC / M. ALLEN, PLANTATION, FL
INST OF MARINE SCIENCES / LIB, PORT ARANSAS, TX
INSTITUTE OF MARINE SCIECES / MOREHEAD CITY, NC
IOWA STATE / AMES, IA
JOHN HOPKINS UNIV / CE DEPT, JONES, BALTIMORE, MD

JOHN J MC MULLEN ASSOC / LIB, NEW YORK, NY
KAISER PERMANENTE MEDCIAL CARE PROGRAM / OAKLAND, CA
LANTNAVFACENGCOM / CODE 411, NORFOLK, VA
LAWRENCE LIVERMORE NATIONAL LAB / LIVERMORE, CA; FJ TOKARZ, LIVERMORE, CA; PLANT ENGRG LIB (L-654), LIVERMORE, CA
LAWRENCE UNIV / SOUTHFIELD, ME
LEHIGH UNIV / BETHLEHAM, PA
LEO A DALY CO / HONOLULU, HI
LOCKHEED / RSCH LAB (M. JACOBY), PALO ALTO, CA; RSCH LAB (P UNDERWOOD), PALO ALTO, CA
MAINE MARITIME ACADEMY / LIB, CASTINE, ME
MARATHON OIL CO / GAMBLE, HOUSTON, TX
MARC ANALYSIS RSCH CORP / HSU, PALO ALTO, CA
MARITECH ENGRG / DONOGHUE, AUSTIN, TX
MC DERMOTT, INC / E&M DIV, NEW ORLEANS, LA
MCCLELLAND ENGRS / HOUSTON, TX
MCDONNELL DOUGLAS CORP / R CARSON, ST LOUIS, MO
MICHIGAN TECH UNIV / HOUGHTON, MI; CO DEPT (HAAS), HOUGHTON, MI
MIT / R.V. WHITMAN, CAMBRIDGE, MA
MOBIL R&D CORP / OFFSHORE ENGRG LIB, DALLAS, TX
MT DAVISSON / CE, SAVOY, IL
NATL ACADEMY OF ENGRY / ALEXANDRIA, VA
NATL ACADEMY OF SCIENCES / BRB, (SMEALLIE), WASHINGTON, DC; NRC, DR. CHUNG, WASHINGTON, DC
NAVEODTECHCEN / TECH LIB, INDIAN HEAD, MD
NAVFACENGCOM / CODE 04A3, ALEXANDRIA, VA; CODE 04B (J. CECILIO), ALEXANDRIA, VA; CODE 04BE (WU), ALEXANDRIA, VA; CODE 07, ALEXANDRIA, VA; CODE 07M (BENDER), ALEXANDRIA, VA; CODE 163, ALEXANDRIA, VA
NAVSAFECEN / CODE 43, NORFOLK, VA
NAVSCOLCECOFF / CODE C35, PORT HUENEME, CA
NAVSEACENPAC / CODE 420, SAN DIEGO, CA
NAVSEASYSCOM / CODE 56W23, WASHINGTON, DC; CODE 0622, WASHINGTON, DC
NAVSURFWARCEN COASTSYSTA / CODE 0222, PANAMA CITY, FL
NAVSWC / CO, DAHLGREN, VA; DET, WHITE OAK LAB, LIB, SILVER SPRING, MD
NAVWPNCEN / CODE 3276, CHINA LAKE, CA
NAVWPNSTA / CODE 09, CONCORD, CA; SAFETY BR, SEAL BEACH, CA
NAVWPNSTA EARLE / CODE 8052, COLTS NECK, NJ
NAWS / CODE 1018, POINT MUGU, CA
NCSC / PANAMA CITY, FL
NEW ZEALAND CONCRETE RSCH ASSN / LIB, PORIRUA
NIEDORODA, AW / GAINESVILLE, FL
NOAA / JOSEPH VADUS, ROCKVILLE, MD
NORTHNAVFACENGCOM / CO, PHILADELPHIA, PA; CODE 04, PHILADELPHIA, PA
NORTHWESTERN UNIVERSITY / EVANSTON, IL; BAZANT, EVANSTON, IL; CE DEPT (BELYTSCHKO), EVANSTON, IL
NRL / CODE 2511, WASHINGTON, DC; CODE 2530.1, WASHINGTON, DC; CODE 4670, WASHINGTON, DC; RATH, ARLINGTON, VA
NSF / STRUC & BLDG SYSTEMS (KP CHONG), WASHINGTON, DC
NUHN & ASSOC / A.C. NUHN, WAYZATA, NM
OCNR / CODE 10P4 (KOSTOFF), ARLINGTON, VA; SILVA, ARLINGTON, VA
OMEGA MARINE, INC. / SCHULZE, LIBRARIAN, HOUSTON, TX
ONR / CODE 1132SM, ARLINGTON, VA

OREGON STATE UNIV / CORVALLIS, OR; CE DEPT (YIM), CORVALLIS, OR; DEPT OF MECH ENGRG (SMITH), CORVALLIS, OR
PACIFIC MARINE TECH / M. WAGNER, DUVALL, WA
PAYE-KOSANOWSKY, S / POND EDDY, NY
PENNSYLVANIA STATE UNIV / GOTOLSKI, UNIVERSITY PARK, PA; LAB, STATE COLLEGE, PA; RSCH LAB, STATE COLLEGE, PA
PERKOWSKI, MICHAEL T. / TIPPECANOE, OH
PILE BUCK, INC / SMOOT, JUPITER, FL
PORTLAND CEMENT ASSOC / AE FIORATO, SKOKIE, IL
PORTLAND STATE UNIV / MIGLIORI, PORTLAND, OR
PURDUE UNIV / CE SCOL (CHEN), WEST LAFAYETTE, IN
PURDUE UNIVERSITY / WEST LAFAYETTE, IN
SAN DIEGO STATE UNIV / CE DEPT (KRISHNAMOORTHY), SAN DIEGO, CA
SANDIA LABS / LIB, LIVERMORE, CA
SARGENT & HERKES, INC / JP PIERCE, JR, NEW ORLEANS, LA
SCHUPACK SUAREX ENGRS INC / SCHUPACK, NORWALK, CT
SCOPUS TECHNOLOGY INC / (B. NOUR-OMID), EMERYVILLE, CA; (S. NOUR-OMID), EMERYVILLE, CA
SEATTLE UNIV / SEATTLE, WA
SHANNON AND WILSON INC / SEATTLE, WA
SHELL OIL CO / E. DOYLE, HOUSTON, TX
SIMPSON, GUMPERTZ & HEGER, INC / HILL, ARLINGTON, MA
SMELSER, D / SEVIERVILLE, TN
SOUTHNAVFACENGCOM / CODE 04A, CHARLESTON, SC; CODE 1622, CHARLESTON, SC
SOUTHWEST RSCH INST / ENERGETIC SYS DEPT (ESPARZA), SAN ANTONIO, TX; KING, SAN ANTONIO, TX; M. POLCYN, SAN ANTONIO, TX; MARCHAND, SAN ANTONIO, TX; THACKER, SAN ANTONIO, TX
SOWESTNAVFACENGCOM / LANGSTRAAT, SAN DIEGO, CA
SRI INTL / ENGRG MECH DEPT (GRANT), MENLO PARK, CA; ENGRG MECH DEPT (SIMONS), MENLO PARK, CA
STANFORD UNIV / APP MECH DIV (HUGHES), STANFORD, CA; CE DEPT (PENSKY), STANFORD, CA; DIV OF APP MECH (SIMO), STANFORD, CA
STATE UNIV OF NEW YORK / CE DEPT, BUFFALO, NY
TECHNOLOGY UTILIZATION / K WILLINGER, WASHINGTON, DC
TEXAS A&M UNIV / CE DEPT (MACHEMEHL), COLLEGE STATION, TX; CE DEPT (NIEDZWECKI), COLLEGE STATION, TX; OCEAN ENGR PROJ, COLLEGE STATION, TX
TRW INC / ENGR LIB, CLEVELAND, OH
TUDOR ENGRG CO / ELLEGOOD, PHOENIX, AZ
TUFTS UNIV / SANYEI, MEDFORD, MA
UNIV OF CALIFORNIA / CE DEPT (FENVES), BERKELEY, CA; CE DEPT (FOURNEY), LOS ANGELES, CA; CE DEPT (HERRMANN), DAVIS, CA; CE DEPT (KUTTER), DAVIS, CA; CE DEPT (RAMEY), DAVIS, CA; CE DEPT (WILLIAMSON), BERKELEY, CA; CTR FOR GEOTECH MODEL (IDRISS), DAVIS, CA; MECH ENGRG DEPT (BAYO), SANTA BARBARA, CA; MECH ENGRG DEPT (BRUCH), SANTA BARBARA, CA; MECH ENGRG DEPT (LECKIE), SANTA BARBARA, CA; MECH ENGRG DEPT (MCMEEKING), SANTA BARBARA, CA; MECH ENGRG DEPT (MITCHELL), SANTA BARBARA, CA; MECH ENGRG DEPT (TULIN), SANTA BARBARA, CA
UNIV OF COLORADO / CE DEPT (HON-YIM KO), BOULDER, CO; MECH ENGRG DEPT (PARK), BOULDER, CO
UNIV OF CONN / LEONARD, STORRS, CT; LIBRARY, GROTON, CT
UNIV OF HAWAII / CE DEPT (CHIU), HONOLULU, HI; MANOA, LIB, HONOLULU, HI
UNIV OF ILLINOIS / CE LAB (PECKNOLD), URBANA, IL; METZ REF RM, URBANA, IL

UNIV OF MARYLAND / CE DEPT, COLLEGE PARK, MD
UNIV OF MICHIGAN / CE DEPT (RICHART), ANN ARBOR, MI
UNIV OF N CAROLINA / CE DEPT (AHMAD), RALEIGH, NC; CE DEPT (GUPTA), RALEIGH, NC; CE DEPT (TUNG), RALEIGH, NC
UNIV OF NEW MEXICO / NMERI (BEAN), ALBUQUERQUE, NM; NMERI (FALK), ALBUQUERQUE, NM; NMERI (TAPSCOTT), ALBUQUERQUE, NM; NMERI, HL SCHREYER, ALBUQUERQUE, NM
UNIV OF NEW YORK / BUFFALO, NY; REINHORN, BUFFALO, NY
UNIV OF PENNSYLVANIA / DEPT OF ARCH, PHILADELPHIA, PA
UNIV OF RHODE ISLAND / CE DEPT (KARAMANLIDIS), KINGSTON, RI; CE DEPT (KOVACS), KINGSTON, RI; CE DEPT (TSIATAS), KINGSTON, RI; DR. VEYERA, KINGSTON, RI
UNIV OF TENNESSEE / KNOXVILLE, TN
UNIV OF TEXAS / CONSTRUCTION INDUSTRY INST, AUSTIN, TX; ECJ 4.8 (BREEN), AUSTIN, TX
UNIV OF WASHINGTON / CE DEPT (HARTZ), SEATTLE, WA; MATTOCK, SEATTLE, WA
UNIV OF WEST VIRGINIA / BLACKSBURG, WV
UNIV OF WISCONSIN / MILWAUKEE, WI; GREAT LAKES STUDIES CEN, MILWAUKEE, WI
UNIV OF WYOMING / SCHMIDT, LARAMIE, WY
US DEPT OF INTERIOR / BLM, ENGRG DIV (730), WASHINGTON, DC
US MERCHANT MARINE ACADEMY / KINGS POINT, NY
US NUCLEAR REGULATORY COMMISSION / KIM, WASHINGTON, DC
USA BELVOIR / FORT BELVOIR, VA
USACOE / CESPD-CO-EQ, SAN FRANCISCO, CA
USAE / CEWES-IM-MI-R, VICKSBURG, MS
USAMMRC / DRXMR-SM, WATERTOWN, MA
USDA FOREST SERVICE / SAN DIMAS, CA; REG BRIDGE ENGR, ALOHA, OR
USNA / CH, MECH ENGRG DEPT (C WU), ANNAPOLIS, MD; SYS ENGRG, ANNAPOLIS, MD
USPS / BILL POWELL, WASHINGTON, DC
VALLEY FORGE CORPORATE CENTER / FRANKLIN RESEARCH CENTER, NORRISTOWN, PA
VAN ALLEN, B / KINGSTON, NY
VIRGINIA INST OF MARINE SCI / GLOUCESTER POINT, VA
VSE CORP / LOWER, ALEXANDRIA, VA
VULCAN IRON WORKS, INC / DC WARRINGTON, CLEVELAND, TN
WESTERN INSTRUMENT CORP / VENTURA, CA
WESTINGHOUSE ELECTRIC CORP / LIB, PITTSBURG, PA; OCEANIC DIV LIB, ANNAPOLIS, MD
WESTNAVFACENGCOM / CO, SAN BRUNO, CA; CODE 402, SAN BRUNO, CA; CODE 404.2 (JEUNG), SAN BRUNO, CA; CODE 411, SAN BRUNO, CA; VALDEMORO, SAN BRUNO, CA
WISS, JANNEY, ELSTNER, & ASSOC / DW PFEIFER, NORTHBROOK, IL
WISWELL, INC. / SOUTHPORT, CT
WOODWARD CLYDE CONSULTANTS / OAKLAND, CA
WORCHESTER POLYTECH / SULLIVAN, WORCESTER, MA

DISTRIBUTION QUESTIONNAIRE

The Naval Civil Engineering Laboratory is revising its primary distribution lists.

SUBJECT CATEGORIES

1 **SHORE FACILITIES**
1A Construction methods and materials (including corrosion control, coatings)
1B Waterfront structures (maintenance/deterioration control)
1C Utilities (including power conditioning)
1D Explosives safety
1E Aviation Engineering Test Facilities
1F Fire prevention and control
1G Antenna technology
1H Structural analysis and design (including numerical and computer techniques)
1J Protective construction (including hardened shelters, shock and vibration studies)
1K Soil/rock mechanics
1L Airfields and pavements
1M Physical security
2 **ADVANCED BASE AND AMPHIBIOUS FACILITIES**
2A Base facilities (including shelters, power generation, water supplies)
2B Expedient roads/airfields/bridges
2C Over-the-beach operations (including breakwaters, wave forces)
2D POL storage, transfer, and distribution
2E Polar engineering
3 **ENERGY/POWER GENERATION**
3A Thermal conservation (thermal engineering of buildings, HVAC systems, energy loss measurement, power generation)
3B Controls and electrical conservation (electrical systems, energy monitoring and control systems)
3C Fuel flexibility (liquid fuels, coal utilization, energy from solid waste)
3D Alternate energy source (geothermal power, photovoltaic power systems, solar systems, wind systems, energy storage systems)
3E Site data and systems integration (energy resource data, integrating energy systems)
3F EMCS design
4 **ENVIRONMENTAL PROTECTION**
4A Solid waste management
4B Hazardous/toxic materials management
4C Waterwaste management and sanitary engineering
4D Oil pollution removal and recovery
4E Air pollution
4F Noise abatement
5 **OCEAN ENGINEERING**
5A Seafloor soils and foundations
5B Seafloor construction systems and operations (including diver and manipulator tools)
5C Undersea structures and materials
5D Anchors and moorings
5E Undersea power systems, electromechanical cables, and connectors
5F Pressure vessel facilities
5G Physical environment (including site surveying)
5H Ocean-based concrete structures
5J Hyperbaric chambers
5K Undersea cable dynamics

ARMY FEAP
BDG Shore Facilities
NRG Energy
ENV Environmental/Natural Responses
MGT Management
PRR Pavements/Railroads

TYPES OF DOCUMENTS

D = Techdata Sheets; **R** = Technical Reports and Technical Notes; **G** = NCEL Guides and Abstracts; **I** = Index to TDS; **U** = User Guides; ☐ None - remove my name

Old Address:

_____

_____

_____

_____

Telephone No.: _____

New Address:

_____

_____

_____

_____

Telephone No.: _____

INSTRUCTIONS

The Naval Civil Engineering Laboratory has revised its primary distribution lists. To help us verify our records and update our data base, please do the following:

- Add - circle number on list
- Remove my name from all your lists - check box on list.
- Change my address - line out incorrect line and write in correction **(DO NOT REMOVE LABEL).**
- Number of copies should be entered after the title of the subject categories you select.
- Are we sending you the correct type of document? If not, circle the type(s) of document(s) you want to receive listed on the back of this card.

Fold on line, staple, and drop in mail.

DEPARTMENT OF THE NAVY
Naval Civil Engineering Laboratory
560 Laboratory Drive
Port Hueneme CA 93043-4328

Official Business
Penalty for Private Use, $300

NO POSTAGE NECESSARY IF MAILED IN THE UNITED STATES

BUSINESS REPLY CARD
FIRST CLASS PERMIT NO. 12503 WASH D.C.

POSTAGE WILL BE PAID BY ADDRESSEE

COMMANDING OFFICER
CODE L34
560 LABORATORY DRIVE
NAVAL CIVIL ENGINEERING LABORATORY
PORT HUENEME CA 93043-4328

NCEL DOCUMENT EVALUATION

You are number one with us; how do we rate with you?

We at NCEL want to provide you our customer the best possible reports but we need your help. Therefore, I ask you to please take the time from your busy schedule to fill out this questionnaire. Your response will assist us in providing the best reports possible for our users. I wish to thank you in advance for your assistance. I assure you that the information you provide will help us to be more responsive to your future needs.

R. N. STORER, Ph.D, P.E.
Technical Director

DOCUMENT NO. _____ TITLE OF DOCUMENT: _____

_____

Date: _____ Respondent Organization : _____

Name: _____ Activity Code: _____
Phone: _____ Grade/Rank: _____

Category (*please check*):

Sponsor ____ User ____ Proponent ____ Other (*Specify*) _____

Please answer on your behalf only; not on your organization's. Please check (*use an X*) only the block that most closely describes your attitude or feeling toward that statement:

SA Strongly Agree A Agree O Neutral D Disagree SD Strongly Disagree

---

	SA	A	N	D	SD
1. The technical quality of the report is comparable to most of my other sources of technical information.	( )	( )	( )	( )	( )
2. The report will make significant improvements in the cost and or performance of my operation.	( )	( )	( )	( )	( )
3. The report acknowledges related work accomplished by others.	( )	( )	( )	( )	( )
4. The report is well formatted.	( )	( )	( )	( )	( )
5. The report is clearly written.	( )	( )	( )	( )	( )
6. The conclusions and recommendations are clear and directly supported by the contents of the report.	( )	( )	( )	( )	( )
7. The graphics, tables, and photographs are well done.	( )	( )	( )	( )	( )

Do you wish to continue getting NCEL reports? ☐ YES ☐ NO

Please add any comments (e.g., in what ways can we improve the quality of our reports?) on the back of this form.

Comments:

Fold on line, staple, and drop in mail.

DEPARTMENT OF THE NAVY
Naval Civil Engineering Laboratory
560 Laboratory Drive
Port Hueneme CA 93043-4328

Official Business
Penalty for Private Use, $300

NO POSTAGE NECESSARY IF MAILED IN THE UNITED STATES

BUSINESS REPLY CARD
FIRST CLASS PERMIT NO. 12503 WASH D.C.

POSTAGE WILL BE PAID BY ADDRESSEE

COMMANDING OFFICER
CODE L03
560 LABORATORY DRIVE
NAVAL CIVIL ENGINEERING LABORATORY
PORT HUENEME CA 93043-4328